THE UNIVERSITY
of EDINBURGH

Exploring the role of Kindlin-1 in skin homeostasis and Squamous Cell Carcinoma

Ifigeneia Stavrou

THE UNIVERSITY of EDINBURGH

The University of Edinburgh

Doctor of Philosophy

2017

Declaration

I hereby declare that I am the sole author of this thesis and that work contain herein is the result of my own independent investigation, except where acknowledgment has been specified in the text. No part of this thesis has been submitted for any other degree or qualification, except where noted.

Ifigeneia Stavrou

23 | 03 | 2017

To my family

Acknowledgments

First and foremost I wish to thank my supervisor Prof. Val Brunton, to whom I am extremely grateful for her invaluable guidance and support over the last 4 years. I truly enjoyed my PhD and, besides the project itself, a key reason for this was being a member of her lab and having her as my mentor. I would also like to extend my gratitude to my second supervisor Prof. Margaret Frame for her advice and encouragement during my PhD. Moreover, I would like to acknowledge my day-to-day supervisor and friend Dr Hitesh Patel for all that he has done; whether that was to offer his assistance and advice, or to buy me a (multiple) glass(es) of wine in the pub on Friday afternoons. Thank you also to Dr Viji Draviam and Dr Roshan Shrestha from the University of Cambridge for their collaboration, for introducing me to the world of live-cell imaging and for their hospitality, which made my 2-week stay in Cambridge a truly memorable experience. Thank you to Dr Martin Lee for being an awesome office neighbour, accompanying me to my short-lived effort in running and helping me with the second harmonic microscopy. Thank you to Morwenna Muir for her vital support with the animal experiments and to Dr Stuart Aitken for the RNA-Seq data analysis. I would also like to acknowledge Dr Hila Emmert and Georgia Dodd for allowing me to include one of their figures in the discussion of my thesis. Also, a great thank you to my friends and future doctors Mina and Laura for their friendship and all the wonderful moments that we spent together in and out of the lab, as well to my friends back home, Antreas, Eleni and so many more, who continue to grant me with priceless memories and laughter every time I see them.

Special thanks to Dr Georgios Kanellos for his love, support, patience and encouragement, and for keeping me sane throughout these 4 years. Finally, my deepest gratitude goes to my parents, brother and grandparents for their unconditional love and for always believing in me and standing by my side. I dedicate my PhD thesis to them and especially to my grandmother Ifigeneia who I miss dearly.

table of contents

Declaration **Error! Bookmark not defined.**

list of abbreviations 10

list of figures and tables 13

abstract 17

lay reader summary 19

Chapter 1: introduction 21

1.1. Overview of Kindler Syndrome 21

1.2. Overview of Epidermolysis Bullosa 22

1.3. Kindlins and talins in FERM adhesion 25

1.4. Kindlins and talins cooperate to induce integrin activation 29

1.5. Models of talin/kindlin-mediated integrin activation 30

1.6. Kindlins and talins control bidirectional integrin signalling 33

1.7. Functional roles of kindlins in biological processes such as cell adhesion, spreading and migration 34

1.7.1. Cellular roles of Kin1 35

1.7.2. Cellular roles of Kin2 and Kin3 36

1.7.3. Overlapping and distinct cellular roles of Kin1 and Kin2 37

1.8. Kindlins in cancer 38

1.8.1. Roles of kindlins in tumour promotion 38

1.8.2. Roles of kindlins in tumour suppression 40

1.9. project aims 41

Chapter 2: materials and methods 43

2.1. Cell culture 43

2.1.1. Cell line maintenance 43

2.1.2. Generation of MDA-MB-231$^{H2B:DsRed}$ cell line 43

2.1.3. RNA interference and live cell imaging 44

2.1.3.1. RNA interference in MDA-MB-231 and HeLa cell lines 44

2.1.3.2. Live cell imaging of MDA-MB-231 and HeLa cell lines 44

2.1.3.3. Alamar Blue viability assay in HeLa cells 44

2.1.4. Incucyte cell count proliferation assay 45

2.1.5. Methylcellulose-over-agarose proliferation assay 46
2.2. Animal models and cell culture 46
2.2.1. Generation of mouse model of Kin1 loss 46
2.2.2. Isolation of mouse primary keratinocytes 47
2.2.3. Generation of mouse SCC tumour cell lines: 117 SCC cells, 130 SCC cells and 145 SCC cells 48
2.3. Cloning, cell infections and generation of $Kin1^{null}$, $Kin1^{wt}$ and $Kin1^{AA}$ mouse SCC cell lines 48
2.4. Development of $Kin1^{null}$, $Kin1^{wt}$ and $Kin1^{AA}$ SCC tumours 50
2.5. Immunoblotting, Immunohistochemistry and Immunofluorescence 50
2.5.1. Cell lysis, protein quantification and Immunoblotting 50
2.5.2. Immunohistochemistry 52
2.5.3. Immunofluorescence 53
2.6. Second harmonic imaging microscopy 56
2.7. Tumour and cell RNA extraction, RNA Sequencing and quantitative real-time PCR 56
2.7.1. RNA extraction 56
2.7.2. RNA-Sequencing and analysis 57
2.7.3. Quantitative real-time PCR 57
2.8. Data statistical analysis 59

Chapter 3: development and characterisation of a mouse model of Kin1 loss 61
3.1. Use of Cre-Lox recombination system to achieve conditional knockout of *Fermt1* in the epidermis of adult mice 62
3.2. Phenotypic analysis and histological examination of K14-Cre-$Kin1^{fl/fl}$ mouse epidermis 65
3.3. Characterisation of the proliferative and mitotic capacity in keratinocytes of K14-Cre-$Kin1^{fl/fl}$ mouse epidermis 68
3.4. Characterisation of mitosis in keratinocytes of K14-Cre-$Kin1^{fl/fl}$ mouse epidermis 71
3.5. Characterisation of the apoptotic capacity of K14-Cre-$Kin1^{fl/fl}$ mouse epidermis 75
3.6. Discussion 76

3.6.1. Kin1 plays a role in regulation of keratinocyte proliferation and mitosis in mouse epidermis 76
3.6.2. Evaluation of K14-Cre-Kin1$^{fl/fl}$ mouse model of Kin1 loss 79
3.6.3. Summary and future work 81

Chapter 4: exploring the role of Kin1 and Kin2 in mitosis 83
4.1. Establishment of MDA-MB-231$^{H2B:DsRed}$ cell line 84
4.2. Kin1 depletion in MDA-MB-231$^{H2B:DsRed}$ cell line 86
4.3. Morphological assessment of si-NT and si-Kin1 treated MDA-MB-231 cells 87
4.4. Assessment of duration of mitosis and mitotic spindle phenotypes in si-NT and si-Kin1 treated MDA-MB-231 cells 88
4.5. Characterisation of HeLa$^{H2B:GFP/\beta\text{-}tub:DsRed}$ cell line 93
4.6. Individual depletion of Kin1 and Kin2, and co-depletion of Kin1+Kin2 in HeLa cells 94
4.7. Morphological assessment of si-Kin1, si-Kin2 and si-Kin1+Kin2 in HeLa cells 95
4.8. Assessment of duration of mitosis and mitotic spindle phenotypes in si-NT, si-Kin1, si-Kin2 and si-Kin1+Kin2 treated HeLa cells 96
4.9. Discussion 101
4.9.1. Kin1 regulates chromosome segregation in MDA-MB-231 cells 101
4.9.2. Kin1 regulates spindle orientation in MDA-MB-231 cells 102
4.9.3. Kin1 and Kin2 display overlapping and distinct functions in regulating mitotic homeostasis 103
4.9.4. Kin1 and Kin2 display distinct functions in regulating cell morphology 104
4.9.5. Summary and future work 105

Chapter 5: exploring the role of Kin1 in SCC 106
5.1. Characterisation of mouse SCC cell lines 108
5.2. Cre-Lox recombination system-mediated conditional knockout of *Fermt1* in mouse SCC cells 110
5.3. Characterisation of Kin1^{null}, Kin1^{wt} and Kin1^{AA} mouse SCC cell lines 111
5.4. Subcellular localisation of Kin1 and Kin2 within Kin1^{null}, Kin1^{wt} and Kin1^{AA} mouse SCC cell lines 113

5.5. *In vitro* assessment of proliferation and clonogenicity in Kin1^{null}, Kin1^{wt} and Kin1^{AA} mouse SCC cell lines 115
5.6. *In vivo* assessment of Kin1^{null}, Kin1^{wt} and Kin1^{AA} mouse SCC tumour growth 119
5.7. Morphological assessment of Kin1^{null}, Kin1^{wt} and Kin1^{AA} mouse SCC tumours 122
5.8. Immunohistochemical assessment of proliferation, apoptosis and vascularization in Kin1^{null} and Kin1^{wt} mouse SCC tumours 127
5.9. Comparative RNA-Seq analysis of gene expression changes in Kin1^{null} and Kin1^{wt} mouse SCC tumours 131
5.10. Exploring gene expression changes identified through RNA-Seq in Kin1^{null} and Kin1^{wt} mouse SCC tumours, and in Kin1^{null}, Kin1^{wt} and Kin1^{null} and Kin1^{AA} mouse SCC cell lines 133
5.10.1. Validation of genetic loss of Fermt1 gene in Kin1^{null} mouse SCC tumours 134
5.10.2. Analysis of expression of Metalloproteinase genes in Kin1^{null} and Kin1^{wt} mouse SCC tumours, and in Kin1^{null}, Kin1^{wt} and Kin1^{AA} mouse SCC cells 135
5.10.2.1. Analysis of expression of "classical" Matrix Metalloproteinase (MMP) genes *Mmp3* and *MMP13* in Kin1^{null} and Kin1^{wt} mouse SCC tumours, and in Kin1^{null}, Kin1^{wt} and Kin1^{AA} mouse SCC cells 136
5.10.2.2. Analysis of expression of Membrane-Type Matrix Metalloproteinase (MT-MMP) genes *Mmp15* in Kin1^{null} and Kin1^{wt} mouse SCC tumours 142
5.10.2.3. Analysis of expression of "A Disintegrin and Metalloproteinase with Thrombospondin motif" (ADAMTS) genes *Adamts6*, *Adamts12* and *Adamts17* in Kin1^{null} and Kin1^{wt} mouse SCC tumours 144
5.10.3. Analysis of expression of angiogenesis factors in Kin1^{null} and Kin1^{wt} mouse SCC tumours 146
5.10.3.1. Analysis of expression of *Hif1α* gene in Kin1^{null} and Kin1^{wt} mouse SCC tumours 147
5.10.3.2. Analysis of expression of *Vegfa (Vascular endothelial growth a), Flt1 (FMS-like tyrosine kinase 1)* and *Kdr (Kinase insert domain receptor)* gene in Kin1^{null} and Kin1^{wt} mouse SCC tumours 148
5.10.3.3. Analysis of expression of Thbs1 gene in Kin1^{null} and Kin1^{wt} mouse SCC tumours 150
5.10.4. Analysis of expression of chemokines in Kin1^{null} and Kin1^{wt} mouse SCC tumours 152
5.11. Discussion 155
5.11.1. Role of Kin1 in *in vitro* proliferation 155
5.11.2. Role of Kin1 in tumour growth and progression 157
5.11.3. Role of Kin1-integrin interaction in tumour growth and proliferation 158
5.11.4. Role of Kin1 in regulating the tumour microenvironment 160

5.11.4.1. Role of Kin1 in regulating angiogenesis 160
5.11.4.2. Role of Kin1 in regulating the ECM 162
5.11.4.2.1. Role of Kin1 in regulating MMPs 162
5.11.4.2.2. Role of Kin1 in regulating ADAMTSs 165
5.11.4.3. Role of Kin1 in regulating the immune system 166
5.11.5. Role of Kin1 in tumour growth in $Kin1^{null}$, $Kin1^{wt}$ and $Kin1^{AA}$ Met-1 mammary tumours 169
5.11.6. Summary and future work 170

Chapter 6: discussion 172
6.1. Therapeutic avenues for KS and other types of EB 172
6.1.1. Allogeneic bone marrow transplantation 172
6.1.2. Autologous gene therapy 173
6.1.3. Revertant mosaicism 173
6.2. A role for Kin1 in skin homeostasis 175
6.3. A role for Kin1 in the development of SCC 177
6.4. Concluding Remarks 179

Bibliography 182

list of abbreviations

4OHT	4-hydroxytamoxifen
α-tub	α-tubulin
ac-tub	acetylated α-tubulin
ACD	Asymmetrical Cell Division
ADAM	A Disintegrin and Metalloproteinase
ADAMTS	A Disintegrin and Metalloproteinase with Thrombospondin Motif
AMPK	AMP-activated Protein Kinase
ANOVA	one-way analysis of variance
BM	Bone Marrow
BSA	Bovine Serum Albumin
C57BL/6	C57Black/6
C. elegans	Caenorhabditis elegans
CAF	Cancer-associated fibroblast
Casp-3	Cleaved caspase-3
Ccl	C-C motif ligand
CHO	Chinese Hamster Ovary
CTC	Circulating Tumour Cells
Cxcl1	Cxcl1 (C-X-C motif ligand 1)
DMBA	7,12-Dimethylbenz[a]Anthracene
DMEM	Dulbecco's Modified Eeagle's Medium
DSP	Desmoplakin
DEB	Dystrophic Epidermolysis Bullosa
EB	Epidermolysis Bullosa
EB1	End Binding 1
EBS	Epidermolysis Bullosa Symplex

ECM	Extracellular Matrix
EMT	Epithelial-to-Mesenchymal Transition
FACS	Fluorescence-Activated Cell Sorting
FAK	Focal Adhesion Kinase
FBS	Fetal Bovine Serum
FERM	Four-point-one, Ezrin, Radixin, Moesin
FERMT1	Fermitin family member 1
Flt1	FMS-like tyrosine kinase 1
H&E	Haematoxylin & Eosin
HB-EGF	Heparin-Binding Epidermal Growth Factor-like growth factor
HDAC6	Histone Deacetylase 6
Hif1α	Hypoxia-inducible factor 1α
ICAP-1	Integrin Cytoplasmic domain-Associated Protein-1
IF	Immunofluorescence
IGF	Insulin-like Growth Factor
IHC	Immunohistochemistry
IL-6	Interleukin-6
JEB	Junctional Epidermolysis Bullosa
Kdr	Kinase insert domain receptor
Kin1	Kindlin-1
Kin2	Kindlin-2
Kin3	Kindlin-3
KS	Kindler Syndrome
LAD-III	Type III Leukocyte Adhesion Deficiency
MMP	Matrix Metalloproteinase
MT-MMP	Membrane-type Matrix Metalloproteinase
PAT-3	Paralysed Arrest at two-fold-3

PCA	Principle Component Analysis
PH	Pleckstrin Homology
pHH3	phospho-histone H3
PIP2	Phosphatidylinositol 4,5-bisphosphate
PIP3	phosphatidylinositol-3,4,5-triphosphate
PLK1	Polo-Like Kinase 1
PKP1	Plakophilin-1
PTB	Phosphotyrosine-Binding
qRT-PCR	Quantitative real-time PCR
RM	Revertant Mosaicism
RNA-Seq	RNA-Sequencing
SCC	Squamous Cell Carcinoma
siRNA	small Interfering RNA
SCD	Symmetrical Cell Division
TAM	Tumour-associated macrophage
TGF-β	Transforming Growth Factor-β
TPA	12-O-Tetradecanoylphorbol 13-Acetate
Vcam1	Vascular cell adhesion molecule-1
VEGF	Vascular Endothelial Growth Factor
VSA	Vascular Surface Area

list of figures and tables

Chapter	Figure / Table	Page
1	**Figure 1:** Schematic representation of the proteins affected in the 4 different types of inherited Epidermolysis Bullosa: EBS, KS, JEB and DEB.	24
1	**Figure 2:** Talin and kindlin-mediated integrin activation.	28
1	**Figure 3: The spectrum of mutations of *FERMT1*.**	28
1	**Figure 4:** Models of synergy between talin and kindlin to achieve integrin activation.	32
3	**Figure 5:** Conditional knockout of *Fermt1* gene in the epidermis of adult mice.	63
3	**Figure 6:** Loss of Kin1 in the epidermis of adult K14-Cre-Kin1$^{fl/fl}$ adult mice.	64
3	**Figure 7:** Loss of Kin1 in the epidermis of K14-Cre-Kin1$^{fl/fl}$ adult mice did not alter skin phenotype or hair growth.	66
3	**Figure 8:** Loss of Kin1 in the epidermis of K14-Cre-Kin1$^{fl/fl}$ adult mice did not alter epidermal morphology.	67
3	**Figure 9:** Short-term loss of Kin1 in the epidermis of K14-Cre-Kin1$^{fl/fl}$ adult mice significantly decreased the number of proliferating cells.	69
3	**Figure 10:** Short-term loss of Kin1 in the epidermis of K14-Cre-Kin1$^{fl/fl}$ adult mice significantly decreased the number of mitotic cells.	70
3	**Figure 11:** Short-term loss of Kin1 in the epidermis of K14-Cre-Kin1$^{fl/fl}$ adult mice significantly increased the incidence of ACD.	72
3	**Figure 12:** Short-term loss of Kin1 in the epidermis of K14-Cre-Kin1$^{fl/fl}$ adult mice significantly reduced levels of microtubule acetylation.	74
3	**Figure 13:** Short-term loss of Kin1 in the epidermis of K14-Cre-Kin1$^{fl/fl}$ adult mice did not alter the level of apoptosis.	75
4	**Figure 14:** MDA-MB-231 cells express Kin1, but not Kin2.	84
4	**Figure 15:** Expression of Histone H2B:DsRed as a chromatin marker in MDA-MB-231$^{H2B:DsRed}$ cell line.	85
4	**Figure 16:** Depletion of Kin1 in MDA-MB-231 cells.	86
4	**Figure 17:** Depletion of Kin1 in MDA-MB-231$^{H2B:DsRed}$ cells.	87

4	**Figure 18:** Morphological characterisation of si-NT and si-Kin1 treated MDA-MB-231 cells.	87
4	**Figure 19:** Assessment of mitosis in MDA-MB-231 cells from prophase to telophase with the use of live cell imaging.	88
4	**Figure 20:** Assessment of duration of mitosis in si-NT and si-Kin1 treated MDA-MB-231 cells with the use of live cell imaging.	89
4	**Figure 21:** Phenotypic analysis of spindle orientation, chromosome segregation and spindle formation in MDA-MB-231 cells	90
4	**Figure 22:**Assessment of spindle orientation, chromosome segregation and mitotic spindle formation in si-NT, si-Kin1 and si-Kin1^{+Tub} treated MDA-MB-231 cells with the use of live cell imaging.	92
4	**Figure 23:** Expression of Histone H2B:GFP as a chromatin marker and β-tubulin:DsRed as a microtubule marker in HeLa$^{H2B:GFP/\beta\text{-}tub}$ cell line.	93
4	**Figure 24:** Individual depletion of Kin1 and Kin2, and co-depletion of Kin1+Kin2 in HeLa cells.	94
4	**Figure 25:** Morphological characterisation of si-NT, si-Kin1, si-Kin2 and si-Kin1+Kin2 treated HeLa cells.	95
4	**Figure 26:** Assessment of mitosis in HeLa cells was performed from prophase to telophase with the use of live cell imaging.	96
4	**Figure 27:** Assessment of duration of mitosis in si-NT, si-Kin1, si-Kin2 and si-Kin1+Kin2 treated HeLa cells with the use of live cell imaging	97
4	**Figure 28:** Phenotypic analysis of spindle orientation, chromosome segregation and spindle formation in HeLa cells.	98
4	**Figure 29:** Assessment of mitotic spindle phenotypes in si-NT, si-Kin1, si-Kin2 and si-Kin1+Kin2 treated HeLa cells.	100
5	**Figure 30:** Development and characterisation of mouse SCC cell lines.	109
5	**Figure 31:** Development and characterisation of *in vitro* mouse SCC model: Kin1^{null}, Kin1^{wt} and Kin1^{AA} SCC cell lines.	112
5	**Figure 32:** Subcellular localisation of Kin1 and Kin2 in Kin1^{null}, Kin1^{wt} and Kin1^{AA} SCC cell lines.	114
5	**Figure 33:** *In vitro* assessment of proliferation of Kin1^{null}, Kin1^{wt} and Kin1^{AA} SCC cell lines in 2D cell culture.	116
5	**Figure 34:** *In vitro* assessment of proliferation and clonogenicity of Kin1^{null}, Kin1^{wt} and Kin1^{AA} SCC cell lines in 3D cell culture.	118
5	**Figure 35:** *In vivo* assessment of Kin1^{null}, Kin1^{wt} and Kin1^{AA} SCC tumour growth.	121

5	**Figure 36:** Morphological assessment of Kin1^{null}, Kin1^{wt} and Kin1^{AA} SCC tumours.	122
5	**Figure 37:** Analysis of nuclear length, nuclear area and nuclear density in Kin1^{null}, Kin1^{wt} and Kin1^{AA} SCC tumours.	124
5	**Figure 38:** Analysis of collagen-I deposition in Kin1^{null} and Kin1^{wt} SCC tumours.	126
5	**Figure 39:** Analysis of proliferation in Kin1^{null} and Kin1^{wt} SCC tumours.	127
5	**Figure 40:** Analysis of apoptosis in Kin1^{null} and Kin1^{wt} SCC tumours.	128
5	**Figure 41:** Analysis of VSA in Kin1^{null} and Kin1^{wt} SCC tumours.	129
5	**Figure 42:** PCA of RNA-Seq results from Kin1^{null} and Kin1^{wt} SCC tumours.	131
5	**Figure 43:** Analysis of *Fermt1* gene expression levels in Kin1^{null} and Kin1^{wt} tumours.	134
5	**Figure 44:** Analysis of Mmp3 gene expression levels in Kin1null and Kin1wt SCC tumours and Kin1null, Kin1wt and Kin1AA SCC cell lines.	137
5	**Figure 45:** Analysis of MMP3 protein expression levels in Kin1null and Kin1wt SCC tumours and in Kin1null, Kin1wt and Kin1AA SCC cell lines.	139
5	**Figure 46:** Analysis of Mmp13 gene expression levels in Kin1null and Kin1wt SCC tumours and Kin1null, Kin1wt and Kin1AA SCC cell lines.	141
5	**Figure 47:** Analysis of *Mmp15* gene expression levels in Kin1^{null} and Kin1^{wt} SCC tumours.	143
5	**Figure 48:** Analysis of *Adamts6, Adamts12* and *Adamts17* gene expression levels in Kin1^{null} and Kin1^{wt} SCC tumours.	145
5	**Figure 49:** Analysis of Hif1α gene expression levels in Kin1null and Kin1wt SCC tumours.	147
5	**Figure 50:** Analysis of *Vegfa, Flt1* and *Kdr* gene expression levels in Kin1^{null} and Kin1^{wt} SCC tumours.	149
5	**Figure 51:** Analysis of *Thbs1* gene expression levels in Kin1^{null} and Kin1^{wt} SCC tumours.	151
5	**Figure 52:** Analysis of *Cxcl1, Ccl2* and *Ccl7* gene expression levels in Kin1^{null} and Kin1^{wt} SCC tumours.	153
5	**Figure 53:** Analysis of β1 integrin activation in Kin1^{null}, Kin1^{wt} and Kin1^{AA} SCC cells.	159
5	**Figure 54:** Assessment of Kin1^{null}, Kin1^{wt} and Kin1^{AA} Met-1 tumour growth.	170

6	**Figure 55:** The role of Kin1 in skin homeostasis and the development of SCC	180
2	**Table 1:** List of primers for wild-type *Fermt1* gene and *Fermt1* gene with QW611/612AA mutation	49
2	**Table 2:** List of antibodies used for WB (western blot), IHC (Immunohistochemistry) and IF (Immunofluorescence).	55
2	**Table 3:** List of primers used for q-PCR.	59
5	**Table 4:** Analysis of RNA-Seq results from Kin1^{null} and Kin1^{wt} SCC tumours.	132
5	**Table 5:** Correlation Coefficient Interpretation Guide.	134
5	**Table 6:** Summary of the most important gene expression alterations between Kin1^{null} and Kin1^{wt} SCC tumours.	154

abstract

Kindlin-1 (Kin1) is an epithelial focal adhesion protein that plays a key role in integrin-mediated anchorage of cells to the extracellular matrix. Congenital loss of Kin1 leads to Kindler Syndrome (KS), whose symptoms include progressive epidermal atrophy, reduced keratinocyte proliferation, skin blistering and increased incidence of aggressive Squamous Cell Carcinoma (SCC). Objectives of this study were to examine the role of Kin1 in skin homeostasis and in the development of aggressive SCC in KS, as the molecular aetiologies for these pathologies are yet to be clearly understood.

We first examined whether the recently discovered role of Kin1 in mitosis contributes to reduced keratinocyte proliferation observed in KS epidermis. We discovered that short-term loss of Kin1 in adult mouse epidermis reduced keratinocyte proliferation. We also found that Kin1 loss increased mitotic spindle misorientation that, according to the model of cell division in skin homeostasis, decreases cell proliferative potential, and, thus, may account for the reduced proliferation in our model. As spindle misorientation can stem from microtubule instability, we believe that the reduction in acetylated α-tubulin (ac-tub), a known marker of stable microtubules, that we also observed in mouse epidermis following Kin1 loss could account for the defective spindle orientation phenotype.

The role of Kin1 in spindle orientation was also evident *in vitro*. Moreover, data from our lab revealed showed reduction in spindle ac-tub following Kin1 depletion, mirroring our *in vivo* observation. Additionally to orientation defects, *in vitro* depletion of Kin1 led to enhanced chromosome missegregation, which is likely to result from reduced microtubule stability due to low levels of ac-tub. We showed that role of Kin1 in spindle orientation and chromosome segregation is dependent on HDAC6, a known inhibitor of

ac-tub. Overall, our results uncover an *in vitro* and *in vivo* role of Kin1 in mitotic spindle fidelity that could be crucial to skin homeostasis, and, when disturbed, may lead to reduced keratinocyte proliferation. Interestingly, our *in vitro* studies also revealed that in mitosis Kin1 and Kindlin-2 (Kin2) had overlapping, but also distinct roles, which is in line with various reports that show different biological functions for the two protein isoforms.

Our next and final aim was to explore the roles of Kin1 in the development and progression of SCC, which would help us comprehend the reason behind the cancer's aggressive nature in KS. By employing *in vitro* and *in vivo* SCC growth assays and tumour immunohistochemical staining we found that absence of Kin1 in SCC cells and tumours enhanced proliferation and growth, and enhanced tumour vascularisation. RNA sequencing of tumour material revealed that lack of Kin1 increased expression of matrix metalloproteinases and chemokines, which have been implicated in tumour progression via promotion of angiogenesis and invasion in a plethora of studies, and of various angiogenesis markers. Together this provides an insight into the mechanisms via which Kin1 controls tumour microenvironment and, ultimately, SCC tumour growth and development.

Overall, we report an *in vitro* and *in vivo* role for Kin1 in mitotic spindle stability, which affects a variety of mitotic processes and may be linked to reduced keratinocyte proliferation observed in epidermis of KS patients, thus contributing to skin homeostasis. Moreover, we describe a role for Kin1 in regulation of SCC tumour growth and progression, which may ultimately offer an explanation for the aggressive and life-threatening nature of SCC developed in KS.

lay reader summary

Kindler Syndrome (KS) is a rare genetic disease. Most of its symptoms manifest at birth and include very thin and fragile skin (atrophy) prone to blistering, photosensitivity as well as a propensity to develop a form of skin cancer known as Squamous Cell Carcinoma (SCC). The disorder results from the lack of a protein called Kindlin-1 (Kin1) whose most studied role is enabling cells to adhere to their surroundings. Currently, there is no cure for KS, nor a comprehensive understanding of how Kin1 contributes to the maintenance of a healthy skin. We, therefore, sought to explore the cellular roles of Kin1, which will enhance our understanding on how the KS pathologies develop and can be treated. Our interest was examining the role of Kin1 in mouse epidermis cell proliferation, which is the ability of cells to multiply, as well as in the development of aggressive SCC, due to its life-threatening nature.

To study the pathology of reduced cell proliferation, which has been observed in the atrophic skin of KS patients, we deleted Kin1 from mouse epidermis and compared it to that of healthy mice. We observed that lack of Kin1 in mouse epidermis reduced the number of mouse cells that are able to multiply, which is a feature of the epidermis of KS patients. Further investigation into the process of cell division revealed that the molecular structure that captures DNA during mitosis - the mitotic spindle - had a higher chance of being unstable and abnormally formed in cells lacking Kin1. We confirmed our findings by performing live cell imaging, which allowed us to track cells during cell division and showed a variety of mitotic spindle abnormalities in cells without Kin1. Our findings therefore offer an insight into the role of Kin1 in maintaining a healthy mitotic spindle during cell division, thus indicating a potential mechanism through which skin atrophy may arise in KS.

To assess the role of Kinı in SCC, we compared the growth and morphology of mouse SCC tumours that had or lacked Kinı. We discovered that when compared to tumours that had Kinı, SCC tumours without Kinı were bigger, had a greater number of multiplying cells, and a greater number of blood vessels that are known positively influence tumour growth by transporting oxygen and nutrients. Moreover, we discovered that tumours without Kinı had higher levels of various MMPs (Matrix Metalloproteinases), which are proteins that degrade the matrix surrounding the cells (extracellular matrix) and, thus, allow cells to multiply and invade other tissues in many types of cancer. Finally, SCC tumours without Kinı revealed higher levels of various immune system molecules known as chemokines, which have also previously been shown to support tumour growth and progression via various ways, such as promoting growth of new blood vessels. Thus, our findings show that presence of Kinı is inhibitory to the expression of tumour-promoting factors, providing a mechanistic explanation for why loss of Kinı in KS leads to the development of aggressive SCC.

Overall, we offer an insight into a novel role of Kinı in ensuring that cells have normal mitotic spindles, which could, ultimately, contribute to maintenance of healthy skin, and a role of Kinı in protecting cells against growth and progression of SCC.

Chapter 1: introduction

1.1. Overview of Kindler Syndrome

Kindler Syndrome (KS) is a rare, autosomal recessive genodermatosis first described in 1954 by dermatologist Dr Theresa Kindler. Symptoms first appear in infancy and include acral blistering, which develops spontaneously or after mechanical trauma, severe epidermal atrophy, photosensitivity, hyper- or hypo- pigmentation and poikiloderma [1]–[4]. According to various case reports, some of the pathologies, such as blistering and photosensitivity, tend to subside after the first few years of age, in contrast to epidermal atrophy which is often progressive and, therefore, one of the major clinical features of the disease [5]–[7]. As a result, the skin of KS patients tears easily and presents a characteristic cigarette paper-like wrinkling [7][8].

KS patients also present a predisposition to aggressive Squamous Cell Carcinoma (SCC), with the risk of malignancy being reported to 70% for subjects older than 45 years old [9]. According to KS case studies, cancer often develops on the hand, leg and lip, and less frequently on the oral mucosa and the larynx of individuals [2][10]–[12]. The nature of SCC developed in KS patients, particularly in limbs, is extremely aggressive and metastatic, often requires amputation and lymph node excision [13][14]. Development of SCC is sometimes fatal for various KS patients [2][15], making it a main cause of morbidity and mortality in KS amongst the disease's pathologies.

Manifestations of the disease are not restricted in the epidermis. Clinical intraoral findings, such as gingivitis, gum haemorrhage, and early-onset aggressive periodontitis, have been recorded in a great number of patients [16]–[19]. Incidence of other features such as ulcerative haemorrhagic colitis, syndactyly and nail dystrophy varies between cases [1][20]–[22].

The disease is extremely rare. More than 120 cases have been reported since 1954, with the largest series being a group of 26 KS patients identified within a tribe on the Northwestern Carribean coast of Panama [6]. KS shows an autosomal pattern of transmission [4][23], but sporadic cases have also been recorded [1][6][22]. A variety of patients of consanguineous descent have been documented [7][24].

1.2. Overview of Epidermolysis Bullosa

Kindler Syndrome is part of a heterogeneous simplex of inherited genodermatoses known as Epidermolysis Bullosa (EB), which affects approximately half million people worldwide. All variants of EB are generally characterised by similar symptoms, including spontaneous or trauma-induced blistering of inherently atrophic skin, predisposition to aggressive SCC, which can be fatal, and a variety of extracutaneous manifestations including periodontitis and gastrointestinal complications [25]–[28]. Besides development of SCC, mortality for severe EB cases can often result from mucosal strictures in sites such as in the gastrointestinal tract and deleterious consequences of infections in affected skin.

As there is currently no single optimal therapy option for EB patients, treatment is mainly symptomatic and includes wound maintenance and healing, which can be aided by use of glucocorticoids, photoprotection, avoidance of physical trauma and good oral hygiene. As it will be discussed extensively in **Chapter 6**, various therapeutic avenues have been proposed, which hold potential for disease modification and cure.

According to the first classification scheme, proposed in 1962, EB was categorised in three major types, Epidermolysis Bullosa Symplex (EBS), JEB Junctional Epidermolysis Bullosa (JEB) and Dystrophic Epidermolysis Bullosa (DEB), based on the constellations of structural differences on patients' skin

[29]. Gaining a greater insight on clinical, molecular, histopathological and mutational features of EB genodermatoses led to the addition of KS as the fourth major type of EB a decade ago, as decided during the "Third International Consensus Meeting on diagnosis and classification of EB" [29].

Intriguingly, whereas, similarly to KS, JEB is inherited in a recessive fashion [30], EBS and DEB have a dominant or recessive pattern of inheritance [31][32]. Moreover, in contrast to KS, EBS, JEB and DEB are further classified into more subtypes, based on the ultrastructural site of skin findings and gene mutational analysis. For example, localised EBS affects the basal cell layer of the epidermis and presents mutations in genes that encode keratins, such as *KRT5* and *KRT14*, whereas EBS with plakophilin-1 deficiency affects desmosomes of suprabasal layer of skin, and its patients have mutations in *PKP1* (*Plakophilin-1*) and *DSP* (*Desmoplakin*) [29].

Mutational analysis has revealed that EB arises from nonsense, missense, indel or splice variant mutations that overall affect skin homeostasis. In particular, EB variants present abnormalities at the cutaneous basement membrane zone, also known as the dermoepidermal junction, which provides structural adhesion between the epidermis and the underlying dermis, preserves tissue architecture and grants skin resistance against shearing forces [33] **(Fig.1.)**.

Mutations in EBS mainly target genes that encode cytoplasmic intermediate filaments (IFs) keratin 5 and 14, forming the cytoskeletal network of basal epithelial cells [34]. EBS also affects Plakophilin-1 and Desmoplakin, required for normal assembly of desmosomes intercellular junctions that tether the aforementioned keratin IFs to the plasma membrane [35], and plectin, which links keratin IFs to transmembrane receptor integrin α6β4 at cell-Extracellular Matrix (ECM) adhesion contacts [29][36]. The genetic basis of KS is loss-of-functin mutations in *FERMT1 (Fermitin family member 1)* gene, which target an

adaptor protein known as Kindlin-1 (Kin1), a member of cell adhesion macromolecular complexes that mediate anchorage between cell cytoskeleton and ECM through interactions with β integrins [24][37]. JEB results from mutations in genes that encode protein anchors between cell and ECM, such as laminin-332, collagen XVII and integrin α6β4 [38]–[40]. Interestingly, α6β4 integrin mutations also appear in one subtype of EBS [29]. Finally, DEB mutations affect collagen VII, the major component of the anchoring fibrils at the dermoepidermal junction, providing a connection between lamina densa, a layer of the basement membrane, and the underlying dermis [32]. Detailed schematic representation of the aforementioned proteins targeted in the four major types of EB can be found at **Figure 1**.

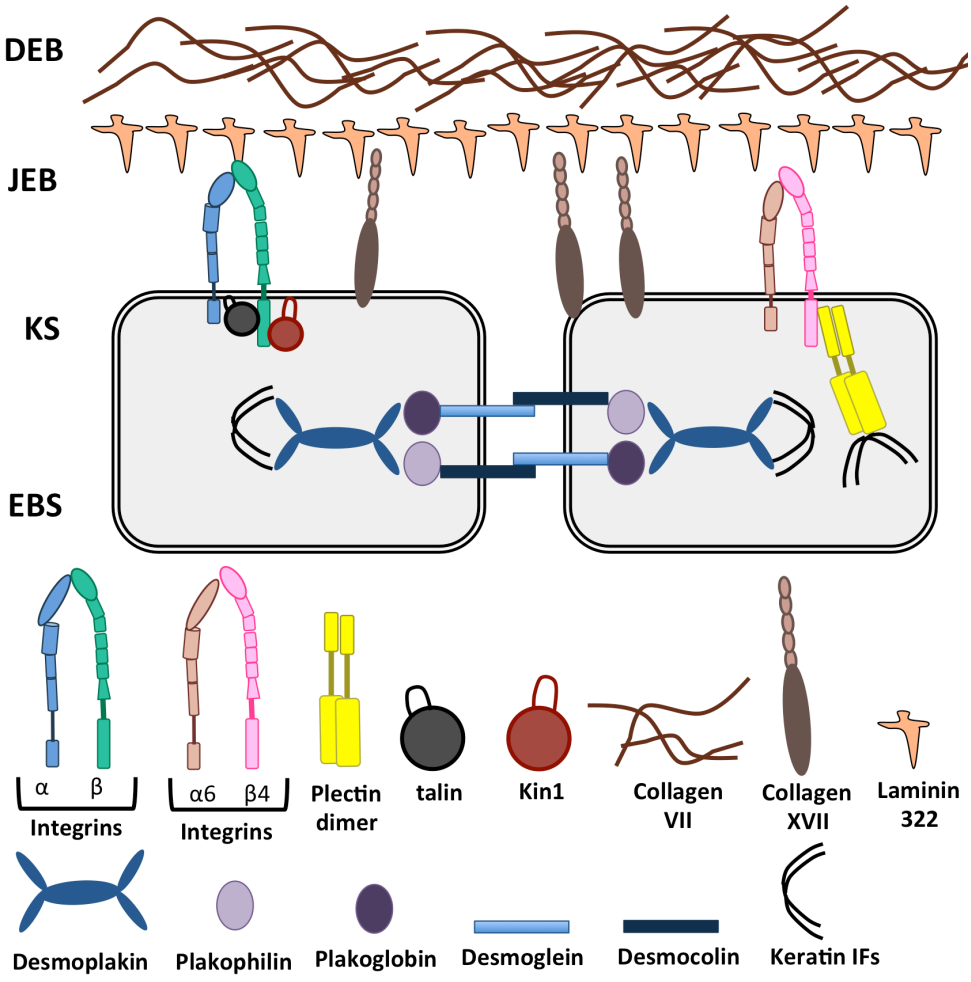

Figure 1: Schematic representation of the proteins affected in the 4 different types of inherited Epidermolysis Bullosa: EBS, KS, JEB and DEB.

1.3. Kindlins and talins in FERM adhesion

Nomenclature of *FERMT1* gene indicates that Kin1 is a FERM (Four-point-one, ezrin, radixin, moesin) domain-containing protein. FERM domain is found in various other mammalian proteins that function towards sustaining an adhesive link between cells and ECM, such as Focal Adhesion Kinase (FAK) and talin [41].

FERM domains consist of 3 globular subdomains F1, F2 an F3, which compose the domain core preceded by a less well-defined Fo subdomain. In the human genome there are approximately 50 distinct types of FERM domains, encoded by over 30 genes [42]. Aminoacid sequence similarity of FERM domain is highly conserved amongst Kin1, Kindlin-2 (Kin2) and Kindlin-3 (Kin3), which together compose kindlin protein family. FERM domain sequence of kindlins resembles FERM domain sequence of talins cell adhesion proteins that also share have functional similarities to kindlins. In particular, kindlin Fo, F1, F2 and F3 subdomains are 36-55% similar to the equivalent talin subdomains, with the highest similarity being found within F1, F2 and F3 subdomains [43].

The structure of talin-1 and talin-2, which compose the vertebrate talin protein family, contains the talin head, which is located in the N-terminus and is composed of the F1, F2 and F3 subdomains that are preceded by the Fo subdomain, and a flexible C-terminal rod [44][45] **(Fig.2.)**. Kindlins lack a C-terminal rod, but also contain Fo, F1, F2 and F3 subdomains **(Fig.2.)**.

Through their FERM subdomains, kindlins and talins can interact with the cell membrane as well as with integrins transmembrane αβ heterodimer receptors. Integrin family contains 18α and 8β subunits, which assemble into 24 distinct heterodimer combinations, and they all span the cell membrane and establish a connection between the actin cytoskeleton and ECM [46]. Talins/kindlins and integrins interactions foster conformational alterations in integrins, from

a bent and clasped inactive conformation to an extended, active integrin form with high affinity for ECM ligands [47] **(Fig.2.)**.

F3 subdomain contains a structurally conserved mechanism that allows both talins and kindlins to bind β-integrin tails and potentiate integrin activation that is critical for cell adhesion and numerous other cellular functions. In particular, the F3 subdomain of talins and kindlins harbours a Phosphotyrosine-binding (PTB) domain that potentiates interaction of talins and kindlins to NpxY membrane-proximal and NxxY membrane-distal NxxY motifs in β-integrin subunits, respectively [48]–[51]. Mutational analysis showed that disruption of NPxY and NxxY motifs inhibits binding of talins or kindlins to integrin tails and talin/kindlin-mediated integrin activation [48][49][52].

F3 subdomain of Kin1, Kin2 and Kin3 is able to bind and activate β1 and β3 integrin tails, whilst Kin1 can also bind β6 integrin, and Kin3 is also capable of β2 integrin interaction. It was also found that in Chinese Hamster Ovary (CHO) cells, W612, K610 and I651, as well as W615 are key F3 sites on Kin1 and Kin2, respectively, for binding to β1 integrin tails [49]. Similarly, the importance of Kin1 W612 site on β1 and β3 integrin activation was shown in MDA-MB-231 breast cancer cells and keratinoctes, as well as in CHO cells, respectively [53]–[55].

Integrins consist of an ectodomain embedded into the ECM, a transmembrane domain, and a tail projecting to the intracellular space. Interestingly, integrins are locked to an inactive state through a variety of interactions, including salt bridges formed between the cytoplasmic tails and transmembrane domain of integrins, and electrostatic interactions between the head and tail of integrin subunits [56][57]. It was shown that talin F3 subdomain forms salt bridge with

β integrin tail, thus disrupting the salt bridges between α and β subunits [57][58].

Integrin activation also depends on binding of kindlins and talins to the cell membrane. Namely, a patch of positively charged aminoacid residues, termed "membrane orientation patch", was identified on talin F2 subdomain, allowing talin to interact with negatively charged membrane phospholipids such as Phosphatidylinositol 4,5-bisphosphate (PIP2) [58][59]. This orientates talin to disrupt the salt bridge between the αβ heterodimeric integrin transmembrane complex, promoting integrins to adopt their extended form. Furthermore, it was found that binding of talin F2 and F3 subdomains to a membrane-embedded dimer fragment of α2β3 integrin induces integrin orientation in a fashion that dissociates the salt transmembrane contact between α and β subunits [60].

Besides enabling integrin activation, PIP2 interaction is critical for talin activation. NMR spectroscopy revealed that binding of talin rod to talin head restrains talin in a closed conformation and masks an integrin-binding region in the talin PTB domain [61]. Talin PTB domain-PIP2 interaction displaces inhibitory talin rod, thus preventing talin structural autoinhibition, and exposes the talin β-integrin binding site [61].

Talin can also bind PIP2 via a loop in its F1 subdomain, a feature shared by Kin1, and disruption of talin/kindlin F1-PIP2 bond impairs activation of integrins [62][63]. Interactions between kindlin and anionic phospholipids are also feasible through basic residues on Fo subdomain [64][43] and through a Pleckstrin Homology (PH) domain that interrupts F2 subdomain of kindlins [51][65][66], a feature not shared by talins. Fo and PH domains are key for integrin activation. This is evident by impairment of integrin activation in

CHO cells that lack Kin1 Fo subdomain [43] or have disrupted membrane binding due to mutated Kin2 Fo or PH domains [64][65].

A number of the most important domains and active sites of *FERMT1* that are subjected to mutations is displayed in **Figure 3**. The mutational range includes nonsense mutations such as S114X in Fo subdomain, where Serine 114 is replaced by a premature stop codon, thus, resulting in a truncated protein, insertions such as 1714insA in F2 subdomain, where an Alanine is inserted in position 1714, and deletions such as 1909delA in F3 subdomain, where Alanine 1909 is deleted.

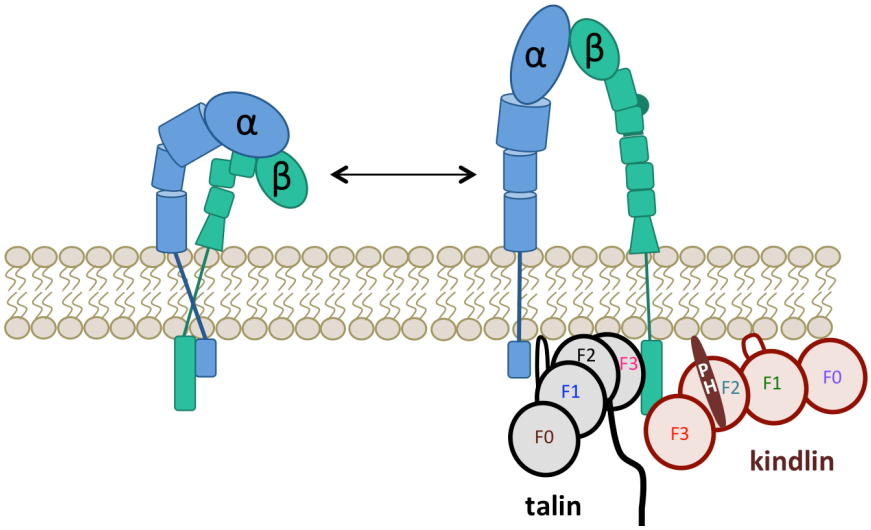

Figure 2: Talin and kindlin-mediated integrin activation. Interaction of talins and kindlins to β-integrin tails leads to conformation changes that transform the bent, inactive integrin state to an extended, active form with an increased affinity for extracellular ligands.

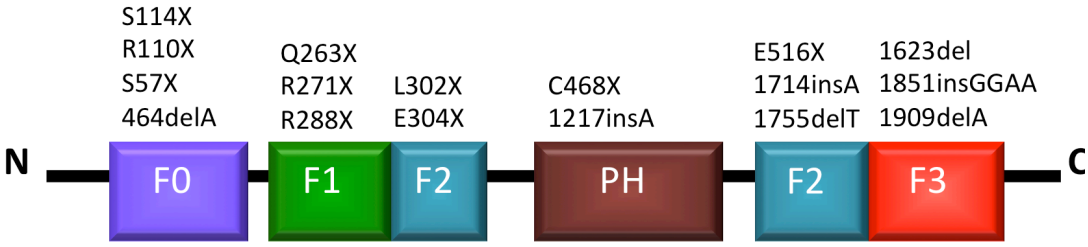

Figure 3: The spectrum of mutations of *FERMT1*. Schematic representation of *FERMT1*, which encodes Kin1 protein, and the most well-documented mutations that the various subdomains and active *FERMT1* sites are subjected to.

1.4. Kindlins and talins cooperate to induce integrin activation

The landmark discovery of talin-mediated integrin activation occurred from talin knockdown studies in CHO cells [67], prior to detecting the importance of kindlins in integrin activation. Talins are required for integrin activation, with block of talin-integrin interactions resulting in complete abolition of talin- and kindlin-mediated integrin activation [68]. Nevertheless, kindlin knockdown experiments along with expression of integrin-binding mutants implicate kindlins in integrin activation as well.

The first study to highlight the importance of kindlins in integrin function was performed in Caenorhabditis elegans (C. elegans) and published in 2000. It demonstrated that homozygous null mutations in *unc-112,* a gene encoding a membrane-linked, intracellular protein, resulted in similarly severe abnormalities to those caused by mutations in genes that encode C. elegans orthologs of β-integrin and ECM component perlecan [69]. All mutations resulted in a paralysed phenotype characterised by a defective formation of embryonic body-wall muscle [69]. UNC-112 showed colocalisation with β-integrin ortholog Paralysed Arrest at two-fold-3 (PAT-3) and was required for PAT-3's localisation in the muscle cell membrane of C. elegans [69]. In 2003 it was shown that loss-of-function mutations in KS patients mapped in *FERMT1*, a gene encoding the human homolog of *unc-112* that was named Kin1 [24][70].

However, it wasn't until 2008 that kindlins were shown to be key for integrin activation induction, when *FERMT3* null mutations reduced integrin activation in platelets, despite normal expression of talin [52]. Similarly, despite expression of normal levels of talin, overexpression and depletion of Kin2 increased and impaired β integrin activation in podocytes, respectively [71]. Additionally, as explained in **Section 1.3.**, individual disruption of kindlin Fo, F3 and PH subdomains perturbs integrin activation, despite talin expression, showing the importance of kindlins towards integrin activation.

However, kindlin depletion, or expression of integrin-binding kindlin mutants significantly reduces, but does not completely abrogate integrin activation, suggesting a synergistic effect of kindlins and talins towards maximal integrin activation. In line with this theory, whilst overexpression of Kin2 alone showed a mild effect, and expression of talin alone had a moderate effect on β3 integrin activation, co-expression of Kin2 and talin dramatically enhanced integrin activation compared to the individual effect of Kin2 or talin in CHO cells [50].

In CHO cells, Kin1 and Kin2 overexpression was surprisingly shown to inhibit activation of β3 integrins [49]. Although the molecular explanation behind this is not clear yet, it may result from the fact that kindlin overexpression uncouples potential kindlin-induced recruitment of kindlin-binding adaptor proteins that cooperate with talin towards integrin activation. Nevertheless, co-expression of Kin1 and Kin2 with talin head strongly stimulated activation of β3 integrins in CHO cells [49].

It is, thus, clear, that whereas talin is necessary for integrin activation, inability of kindlins to bind and activate integrins reduces an activation enhancement effect and prevents maximal integrin activation, which showcases the cooperation between talins and kindlins in this biological process.

1.5. Models of talin/kindlin-mediated integrin activation

Whilst synergy between talins and kindlins in integrin activation is clear, the exact nature of integrin activation remains controversial. Moreover, whereas we have a considerable understanding on how talin activates integrins, steps of kindlin-mediated integrin activation are yet to be determined. It is possible that binding of kindlin to β-integrin tail and cell membrane exposes talin-binding sites on β-integrin tail, thus, directly promoting talin-mediated

integrin activation **(Fig.4.A.)**. Nevertheless, alternative models of synergy between talin and kindlin towards integrin activation have also been proposed.

Integrin inhibitor filamin competes with talin for β-integrin binding, as both proteins were shown to occupy overlapping sites on β-integrins tails, and filamin loss stimulated integrin activation [72]. Filamin shares the same integrin-binding site as Migfilin, a kindlin-binding protein recruited at cell-ECM adhesion sites by kindlin [73]. Expression of migfilin has shown to enhance integrin activation [74][75], potentially due to the fact that migfilin-integrin binding disconnects filamin from β integrin tail, resulting in talin/integrin interaction and integrin activation [76]. Finally, kindlins and filamins also share overlapping β-integrin sites [77]. Likewise, there is overlap of integrin binding sites between kindlins and other inhibitors of integrin activation, such as Integrin Cytoplasmic domain-Associated Protein-1 (ICAP-1) [78][79]. These findings suggest that kindlins alone or through recruitment of other integrin-activating proteins, such as migfilin, could displace inhibitors of integrin activation, thus exposing talin-binding integrin domains and facilitate talin-mediated integrin activation **(Fig.4.B.)**.

It is possible that kindlins also influence integrin clustering, thus promoting integrin interaction with multiple ECM ligands rather than with a monovalent ligand **(Fig.4.C.)**. Multiplicity of integrin-binding motifs on filamin sequence could permit filamin to provoke integrin clustering, and migfilin, a protein with multiple filamin binding sites, would allow clusters of integrin to undergo activation following filamin displacement [80].

In an alternative model, it is thought that kindlin influences integrin activation events following the recruitment of talin to the integrin tail. This hypothesis developed from the observation that Kin2 depletion or overexpression did not disturb recruitment of talin to cell membrane or the

talin-β3-integrin interaction in CHO cells [81]. In agreement, binding of Kin2 to integrin did not enhance talin-β3-integrin interaction, or vice versa, and no interaction has been reported between talin and kindlin [82]. It has been shown that recruitment of talin in neutrophils was sufficient to induce low-affinity β2-integrins to change into an intermediate-affinity form, whilst synergy between talin and Kin3 was required for high-affinity integrin conformation **(Fig.4.D.)**. Finally, Kin2 was found unable to unclasp the complex formed between α and β integrin cytoplasmic tails, whereas, as mentioned in **Section 1.3.**, talin is capable of breaking the low-affinity integrin conformation [82], indicating that talin-integrin interactions may precede kindlin-integrin binding and provide the initial step towards integrin activation.

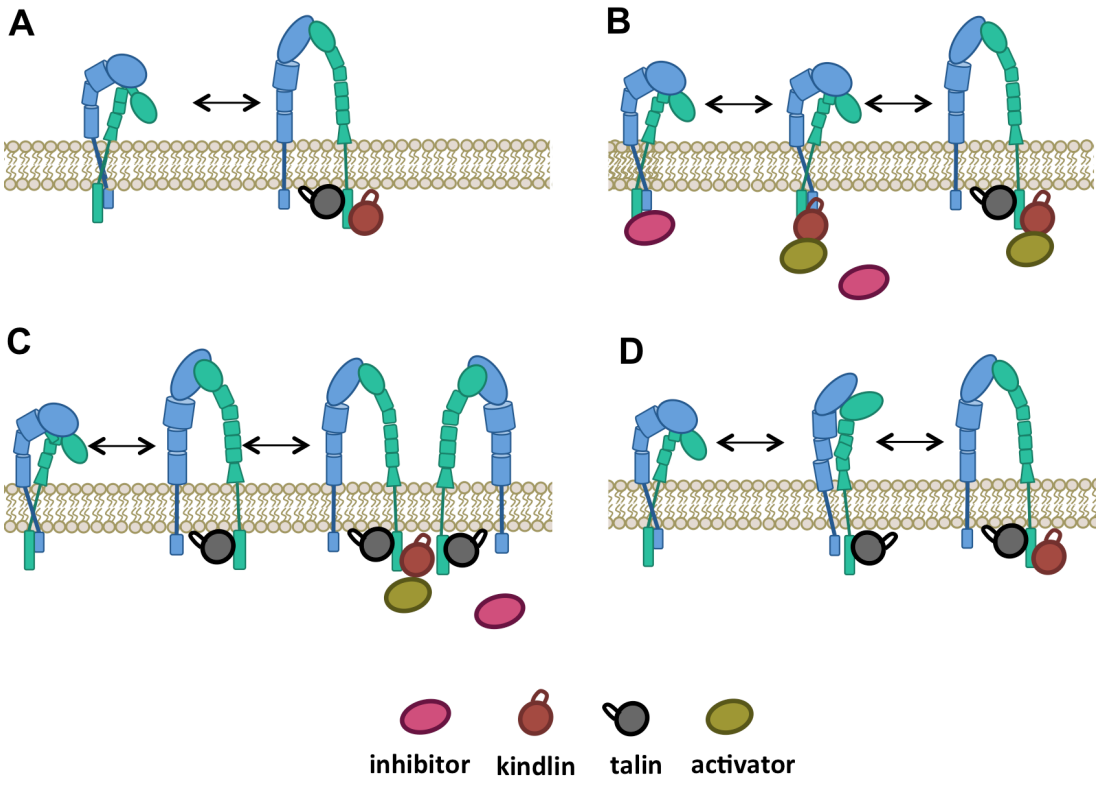

Figure 4: Models for synergy between talin and kindlin to achieve integrin activation. A: Kindlin-integrin and kindlin-membrane interactions could directly enable talin-mediated integrin activation by exposing talin-binding sites on β-integrin tail. **B:** Kindlin alone or via recruitment of other integrin-

activating proteins could displace inhibitor that occupies talin binding sites on β-integrin tail, facilitating talin binding and integrin activation. **C:** Kindlin alone or via recruitment of other integrin-activating proteins could displace inhibitors that occupy talin binding sites on multiple β-integrin tails, thus facilitating talin binding and activation of integrin clusters. **D:** Finally, kindlin could be recruited to integrin sites following initial talin-integrin binding, and alter an intermediate integrin conformation to a fully extended, high-affinity integrin conformation. (Figure adapted from [83]).

1.6. Kindlins and talins control bidirectional integrin signalling

Talin-kindlin-mediated integrin activation enhances affinity of individual integrins or small integrin clusters for ECM adhesive ligands and is known as inside-out signalling. Signal transduction is a key role of integrins, which can transmit signals bidirectionally.

Upon interaction of extracellular integrin head with ECM ligands, such as fibronectin, integrins undergo conformational changes that initiate outside-in signalling, which transduces signals to the cell's interior and regulates biological processes such as cell proliferation, spreading, survival and assembly of cell adhesion macromolecular complexes termed focal adhesions [84].

Thus, the valence of talin/kindlin-integrins binding regulates the extend of inside-out and outside-in signalling. Reciprocally, ligand-integrin head interactions may also influence inside-out signalling, as binding to ECM ligands was suggested to separate α and β integrin transmembrane and cytoplasmic domains, enhancing talin/kindlin access to β-integrin tail [85]. The necessity of integrin subunit separation for outside-in signalling was emphasised after block of dissociation of α and β transmembrnae domains led to defective cell spreading and focal adhesion formation [86].

Focal adhesion assembly is triggered by integrin clustering, an event that, as described earlier, is influenced by inside-out clustering. As principle components of inside-out signalling, kindlins and talin are also key

components of focal adhesions and can also regulate focal adhesion formation. Specifically, it was shown that talin-deleted embryonic stem cells were unable to form paxilin- or vinculin-containing focal adhesions [87], and loss of Kin2 affected the formation of talin-containing focal adhesions in immortalised keratinocytes [88]. Intriguingly, ECM ligand-integrin binding further augments clustering of activated integrins, which result in formation of focal adhesions enriched in proteins such as FAK, talin and kindlin [89][90].

1.7. Functional roles of kindlins in biological processes such as cell adhesion, spreading and migration

Kin1 and Kin2 share a 62% amino acid identity between them, and a 49-53% homology with Kin3, from which they evolutionary diverged. Kindlins have differences in tissue expression, as expression of Kin1 is epithelium-specific and expression of Kin2 is ubiquitous with the exception of haematopoietic cells in which Kin3 is mainly recorded [91]. It was shown that Kin3 is also expressed in non-haematopoietic cells, such as breast, skin and lung [92]. Nevertheless, when compared to haematopoietic cells expression of Kin3 in endothelial cells was significantly lower, and Kin2 levels were higher in endothelial cells but lower in haematopoietic cells, when compared to Kin3 [93].

As described earlier, kindlins play a key role as integrin co-activators and influence important cellular processes through control of inside-out or outside-in signalling. Specific kindlin cellular roles can be appreciated from the profound in *in vivo* and *in vitro* defects observed following kindlin depletion or mutations that impair kindlin function.

1.7.1. Cellular roles of Kin1

Besides reduced integrin activation *in vitro*, as described earlier, loss of Kin1 results in decreased β1 integrin activation *in vivo*, as observed in KS skin [37], and in intestinal epithelium of mice with genetic loss of Kin1 [54]. Intriguingly, Kin1 was also shown to regulate β1 integrin expression and trafficking in keratinocytes, as a great proportion of immortalised KS cells were unable to redistribute internalised integrins to the plasma membrane, a process that depended on Kin1 F3 subdomain [94].

Cultivated KS keratinocytes present reduced adhesion to fibronectin and laminin 322, which are well-characterised integrin ligands [8][37][94]. Perturbed adhesion is likely to aggravate skin atrophy and fragility in KS patients, as KS skin is characterised by tissue separation, either within or below the basal keratinocyte layer [8]. Severe adhesion defect was also observed in Kin1-null mouse intestine, where intestinal epithelial cells detacheded from the underlying basement membrane, triggered by reduced integrin activation [54]. This led to loss of intestinal epithelial barrier and mouse post-natal lethality, and is likely to provide a molecular explanation for ulcerative colitis in KS patients. Parallels between KS epidermis and β1 integrin mouse deficient skin, which present disorganised basement membrane and discontinuous pattern of proteins such as collagen IV and laminin 322 [8][37][95][96], suggest a functional relation between β1 integrin and Kin1 that could explain skin blistering in KS. KS keratinocytes also show abnormal cell shape, demonstrated in keratinocytes of deficient β1 integrin mouse epidermis as well, and undirected migration and polarisation [8][37][94][96]. Kin1 was also important in cell spreading, as observed in cultured KS keratinocytes and after Kin1 knockdown in HaCat immortalised keratinocytes [97][94].

Kin1 loss was also shown to impair proliferation *in vitro* and *in vivo* [8], as well as reduce stem cell markers in KS skin and lower the colony-forming ability of

KS keratinocytes *in vitro* [37], highlighting a role for Kin1 in these processes. Complementing these findings is the observation of early stem cell marker depletion and precocious senescence in primary cultured KS keratinocytes in contrast to healthy counterparts [98]. Induction of premature senescence in keratinocytes in the absence of Kin1 could be a potential cause for KS skin atrophy.

Finally, a novel role for Kin1 in mitosis was discovered a few years ago *in vitro*. Kin1 localisation was observed in centrosomes of mitotic cells where it was shown to be phosphorylated by Plk-1 (polo-like kinase-1), a function required for correct mitotic spindle formation and orientation [53].

1.7.2. Cellular roles of Kin2 and Kin3

Similarly to Kin1, Kin2 and Kin3 play a pivotal role in integrin activation *in vivo*, but since kindlins are expressed in distinct tissues, their loss leads to different phenotypes.

Disruption of *Fermt2* gene during mouse embryonic development results in peri-implantation lethality due to diminished integrin activation and detachment of epiblast and endoderm from embryonic basement membrane [99]. On the other hand, human subjects with Kin3 mutations leading to protein loss suffer from LAD-III (type III Leukocyte Adhesion Deficiency), a haematopoietic disorder with symptoms of severe bleeding tendency and recurrent infections [100][101]. Symptoms are derived from inability of leukocytes and platelets to adhere and aggregate, respectively, and from compromised activation of β1, β2 and β3 integrins, as observed by studies on cells isolated from LAD-III patients. Mice that lack Kin3 expression died within a week of birth due to severe haemorrhages in gastrointestinal tract, brain, bladder and skin that derived from platelet adherence dysfunction and lower β3 integrin activation [52].

Besides integrin activation, Kin2 and Kin3 play a role in integrin trafficking, which is in line with the role of Kin1 in this process [52][102][103]. Intriguingly, *in vitro* Kin2 loss not only reduced surface expression of β1 integrins, but also resulted in β1 integrin accumulation in lysosomes and enhanced β1 integrin degradation [102].

Finally, Kin2 and Kin3 also play a role in Kin1-regulated cell features such as spreading, cell migration and proliferation. Due to its ubiquitous expression, Kin2 regulates these processes in a variety of cell types. For example, Kin2 demonstrated a role in cell spreading in mouse embryonic stem cells and mouse osteoblasts, and in migration in vascular smooth muscle cells [99][104][105]. Moreover, Kin2-null mice showed reduced chondrocyte proliferation, and Kin2 depletion decreased mouse osteoblast proliferation *in vitro*, highlighting the role of Kin2 in proliferation [104][106]. In a similar manner, Kin3 controls cell spreading in haematopoietic cells, such as platelets and neutrophils, is required to retain proliferation of haematopoietic stem cells, and demonstrates a role in regulation of cell migration in leukocytes isolated from LAD-III patients [52][101][107][108].

1.7.3. Overlapping and distinct cellular roles of Kin1 and Kin2

Due to similarities in various Kin1 and Kin2 functions, and expression of Kin1 and Kin2 in epithelial cells, studies have scrutinised whether the two proteins also share overlapping functions in tissues where they are co-expressed, and if they can compensate for each other's loss. Kin1 and Kin2 show functional redundancy in cell adhesion, survival and β_1 integrin activation [88][94]. Nonetheless, presence of endogenous Kin2 is unable to compensate the loss of Kin1 in KS and mouse models of Kin1 loss, suggesting that distinct functions may exist between the two protein isoforms.

Indeed, whereas cell-cell contacts and talin-containing focal adhesions in Kin1-depleted keratinocytes resembled the ones formed by control cells to a great extend, they were severely malformed in Kin2-depleted cells [88]. Likewise, migration of keratinocytes was particularly impacted by lack of Kin2 compared to Kin1, highlighting important distinct functions between the two protein isoforms [88]. Additionally, despite its normal expression and effective focal adhesion localisation, Kin1 was unable to rescue impaired keratinocyte spreading in Kin2-depleted keratinocytes, further emphasising functional differences between Kin1 and Kin2 [109]. Interestingly, Kin2, but not Kin1, showed localisation at cell-cell contacts *in vitro* and *in vivo*, indicating that differential subcellular compartment localisation of the two proteins, and could justify why Kin1 and Kin2 cannot compensate for each other's loss *in vitro* or *in vivo* [54][91] .

1.8. Kindlins in cancer

1.8.1. Roles of kindlins in tumour promotion

Kindlin overexpression has been reported in a variety of primary tumours and cancer cell lines. Particularly, enhanced expression levels of Kin1 were found in lung, colon and hepatocellular carcinoma as well as pancreatic cancer cell lines [110]–[112], of Kin2 in malignant mesothelioma cell lines [113], and of Kin3 in breast cancer [114].

A plethora of studies has implicated kindlins in cancer progression via the employment of various signalling pathways. Kin1 expression showed positive correlation with breast cancer lung metastasis, and orthotopic injection of Kin1-depleted breast cancer cells reduced tumour growth and inhibited breast cancer-lung metastasis [115]. *In vitro*, Kin1 overexpression in poorly metastatic breast cancer cell line enhanced proliferation and migration, and induced transforming growth factor-β (TGF-β) dependent epithelial to mesenchymal

transition (EMT) [115]. Notably, Kin1 expression levels are also higher in other types of epithelial tumours that spread to the lungs such as colon and bladder, compared to cancers that do not show lung metastasis such as ovarian and prostate [115]. Moreover, Kin1 expression correlated positively with metastatic status and tumour size and aggressiveness in hepatocellular carcinoma, and inhibition of Kin1 supressed pancreatic cancer cell migration and invasion although no underlying molecular mechanism has been proposed for these observations [111][112].

Concurrent enhanced expression of Kin2 and ILK at the invasion front of malignant mesothelioma tumours suggested a putative link between the two proteins in tumour progression, although this is yet to be examined [113]. Interestingly, *in vitro* expression of ILK in malignant mesothelioma rescued impaired cell migration caused by Kin2 depletion, which strengthened the hypothesis for potential association between Kin2 and ILK in tumour progression [113]. Furthermore, Kin2 promoted breast cancer cell invasion *in vitro* and tumour growth *in vivo*, which was achieved via epigenetic repression of micro RNA miR-200b [116]. In particular Kin2 formed a complex with DNA methyltransferase 3A, which occupied miR-200b promoter and induced CpG island hypermethylation of miR-200b [116]. An alternative mechanism for Kin2-induced tumour progression in breast cancer has also been proposed, as Kin2 was shown to interact with EGFR, and stabilise EGFR expression by inhibiting its degradation, ultimately promoting EGF-induced breast cancer cell migration [117]. Finally, Kin2 demonstrated a pivotal role in prostate angiogenesis and normal vessel formation and maturation *in vivo*, which, in turn, regulated tumour growth and was dependent on Kin2-mediated β3 integrin activation [118].

Kin3 also demonstrated a role in tumour progression via regulation of angiogenesis. *In vivo*, expression of Kin3 was significantly higher in breast

tumours compared to normal tissue, and breast tumours with higher levels of Kin3 had increased vascularisation and lung metastasis [114]. Mechanistically, Kin3 overexpression in breast cancer cells was accompanied by enhanced β1 integrin activation and increased production of Twist, a tumour angiogenesis-promoting transcription factor, and vascular endothelial growth factor (VEGF) [114]. It was established that Kin3 maintains a crosstalk between β1 integrins and Twist to promote VEGF production and enhance tumour angiogenesis, which is likely to contribute to the metastasis observed in this model.

1.8.2. Roles of kindlins in tumour suppression

Nonetheless, kindlin expression was also demonstrated to hinder tumour progression, and tumour-suppressor mechanisms for kindlins have been identified over the years.

As aforementioned in **Section 1.1.**, one of the main pathologies of KS is the predisposition to aggressive SCC that often results in patient mortality. A single study has addressed the mechanism for SCC predisposition, by concluding that Kin1 sustains an equilibrium between Wnt tumour-promoting signals and TGF-β tumour-supressing signals, which is disturbed following loss of Kin1, resulting in cutaneous stem cell hyperactivation and enhanced growth of skin tumours [119]. Despite the pathology's severity, the molecular reason underlying aggressiveness of SCC developed KS is yet to be addressed.

Expression of Kin1 in non-small-cell lung cancer was also shown to inhibit *in vitro* cell migration and *in vivo* tumour growth via inhibition of EMT [120]. Notably, Kin1 and Kin2 presented counteracting functional roles in this model, as Kin2 expression in non-small-cell lung cancer promoted EMT, cell migration and tumour growth. In sharp contrast, Kin2 expression was reduced in serous epithelial ovarian cancer where Kin2 induced mesenchymal-to-epithelial transition and inhibited cell peritoneal dissemination, a process that

can normally lead to metastasis [121]. Clinically, low Kin2 levels showed positive correlation with tumour grade and longer survival [121].

Finally, Kin3 expression in melanoma, lung and breast cancer was significantly reduced when compared to normal tissue, which, as suggested, was achieved by the significantly higher levels of *FERMT3* promoter hypermethylation found in tumours samples [92]. Kin3 downregulation enhanced lung metastasis in melanoma and breast cancer cell lines, led to *in vitro* impairment of talin-integrin interaction and reduction of β3 integrin activation, and promoted internalisation of active β3 integrins [92]. Consequences of impaired integrin function after Kin3 depletion decreased cell adhesion and enhanced cell invasion, which can justify *in vivo* enhancement of metastasis [92].

1.9. project aims

Skin atrophy, which has been linked to reduced keratinocyte proliferation in KS epidermis, and development of aggressive SCC are two of the most prominent pathologies of KS. In particular, the progressive nature of epidermal atrophy leads to a lifetime of cutaneous fragility that, in turn, causes skin tears, wounds and bleeding, whilst the aggressive behaviour of SCC increases morbidity and risk of fatality in KS patients. As molecular mechanisms that underline reduced keratinocyte proliferation, which could contribute to skin atrophy, and development of SCC in KS are undefined, this thesis has focused in establishing a role of Kin1 in skin homeostasis and development of SCC.

The aims of this study were:

1. Develop and characterise the epidermis of a mouse model of Kin1 loss.
2. Use mouse model of Kin1 loss in order to explore the recently discovered role of Kin1 in mitosis, in the context of skin homeostasis.

3. Use live cell imaging and characterise in detail the role of Kin1 and Kin2 in mitosis in epithelial cells.

4. Examine if Kin1 and Kin2 have overlapping or distinct functions in mitosis in epithelial cells.

5. Generate and characterise growth kinetics of mouse SCC cell lines that lack Kin1, express Kin1 or express integrin-binding mutant of Kin1.

6. Generate mouse SCC tumours that lack Kin1 or express Kin1.

7. Explore roles of Kin1 in SCC tumour development and progression.

Chapter 2: materials and methods

2.1. Cell culture

2.1.1. Cell line maintenance

Unless stated otherwise, all cell lines were cultured in DMEM (Dulbecco's modified eagle's medium) (Invitrogen) with 10% FBS (Fetal Bovine Serum) (Invitrogen), supplemented with 2mM L-glutamine (Gibco), and incubated at 37°C and 5% CO2. Cell lines were routinely tested for mycoplasma and were negative. Routine subculture was performed twice a week when cells reached 70-80% confluency.

2.1.2. Generation of MDA-MB-231$^{H2B:DsRed}$ cell line

MDA-MB-231 cells (American Type Culture Collection) were transfected using 1µg of Histone H2B:DsRed plasmid DNA and Lipofectamine RNAiMAX (Invitrogen) according to manufacturer's instructions. The plasmid used was based on pcDNA2.1 backbone and was kindly given to us by Dr Viji Draviam. Prior to transfection, One Shot TOP10 chemically competent bacteria (ThermoFischer Scientific) were transformed using heat-shock protocol and selected with Ampicillin, and plasmid isolation was performed with Miniprep kit.

Transfected cells were subsequently incubated for 72 hours in DMEM+10% FBS, at 37°C and 5% CO2. Subsequently, $5x10^7$ cells at concentration of $1x10^7$ cells/ml were subjected to fluorescence-activated cell sorting (FACS) with the use of 594nm laser for DsRed excitation. Resulting MDA-MB-231$^{H2B:DsRed}$ cells were maintained in DMEM+10% FBS supplemented with 1:100 ampicillin (ThermoFischer Scientific), in order to sustain selection of H2B:DsRed-expressing cells, at 37°C and 5% CO2.

HeLa$^{H2B:GFP/\beta\text{-}tub:DsRed}$ cells, which were kindly given to us by Dr Viji Draviam, were maintained in DMEM+10% FBS supplemented with 1:100 geneticin (G-418) (ThermoFischer Scientific), in order to sustain selection of H2B:DsRed-expressing cells, at 37°C and 5% CO2.

2.1.3. RNA interference, live cell imaging and cell viability assay

2.1.3.1. RNA interference in MDA-MB-231 and HeLa cell lines

Small interfering RNA (siRNA) treatments in MDA-MB-231$^{H2B:DsRed}$ and HeLa$^{H2B:GFP/\beta\text{-}tub:DsRed}$ cells were performed with the use of Lipofectamine RNAiMAX (Life Technologies), according to manufacturer's instructions. All siRNA oligos were purchased from Dharmacon RNAi Technologies and were used at a final concentration of 60nM for MDA-MB-231$^{H2B:DsRed}$ cells and 90nM for HeLa$^{H2B:GFP/\beta\text{-}tub:DsRed}$ cells. For Kin1+Kin2 co-depletion in HeLa$^{H2B:GFP/\beta\text{-}tub:DsRed}$ cells, combination of Kin1^{UTR1}, Kin1^{UTR2}, Kin2^{ORF1} and Kin2^{ORF2}. siRNA oligos were used at a final concentration of 90nM. Media was changed 24 hours post-transfection, with the addition of fresh DMEM+10%FBS. Duration of siRNA treatment lasted 48 hours for MDA-MB-231$^{H2B:DsRed}$ cells and 72 hours for HeLa$^{H2B:GFP/\beta\text{-}tub:DsRed}$ cells, after which cells were either lysed or used for live cell imaging. siRNA was performed in dishes if cells were destined for lysis, and in chambered glass coverslips (Cover glass Lab-tek Chambers, FISHER) covered with collagen I diluted in acetic acid (3.33µl/ml) if cells were destined for live cell imaging.

2.1.3.2. Live cell imaging of MDA-MB-231 and HeLa cell lines

Prior to live cell imaging, cell media was replaced with Leibovitz's L-15 Medium (ThermoFischer Scientific), which supports cell growth in environments that lack CO equilibrium. Cells were imaged at 37°C. Images were captured every 10 minutes for a total of 8 hours with a 40x0.85 NA Plan-Apochromat objective lens (CarlZeiss UK, Cambridge, UK) on a Zeiss Axio-

Observer Z1 inverted microscope equipped with a Lumencor Spectra XLED light source (Lumencor Inc, Beaverton, OR) and a Photometrics Coolsmap HQ2 CCD camera (Photometrics, Tucson, AZ). Exposures of 0.1 seconds were applied for GFP channel and of 0.3 seconds for RFP channel. Every image was captured on five Z planes separated by 1μm. Mitosis images were combined in an 8 hour-long video automatically by Micro-Manager software [122] and phenotype assessment and quantification was performed manually, in a blind fashion.

2.1.3.3. Alamar blue cell viability assay in HeLa cell lines

72 hours following siRNA treatment, alamar blue assay was used to assess cell viability in HeLa cells. To achieve this, cell culture media was removed and was implemented with 10% alamar blue (Thermo Fisher Scientific), and cells were incubated with the mix for 3h at 37°C. Fluorescence was then measured as indicator of cellular activity at 590nm emission wavelength. The assays were performed in 96-well plates, 48h post-siRNA treatments in triplicates.

2.1.4. Incucyte cell count proliferation assay

We used Incucyte real-time live-cell analysis system (Essen Instruments, Ann Arbor, MI, USA) to assess cell proliferation in two-dimensional cell culture conditions, according to manufacturer's instructions. Cells were seeded at a density of 1500 cells/well in 96 well plates, and were immediately transferred in Incucyte system, which was kept within a 37°C+5% CO2 incubator. Phase-contrast images were captured directly after plates were placed within Incucyte, which determined the exact cell density at 0 hours, and every 3 hours after that. Images were, eventually, combined by Incucyte to form time-lapse microscopy movies. Cell density quantification of every phase-contrast image was performed automatically by Incucyte control software.

2.1.5. Methylcellulose-over-agarose proliferation assay

We used methylcellulose-over-agarose assay to assess cell proliferation in three-dimensional cell culture conditions. For this assay, we transformed cell culture plastic dishes into low-adherent dishes by plating a combination of 1.8% UltraPure agarose (Invitrogen) and DMEM+10%FBS to a 1:1 ratio, and subsequently stored at 4°C overnight. On the day of the experiment, desired amount of cells were counted, pelleted and resuspended in DMEM+20%FBS. Resuspended cells were then passed through a single cell filter (Stem Cell Technologies) to ensure single-cell suspension, and cells were added to 3% methylcellulose (StemCell) to a 1:1 ratio. Cells were subsequently plated on the pre-prepared agarose dishes, and immediately phase contrast images were captured. For every cell line there were 3 repeats of methylcellulose-over-agarose dishes, and for every plate 5 low-power field images were captured. Phase contrast images were captured on Day0, Day1, Day3 and Day6 and were used to manually determine the area of every spheroid formed with the use of ImageJ software.

2.2. Animal models and cell culture

2.2.1. Generation of mouse model of Kin1 loss

Kin1 loss in adult mouse epidermis was performed as illustrated in **Figure 6**. Kin1$^{fl/fl}$ transgenic mice, in which exons 4 and 5 of *FERMT1* gene were floxed by loxP sites, was crossed with a K14-Cre-ER^{T2} (K14-Cre) mouse [123] to generate K14-Cre-ER^{T2}-Kin1$^{fl/fl}$ (K14-Cre-Kin1$^{fl/fl}$) conditional knockout mouse line. Cre-ER^{T2} represents the fusion between mouse epidermis Cre-recombinase and estrogen receptor (ER), and was expressed under the control of K14 (keratin 14) promoter [124]. Adult (28-day old) K14-Cre-Kin1$^{fl/fl}$ and K14-Cre mice, were subjected to daily subcutaneous injections of 100μg 4OHT (4-hydroxytamoxifen) (Sigma-Aldrich), resulting in the translocation of cytoplasmic Cre-ER^{T2} to the nucleus [123][124]. In K14-Cre-Kin1$^{fl/fl}$ mice this

resulted in Cre recombination at loxP sites [125], deletion of exons 4 and 5 and knockout of *Fermt1*. Duration of 4OHT treatment lasted 5 days. From the end of the 4OHT treatment until mouse scarification, animals were checked and weighed regularly.

Mice were sacrificed using cervical dislocation, and tails and dorsal skin were collected 5 days, 10 days or 1 year following the end of the 4OHT treatment. Dorsal skin was fixed overnight in neutral-buffered 10% formaldehyde (Surgipath Europe) for later immunohistochemical analysis. Dorsal skin of mice that were kept for 1 year after the termination of 4OHT treatment was shaved 8 months following the end of 4OHT treatment and, subsequently photographed on a regular basis to monitor hair growth and overall skin appearance.

All mice were bred and maintained on an FVB genetic background. Animal husbandry and breeding were carried out by the staff of the Institute of Genetics and Molecular Medicine, University of Edinburgh. Genotyping was performed by Transnetyx with the use of ear notch tissue from at least 14-day old mice. All animal experiments **(Sections 2.2.1., 2.2.3. and 2.4.)** were carried out in compliance with UK Home Office guidelines and with the help of Morwenna Muir.

2.2.2. Isolation of mouse primary keratinocytes

Following mouse sacrifice, skin was removed from tails of mice and was incubated in 4mg/ml dispase (Gibco) diluted in PBS for 3 hours at 37°C. Subsequently, tail epidermis was separated from dermis and dissected into minor pieces that were then incubated in trypsin diluted in PBS-EDTA for 10 minutes at 37°C. To aid cell disaggregation, solution was subjected to brief vortex. Addition of DMEM supplemented with 20% FBS (Invitrogen) neutralised trypsin, and the solution was sieved through a 70μm cell strainer

(Becton Dickinson). Centrifugation collected cells into a pellet that was washed with PBS, and this was repeated two times. Cells were then plated on tissue culture dishes (Greiner bio-one) coated with collagen I diluted in acetic acid (3.33µl/ml) and maintained in keratinocyte basal medium supplemented with SingleQuotes kit (Clonetics) in 37°C and 5% CO_2. Tail keratinocytes were incubated for 4 days, after which they were collected for generation of cell lysate.

2.2.3. Generation of mouse SCC tumour cell lines: 117 SCC cells, 130 SCC cells and 145 SCC cells

Two-stage chemical carcinogenesis protocol [126][127] had been previously applied by Dr Hitesh Patel, as follows, to generate mouse SCC tumours in K14-Cre-Kin1$^{fl/fl}$ mice, as depicted in **Figure 30**. A single application of 7,12-dimethylbenz[a]anthracene (DMBA) was followed by repeated applications of phorbol ester 12-O-tetradecanoylphorbol 13-acetate (TPA). This led to the formation of benign cutaneous papillomas, some of which progressed to form cutaneous SCC tumours in 3 different mice (mouse no.117, no.130 and no.145). Mouse SCC tumours were then removed, dissected into minor pieces and incubated in trypsin diluted in PBS-EDTA for 10 minutes at room temperature. Trypsin was neutralised with addition of DMEM+10%FBS. Cells were subsequently plated and allowed to grow in DMEM+10% FBS supplemented with 100 units penicillin and streptomycin per ml (Sigma-Aldrich) in 37°C and 5% CO_2.

2.3. Cloning, cell infections and generation of Kin1^{null}, Kin1^{wt} and Kin1^{AA} mouse SCC cell lines

This protocol had been previously performed by Dr Hitesh Patel to generate Kin1^{null}, Kin1^{wt} and Kin1^{AA} mouse SCC cell lines. RNA was extracted from mouse mammary mammary epithelial cells with RNeasy kit (Qiagen) according to manufacturer's instructions. SuperScript II Reverse Transcriptase

and random hexameres (SuperScript First-Strand cDNA synthesis kit, Invitrogen) catalysed the conversion of RNA to cDNA. Following DNA synthesis, coding sequence for wild-type and QW611/612AA mutant *Fermt1* (primer sequences at **Table 1**) were amplified by PCR using the PfuUltra Hotstart PCR master mix (Agilent Technologies) and run on a 1% agarose gel. DNA was isolated from the corresponding gel bands with the QIAquick gel extraction kit (Qiagen), and cloned into pWZL-Hygro retroviral vectors with the use of a standard DNA ligation kit protocol (Roche), according to manufacturer's instructions. One Shot TOP10 chemically competent bacteria (ThermoFischer Scientific) were then transformed using heat-shock protocol and selected with Hygromycin (Calbiochem) antibiotic, and plasmid isolation was performed with Maxiprep kit (Qiagen).

Finally, pEco packaging retrovirus producing cells were transfected with 5μgr of pWZL plasmids of Lipofectamine 2000 (Invitrogen) according to manufacturer's instructions. Supernatant containing the produced retroviruses was subsequently collected, filtered through 0.45μm filters (Millipore) and implemented with 10% FBS and 1:1000 polybrene (Millipore). Finally, $Kin1^{null}$ mouse SCC clonal cell line was infected with the retrovirus-contaning supernatant under 1:100 Hygromycin selection (Calbiochem).

Target gene name	Primer	Sequence 5'→3'
Fermt1	forward	*cgccaatatgaagcagtgg*
	reverse	*gtcaaactcgattgccacct*
Fermt1 WQ611/612AA	forward	*ccagttgacattcgccgccttcatattg*
	reverse	*ccagttgacattcgccgccttcatattg*

Table 1: List of primers for wild-type *Fermt1* gene and *Fermt1* gene with QW611/612AA mutation

2.4. Development of Kin1^{null}, Kin1^{wt} and Kin1^{AA} SCC tumours

Kin1^{null}, Kin1^{wt} and Kin1^{AA} mouse SCC cells were grown in T150 culture flasks to a confluency of 80% before being harvested. Following cell counting, the appropriate amount of cells was pelleted, washed in PBS and resuspended in Hank's balanced salt solution (Gibco) to final concentrations of $0.25x10^6$ or $0.50x10^6$ or $1.00x10^6$ cells/ml. Cell suspension was passed through a single cell filter (Stem Cell Technologies) to ensure single-cell suspension.

5-week old female athymic mice received bilateral subcutaneous injections of 100µl of Kin1^{null}, Kin1^{wt} or Kin1^{AA} mouse SCC cells. Animals were monitored for signs of growth, and tumour growth was measured twice a week with the use of a calliper by recording the longest and shorter tumour dimensions. First measurements were performed 3 days after tumour cell implantation. Animals were all culled by cervical dislocation once the first ulcerated tumours began to appear in the study or if tumours reached their maximum permitted size.

On cull, tumours were removed and fixed overnight in neutral-buffered 10% formaldehyde 10% (Surgipath Europe) for later immunohistochemical analysis, and half were snap frozen in liquid N_2 and stored at -80^{o}C for later RNA extraction.

2.5. Immunoblotting, Immunohistochemistry and Immunofluorescence

2.5.1. Cell lysis, protein quantification and Immunoblotting

Cells to be analysed by western blotting were cultured until reaching the desired confluency and placed on ice. Following removal of cell media, ice-cold PBS was used to wash any residual media. Cell lysis was performed by adding cold RIPA cell lysis buffer (10 mM Tris-HCl pH 8.0 (Sigma-Aldirch), 140mM NaCl (Sigma-Aldrich), 1 mM EDTA (Sigma-Aldirch), 0.5% sodium

deoxycholate (Thermo Fisher Scientific), 0.1% SDS (Sigma-Aldrich) and 1% Triton X100 (Sigma-Aldrich)) supplemented with 1 proteinase inhibitor (complete ULTRA tablet, Roche) and 1 phosphatase inhibitors (phosSTOP tablet, Roche), for 15 minutes on ice. Cells were collected in an Eppendorf, and cell lysis was completed by high-speed centrifugation at 13200rpm for 15min at 4°C.

Protein concentration was then defined using a Micro BCA protein assay kit (Thermo Scientific) according to manufacturer's instructions. Quantification of protein concentration was defined by measuring solution absorbance using a plate reader set at 570nm. Unless otherwise stated, 15µg of cell lysate were used for gel electrophoresis by combining with 6x Laemmli sample buffer (292.5mM Tris pH6.8 with HCL (Sigma-Aldrich), 9.36% SDS (Sigma-Aldrich), 0.027% bromophenol blue (BioRad), glycerol (ThermoFisher Scientific), 0.027% bromophenol blue (BioRad) and 10% β-mercaptoethanol (Sigma-Aldrich) and 10% β-mercaptoethanol (Sigma-Aldrich)), and incubating for 10 minutes at 95°C. Protein separation was achieved with SDS-PAGE on 4-15% mini protean TGX stain-free precast gels (Biorad Life Science), facilitated by addition of running buffer (10x Tris-Glycine-SDS running buffer in distilled water). Gels were run at 180V for 40 minutes. 5µl of precision plus protein dual colour standard marker (Biorad) was used, which enabled identification of the desired band. Gels were then transferred on a nitrocellulose trans-blot turbo nitrocellulose transfer packs (BioRad) using the trans-blot turbo transfer system (Biorad), and incubated in 5% bovine serum albumin (BSA) (Calbiochem) diluted in TBST (0.15% Tween-20 (Thermo Fisher Scientific)) (5% TBST-BSA) for 1 hour at room whilst being constantly agitated.

Blots were incubated with primary antibody of interest in 5% TBST-BSA overnight at 4°C whilst being constantly agitated. Following, blots were washed three times in TBST and incubated with the appropriate secondary

antibodies for 1 hour at room temperature, before being washed further 3 times and visualised. Visualisation with LI-COR Odyssey infrared imaging system required use of 680 and 800 IRDye fluorescent secondary antibodies (Li-COR) at concentrations recommended by the manufacturer. HRP anti-mouse and anti-rabbit antibodies were used for blot visualisation with enhanced chemiluminescence detection at the Biorad Chemi Doc MP imaging system.

List of primary antibodies used can be found on **Table 2**.

2.5.2. Immunohistochemistry

Formaldehyde-fixed dorsal skin and tumour specimens were embedded in paraffin and cut into 5µm sections for hematoxylin and eosin (H&E) staining, performed by the University of Edinburgh Histology Service, or antibody staining performed as follows.

Paraffin sections were dewaxed with 2 x 5 minute washes of xylene (Fischer Scientific), followed by rehydration with 5 minute washes in decreasing concentrations of ethanol (100%, 100%, 80% and 50%). Sections were then rinsed with water and were subjected to antigen retrieval by microwaving sections under pressure for 10 minutes in 10mM pre-heated sodium citrate buffer (pH 6.0) (Fisher Scientific). Once cool, sections were briefly washed in tap water and twice with 0.0025% Tween20 (Thermo Fisher Scientific) in TBS, and outlined with an ImmEdge Hydrophobic barrier pen (Vector laboratories). Subsequently, sections were incubated with peroxidase block (DAKO) for 15 minutes at room temperature, which was then removed and sections were washed briefly with water. Sections were then incubated with serum free protein block (DAKO) for 1 hour at room temperature.

Primary antibody, which was diluted in antibody diluent buffer, was then

added to sections, followed by an overnight incubation at 4°C. A negative control was included in all experiments, which consistent of a tissue section incubated with serum free protein block (DAKO) overnight. Following day, sections were washed 2 times in 0.0025% Tween20 in TBS and incubated with mouse or rabbit Envision (DAKO) secondary antibody for 45 minutes at room temperature. Sections were then washed 3 times with TBS and treated with DAB/DAB chromogen (DAKO) for 10 minutes at room temperature, rinsed briefly with water, and counterstained for 2 minutes in haematoxylin (Pioneer Research Chemicals). Following, sections were briefly washed with water, treated for 2 minutes at room temperature with Scott's tap water solution (0.35% sodium bicarbonate (Sigma-Aldrich) and 2% magnesium sulphate (Sigma-Aldrich) in distilled water) and briefly washed with water again. Finally, sections were dehydrated in a series of solutions of increasing ethanol concentrations (50%, 80% 100% and 100%), with 5 minute wash in each solution. Finally, sections were washed twice for 5 minute in xylene before being mounted DPX mounting medium (Fisher).

Sections were scanned using NanoZoomer-XR Digital slide scanner (Hamamatsu) and visualised using NDP view2 Viewing software (Hamamatsu), or visualised using BX-51 microscope (Olympus) and images were captured using Cell^{R} software. Image analysis was performed blind, as specified in each figure legend, either manually, with the use of ImageJ software, or with the use of ImmunoRatio plugin of ImageJ software [128]. Analysis and interpretation of histological staining in Kin1^{null}, Kin1^{wt} and Kin1^{AA} tumours was carried out with assistance of pathologist Dr Mark Arends.

List of primary antibodies used can be found on **Table 2**.

2.5.3. Immunofluorescence

For tissue immunofluorescence, formaldehyde-fixed dorsal skin and tumour

specimens were embedded in paraffin and cut into 5µm sections, and, subsequently, subjected to the same treatment received by sections analysed by Immunohistochemistry **(Section 2.5.2.)**. Variation from Immunohistochemistry protocol was that instead of using mouse/rabbit Envision (DAKO) secondary antibodies, sections were incubated in the dark at room temperature with fluorescent secondary antibodies (488 and 594 Alexa Fluor, Invitrogen) that were diluted in antibody diluent (Dako). Subsequently, secondary antibody was washed 3 times with TBS in the dark, and sections were mounted with DAPI-containing Vectashield mounting medium (Vector Laboratories). Sections were scanned using NanoZoomer-XR Digital slide scanner (Hamamatsu) and visualised using NDP.view2 Viewing software (Hamamatsu). Image analysis was performed blind, as specified in each figure legend, either manually, with the use of ImageJ software, or with the use of ImmunoRatio plugin of ImageJ software [128].

For cell immunofluorescence, cells were plated on sterile 19mm glass coverslips (VWR collection) and fixed and permeabilised on ice for 10 minutes in cold fixation solution (3.7% formaldehyde (Thermo Fisher Scientific), 100mM PIPES (Sigma-Aldrich), 1mM $MgCl_2$ (Sigma-Aldrich), 10mM EGTA (Sigma-Aldrich) and 0.2% Triton X100 (Sigma-Aldrich)). Following, cells were washed 3 times on ice with 0.1% Triton X100 in TBS and blocked for 1 hour on ice with 2% BSA (Calbiochem) in TBST. Coverslips were overnight at $4^{o}C$ with the appropriate primary antibodies in 2% BSA in TBST, followed by 3 TBST washes on ice the following day. Subsequently, coverslips were incubated for 45 minutes on ice in the dark with secondary fluorescent antibodies (488, 594 Alexa Fluor, Invitrogen). Finally, coverslips were washed 3 times on ice in the dark with TBST, before being mounted with DAPI-containing Vectashield mounting medium (Vector Laboratories).

Visualisation of immunofluorescent staning was performed in Olympus

FV1000 confocal microscope with the use of 60x1.35 NA UPLANSAPO oil immersion objective, and Olympus FluoView FV1000 software.

List of primary antibodies used can be found on **Table 2**.

Antibody	Company	Application and Dilution	Species
Kin1	Abcam	WB 1:2000 IF 1:100	Rabbit
Kin2	Origene	WB 1:3000 IF 1:200	Mouse
β-actin	CST	WB 1:5000	Mouse
Ki-67	Vector	IHC 1:800	Mouse
pHH3	CST	IHC 1:700	Rabbit
α-tub	CST	IF 1:4000	Mouse
ac-tub	CST	IF 1:6000	Rabbit
casp-3	CST	IHC 1:100	Rabbit
E-cadherin	CST	WB 1:1000	Rabbit
FAK	CST	IF 1:200	Mouse, Rabbit
CD31	Abcam	IHC, IF 1:400	Rabbit
MMP3	CST	WB 1:1000 IF 1:200	Mouse

Table 2: List of antibodies used for WB (western blot), IHC (Immunohistochemistry) and IF (Immunofluorescence).

2.6. Second harmonic imaging microscopy

Second harmonic imaging microscopy was performed with the help of Dr Martin Lee and enabled visualisation of collagen-I in paraffin-embedded $Kin1^{null}$ and $Kin1^{wt}$ mouse SCC tumours. A picoEmerald (APE) laser provided both a tunable pump laser (720–990 nm, 7 ps, 80 MHz repetition rate) and a spatially overlapped second beam termed the Stokes laser (1064, nm, 5–6 ps and 80 MHz repetition rate). The laser was inserted into an Olympus FV1000 microscope coupled to an Olympus XLPL25XWMP N.A. 1.05 objective lens using a short-pass 690 nm dichroic mirror (Olympus). Second harmonic generation signals were filtered using the following series of filters: FF552-Di02, FF483/639-Di01 and FF420/40. The pump laser was tuned to 816.8 nm and used 50 mW power as measured at the objective, whilst the Stokes laser used 20 mW power as measured at the objective.

2.7. Tumour and cell RNA extraction, RNA Sequencing and quantitative real-time PCR

2.7.1. RNA extraction

RNA was extracted from snapped-frozen tumours that had been stored in -80°C for RNA preservation. Tumours were disrupted using pestle and mortar that were coated with dry ice for 1 minute and cleaned with 70% ethanol prior to every tumour disruption. RNA was subsequently extracted using the RNeasy kit (Qiagen) according to manufacturer's instructions. RNA concentration was determined with the use of NanoDrop Spectrophotometr (ThermoFischer Scientific). RNA was also extracted from $Kin1^{null}$, $Kin1^{wt}$ and $Kin1^{AA}$ cells grown on two-dimensional cell monolayers, and from $Kin1^{null}$, $Kin1^{wt}$ and $Kin1^{AA}$ cells grown on low-adherent plates (Fischer Scientific), in DMEM+10%FBS. Cells were plated at the same number (500 000 cells) and grown for 48 hours before RNA extraction was performed using the RNeasy kit (Qiagen) according to the

manufacturer's instructions. RNA concentration was determined with the use of NanoDrop Spectrophotometr (ThermoFischer Scientific).

2.7.2. RNA-Sequencing and analysis

RNA-Sequencing (RNA-Seq) was performed on tumour RNA material isolated as aforementioned, using single read sequencing on the Illumina Next-Generation Sequencing platform by the services of GATC Biotech (Constance, Germany). The average number of reads obtained in $Kin1^{null}$ samples was 55 million, and 31 million in $Kin1^{wt}$ samples.

Bioinformatics analysis was performed with assistance of Dr Stuart Aitken. 48 million $Kin1^{null}$ reads and 26 million $Kin1^{wt}$ reads were mapped to the mouse mm9 reference genome using Tophat2 [129] that aligns the reads across splice junctions independently of gene annotations. Overall alignment rates were ~30% due to variable mapping rates across the replicates in each condition. Differential expression was analysed by Cuffdiff [129] and by DESeq2 [130] to obtain lists of differentially expressed genes by two alternative statistical techniques. Finally, reads were used to construct a Principal Component Analysis (PCA), revealing variance in gene expression between different tumour samples.

2.7.3. Quantitative real-time PCR

Tumour RNA was converted into cDNA with the use of SuperScript first-strand cDNA synthesis kit and random hexamer primers (Invitrogen), according to manufacturer's instructions. Quantitative real-time PCR reactions were performed with the use of SensiFAST Hi-ROX kit (Bioline), as instructed by the manufacturer. Primers **(Table 3)** were used at a final concentration of 400nM, and 10-20ng of cDNA were used per 20μl reaction. *Gapdh* expression was used as internal control. Reactions were run on a StepOnePlus Real Time

PCR system (Thermo Fisher Scientific) and quantification of relative gene expression was performed using the ΔΔCt method [131].

Target gene name	Primer	Sequence 5'→3'
Fermt1	forward	*cgccaatatgaagcagtgg*
	reverse	*gtcaaactcgattgccacct*
Mmp3	forward	*ccaagtctaactctctggaacctg*
	reverse	*agagatttgcgccaaaagtg*
Mmp13	forward	*gccagaacttcccaaccat*
	reverse	*tcagagcccagaattttctcc*
Mmp15	forward	*ctaaagacgccgaagtgtacg*
	reverse	*gctggggtaggtagccataga*
Adamts6	forward	*agctcatattactgcaaataccaatc*
	reverse	*caagtaccacggcctgaatc*
Adamts12	forward	*ccttgtggagaatggcaagt*
	reverse	*cacctcctccacaggaccta*
Adamts17	forward	*cactgaatgtggagcagacaa*
	reverse	*gctcctgtaccacaggttcg*
Hif1a	forward	cgctatccacatcaaagcaa
	Reverse	gcactagacaaagttcacctgaga

Vegfa	forward	*aaaaacgaaagcgcaagaaa*
	reverse	*tttctccgctctgaacaagg*
Flt1	forward	*gcctacctcaccgtgcaa*
	reverse	*gagttagaaggagccaaaagagg*
Kdr	forward	*cagtggtactggcagctagaag*
	reverse	*acaagcatacgggcttgttt*
Thbs1	forward	*ccccaaccttcccaactc*
	reverse	*gggttgtaatggaatggacag*
Cxcl1	forward	*gactccagccacactccaac*
	reverse	*tgacagcgcagctcattg*
Ccl2	forward	*catccacgtgttggctca*
	reverse	*gatcatcttgctggtgaatgagt*
Ccl7	forward	*ttctgtgcctgctgctcata*
	reverse	*ttgacatagcagcatgtggat*

Table 3: List of primers used for q-PCR.

2.8. Data statistical analysis

Assessment of normality for all data sets was performed in GraphPad Prism 7 by the recommended D'Agostino & Pearson's normality test. Statistical significance was assessed by using unpaired student's t-test or one-way ANOVA (one-way analysis of variance) with Tukey's multiple comparison in data that were normally distributed. Statistical significance was assessed by

using Mann-Whitney's test or Kruskal-Wallis one-way ANOVA with Dunn's multiple comparison in non-normally distributed data. Pearson's correlation coefficient was calculated via GraphPad Prism 7, and compared correlation between gene expression and tumour volume according to correlation coefficient interpretation guide **(Table 5)** [132] .

Chapter 3:

development and characterisation of a mouse model of Kin1 loss

Part of the findings presented in this chapter have been published in the following article: Patel, H., Stavrou, I., Shrestha, R.L., Draviam, V., Frame, M.C., Brunton, V.G. (2016). Kindlin1 regulates microtubule function to ensure normal mitosis. Journal of Molecular and Cell Biology *8,* 338-348

Skin atrophy is one of the main clinical pathologies of KS, which in contrast to other KS symptoms that tend to improve by age, such as skin blistering, it becomes progressively worse [5]–[7]. Skin atrophy has been linked to proliferation defects that are present in keratinocytes of KS patients and of Kin1-null mice with KS-like features [8][54]. However, the molecular mechanisms via which Kin1 controls keratinocyte proliferation and, hence, skin homeostasis have not been fully elucidated.

Recent data on MDA-MB-231 breast cancer epithelial cells demonstrated that Kin1 regulates mitotic spindle formation *in vitro* [53]. Consequently, we wanted to generate a mouse model of Kin1 loss to assess whether and how Kin1 regulates mitosis *in vivo*, and whether this role of Kin1 is implicated in the reduced keratinocyte proliferation and, potentially, skin atrophy observed in the epidermis of KS patients.

Specific aims of this section of the chapter are:

1. Development of a mouse model of Kin1 loss by performing conditional knockout of *Fermt1* gene in mouse epidermis**.**
2. Examination and characterisation of potential morphological, proliferation and mitotic defects in epidermal keratinocytes following loss of Kin1 in mouse epidermis.

3.1. Use of Cre-Lox recombination system to achieve conditional knockout of *Fermt1* in the epidermis of adult mice

A number of KS patients suffer from ulcerative colitis that first develops during infancy [20][21][133]. Whereas this pathology is not lethal in humans, deletion of *Fermt1* in mice leads to lethal neonatal gastrointestinal dysfunction [54]. To circumvent the lethality of a constitutive *Fermt1* ablation, we established a unique model of Kin1 loss in which deletion of *Fermt1* gene was performed only in the epidermis of adult mice in a temporally controlled manner.

To achieve this, we engineered a Kin1$^{fl/fl}$ transgenic mouse, in which exons 4 and 5 of *Fermt1* gene were floxed, and crossed it with a K14-Cre-ER^{T2} (K14-Cre) mouse to generate K14-Cre-ER^{T2}-Kin1$^{fl/fl}$ (K14-Cre-Kin1$^{fl/fl}$) double transgenic progeny, in which Cre-ER^{T2} was under the control of K14 skin promoter [123][124] **(Fig.5.1.)**. Adult K14-Cre-Kin1$^{fl/fl}$ mice and adult K14-Cre mice, which were used as control, were treated with 4OHT **(Fig.5.2.)**. In K14-Cre-Kin1$^{fl/fl}$ mice this resulted in Cre recombination at loxP sites [125], thus inducing deletion of exons 4 and 5 and, therefore, deletion of *Fermt1* **(Fig.5.3.)**. Any subsequent mention of K14-Cre and K14-Cre-Kin1$^{fl/fl}$ mice refers to K14-Cre and K14-Cre-Kin1$^{fl/fl}$ mice treated with 4OHT.

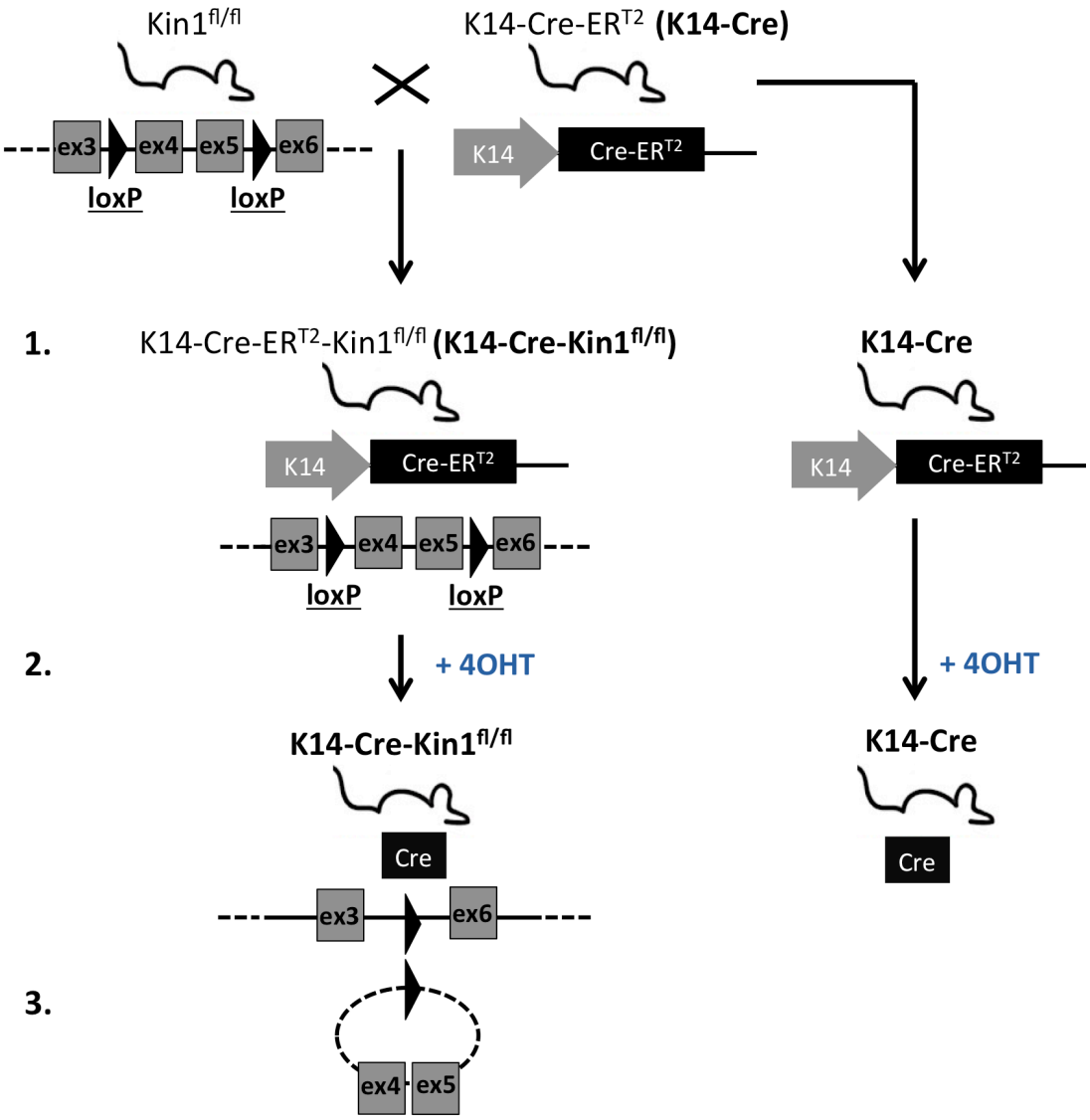

Figure 5: Conditional knockout of *Fermt1* gene in the epidermis of adult mice. 1: Mice with floxed *Fermt1* exons 4 and 5 (Kin1$^{fl/fl}$) were crossed with K14-Cre-ER^{T2} (K14-Cre) mice to generate K14-Cre-ER^{T2}-Kin1$^{fl/fl}$ (K14-Cre-Kin1$^{fl/fl}$) double transgenic mice. **2:** Subsequently, adult K14-Cre-Kin1$^{fl/fl}$ mice and adult K14-Cre mice, which were used as controls, were treated with 4OHT. **3:** This induced Cre-mediated recombination at loxP sites, deletion of the above exons and, thus, knockout of *Fermt1* in the epidermis of adult K14-Cre-Kin1$^{fl/fl}$ mice.

Our initial aim was to confirm the loss of Kin1 in the epidermis of K14-Cre-Kin1$^{fl/fl}$ mice. Thus, lysates from tail epidermal keratinocytes of K14-Cre and K14-CreKin1$^{fl/fl}$ mice were analysed by western blot, which confirmed the loss of Kin1 in the epidermis of the latter (**Fig.6.**).

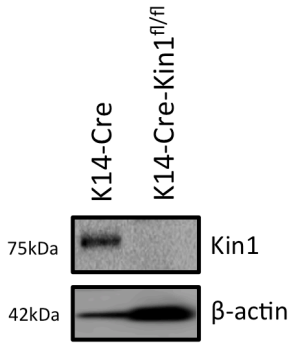

Figure 6: Loss of Kin1 in the epidermis of adult K14-Cre-Kin1$^{fl/fl}$ adult mice. Tail keratinocytes were isolated from the epidermis of K14-Cre and K14-Cre-Kin1$^{fl/fl}$ mice 10 days following the end of the 4OHT treatment. Western blot analysis of Kin1 expression in the epidermis of K14-Cre and K14-Cre-Kin1$^{fl/fl}$ mice. β-actin was used as loading control. Due to the low yield of keratinocytes from each tail, it was necessary to pool keratinocytes from multiple tails together [K14-Cre (n=3), K14-Cre-Kin1$^{fl/fl}$ (n=6)] . The difference in the amount of β-actin reflects the variability in the number and size of mice tails used.

3.2. Phenotypic analysis and histological examination of K14-Cre-Kin1$^{fl/fl}$ mouse epidermis

We first performed a visual inspection of K14Cre-Kin1$^{fl/fl}$ epidermis, but detected no signs of skin atrophy or other KS symptoms **(Fig.7.A.)**. Moreover, we assessed hair coat development in K14Cre-Kin1$^{fl/fl}$ mice over the course of 2 months, as mice with congenital loss of Kin1 were previously shown to develop irregular hair coat with alternating patches of dense hair and areas of alopecia [119]. To achieve this we shaved the back of K14Cre-Kin1$^{fl/fl}$ and K14-Cre mice **(Fig.7.B.)** and observed hair re-growth over time. We detected normal hair coat development, both in K14Cre-Kin1$^{fl/fl}$ and K14-Cre mice and normal skin pigmentation **(Fig.7.C,D)**.

Following, we examined whether the epidermis of K14-Cre-Kin1$^{fl/fl}$ mice presented any morphologic aberrations in comparison to K14-Cre mouse epidermis. In order to determine the effects of short-term and long-term epidermal loss of Kin1 on skin morphology, dorsal skin from K14-Cre and K14-Cre-Kin1$^{fl/fl}$ mice was collected 5 days **(Fig.8.A.)**, 10 days **(Fig.8.B.)** and 1 year **(Fig.8.C.)** after the end of the 4OHT treatment. Histological H&E examination revealed no epidermal structural changes between K14-Cre and K14-Cre-Kin1$^{fl/fl}$ mice **(Fig.8.A-C.)**.

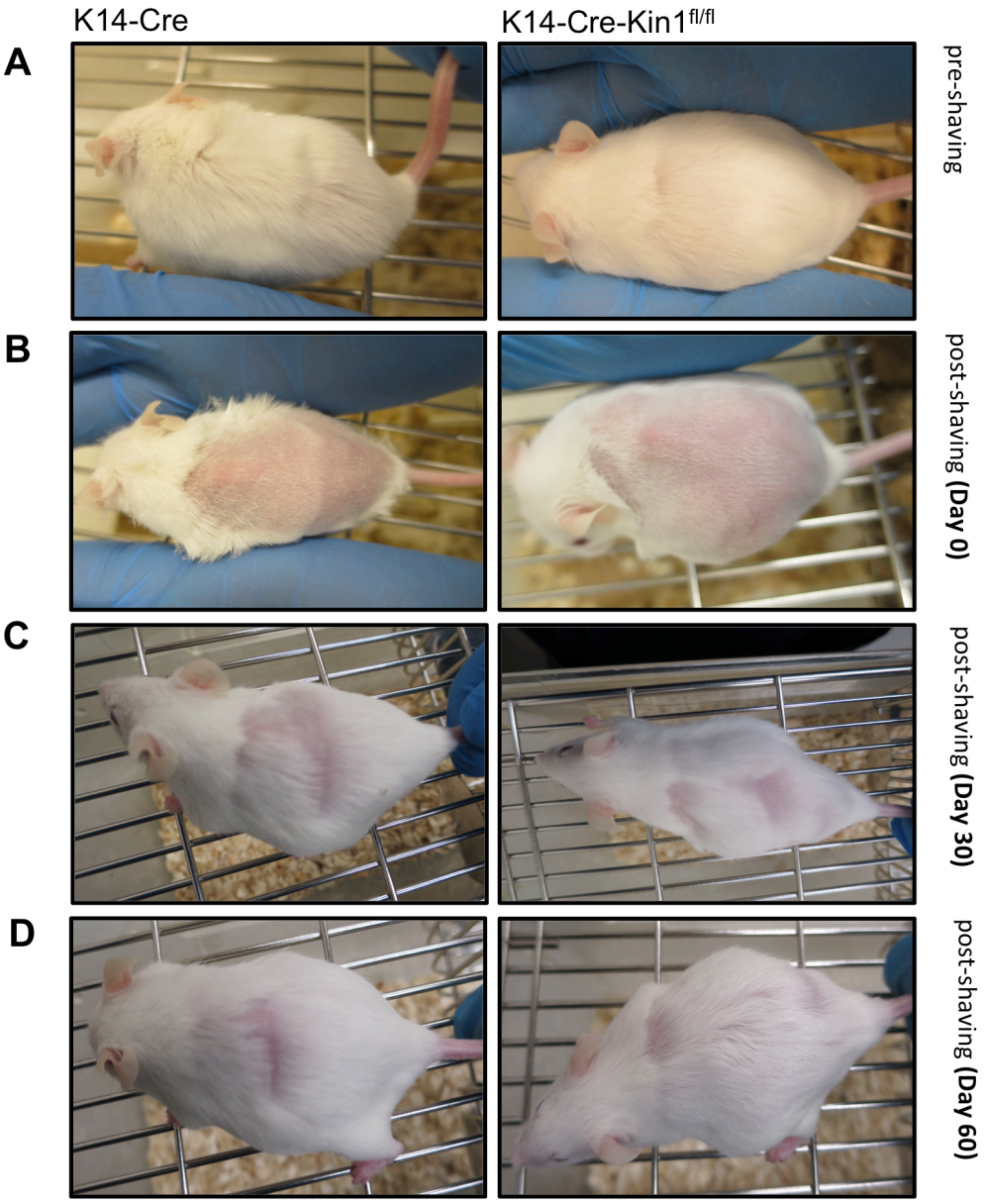

Figure 7: Loss of Kin1 in the epidermis of K14-Cre-Kin1$^{fl/fl}$ adult mice did not alter skin phenotype or hair growth. Representative photographs of mice **A:** before shaving, **B:** the day of shaving and **C:** 30 days post-shaving, **D:** 60 days post-shaving.

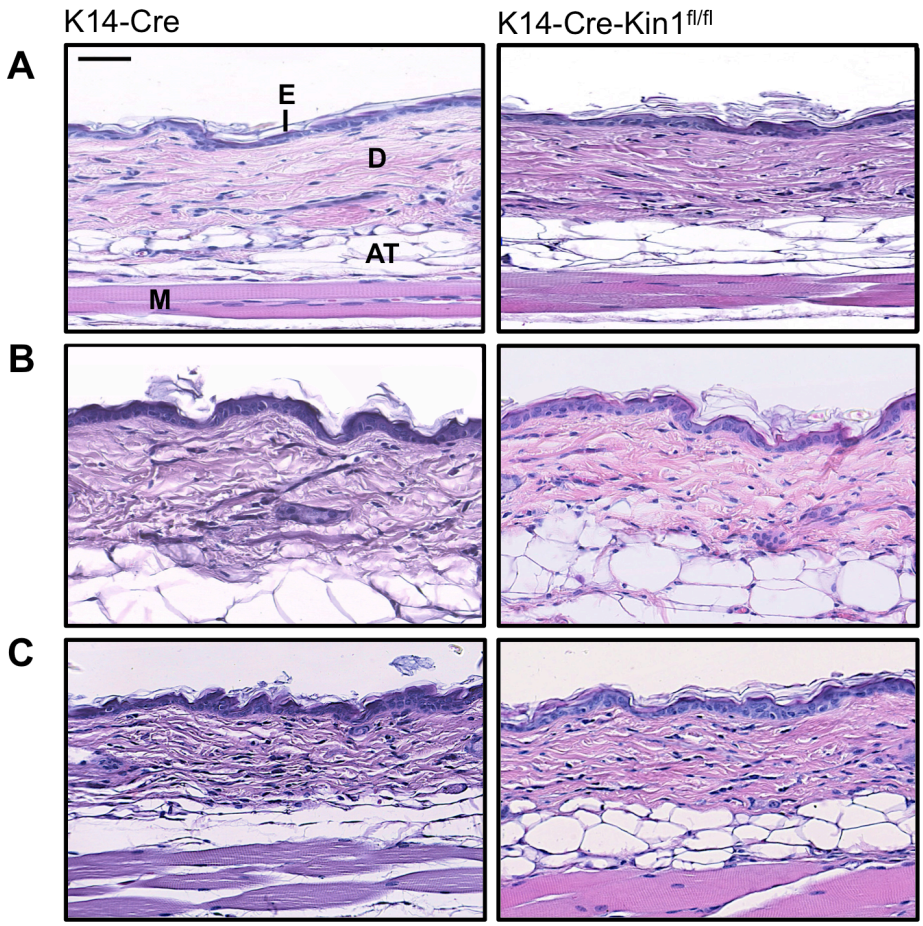

Figure 8: Loss of Kin1 in the epidermis of K14-Cre-Kin1$^{fl/fl}$ adult mice did not alter epidermal morphology. Representative images of H&E staining that was performed on sections of dorsal skin isolated from K14-Cre and K14-Cre-Kin1$^{fl/fl}$ mice **A:** 5 days, **B:** 10 days and **C:** 1 year following the end of the 4OHT treatment. E= epidermis, D= dermis, AT= adipose tissue, M= muscle. Mag x40. The scale bar represents 50µm.

3.3. Characterisation of the proliferative and mitotic capacity in keratinocytes of K14-Cre-Kin1$^{fl/fl}$ mouse epidermis

KS keratinocytes exhibit minimal proliferation in comparison to healthy counterparts, both in vitro and in vivo [8][54][98], which led us to explore whether the epidermis of K14-Cre-Kin1$^{fl/fl}$ mice presented any proliferation defects when compared to K14-Cre epidermis.

Proliferative capacity of cells was determined via immunolabeling of dorsal skin from K14-Cre and K14-Cre-Kin1$^{fl/fl}$ mice with Ki-67 proliferation marker **(Fig.9.A)**. We observed that ~50% of K14-Cre nuclei scored positive for Ki-67, which was significantly reduced by ~16% in nuclei of K14-Cre-Kin1$^{fl/fl}$ epidermis **(Fig.9.B)**.

Recent findings uncovered a novel role for Kin1 in the regulation of mitotic spindle formation, as depletion of Kin1 in MDA-MB-231 breast cancer epithelial cells significantly increased the presence of abnormal spindles and decreased cell survival [53]. We, therefore, assessed whether epidermal keratinocytes of K14-Cre-Kin1$^{fl/fl}$ mice displayed mitotic defects compared to K14-Cre keratinocytes.

We determined the mitotic index of basal keratinocytes by scoring the percentage of epidermal nuclei that were positive for phospho-histone H3 (pHH3), a mitotic marker expressed during late G2 and M phases [134], on dorsal skin from K14-Cre and K14-Cre-Kin1$^{fl/fl}$ mice **(Fig.10.A.)**. We detected a statistically significant reduction in keratinocyte mitosis following loss of Kin1, as only ~6% of K14-Cre-Kin1$^{fl/fl}$ cells were undergoing mitosis compared to ~11% of K14-Cre cells **(Fig.10.B.)**.

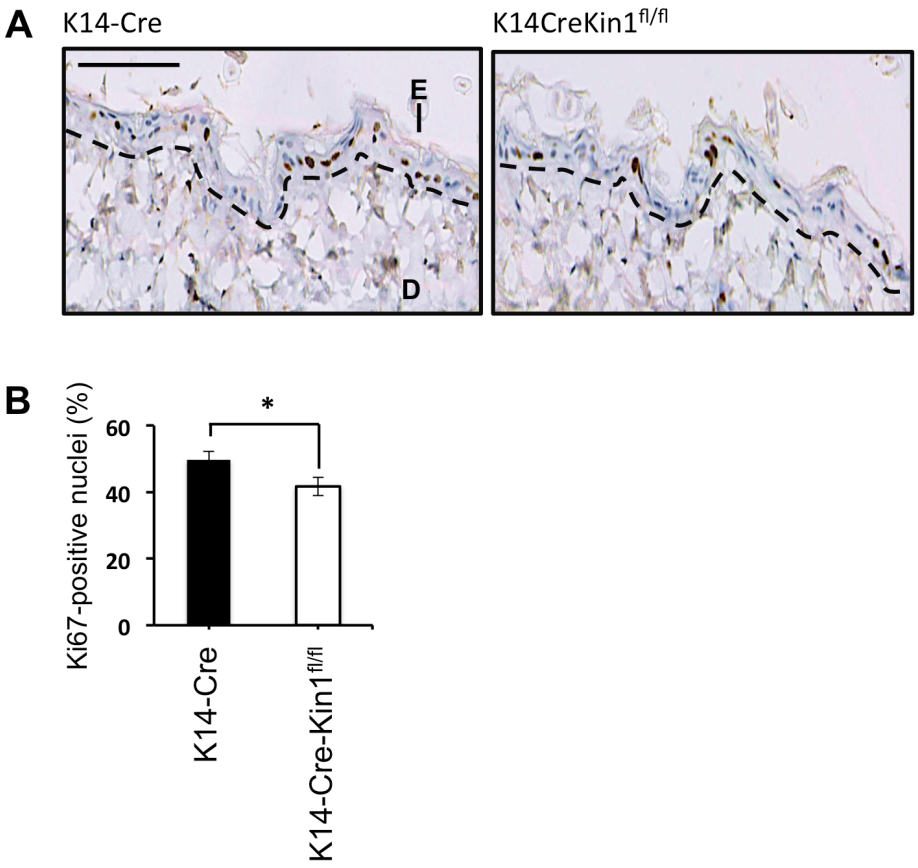

Figure 9: Short-term loss of Kin1 in the epidermis of K14-Cre-Kin1$^{fl/fl}$ adult mice significantly decreased the number of proliferating cells. IHC was performed with a Ki-67 antibody on sections of dorsal skin isolated from K14-Cre and K14-Cre-Kin1$^{fl/fl}$ mice 10 days following the end of the 4OHT treatment. **A:** Representative IHC images of Ki-67 staining. The basement membrane is indicated with a dotted black line. E= epidermis, D= dermis. Mag x80. Scale bar represents 50µm. **B:** Quantification of the percentage of Ki-67-positive nuclei was performed manually by scoring the selected epidermis. Cells from 10 or more representative low-power fields were analysed per K14-Cre (n=4) and K14-Cre-Kin1$^{fl/fl}$ mouse (n=4). Results presented as mean ± SEM. Unpaired t-test; * p-value < 0.05.

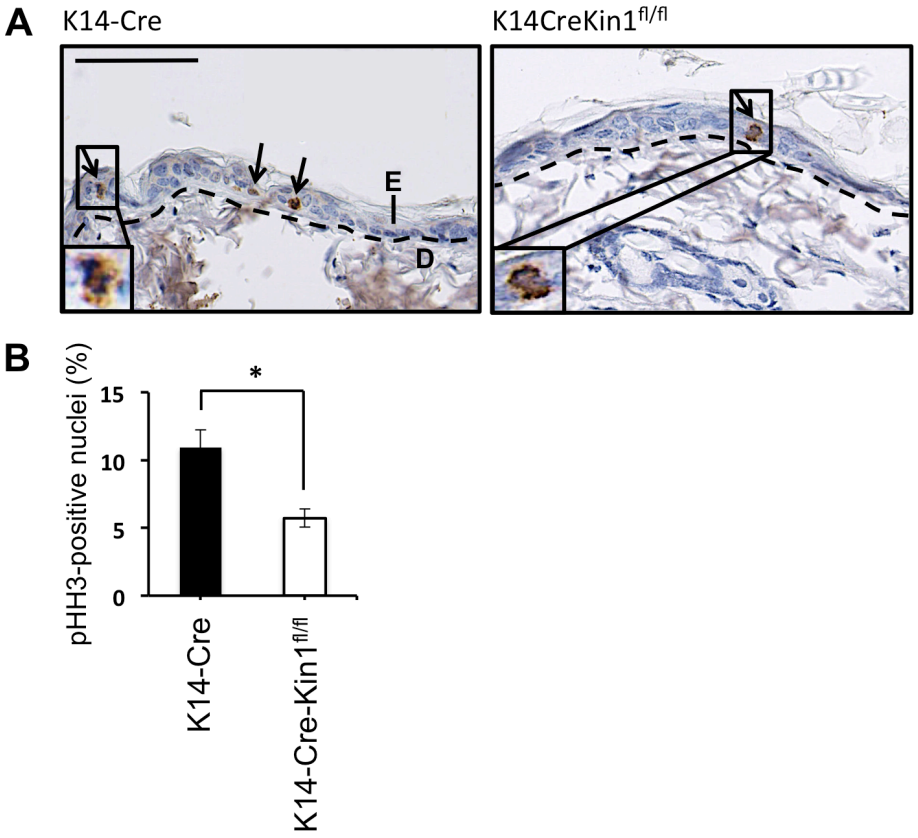

Figure 10: Short-term loss of Kin1 in the epidermis of K14-Cre-Kin1$^{fl/fl}$ adult mice significantly decreased the number of mitotic cells. IHC was performed with a pHH3 antibody on sections of dorsal skin isolated from K14-Cre and K14-Cre-Kin1$^{fl/fl}$ mice 10 days following the end of the 4OHT treatment. **A:** Representative IHC images of pHH3 staining. Arrows indicate pHH3-positive nuclei. Magnified cells are undergoing anaphase. The basement membrane is indicated with a dotted black line. E= epidermis, D= dermis. Mag x100. Scale bar represents 50µm. **B:** Quantification of the percentage of pHH3-positive nuclei was performed manually by scoring the selected epidermis. Cells from 6 or more representative low-power fields were analysed per K14-Cre (n=4) and K14-Cre-Kin1$^{fl/fl}$ mouse (n=4). Results presented as mean ± SEM. Unpaired t-test; * p-value < 0.05.

3.4. Characterisation of mitosis in keratinocytes of K14-Cre-Kin1$^{fl/fl}$ mouse epidermis

Epidermal progenitors must maintain a theoretical balance between self-division and generation of differentiated progeny, in order to maintain skin homeostasis. To accomplish this, basal keratinocytes divide symmetrically, which yields two basal, proliferative daughter cells and, thus, increases surface area, and asymmetrically, which results in one basal, proliferative and one suprabasal, non-proliferative cell that engages in terminal differentiation, thus promoting epidermal stratification [135] **(Fig.11.A.)**. Symmetrical Cell Division (SCD) is achieved by aligning the mitotic spindles parallel to the underlying substrate (basement membrane), whereas during Asymmetrical Cell Division (ACD) mitotic spindles are misorientated and form perpendicularly to the substrate **(Fig.11.A.)**.

We, thus, sought to determine if the significant reduction in the number of proliferative and mitotic K14-Cre-Kin1$^{fl/fl}$ keratinocytes is accompanied by a shift in the SCD/ACD balance. Using α-tubulin (α-tub) as a mitotic spindle marker, we scored the incidence of SCD and ACD in the epidermis of K14-Cre and K14-Cre-Kin1$^{fl/fl}$ mice **(Fig.11.B.)**. In the K14-Cre epidermis ~29% of mitotic keratinocytes underwent ACD, whereas the incidence significantly increased to ~50% in the K14-Cre -Kin1$^{fl/fl}$ epidermis **(Fig.11.C.)**.

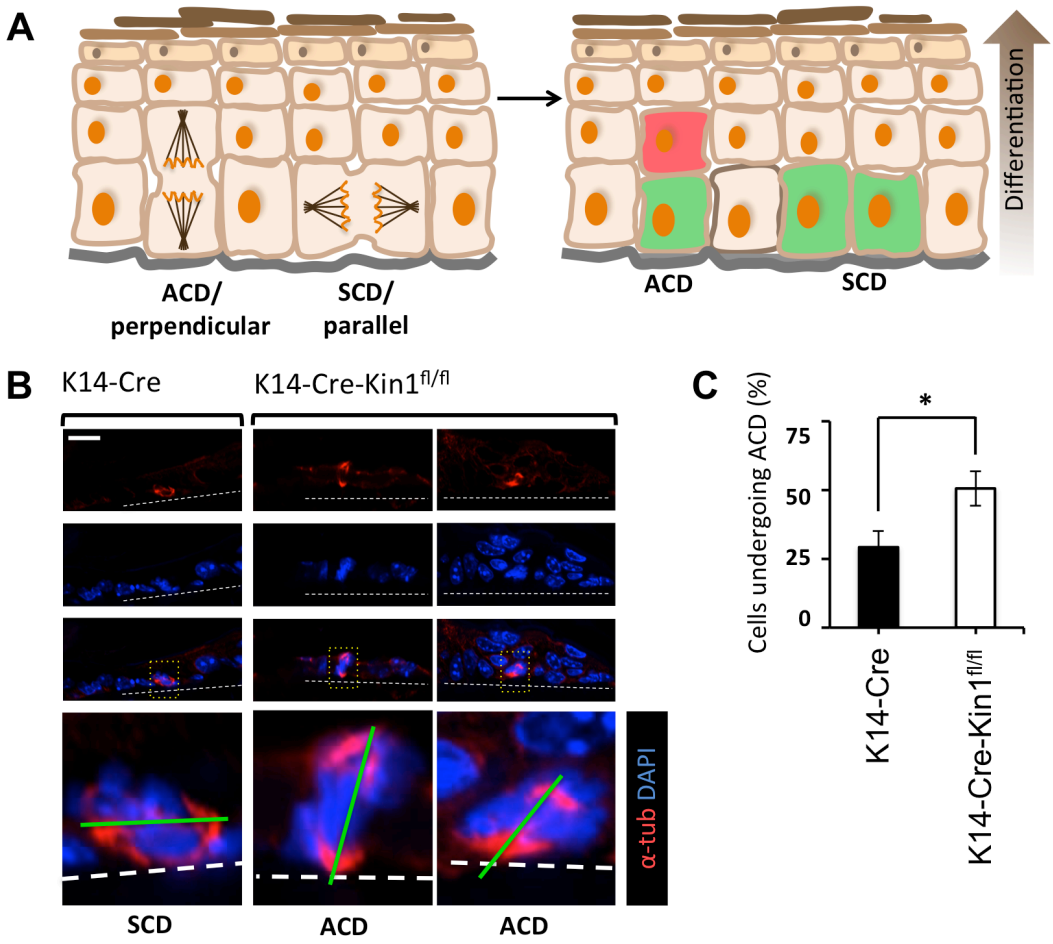

Figure 11: Short-term loss of Kin1 in the epidermis of K14-Cre-Kin1$^{fl/fl}$ adult mice significantly increased the incidence of ACD. IF was performed with an α-tub antibody on sections of dorsal skin isolated from K14-Cre and K14-Cre-Kin1$^{fl/fl}$ mice **A:** Diagram of SCD and ACD accomplished by a plane of division which is parallel or misorientated/perpendicular to the underlying basement membrane (gray line), respectively. SCD results in two basal, proliferative daughter cells (green), whereas ACD generates one basal (green) and one suprabasal, non-proliferative daughter cell (red) that terminally differentiates (Figure adapted from [136]). **B:** Representative IF images of α-tub staining. Examples of mitotic keratinocytes undergoing SCD and ASD are shown. The dotted white line represents the basement membrane and the green solid line represents the axis of cell division. Scale bar represents 10µm. **C:** Quantification of the percentage of cells undergoing ACD was performed manually by scoring the epidermis, which is separated from the dermis by the indicated basement membrane. Overall, 41 cells from K14-Cre (n=4) and 45 cells from K14-Cre-Kin1$^{fl/fl}$ mice (n=4) were analysed. Results presented as mean ± SEM. Unpaired t-test; * p-value < 0.05.

Spindle orientation parallel to the underlying substrate relies on a stable mitotic spindle [137][138]. Spindle stability can be assessed by the acetylation status of microtubules, the major structural element of mitotic spindles, with acetylated microtubules representing more stable and longer-lived microtubules [139]–[142].

Our aim was, therefore, to examine if the significant increase in the occurrence of misorientated spindles and, consequently, ACD in K14-Cre-Kin1$^{fl/fl}$ keratinocytes is linked to a reduction in microtubule acetylation. We used IF to stain the epidermis of K14-Cre and K14-Cre-Kin1$^{fl/fl}$ mice with α-tub and acetylated-α-tubulin (ac-tub) **(Fig.12.A.)** and subsequently evaluated the degree of microtubule acetylation by quantifying the ac-tub:α-tub ratio of each mitotic spindle. Our results revealed a ~35% reduction in the ac-tub:α-tub ratio in K14-Cre-Kin1$^{fl/fl}$ mitotic keratinocytes compared to K14-Cre mitotic keratinocytes **(Fig.12.B.)**.

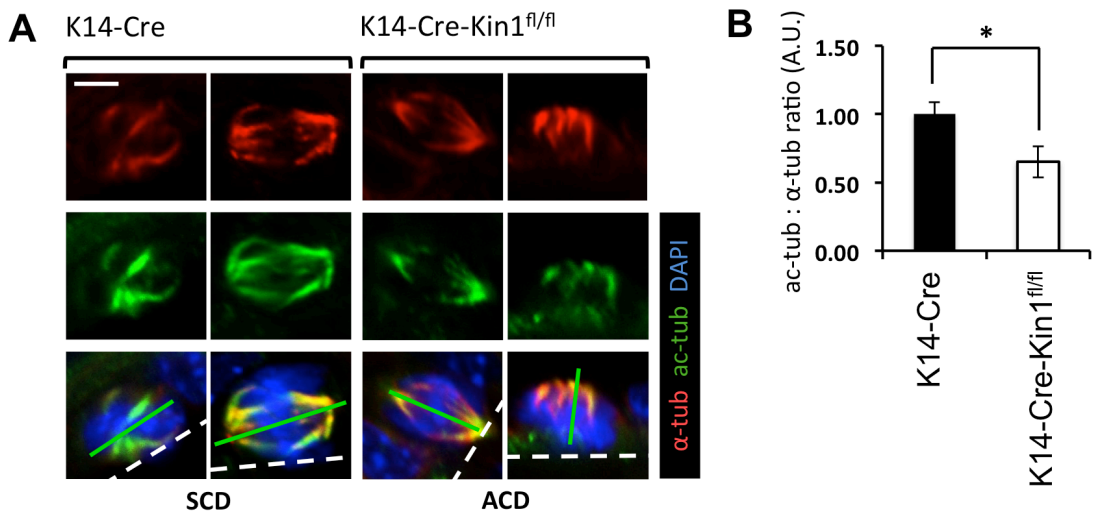

Figure 12: Short-term loss of Kin1 in the epidermis of K14-Cre-Kin1$^{fl/fl}$ adult mice significantly reduced levels of microtubule acetylation. IF was performed with α-tub and ac-tub antibodies on sections of dorsal skin isolated from K14-Cre and K14-Cre-Kin1$^{fl/fl}$ mice. **A:** Representative IF images of α-tub and ac-tub staining in mitotic keratinocytes undergoing SCD and ACD. The dotted white line represents the basement membrane and the green solid line represents the axis of cell division. Scale bar represents 2.5μm. **B:** Quantification of the α-tub:ac-tub ratio in the mitotic spindles of cells was performed with ImageJ software by measuring the Raw Integrated Density (sum of pixel value) of every image. Overall, 55 mitotic spindles from K14-Cre mice (n=4) and 48 mitotic spindles from K14-Cre-Kin1$^{fl/fl}$ mice (n=4) were analysed. Results presented as mean ± SEM. Unpaired t-test; * p-value < 0.05.

3.5. Characterisation of the apoptotic capacity of K14-Cre-Kin1$^{fl/fl}$ mouse epidermis

As prominent epidermal apoptosis had been previously reported in the skin of KS patients [8][143], we investigated the apoptotic status of our mouse model epidermis by manually scoring keratinocytes that stained positive for the apoptotic marker cleaved-caspase-3 (casp-3) **(Fig.13.A.)**. Subsequent quantification revealed no significant difference in the percentage of apoptotic cells between K14-Cre and K14-Cre-Kin1$^{fl/fl}$ mice **(Fig.13.B.)**.

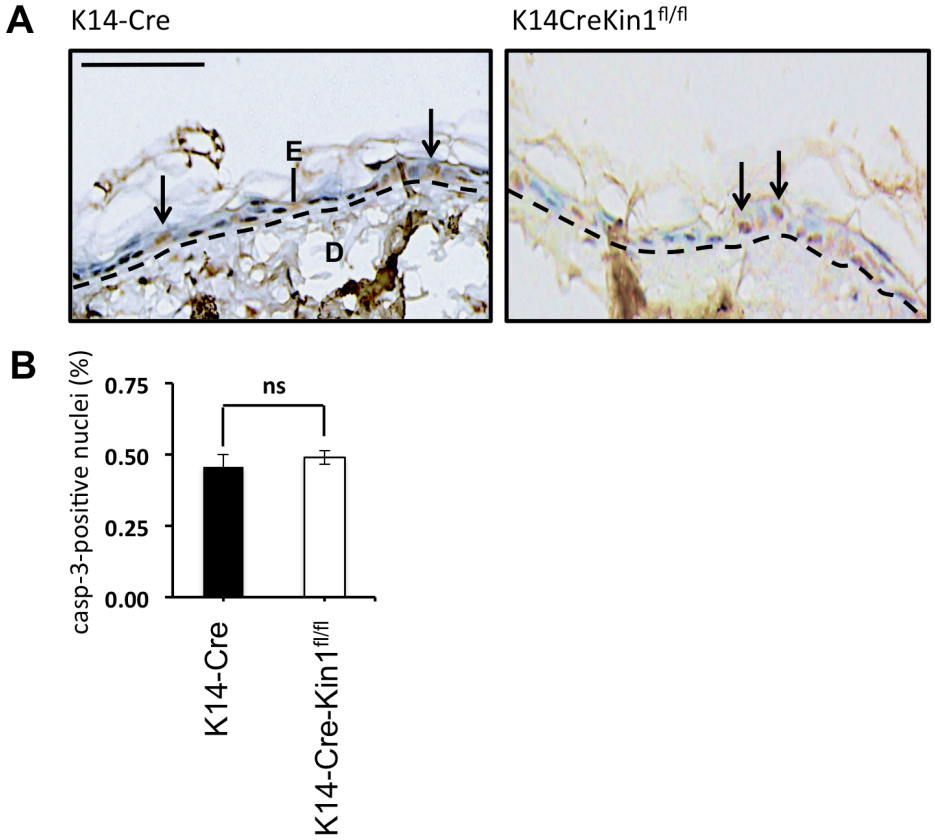

Figure 13: Short-term loss of Kin1 in the epidermis of K14-Cre-Kin1$^{fl/fl}$ adult mice did not alter the level of apoptosis. IHC was performed with a casp-3 antibody on sections of dorsal skin isolated from K14-Cre and K14-Cre-Kin1$^{fl/fl}$ mice. **A:** Representative IHC images of casp-3 staining. Arrows indicate casp-3-positive nuclei. The basement membrane is indicated with a dotted black line. E= epidermis, D= dermis. Mag x100. Scale bar represents 50µm. **B:** Quantification of the percentage of casp-3-positive nuclei was performed manually. Cells from 6 or more representative low-power fields were analysed per K14-Cre (n=4) and K14-Cre-Kin1$^{fl/fl}$ (n=4) mouse. Results presented as mean ± SEM. Unpaired t-test; ns (non-significant): p-value > 0.05.

3.6. Discussion

Kin1 is a well-documented integrin co-activator [49][97], a role that is often associated with the molecular mechanism underlying a number of KS features. In particular, intestinal epithelial dysfunction, as well as reduced adhesion in cultivated KS keratinocytes have been attributed to inadequate integrin activation [54][144].

3.6.1. Kin1 plays a role in regulation of keratinocyte proliferation and mitosis in mouse epidermis

The aetiology that underlies reduced keratinocyte proliferation, which is a characteristic of KS keratinocytes and a KS symptom linked to skin atrophy, is still unclear [8][54]. An *in vitro* study that emerged a few years ago defined a role for Kin1 in mitotic spindle formation [53]. No subsequent studies have addressed the mitotic role of Kin1 *in vivo* or its possible contribution to KS features such as reduced cell proliferation.

Here we show for the first time that Kin1 plays a role in mitotic spindle stability and orientation *in vivo*, which we believe to be associated with proliferation defects observed in KS epidermis. To examine the effects of Kin1 loss *in vivo*, we performed short-term (10-day) epidermis-restricted deletion of *Fermt1* in adult mice **(Fig.5,6)**, and employed a variety of immunological stains on their dorsal skin.

Consistent with previous observations of lower keratinocyte proliferation in KS skin, our data displayed significant decrease in the number of proliferating keratinocytes following loss of Kin1 in adult mouse epidermis **(Fig.9.)** and, thus, indicated an *in vivo* function for Kin1 in keratinocyte proliferation. We proceeded to show for the first time that Kin1 also played a mitotic role *in vivo*,

as we detected a significantly lower mitotic capacity in K14-Cre-Kin1$^{fl/fl}$ keratinocytes compared to K14-Cre counterparts **(Fig.10.)**.

As proposed over a decade ago, the outcome of cell division in the skin depends on the axis of cell division, primarily governed by orientation of mitotic spindles in relation to the underlying basement membrane. SCD occurs when mitotic spindles are parallel to the substratum and yields two basal proliferative cells, whereas ACD is marked by spindles off-parallel/perpendicular to the substrate plane and produces one basal proliferative and one suprabasal non-proliferative keratinocyte that terminally differentiates [135] **(Fig.11.A.)**. The reduction in proliferative and mitotic capacity in K14-Cre-Kin1$^{fl/fl}$ keratinocytes could stem from the significant rise in the percentage of misorientated spindles and, thus, in cells undergoing ACD observed in K14-Cre-Kin1$^{fl/fl}$ epidermis **(Fig.11.B-C.)**. Our data parallel the findings of the *in vitro* study on mitotic role of Kin1, which also showed that a significantly higher percentage of Kin1-depleted epithelial cells failed to orient their spindles parallel to the substrate plane compared to control cells [53].

Orientation of mitotic spindle parallel to underlying substrate relies on stable microtubules [137][138]. The degree of mitotic spindle stability can be assessed by the microtubule acetylation status, as stable microtubules are known to possess high levels of ac-tub [139]–[142]. Our findings showed a role for Kin1 in regulation of ac-tub and, therefore, spindle stability in K14-Cre-Kin1$^{fl/fl}$ epidermis **(Fig.12.)**, which could potentially account for the rise in ACD.

Integrin-deficient keratinocytes also present proliferation defects, both *in vitro* [145][146] and *in vivo* [96]. Interestingly, inhibition of β1 integrin function results in abnormalities in spindle formation and orientation, indicating an integral role for integrins in spindle biology [53][137][147].

According to literature, appropriate alignment of mitotic spindles parallel to the substratum can occur via integrin-dependent and integrin-independent mechanisms, such as regulation of cortical contractile forces and cell-substrate adhesion. *In vitro*, β1 integrin promoted accumulation of phosphatidylinositol-3,4,5-triphosphate (PIP_3) in metaphase cell midcortex during anaphase, which allowed dynein-dynactin motor complex to exert contractile forces that correctly orient mitotic spindles [148]. Moreover, regulation of dynein-dynactin complex by β1 integrin was also essential for proper spindle alignment in mouse epidermis [135], and interaction of dynactin-1 and dynactin-2 subunits of the dynein-dynactin complex with β1 integrins was required for spindle orientation in HeLa cells [149]. Mitotic spindles were severely misorientated in HeLa cells plated on poly-L-lysine, an artificial substrate that does not adhere to integrins [150], or treated with anti-β1 integrin antibody or RGD peptide, which prevents integrin-mediated signalling [151], highlighting the importance of β1 integrin-mediated cell-substrate adhesion and overall function in spindle orientation [137]. Finally, β1 integrin inactivation in the embryonic ventricular zone of mouse cerebral cortex resulted in ventricular zone detachment, impaired proliferation of neural stem cells and defective adhesion to their niche, and misorientated divisions [152].

Finally, microtubule stability, which is another key factor that ensures appropriate spindle alignment, also occurs via mechanisms dependent and independent of integrins. Integrins promoted microtubule stabilisation and proper orientation in Drosophila eye disc epithelium [141], and glandular epithelium [153]. Nevertheless, microtubule stability can also be achieved in integrin-independent manner. In particular, various integrin-independent factors were shown to promote stability of astral microtubules, a subset of microtubules that attach to cell cortex and are required for spindle stabilisation and positioning [154]. Examples include End Binding 1 (EB1) [137],

Cylindromatosis [138] and AMP-activated Protein Kinase [155], and their deficiency leads to short and unstable astral microtubules, improper astral microtubule-cell cortex interactions and, ultimately, spindle misorientation *in vitro*.

In vitro study from our lab previously showed that the role of Kin1 in proper mitotic spindle formation occurred in a manner both dependent and independent of the protein's role in integrin interaction and activation. In particular, expression of Kin1-W612A mutant, which is unable to bind and activate integrins [49], was unable to rescue the abnormal spindle phenotypes, including elevated misorientation, that were observed after depletion of Kin1 in MDA-MB-231 epithelial cells [53]. However, the study also showed that Kin1 is phosphorylated by polo-like kinase 1 (PLK1) *in vitro*, which is what renders Kin1 able to regulate spindle orientation and formation, and that whilst expression of non-Plk1 phosphorylatable Kin1 mutant failed to rescue mitotic defects, it did not affect integrin activation [53].

Collectively, the aforementioned literature findings raise the possibility that the role of Kin1 in proliferation and mitotic spindle stability and orientation in mouse epidermis could be integrin-dependent and/or -independent. One way that this could be addressed is to examine expression of pKin1^{T30}, where T30 represents a strong PLK1 phosphorylation consensus site on Kin1 [53], in mouse epidermis. pKin1^{T30} was previously shown to localise across spindle microtubules [53], where Kin1 is thought to be phosphorylated by Plk1 to employ its function in spindle stability [156].

3.6.2. Evaluation of K14-Cre-Kin1$^{fl/fl}$ mouse model of Kin1 loss

Defects in keratinocyte proliferation were shown to accompany the pathology of skin atrophy in KS patients and Kin1-null mice with KS-like phenotypes [8][54]. However, despite the significant reduction in the number of

proliferating keratinocytes following a short-term (10-day) loss of Kin1 in K14Cre-Kin1$^{fl/fl}$ epidermis **(Fig.9.)**, no indications of skin atrophy or other morphological aberrations were observed **(Fig.7.)**. Likewise, structural comparison between K14Cre-Kin1$^{fl/fl}$ and K14-Cre epidermis after a 5-day **(Fig.8.A.)** or 1-year **(Fig.8.C.)** Kin1 loss mirrored the results of a 10-day Kin1 loss **(Fig.8.B.)**, thus excluding the possibility of a transient or long-term KS-like phenotype in our model.

C57BL/6 (C57Black/6) mice with long-term (>6 months) loss of Kin1 in the epidermis, which occurred during development, developed poikiloderma, signs of skin atrophy and irregular hair coat [119]. This occurred due to enlarged stem cell compartments and provoked hypeproliferation and eventual exhaustion of cutaneous stem cells [119]. However, K14Cre-Kin1$^{fl/fl}$ mice with 1-year old *Fermt1* deletion showed no histological signs of abnormal epidermis **(Fig.8.C.),** developed a normal hair coat and presented no signs of poikiloderma **(Fig.7.)**.

A possible explanation for lack of KS phenotypes, such as skin atrophy, or poikiloderma in our model is that in our study deletion of *Fermt1* was performed in adult mice. Aberrations in keratinocyte stem cell compartments in C57BL/6 mice, which occurred following loss of Kin1 during development and resulted in KS-like phenotypes, allow us to hypothesise that Kin1 could regulate development of bulge stem cells during embryonic morphogenesis, but exert minimal effects on an established adult stem cell population. Indeed, our findings displayed a reduction of only ~16% in adult keratinocyte proliferation following loss of Kin1 in adult mice **(Fig.9.)**, which is not substantial to cause skin atrophy, thus supporting the above hypothesis.

Different mouse strains, including FVB and C56BL/6, have inherent variations in various features, such as susceptibility to skin carcinogenesis [157].

Therefore, lack of atrophy-like abnormalities in our model could stem from the fact that epidermal stem cell population of C57BL/6 mice is more susceptible to Kin1 loss compared to that in FVB mice. Finally, Kin1 loss in C57BL6/6 mice was achieved via the K5 skin promoter, which drives a 4OHT-independent activity of Cre recombinase and, thus, resulted in spontaneous epidermal loss of Kin1 during embryogenesis [119]. K5 and K14 promoters target slightly different stem cell populations [158][159], which could also contribute to the differences observed between the two models.

We believe that it is unlikely that poor K14-Cre recombination efficiency accounts for the lack of KS phenotype in our model. Although we could not examine Kin1 loss at single level, due to the lack of efficient Kin1 antibody for IHC, western blot analysis showed complete loss of Kin1 band in tail keratinocytes **(Fig.6)**, indicating highly efficient disruption of *Fermt1* gene. Moreover, other studies have demonstrated the ability of K14-Cre mouse to recombine floxed sequences in a highly efficient and keratinocyte-specific manner [158][160][161].

3.6.3. Summary and future work

In summary, our data reveal a novel role of Kin1 in skin homeostasis. We show that Kin1 regulates mitotic capacity, spindle orientation and α-tub acetylation in mouse epidermis, and show that loss of Kin1 reduced keratinocyte proliferation, an observation that was previously reported in mouse and human KS epidermis. We hypothesise that that disturbance of spindle orientation and α-tub acetylation upon loss of Kin1 could produce a smaller number of keratinocytes that bear a mitotic and proliferative capacity.

For future studies we suggest establishment of K5-Cre/Kin1$^{fl/fl}$ mice, in which spontaneous deletion of *Fermt1* during embryogenesis will recapitulate the genetic background of KS patients. Moreover, we propose a shift from mice

with FVB background to C57BL/6 mice, to enhance the likelihood of development of KS features and examine the mitotic role of Kin1 in the KS-like skin atrophy.

Chapter 4:

exploring the roles of Kin1 and Kin2 in mitosis

Part of the findings presented in this chapter have been published in the following article: Patel, H., Stavrou, I., Shrestha, R.L., Draviam, V., Frame, M.C., Brunton, V.G. (2016). Kindlin1 regulates microtubule function to ensure normal mitosis. Journal of Molecular and Cell Biology *8,* 338-348

In **Chapter 3** we showed that Kin1 plays a mitotic role *in vivo*, with loss of Kin1 in mouse epidermis enhancing the presence of misorientated spindles. Increase in abnormally orientated spindles had been previously shown following depletion of Kin1 in MDA-MB-231 breast cancer epithelial cells [53].

The aforementioned *in vitro* study as well as our study on mouse epidermis analysed spindle defects on fixed mitotic cells, following depletion or loss of Kin1, respectively. However, as mitosis is not a static process, we next sought to analyse in greater detail the temporal and dynamic nature of mitotic spindle abnormalities in Kin1 depleted cells. For this, we employed live cell imaging, a time-lapse microscopy technique that allows surveillance of mitosis in real time, in contrast to immunostaining on fixed cells or tissue that only provides a snapshot of a single time point. As live cell imaging provides high-resolution imaging of chromosomes and spindles throughout mitosis in live cells, we were able to extensively study the role of Kin1 and Kin2 in processes such as chromosomal alignment at the metaphase plate, chromosome segregation during anaphase, as well as mitotic spindle formation and orientation.

Specific aims of this section of the chapter are:

1. Use of live cell imaging to explore the roles of Kin1 and Kin2 in mitosis in a comprehensive manner.
2. Explore if Kin1 and Kin2 have redundant or distinct functions in mitosis

4.1. Establishment 4.9.5 – 105

of MDA-MB-231$^{H2B:DsRed}$ cell line

Kin1 and Kin2 share a variety of partially redundant roles *in vitro* and *in vivo* including maintenance of muscle integrity in Drosophila [162], and cell adhesion, survival and β1 integrin activation [88][94]. As a result, we initially set out to examine the outcome of Kin1 depletion during mitosis in cells that expressed no other member of the kindlin protein family. This allowed us to clearly establish the function of Kin1 towards mitotic fidelity without any potential compensation from Kin2.

The vast majority of epithelial cell lines express Kin1 and Kin2, as Kin1 is an epithelium-specific protein, whereas Kin2 is expressed ubiquitously. Nevertheless, MDA-MB-231 epithelial cell line, which is the cell line in which the mitotic role of Kin1 was first described, expresses readily detectable levels of Kin1, but no obvious levels of Kin2 **(Fig.14. by Dr Hitesh Patel)** [53] .

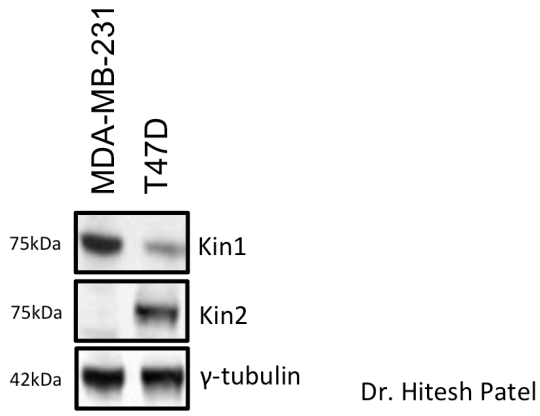

Figure 14: MDA-MB-231 cells express Kin1, but not Kin2. Western blot analysis of Kin1 and Kin2 expression in MDA-MB-231 and T47D breast cancer epithelial cell lines. γ-tubulin was used as loading control. Data reproduced from [53] with permission of Dr Hitesh Patel.

We transfected MDA-MB-231 cells with human histone *H2B* gene fused to the gene encoding red fluorescent protein DsRed of Discosoma coral, resulting in expression of H2B:DsRed fusion protein by a number of cells. Subsequently, DsRed-positive cells were selected with the use of FACS and pooled together to generate a stable cell line constitutively expressing H2B:DsRed (MDA-MB-231$^{H2B:DsRed}$ cell line) **(Fig.15.)**. As histones are principle components of chromatin and, thus, eukaryotic chromosomes, this allowed us to study chromosomal movement and dynamics in live MDA-MB-231$^{H2B:DsRed}$ cells throughout mitosis.

Our initial aim was to also fluorescently tag microtubules, the most abundant component of the mitotic spindle, in order to monitor spindle formation and orientation throughout mitosis. However, this was not feasible due to lack of appropriate fluorescent tag for β-tubulin, one of the basic structures of microtubules. Nevertheless, we were able to deduce the formation and orientation of mitotic spindle based on chromosomal positioning during metaphase and anaphase, as described later on.

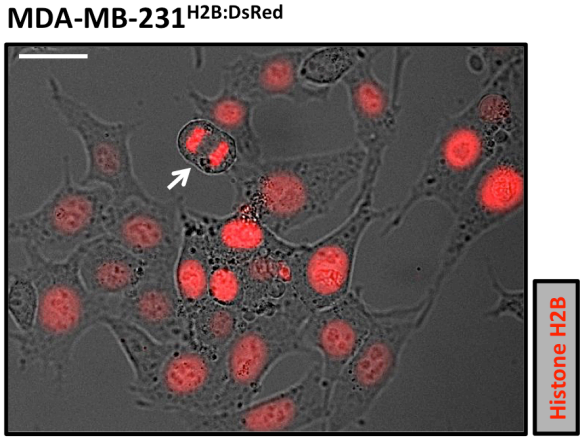

Figure 15: Expression of Histone H2B:DsRed as a chromatin marker in MDA-MB-231$^{H2B:DsRed}$ cell line. Representative phase contrast fluorescent image showing expression of Histone H2B:DsRed in MDA-MB-231$^{H2B:DsRed}$ cells, which allowed us to explore chromosome movement throughout the

various phases of mitosis. White arrow indicates a mitotic cell undergoing anaphase. Scale bar represents 20μm.

4.2. Kin1 depletion in MDA-MB-231$^{H2B:DsRed}$ cell line

Our lab has previously shown depletion of Kin1 in MDA-MB-231 cells with the use of a pool of 4 siRNAs oligos (si-Kin1^{pool}), consisting of two oligos directed against the translated and two against the untranslated region of *FERMT1* [53]. Moreover, depletion was shown with the use of two single siRNA oligos directed against the untranslated *FERMT1* region individually (si-Kin1^{UTR1}, si-Kin1^{UTR2}) and in combination (si-Kin1$^{UTR1+UTR2}$) [53]. Transfection of cells with si-Kin1^{pool}, si-Kin1^{UTR1} and si-Kin1$^{UTR1+UTR2}$ induced similar level of Kin1 knockdown and of spindle abnormalities **(Fig.16.A,B. by Dr Hitesh Patel)** [53]. Re-expression of si-RNA resistant Kin1 concomitantly to si-Kin1$^{UTR1+UTR2}$ treatment achieved exogenous Kin1 expression, but to lower levels compared to endogenous levels of Kin1 in cells treated with scrambled siRNA (si-Scram) (non-targeting siRNA) [53]. This resulted in partial rescue of the abnormal spindle phenotypes, indicating that effects of Kin1$^{UTR1+UTR2}$ on mitotic spindles were specific and not off-target.

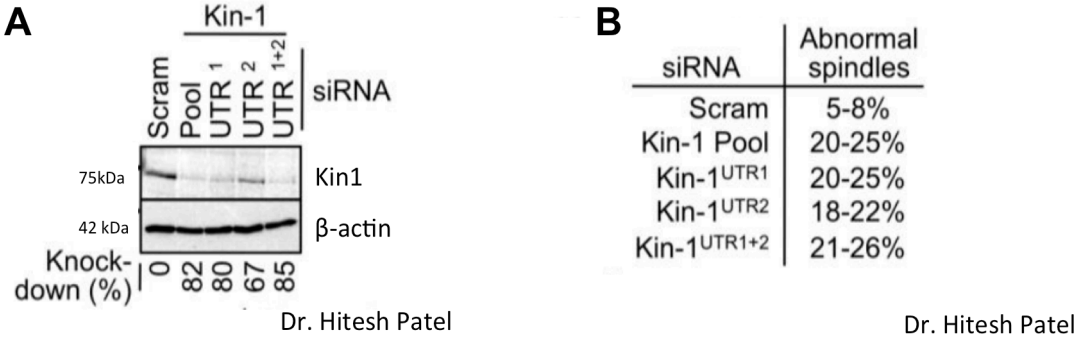

Figure 16: Depletion of Kin1 in MDA-MB-231 cells. (A) Western blot analysis of Kin1 expression in si-Scram, si-Kin1^{pool}, si-Kin1^{UTR1}, si-Kin1^{UTR2} and si-Kin1$^{UTR1+UTR2}$. β-actin was used as loading control. Quantification of Kin1 depletion (knockdown) relative to treatment with si-Scram is also shown. **(B)** Quantification of the percentage of abnormal spindles following transfection with si-Scram, si-Kin1^{pool}, si-Kin1^{UTR1}, si-Kin1^{UTR2} and si-Kin1$^{UTR1+UTR2}$. Data reproduced from [53] with permission of Dr Hitesh Patel.

We, therefore, used si-Kin1$^{UTR1+UTR2}$ for Kin1 depletion in MDA-MB-231$^{H2B:DsRed}$ cells (**Fig.17.**) and for subsequent live cell imaging experiments in MDA-MB-231$^{H2B:DsRed}$. Hereinafter, MDA-MB-231$^{H2B:DsRed}$ cells will be referred to as MDA-MB-231 cells, si-Kin1$^{UTR1+UTR2}$ as si-Kin1, and non-targeting siRNA as si-NT.

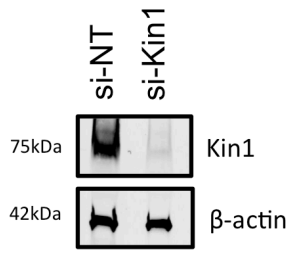

Figure 17: Depletion of Kin1 in MDA-MB-231$^{H2B:DsRed}$ cells. Western blot analysis of Kin1 expression in si-NT and si-Kin1 treated MDA-MB-231$^{H2B:DsRed}$ cells. MDA-MB-231$^{H2B:DsRed}$ cells were lysed 48 hours following si-RNA transfection. β-actin was used as loading control.

4.3. Morphological assessment of si-NT and si-Kin1 treated MDA-MB-231 cells

We observed that 48 hours post-transfection, cells transfected with si-NT had an elongated, spindle-like phenotype, whereas many si-Kin1 transfected cells adopted a rounded morphology (**Fig.18.**).

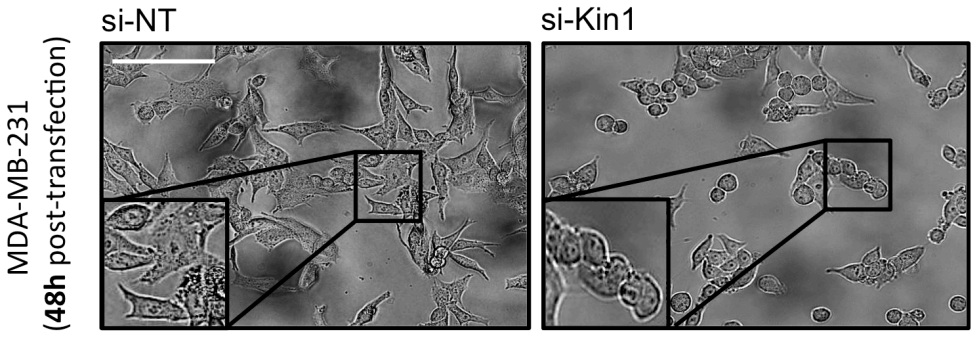

Figure 18: Morphological characterisation of si-NT and si-Kin1 treated MDA-MB-231 cells. Phase-contrast images of si-NT and si-Kin1 treated MDA-MB-231 cells 48 hours post-transfection. Scale bar represents 10μm.

4.4. Assessment of duration of mitosis and mitotic spindle phenotypes in si-NT and si-Kin1 treated MDA-MB-231 cells

Mitosis is a dynamic process divided into a series of stages, which ultimately result in segregation of duplicated chromosomes. Live cell imaging allowed us to monitor chromosome movement during all different stages of mitosis. The initial stage of mitosis is prophase, marked by nuclear envelope breakdown, initiation of chromosome condensation **(Fig.19.i.)** and emergence of spindle fibres from centrosomes. Subsequently, chromosomes continue to condense during prometaphase **(Fig.19.ii.)**, and centrosomes move towards opposite poles and mitotic spindle microtubules attach to kinetochore. In metaphase, chromosomes align at the metaphase plate **(Fig.19.iii.)** and centrosomes are located at opposite poles of the cell. Chromosome segregation occurs during anaphase, with sister chromatids being pulled at opposite poles of the cell **(Fig.19.iv.)** by spindle microtubules. At telophase, sister chromatids arrive at opposite poles and begin to decondense **(Fig.19.v.)**. For each cell we assessed cellular mitosis, from prophase **(Fig.19.i.)** to telophase **(Fig.19.v.)**.

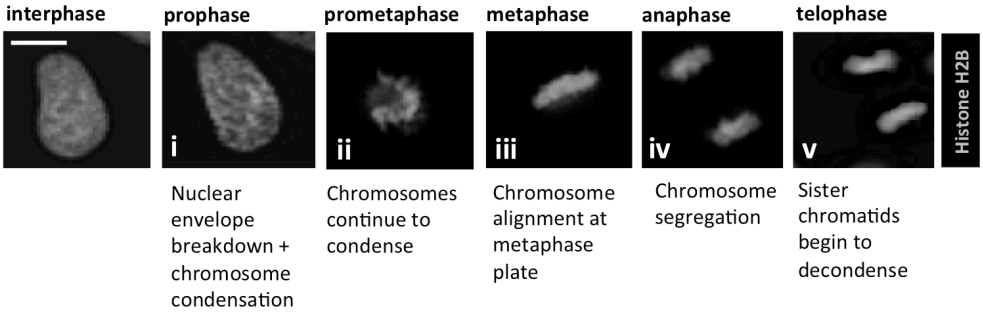

Figure 19: Assessment of mitosis in MDA-MB-231 cells from prophase to telophase with the use of live cell imaging. Representative fluorescent image of an MDA-MB-231 cell undergoing **(i):** prophase, **(ii)** prometaphase, **(iii)** metaphase, **(iv)** anaphase and **(v)** telophase. Main chromosome events that accompany each phase of mitosis are described below each representative image. Scale bar represents 5μm. For visual acuity, Histone H2B:DsRed is represented in grey.

We initiated live cell imaging 48 hours following si-RNA transfection. Initially, we measured the time that cells would spend in mitosis, from prophase until telophase. We observed that the majority of si-NT treated cells completed mitosis within 20-40 minutes, which we considered to be the typical time MDA-MB-231 cells spend to undergo mitosis **(Fig.20.)**. Any cells undertaking longer to complete mitosis (40-80 minutes) were marked as having "mitotic exit delay". No difference in the duration of mitosis was observed between si-NT and si-Kin1 treated cells **(Fig. 19)**.

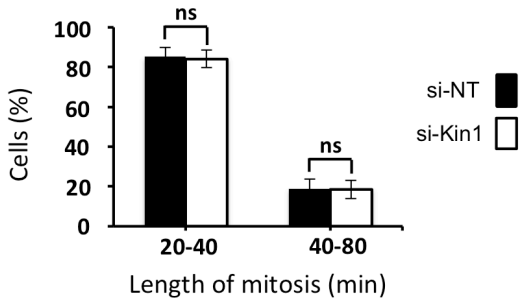

Figure 20: Assessment of duration of mitosis in si-NT and si-Kin1 treated MDA-MB-231 cells with the use of live cell imaging. Live cell imaging was performed in si-NT and si-Kin1 treated MDA-MB-231 cells that had been transfected with Histone H2B:DsRed. Quantification of length of mitosis, from prophase to telophase was performed manually. We categorised cells as spending 20-40 min or 40-80 minutes in mitosis. Results presented as mean ± SEM. Unpaired t-test; ns (non-significant): p-value > 0.05. n=4.

We also assessed spindle orientation relative to the substratum. Evaluation of chromosome alignment at the metaphase plate and segregation during anaphase enabled us to infer whether the mitotic spindle had a normal orientation, parallel to the underlying substratum, or was misorientated by being positioned in a manner off-parallel/perpendicular to the substratum **(Fig.21.A.)**. Moreover, we were able to assess chromosomal segregation fidelity, by observing whether chromosomes segregated completely or missegregated during anaphase **(Fig.21.B.)**. Finally, we evaluated whether spindles formed in a bipolar or multipolar fashion, by assessing chromosome alignment and segregation **(Fig.21.C.)**.

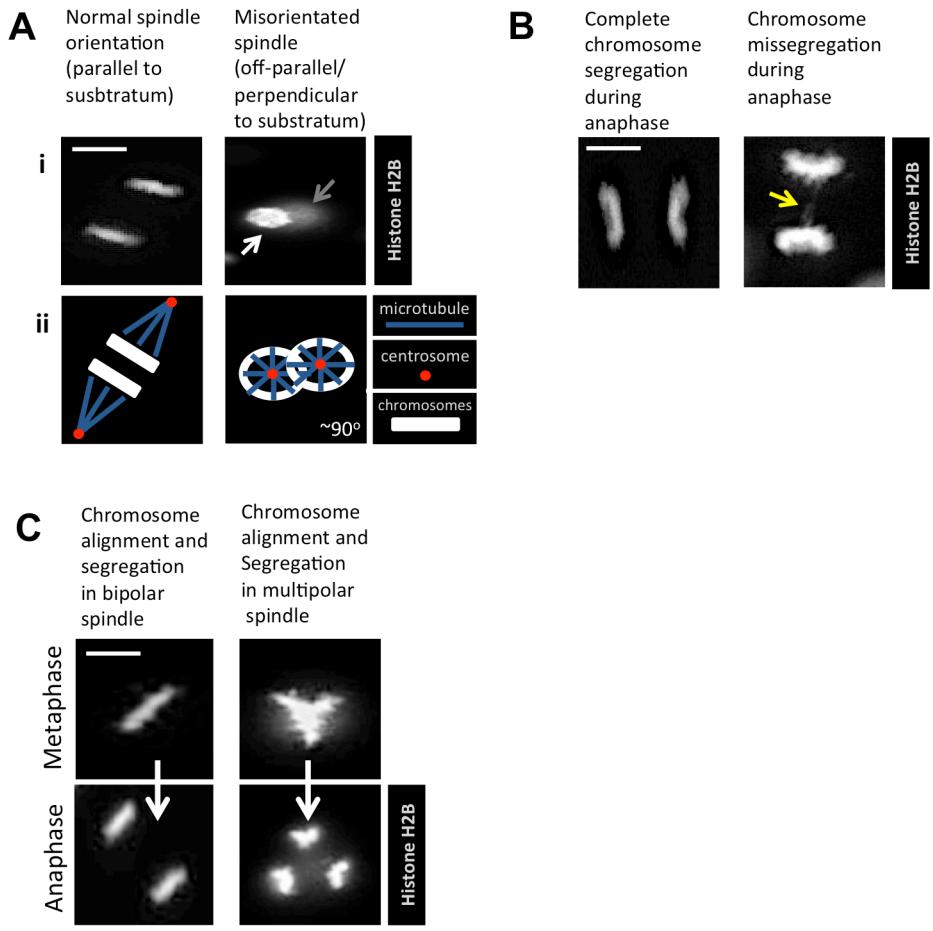

Figure 21: Phenotypic analysis of spindle orientation, chromosome segregation and spindle formation in MDA-MB-231 cells. A(i): Representative fluorescent images of anaphase chromosomes in correctly orientated spindle positioned parallel to the underlying substratum, and in incorrect, misorientated spindle positioned perpendicularly (~90^{o}) to the underlying substratum. White arrow indicates set of chromosomes of the daughter cell that proceeded to adhere to substratum immediately following anaphase. Grey arrow indicates set of chromosomes of the daughter cell in a different focal plane (out of focus), which failed to adhere to substratum immediately following anaphase. **(ii):** Schematic showing microtubules, chromosome positioning and centrosome positioning in a cell with normally orientated spindle and a cell with misorientated spindle. **B:** Representative fluorescent images of complete chromosome segregation and chromosome missegregation during anaphase. Yellow arrow indicates missegregated chromosome. **C:** Representative fluorescent images of chromosome positioning during metaphase and anaphase in a cell with bipolar spindle and a cell with multipolar spindle. **A-C:** Scale bar represents 5µm. For visual acuity, Histone H2B:DsRed is represented in grey.

We considered that cells underwent normal mitosis, when bipolar mitotic spindles orientated parallel to the underlying substrate and there was complete chromosome segregation during anaphase. Overall ~70% of si-NT treated cells underwent normal mitosis, where chromosomes segregated faultlessly during anaphase in a bipolar fashion with their spindle parallel to the underlying substrate. However, the percentage was significantly reduced to ~50% in si-Kin1 treated cells **(Fig.22.A.)**. We detected that percentage of misorientated spindles was significantly increased in si-Kin1 treated cells (~30 %) compared to si-NT treated cells (~10%) **(Fig.22.B.)**. We also observed that si-Kin1 treated cells had a significant increase in the percentage of mitotic spindles with missegregated chromosomes during anaphase compared to si-NT treated cells **(Fig.22.C.)**. Finally, we found no significant difference in the incidence of multipolar spindles following treatment with si-Kin1 **(Fig.22.D.)**.

As shown in **Figure 12**, *in vivo* short-term loss of Kin1 in mouse epidermis led to a significant reduction in ac-tub levels, and *in vitro* data from our lab showed that Kin1 depleted MDA-MB-231 cells had a significant reduction in ac-tub levels, compared to control cells [156]. Acetylation of α-tub is a well-established readout of microtubule stability [137]-[140] and is critically regulated by histone deacetylase 6 (HDAC6), which interacts with and deacetylates α-tub [163][164]. We, thus, next examined if inhibition of HDAC6 with tubacin, a broadly used, highly selective inhibitor of HDAC6 [165] was able to rescue the misorientation and missegregated chromosome phenotype. Tubacin treatment resulted in significant reduction, but partial rescue of the incidence of misorientated spindles, as the resulting percentage of misorientated spindles did not return to levels observed in si-NT treated cells **(Fig.22.B.)**. We saw full rescue of spindles with missegregated chromosomes **(Fig.22.C.)**.

The activity of tubacin was also demonstrated in recently published data from our lab, which showed rescue of ac-tub levels in tubacin-treated Kin1 depleted MDA-MB-231 mitotic and non-mitotic cells [156]. Furthermore, tubacin treatment increased microtubule stability in Kin1 depleted MDA-MB-231 cells as well as in cells treated with non-targeting siRNA, which had been previously subjected to microtubule disruption by cold treatment [156].

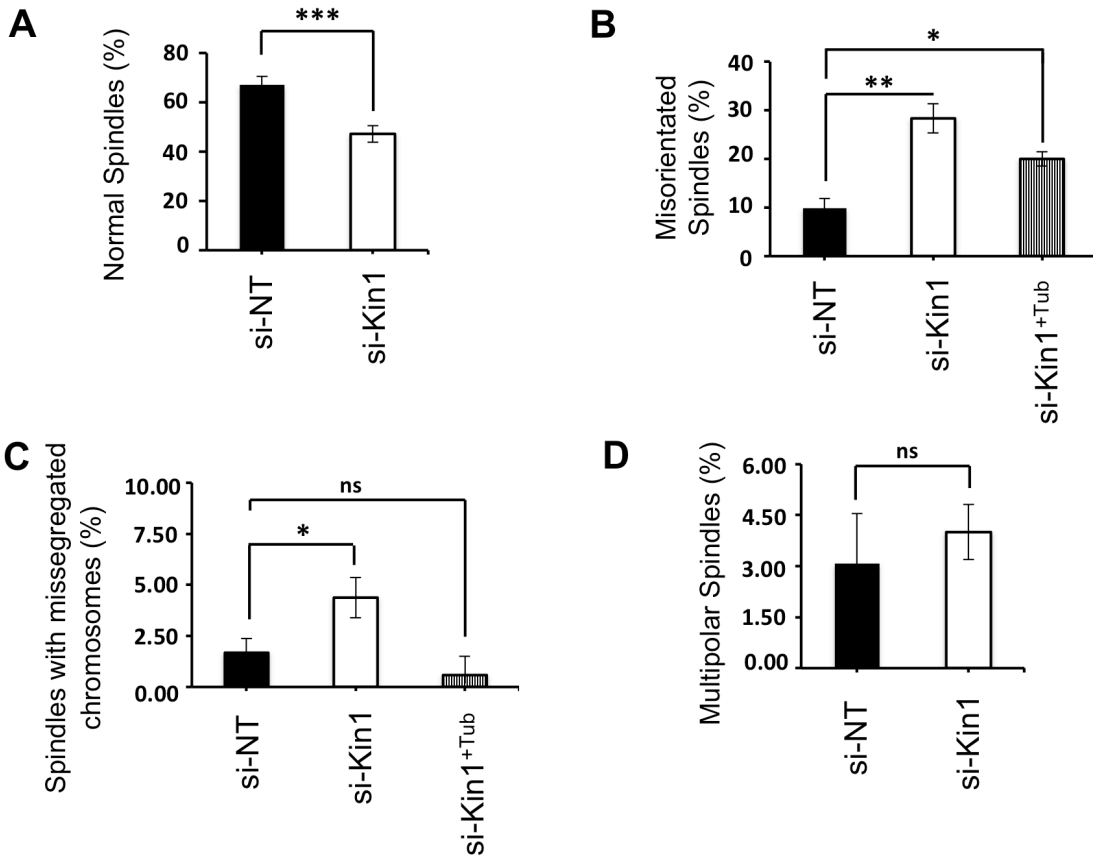

Figure 22: Assessment of spindle orientation, chromosome segregation and mitotic spindle formation in si-NT, si-Kin1 and si-Kin1^{+Tub} treated MDA-MB-231 cells with the use of live cell imaging. Live cell imaging was performed in si-NT and si-Kin1 treated MDA-MB-231 cells that had been transfected with Histone H2B:DsRed. Quantification of percentage of **A:** normal spindles (bipolar, correct spindle orientation during metaphase, complete chromosome segregation during anaphase), **B:** misorientated spindles, **C:** spindles with missegregated chromosomes and **D:** multipolar spindles was performed manually. **A-D:** Results presented as mean ± SEM. n=4. **A,C:** Unpaired t-test; p-value > 0.05, *** p-value ≤ 0.001. **B,C:** one-way ANOVA with Tukey's multiple comparison test; p-value > 0.05, * p-value ≤ 0.05, ** p-value ≤ 0.01. si-Kin1^{+Tub} marks Kin1-depleted cells treated with tubacin, 3mM.

4.5. Characterisation of HeLa$^{H2B:GFP/\beta\text{-tub:DsRed}}$ cell line

Due to the redundant nature of some functions of Kin1 and Kin2, we next set out to determine if Kin2 shares the same mitotic role of Kin1, and whether in mitosis, the two proteins have overlapping or distinct functions and can compensate for each other's depletion. We thus explored cell division in HeLa epithelial cells that express both Kin1 and Kin2 isoforms, and are widely used in studies of mitosis.

We observed mitosis in HeLa$^{H2B:GFP/\beta\text{-tub:DsRed}}$ cells **(Fig.23.)**, which will be referred to as HeLa cells, following depletion of Kin1 or Kin2 or co-depletion of Kin1 and Kin2. HeLa cell line was kindly offered to us by Dr Viji Draviam. Histone H2B chromatin marker allowed us to examine chromosomal dynamics and movement, whereas β-tubulin microtubule marker helped us assess formation and orientation of mitotic spindles in live HeLa cells during the various stages of mitosis.

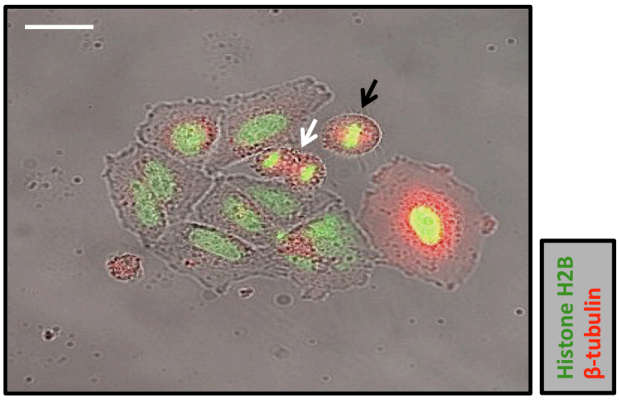

Figure 23: Expression of Histone H2B:GFP as a chromatin marker and β-tubulin:DsRed as a microtubule marker in HeLa$^{H2B:GFP/\beta\text{-tub}}$ cell line. Expression of Histone H2B:GFP and β-tubulin:DsRed allowed us to explore chromosome movement and spindle formation and orientation throughout the various stages of mitosis, respectively. White arrow indicates a mitotic cell undergoing anaphase. Black arrow indicates a mitotic cell undergoing metaphase Scale bar represents 20μm.

4.6. Individual depletion of Kin1 and Kin2, and co-depletion of Kin1 and Kin2 in HeLa cells

Kin1 depletion was achieved with the same si-Kin1 used in MDA-MB-231 cells (**Fig.17.**), and for Kin2 depletion we applied a combination of two single siRNA oligos targeted against *FERMT2* open reading frame, si-Kin2^{ORF_1} and si-Kin2^{ORF_2}, hereinafter mentioned as si-Kin2. Combination of si-Kin1 and si-Kin2 (si-Kin1+Kin2) was used for co-depletion of Kin1 and Kin2. Overall, we did not notice any compensation in protein expression of Kin1 upon depletion of Kin2 or, reciprocally, in expression of Kin2 upon depletion of Kin1 (**Fig.24.B,C.**).

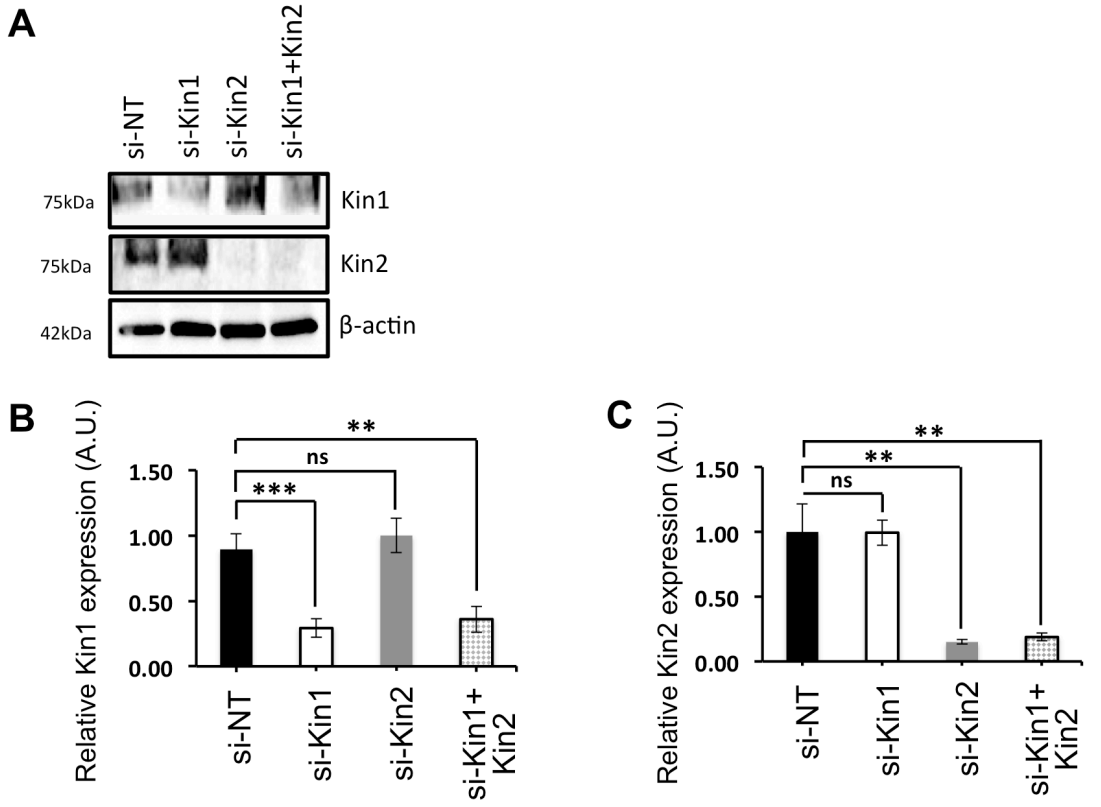

Figure 24: Individual depletion of Kin1 and Kin2, and co-depletion of Kin1+Kin2 in HeLa cells. (A) Western blot analysis of Kin1 and Kin2 expression in si-NT, si-Kin1, si-Kin2 and si-Kin1+Kin2 cells. HeLa cells were lysed 72 hours following si-RNA transfection. β-actin was used as loading control. **B,C:** Quantification of **B:** Kin1 and **C:** Kin2 expression levels was performed in relation to β-actin expression levels via band densitometric analysis with ImageJ software. For each graph, 2 independent western blots were used to calculate protein expression. Results presented as mean ± SEM. one-way ANOVA with Tukey's multiple comparison test; p-value > 0.05, * p-value ≤ 0.05, ** p-value ≤ 0.01, *** p-value ≤ 0.001.

4.7. Assessment of morphology and viability of si-Kin1, si-Kin2 and si-Kin1+Kin2 in HeLa cells

We observed that 72 hours post-transfection, cells transfected with si-NT and si-Kin1 had a cobblestone-like, polygonal morphology **(Fig.25.A.)**. However, HeLa cells treated with si-Kin2 and si-Kin1+Kin2 had lost their cobblestone morphology, with the majority of cells adopting a rounded shape **(Fig.25.A.)**.

Following, we assessed cell viability with the use of alamar blue assay, which revealed that si-Kin2 and si-Kin1+Kin2 treated cells had a ~40% reduction in viability compared to si-NT treated cells **(Fig.25.B.).** No significant change was observed between cells treated with si-NT and si-Kin1 **(Fig.25.B.)**.

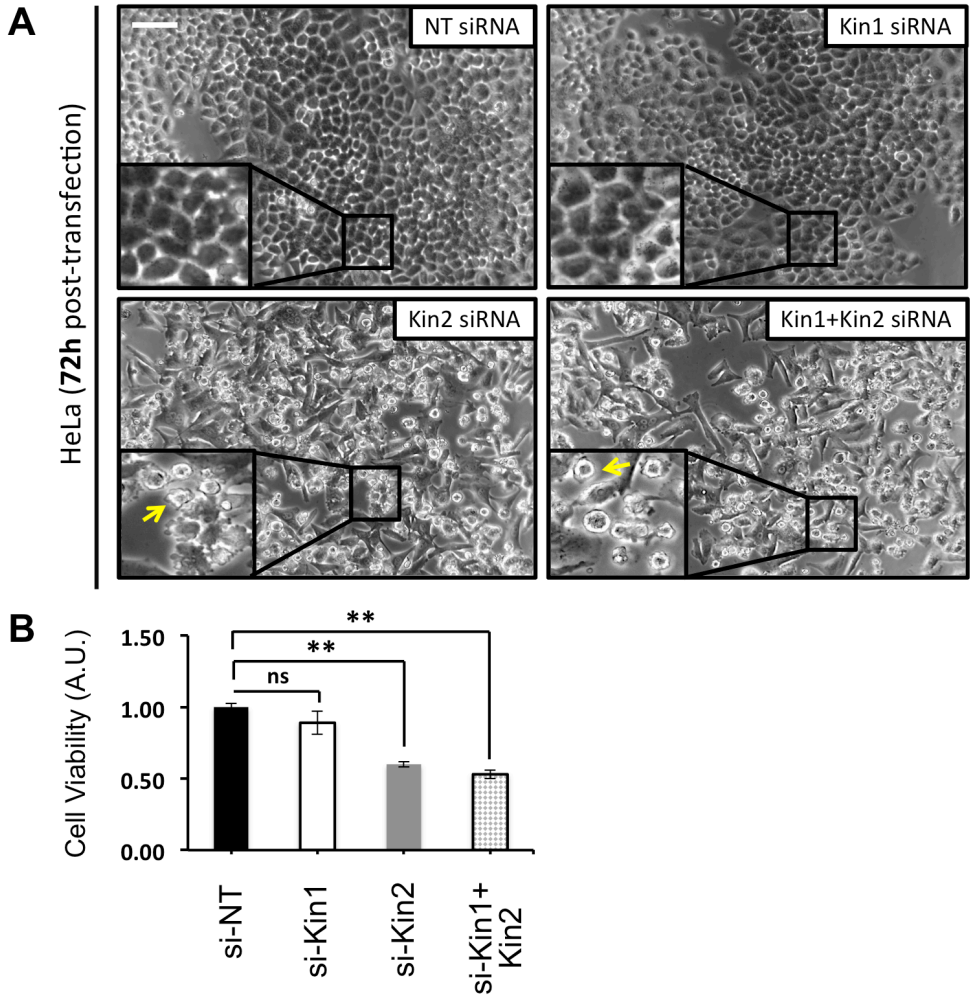

Figure 25: Morphological and viability characterisation of si-NT, si-Kin1, si-Kin2 and si-Kin1+Kin2 treated HeLa cells. A: Phase-contrast images of si-NT, si-Kin1, si-Kin2 and si-Kin1+Kin2 treated HeLa

cells 72 hours post-transfection. Yellow arrows indicate cells with a rounded morphology. Scale bar represents 125µm. **B:** Cell viability of si-NT, si-Kin1, si-Kin2 and si-Kin1+Kin2 treated HeLa cells was assessed 72 hours post-transfection with the use of an alamar blue assay. one-way ANOVA with Tukey's multiple comparison test; ns (non-significant): p-value > 0.05, ** p-value ≤ 0.01. n=3.

4.8. Assessment of duration of mitosis and mitotic spindle phenotypes in si-NT, si-Kin1, si-Kin2 and si-Kin1+Kin2 treated HeLa cells

In a similar manner to MDA-MB-231 cells (**Fig.19.**), we assessed mitosis in HeLa cells from prophase (**Fig.26.i.**) to telophase (**Fig.26.v.**).

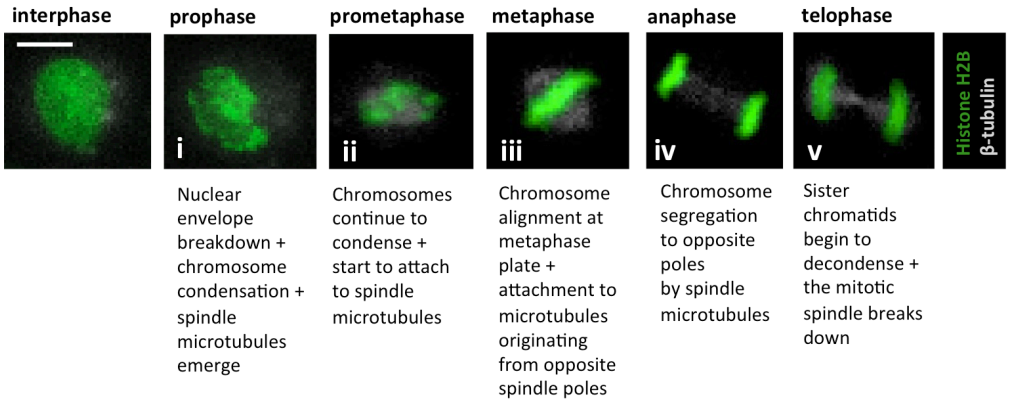

Figure 26: Assessment of mitosis in HeLa cells was performed from prophase to telophase with the use of live cell imaging. Representative fluorescent image of a HeLa cell undergoing **(i):** prophase, **(ii)** prometaphase, **(iii)** metaphase, **(iv)** anaphase and **(v)** telophase. Main chromosome and mitotic spindle events that accompany each phase of mitosis are described below each representative image. Scale bar represents 5µm. For visual acuity, β-tubulin:DsRed is represented in grey.

Live cell imaging was initiated 72 hours following si-RNA transfection. We first assessed duration of mitosis, and observed that the majority of si-NT treated HeLa cells underwent mitosis within 20-40 minutes **(Fig.27.)**, which we perceived as the normal time HeLa cells would spend to complete mitosis. Cells undertaking longer to undergo mitosis (40-80 minutes) were marked as having "mitotic exit delay".

We saw that majority of si-NT (~75%) treated cells completed mitosis within the normal time frame (20-40 minutes), which was significantly greater than the amount of si-Kin2 (~37%) and si-Kin1+Kin2 (~45%) treated cells **(Fig.27.)**. Likewise, a significantly lower amount of si-NT (~25%) treated cells had mitotic exit delay, which was significantly lower than the amount of si-Kin2 (63%) and si-Kin1+Kin2 (55%) treated cells **(Fig.27.)**. We observed no significant difference in the duration of mitosis between si-NT and si-Kin1 treated cells **(Fig.27.)**.

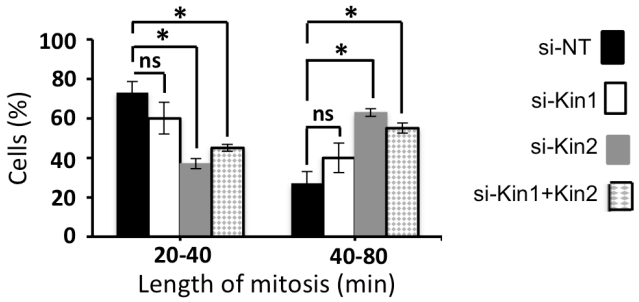

Figure 27: Assessment of duration of mitosis in si-NT, si-Kin1, si-Kin2 and si-Kin1+Kin2 treated HeLa cells with the use of live cell imaging. Live cell imaging was performed in in si-NT, si-Kin1, si-Kin2 and si-Kin1+Kin2 treated HeLa cells that had been transfected with Histone H2B:GFP and β-tubulin:DsRed. Quantification of length of mitosis, from prophase to telophase was performed manually. We categorised cells as spending 20-40 min or 40-80 minutes in mitosis. Results presented as mean ± SEM. one-way ANOVA with Tukey's multiple comparison test; ns (non-significant): p-value > 0.05, * p-value ≤ 0.05. n=4. Thick gray line indicates that statistical testing was performed within cells that received the same siRNA treatment, and compared the percentage of cells divided within 20-40 with percentage of cells divided within 40-80 minutes.

Moreover, we assessed spindle orientation relative to the substratum during metaphase (normal orientation parallel to underlying substratum vs spindle misorientation off-parallel/perpendicular to underlying substratum) **(Fig.28.A)**, chromosomal segregation fidelity during anaphase (normal, complete segregation vs chromosome missegregation) **(Fig.28.B.)**, and formation of mitotic spindle during metaphase (bipolar vs multipolar spindles) **(Fig.28.C.)**.

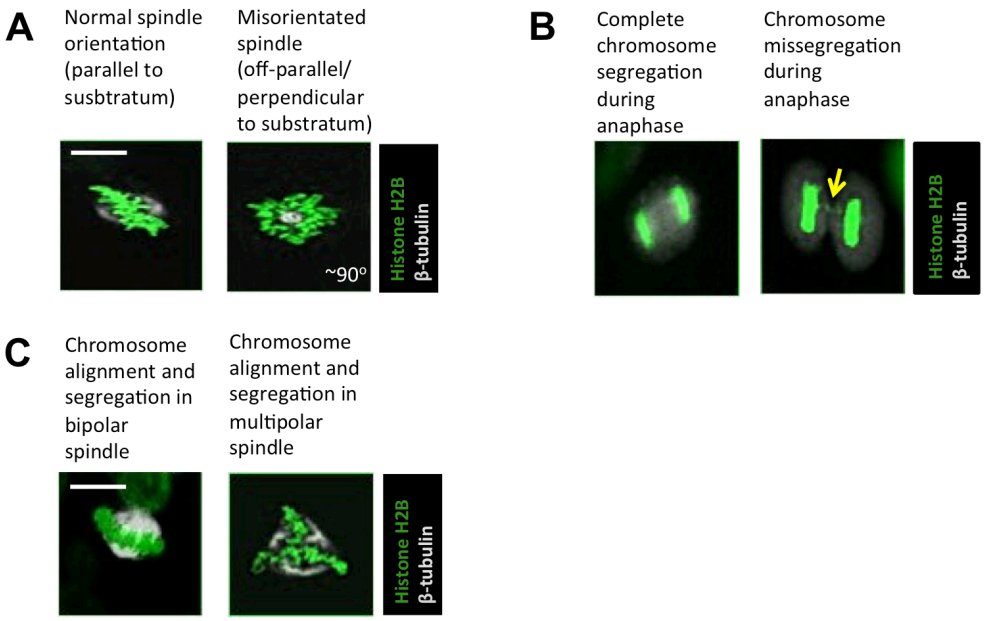

Figure 28: Phenotypic analysis of spindle orientation, chromosome segregation and spindle formation in HeLa cells with the use of live cell imaging. A: Representative fluorescent images of chromosomes and mitotic spindle in metaphase in a cell with correctly orientated spindle positioned parallel to the underlying substratum, and in a cell with incorrect, misorientated spindle positioned perpendicularly (~90^{o}) to substratum. **B:** Representative fluorescent images of complete chromosome segregation, and chromosome missegregation during anaphase. Yellow arrow indicates missegregated chromosome. **C:** Representative fluorescent images of metaphase chromosome positioning in a cell with bipolar spindle or a cell with multipolar spindle. **A-C:** Scale bar represents 5µm. For visual acuity, Histone H2B:DsRed is represented in grey.

We proceeded to analyse phenotypes of mitotic spindles following transfection of si-NT, si-Kin1, si-Kin2 and si-Kin1+Kin2 in HeLa cells. Similar to MDA-MB-231 cells, we considered normal mitosis, when HeLa cells formed bipolar mitotic spindles orientated parallel to the underlying substrate and there was complete chromosome segregation during anaphase.

Compared to si-NT treated cells (~75%), si-Kin1 (~42%), si-Kin2 (~48%) and si-Kin1+Kin2 (~41%) treated cells had significantly lower percentages of normal mitotic spindles **(Fig.29.A)**. Percentage of misorientated spindles was significantly lower in si-NT treated cells (~8%) when compared to si-Kin1 (~20%), si-Kin2 (~30%) and si-Kin1+Kin2 (~27%) treated cells **(Fig.29.B)**. Incidence of spindles with missegregated chromosomes was significantly greater in si-Kin1 (~12%) and si-Kin1+Kin2 treated cells (~12%) compared to si-NT (~4%) treated cells **(Fig.29.C)**. Finally, si-Kin2 (~6%) and si-Kin1+Kin2 (~7%) treated cells had significantly greater incidence of multipolar spindles compared to si-NT (~3%) treated cells **(Fig.29.D.)**.

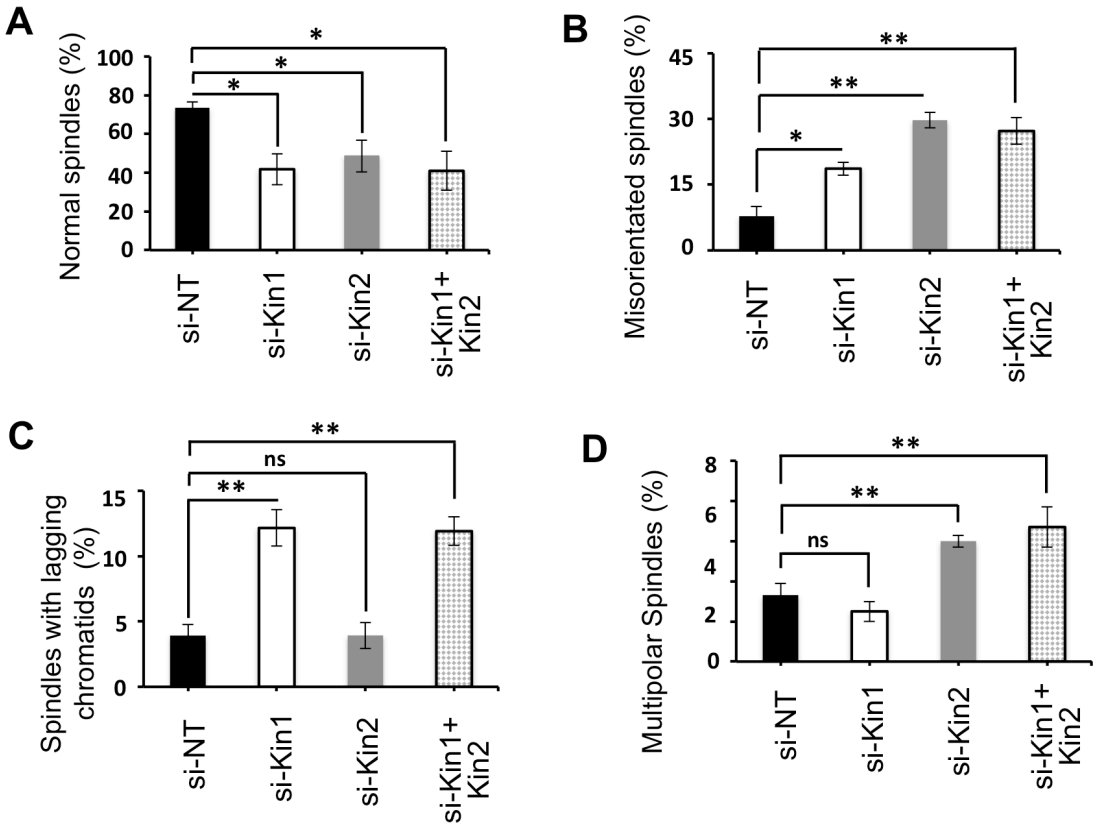

Figure 29: Assessment of mitotic spindle phenotypes in si-NT, si-Kin1, si-Kin2 and si-Kin1+Kin2 treated HeLa cells. Live cell imaging was performed in in si-NT, si-Kin1, si-Kin2 and si-Kin1+Kin2 treated HeLa cells that had been transfected with Histone H2B:GFP and β-tubulin:DsRed. Quantification of percentage of **A:** normal spindles (bipolar, correct spindle orientation during metaphase, complete chromosome segregation during anaphase), **B:** misorientated spindles, **C:** spindles with lagging chromatids and **D:** multipolar spindles was performed manually. **A-D:** Results presented as mean ± SEM. one-way ANOVA with Tukey's multiple comparison test; ns (non-significant): p-value > 0.05, * p-value ≤ 0.05, ** p-value ≤ 0.01. n=4. Total number of mitotic cells assessed: si-NT (308), si-Kin1 (281), si-Kin2 (165), si-Kin1+Kin2 (143).

4.9. Discussion

The role of Kin1 in mitosis emerged a few years ago, when *in vitro* depletion of Kin1 in MDA-MB-231 breast cancer epithelial cells was shown to increase incidence of mitotic spindle defects, as demonstrated by IF staining [53]. This prompted us to study the role of Kin1 in mitosis *in vivo*, which we described in **Chapter 3**, and characterise the role of Kin1 as well as Kin2 in mitosis in a more comprehensive manner, which was the aim of this chapter. We achieved this with the use of live cell imaging that, contrary to the static nature of IF, enabled us to analyse the dynamic and temporal nature of mitosis.

4.9.1. Kin1 regulates chromosome segregation in MDA-MB-231 cells

Live cell imaging uncovered a novel role for Kin1 in chromosome segregation in MDA-MB-231 cells. Erroneous chromosomal segregation is often a result of hypostable spindles, as observed after *in vitro* depletion of spindle-stabilising proteins such as EB1 [166] and csi2p [167].

Notably, recent data showed that α-tub acetyltransferase TgATAT promoted α-tub acetylation, which enhanced spindle stability and was required for correct chromosome segregation in Toxoplasma [168]. This finding linked chromosomal segregation fidelity, microtubule stability and α-tub acetylation, a connection that was also highlighted in our data.

Our *in vivo* observations **(Chapter 3)** and recently published data from our lab showed that loss or depletion of Kin1 in mouse epidermis and MDA-MB-231 cells, respectively, significantly reduced levels of acetylated α-tub **(Fig.12.,** [156]), which is indicative of reduced microtubule stability [137]-[140]. One of the main regulators of ac-tub levels is HDAC6 [161][162]. Data from our lab showed that application of tubacin, a selective HDAC6 inhibitor [163], rescued the reduction in ac-tub levels, in mitotic and interphase cells, and spindle instability in MDA-MB-231 cells [156]. Additionally, incubation with tubacin

followed by gradual washout resulted in si-NT and si-Kin1 treated cells gradually reducing ac-tub levels, which, however, did not occur in HDAC6-depleted cells [53]. Overall, these data showed that Kin1 regulated ac-tub levels and microtubule stability in an HDAC6-dependent manner in MDA-MB-231 cells. By showing full rescue of chromosome missegregation defects in tubacin treated, Kin1 depleted cells **(Fig.22.C.)**, our observations demonstrated that Kin1 controls chromosome segregation fidelity during mitosis via HDAC6 mediated regulation of ac-tub levels and, hence, microtubule stability.

Interestingly, our lab showed that ac-tub levels were similar after expression of wild-type Kin1 and Kin1-W612A integrin-binding mutant in Kin1-depleted cells, demonstrating that Kin1 regulated ac-tub in an integrin-independent manner [156]. This suggests that in our findings Kin1 may regulate chromosome segregation fidelity and ac-tub levels independent of its role in integrin activation.

4.9.2. Kin1 regulates spindle orientation in MDA-MB-231 cells

Live cell imaging also confirmed defects in mitotic spindle orientation in MDA-MB-231 cells upon depletion of Kin1 **(Fig.22.B.)**, which we also observed *in vivo* following loss of Kin1 in mouse epidermis **(Fig.11.C.)**. These findings mirrored previous IF data, showing increased spindle orientation abnormalities in Kin1-depleted MDA-MB-231 cells [53].

Our data showed that the role of Kin1 in spindle orientation in MDA-MB-231 cells also occurs via regulation of HDAC6, as tubacin-mediated HDAC6 inhibition partially rescued misorientation phenotype in Kin1 depleted cells **(Fig.22.B.)**. Nevertheless, partial rescue of abnormal phenotype implies that HDAC6-mediated deacetylation of ac-tub levels is not be the sole cause of spindle misorientation in these cells.

4.9.3. Kin1 and Kin2 display overlapping and distinct functions in regulating mitotic homeostasis

As Kin1 and Kin2 have both overlapping and distinct functions in various biological processes, we questioned whether in HeLa cells the two proteins adopt the same or distinct roles to regulate mitotic homeostasis. After examination of cell division in Kin1, Kin2 and Kin1+Kin2 depleted HeLa cells with the use of live-cell imaging, it became apparent that Kin1 and Kin2 modulated various mitotic features in an overlapping or distinct manner. In particular, we demonstrated that in HeLa cells, Kin1 and Kin2 were both important for spindle orientation **(Fig.29.B.)** while Kin1 regulated segregation fidelity **(Fig.29.C.)**, and Kin2 was important for spindle formation **(Fig.29.D.)**. According to literature, these mitotic features can be regulated in integrin dependent and/or independent ways.

Although the mechanisms that lead to formation of multipolar spindles have not been fully elucidated, perturbed β1 integrin activation was shown as one of the main causes of this phenotype [147][169], raising the possibility that Kin2 controls spindle formation via its role in β1 integrin activation. If this is true, then lack of multipolar spindles following Kin1 depletion could also suggest that Kin2 may play a greater role in integrin activation compared to Kin1 in HeLa cells.

As discussed earlier, chromosomal segregation fidelity depends on microtubule stability mechanisms, such as acetylation of α-tub [168], which we detected in MDA-MB-231 cells. As Kin1 promoted α-tub acetylation independent of integrin activation in MDA-MB-231 cells [156], it is likely that Kin1 could also exert its role in chromosome segregation in HeLa cells via integrin-independent microtubule stability.

Finally, as reviewed extensively in **Chapter 3, Section 3.6.1.**, spindle orientation can occur in various integrin-dependent ways, such as cell-substrate adhesion, and integrin-independent ways, such as via regulation of microtubule stability [137]. Kin1 and Kin2 play a critical role in β1 integrin activation, but not always to the same extent [88]. It is, therefore, likely that greater incidence of spindle misorientation in Kin2 depleted cells compared to Kin1 depleted cells could reflect that in HeLa cells Kin2 may play a greater role in integrin activation compared to Kin1. Nevertheless, this could also result from the fact that Kin1 and Kin2 may control spindle orientation via distinct pathways. For example, Kin1 may control spindle orientation in an integrin-independent pathway, via its role in microtubule stability [156], whereas Kin2 may function towards spindle orientation via its role in β1 integrin activation.

It is, therefore, important to analyse β1 integrin activation after individual depletion or co-depletion of Kin1 and Kin2 in our model, which will help us appreciate if and to which extent Kin1 and Kin2 activate β1 integrins in HeLa cells. Use of W612A and W615A Kin1 and Kin2 β1 integrin-binding mutants, respectively [49][53][99][170], will help us define whether Kin1 and Kin2 control features of mitosis, such as spindle formation and orientation, in an integrin dependent manner.

4.9.4. Kin1 and Kin2 display distinct functions in regulating cell morphology

Besides differential regulation of mitotic features, our findings showed that Kin1 and Kin2 do not exhibit the same role in control of cell morphology. In HeLa cells, Kin2, but not Kin1 depletion led to aberrant cell phenotype (**Fig.25.**), implying that Kin2, contrary to Kin1, may exert a role in cell morphology regulation in this mode. Interestingly, in MDA-MB-231 cells, where Kin1, but not Kin2 is expressed, Kin1 played a role in morphology

(**Fig.18.**), indicating that in that model Kin1 could adopt some functions that in other cell lines, such as HeLa cells, would otherwise be carried out by Kin2.

Rounded cell shape, similar to the one observed in Kin2 and Kin1+Kin2 depleted HeLa cells, was observed in talin-depleted fibroblasts and mouse embryonic stem cells, along with compromised focal adhesion assembly as well as reduced cell-substrate adhesion and decreased expression of total or active β1 integrin [171][87]. Individual loss of Kin1 or Kin2 in different models impairs the formation of focal adhesions, as seen in KS keratinocytes and Kin2-deleted endoderm cells, respectively [94][99]. However, when individual depletion of Kin1 and Kin2 were compared concomitantly in immortalised keratinocytes, effect of Kin2 depletion in focal adhesion formation was much more severe when compared to that of Kin1 depletion, which only affected focal adhesions to a negligible level [88]. We have yet to examine whether implications of Kin2 depletion in HeLa cell morphology are accompanied by defects in β1 integrin-mediated cell adhesion, and whether Kin1 and Kin2 control this process in a differential manner as well.

4.9.5. Summary and future work

Overall, our findings indicated overlapping and different roles of Kin1 and Kin2 in mitotic homeostasis, as individual depletion of the two proteins affected mitosis in similar and separate ways. Distinct Kin1 and Kin2 functions have been reported previously in keratinocytes in cell-cell contact and focal adhesion formation [88]. Examination of rescue of mitotic abnormalities following endogenous depletion of Kin1 and Kin2 and concomitant expression of si-RNA-resistant Kin1 and Kin2, along with use of individual siRNA oligos to deplete Kin1 and Kin2 in HeLa cells, will allow us to evade potential siRNA off-target effects. This, together with re-expression of integrin-binding Kin1 and Kin2 mutants will help to further elucidate Kin1 and Kin2 roles in mitotic homeostasis.

Chapter 5:

exploring the roles of Kin1 in SCC

Kin1 is documented to promote carcinogenesis, invasion and metastasis. It is overexpressed in lung, colon and bladder cancer and promotes progression of pancreatic cancer via enhancement of cell migration and invasion [110][111]. Kin1 was also shown to promote breast cancer lung metastasis [115], and in hepatocellular carcinoma its expression positively correlated with tumour size and aggressiveness, status of metastasis and unfavourable overall survival [112].

Paradoxically, absence of Kin1 also promotes oncogenesis, as KS patients have a propensity to develop aggressive, cutaneous SCC [9][10][13]. A cohort study of 62 patients revealed that 70% of KS patients over 45 years old had developed SCC [9], making it one of the biggest complications within the KS patient population. Little is known about the mechanism that predisposes KS patients to SCC. There is a single *in vivo* study that defines a tumour suppressor role for Kin1 in the skin via control of homeostasis of cutaneous epithelial stem cells, by maintaining a balance between Wnt-β-catenin-mediated growth-stimulating signals and TGF-β-mediated growth-supressing signals [119].

However, to date, no study has addressed the role of Kin1 in development and progression of this pathology. SCC that develops particularly in limbs of KS patients is extremely aggressive and metastatic, and sometimes fatal, often necessitating amputation and lymph node excision [2][13][14]. Search for a comprehensive explanation for the function of Kin1 in KS-developed SCC tumours will provide a mechanistic aetiology for the tumour biology and aggressiveness, and potentially improve patient treatment and overall

prognosis. Thus, here we sought to define a role for Kin1 in cutaneous SCC *in vitro* and *in vivo*.

Specific aims of this chapter include:

1. Characterisation of *in vitro* SCC model of conditional *Fermt1* knockout and re-expression of wild type and integrin-binding mutant *Fermt1*.
2. Development and characterisation of *in vivo* mouse model of SCC, generated with the use of *in vitro* SCC model.

5.1. Characterisation of mouse SCC cell lines

To address the role of Kin1 in cutaneous SCC, we used mouse SCC cell lines that had previously been generated in the lab in K14-Cre-Kin1$^{fl/fl}$ mice, via the application of the well-established two-stage protocol of cutaneous chemical carcinogenesis [126][127] **(Fig.30.A.)**. In particular, application of chemical initiator mutagen DMBA **(Fig.30.A.1.)** was followed by application of pro-inflammatory, pro-proliferative TPA **(Fig.30.A.2.)**, leading to the formation of benign cutaneous papillomas, some of which progressed to form cutaneous SCC tumours **(Fig.30.A.3.)** in 3 K14-Cre-Kin1$^{fl/fl}$ mice (mouse no.117, no.130 and no.145). Subsequent isolation **(Fig.30.A.4.)** and culture **(Fig.30.A.5.)** of SCC cells generated 3 mouse SCC cell lines (117 SCC cells, 130 SCC cells, 145 SCC cells) (Dr Hitesh Patel) with variable expression levels of Kin1 and Kin2 **(Fig.30.B.)**.

We observed that mouse SCC cells were characterised by an overall spindle-shaped morphology **(Fig.30.C.)**. Similar spindle-like morphology was previously observed in mouse SCC cells isolated from DMBA-TPA-induced tumours, and was accompanied by reduced expression of E-cadherin when compared to normal epidermis [172]. In agreement with this observation, we saw that E-cadherin expression was virtually absent from mouse SCC cell lines, in contrast to normal epidermal keratinocytes **(Fig.30.D.)**.

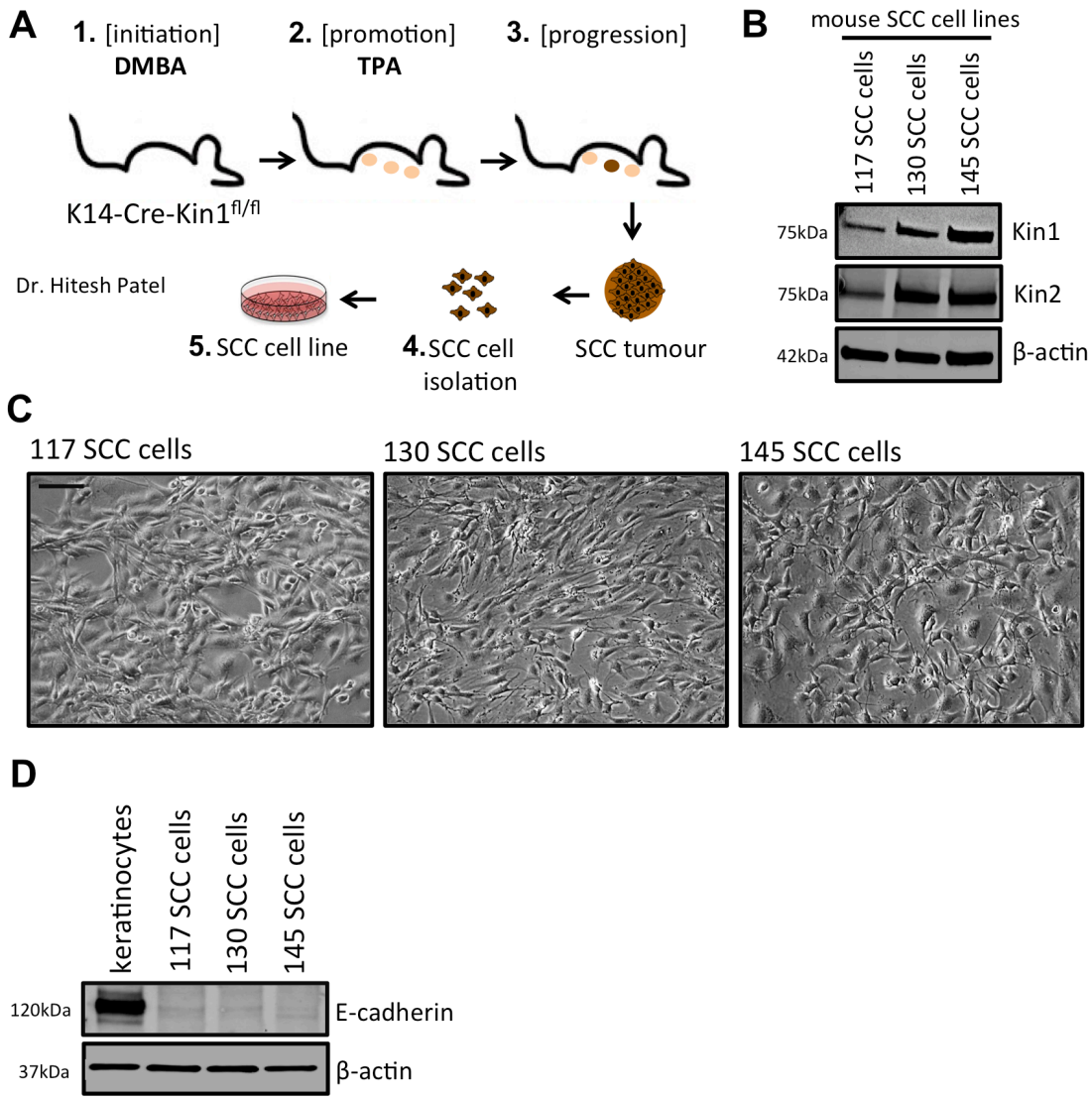

Figure 30: Development and characterisation of mouse SCC cell lines. 3 mouse SCC cell lines (117 SCC cells, 130 SCC cells, 145 SCC cells) had been generated following application of a 2-stage chemical carcinogenesis protocol in 3 K14-Cre-Kin1$^{fl/fl}$ mice (mouse no.117, no.130, no.145). **A:** As instructed by the carcinogenesis protocol **(1.)** application of DMBA, a chemical initiator mutagen, was followed by **(2.)** application of TPA, a pro-inflammatory, pro-proliferative compound. **(3.)** A number of the resulting benign papillomas subsequently progressed to SCC tumours from which cells were **(4.)** isolated and **(5.)** cultured (Dr Hitesh Patel). **B:** Western blot analysis of Kin1 and Kin2 expression in 117, 130 and 145 SCC cells. Each lane contains 15µg of lysate. β-actin was used as loading control. **C:** Representative phase-contrast images of 117, 130 and 145 SCC cells in two-dimensional cell culture. Scale bar represents 125µm. **D:** Western blot analysis of E-cadherin expression in mouse tail keratinocytes, and 117, 130 and 145 SCC cells. Each lane contains 10µg of lysate. β-actin was used as loading control.

5.2. Cre-Lox recombination system-mediated conditional knockout of *Fermt1* in mouse SCC cells

We next used a mouse SCC cell line, previously developed in the lab as follows (Dr Hitesh Patel), in which *Fermt1* deletion recapitulated the Kin1-null background of SCC tumours developed in KS patients.

To achieve *Fertm1* knockout, 117 SCC cells had been treated with 4OHT for 48 hours (117 SCC_{+4OHT}). This induced Cre-mediated genetic deletion of the *Fermt1* gene [125], as 117 SCC cells had been generated in a K14-Cre-$Kin1^{fl/fl}$ mouse **(Fig.30.A.)**. Heterogeneity within a tumour mass and, therefore, a tumour-derived cell line, as well as variability in the success rate of Cre-loxP-mediated gene deletion, exposed the need for identification of individual $Kin1^{null}$ cells within the 117 SCC_{+4OHT} cell population. As a result, single-cell cloning had been employed and aimed to isolate multiple $Kin1^{null}$ SCC cell clones that would, ultimately, be expanded into cell lines. This would enable evaluation of the biological reproducibility and exclude the possibility that any differences between $Kin1^{null}$ and $Kin1^{wt}$ SCC cells were due to clonal variation. However, only a single $Kin1^{null}$ SCC clone had been detected, thus reflecting a low success-rate of Cre-loxP-mediated gene deletion in this system.

5.3. Characterisation of Kin1^{null}, Kin1^{wt} and Kin1^{AA} mouse SCC cell lines

Due to potential variation of individual clones within a cell line population, comparison between the Kin1^{null} clonal SCC cell line with a clonal cell line in which *Fermt1* was still expressed was avoided. Instead, we sought to compare how does re-expression of wild type or mutant *Fermt1* on a Kin1^{null} background regulate SCC growth and behaviour, both *in vitro* and *in vivo*.

For this, we used cell lines that had been previously prepared in the lab (Dr Hitesh Patel) as follows. Kin1^{null} clone obtained via Cre-LoxP-mediated *Fermt1* deletion **(Chapter 5, Section 5.2)** was expanded into a Kin1^{null} SCC cell line to which wild type *Fermt1* (**Fig.31.A.ii.**) and QW611/612AA *Fermt1* mutant, encoding Kin1 unable to interact with integrins (**Fig.31.A.iii.**), were introduced with the use of pWZL retroviral vector. Use of SCC cell line carrying QW611/612AA *Fermt1* mutation (hereinafter referred to as Kin1^{AA} SCC cell line) allowed us to examine whether the role of Kin1 in SCC is dependent upon the protein's ability to bind and activate integrins.

We initially confirmed loss of Kin1 in Kin1^{null} SCC cell line **(Fig.31.B-C.).** Overall, there was differential expression of Kin1 across Kin1^{null}, Kin1^{wt} and Kin1^{AA} SCC cells, and we observed that Kin1^{AA} SCC cells expressed the highest levels of Kin1 amongst the three SCC cell lines **(Fig.31.C.)**. A slight, non-significant difference was observed in expression of Kin2, according to which Kin1^{AA} SCC cells expressed the lowest levels of Kin2, whereas Kin1^{null} SCC cells the highest **(Fig.31.D.)**. Finally, we saw that all cell lines displayed an elongated, spindle-shaped morphology, and there was no phenotypic difference between them **(Fig.31.E.)**.

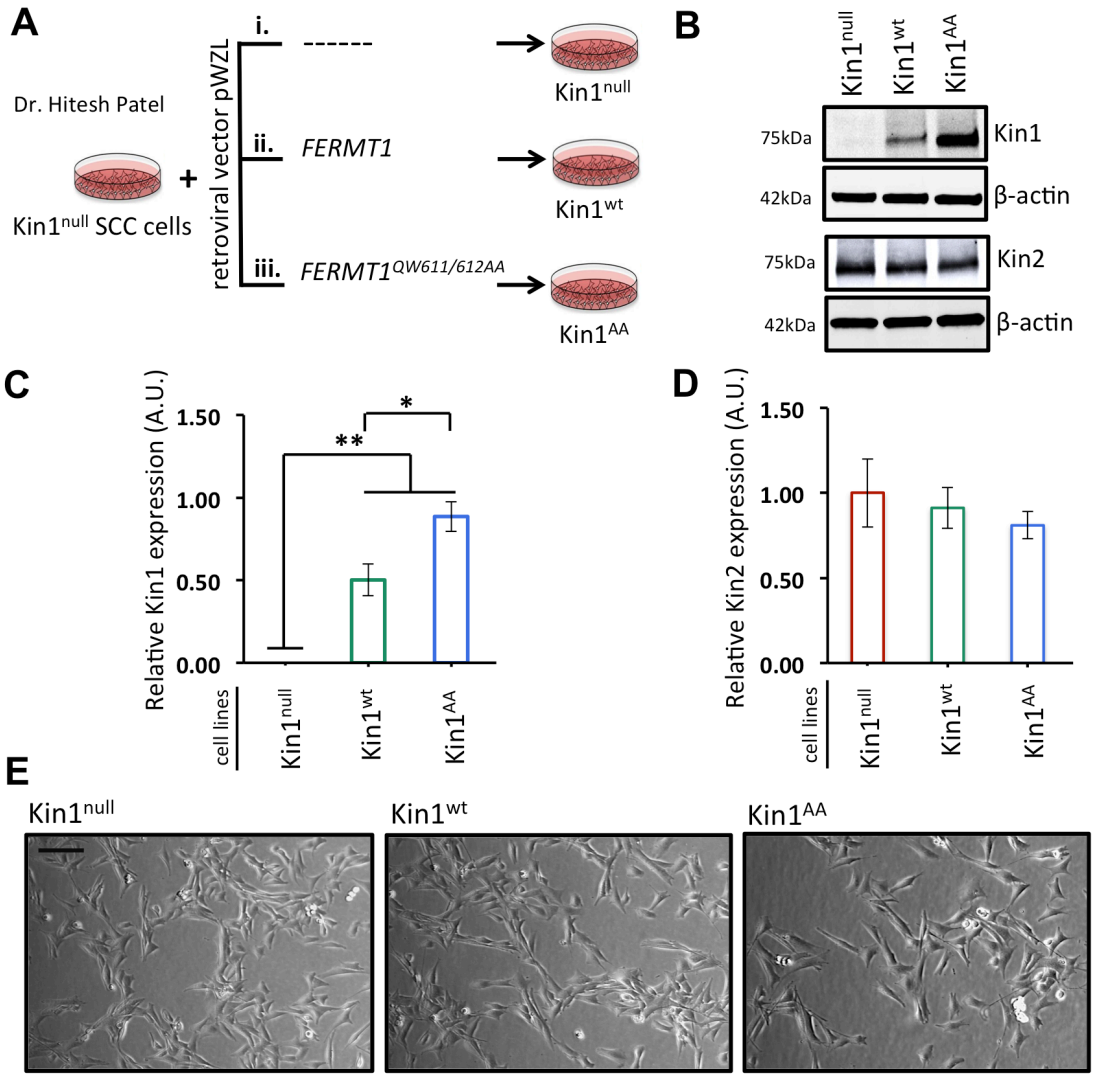

Figure 31: Development and characterisation of *in vitro* mouse SCC model: Kin1^{null}, Kin1^{wt} and Kin1^{AA} SCC cell lines. A: Kin1^{null}, Kin1^{wt} and Kin1^{AA} SCC cell lines had been generated by Dr Hitesh Patel as follows. Kin1^{null} clonal SCC cell line (Kin1^{null} SCC cells) was infected with **(i)** an empty pWZL retroviral vector (Kin1^{null}), **(ii)** pWZL vector with a wild-type *Fermt1* (Kin1^{wt}) or **(iii)** pWZL vector with a *Fermt1*$^{QW611/612AA}$ (Kin1^{AA}). **B:** Western blot analysis of Kin1 and Kin2 expression in Kin1^{null}, Kin1^{wt} and Kin1^{AA} SCC cell lines. Each lane contains 15µg of lysate. β-actin was used as loading control. **C-D:** Quantification of **C:** Kin1 and **D:** Kin2 expression levels was performed in relation to β-actin expression levels via band densitometric analysis with ImageJ software. For each graph, 3 independent western blots were used to calculate protein expression. Results presented as mean ± SEM. one-way ANOVA with Tukey's multiple comparison test; p-value > 0.05, * p-value ≤ 0.05, ** p-value ≤ 0.01. **E:** Representative phase-contrast images of Kin1^{null}, Kin1^{wt} and Kin1^{AA} SCC cell lines in two-dimensional cell culture. Scale bar represents 125µm.

5.4. Subcellular localisation of Kin1 and Kin2 within Kin1^{null}, Kin1^{wt} and Kin1^{AA} mouse SCC cell lines

All members of the kindlin protein family are localised at focal adhesions where they bind to and activate integrins and, ultimately, contribute to the connection between actin cytoskeleton and extracellular matrix [49][97][99][100][173]. We, thus, inspected localisation of Kin1 and Kin2 in subcellular compartments of Kin1^{null}, Kin1^{wt} and Kin1^{AA} SCC cell lines, including focal adhesions, with the use of IF.

As expected, Kin1 was absent from Kin1^{null} SCC cells, and was enriched at focal adhesions, where it colocalised with FAK, as well as in nuclei of Kin1^{wt} SCC cells **(Fig.32.A.)**. Kin1 also localised at focal adhesions and in nuclei of Kin1^{AA} SCC cells **(Fig.32.A.)**. We detected localisation of Kin2 at focal adhesions, but not in nuclei, in all SCC cell lines **(Fig.32.B.)**. Finally, we detected punctate cytoplasmic expression of Kin1 and Kin2 across all lines **(Fig.32.A-B.).**

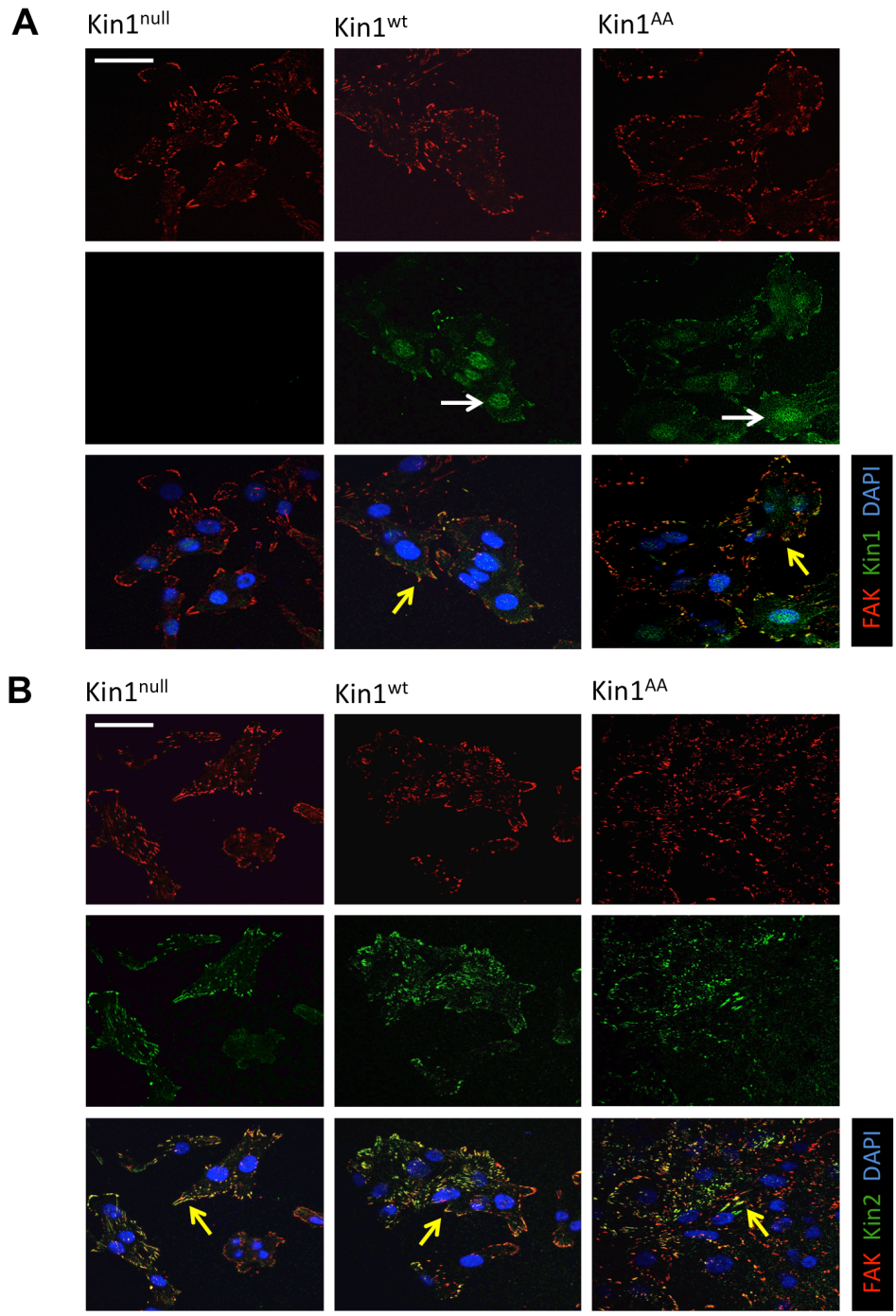

Figure 32: Subcellular localisation of Kin1 and Kin2 in Kin1^{null}, Kin1^{wt} and Kin1^{AA} SCC cell lines. A-B: Representative IF images of **A:** Kin1 and **B:** Kin2 subcellular localisation in Kin1^{null}, Kin1^{wt} and Kin1^{AA} SCC cell lines. White arrows indicate nuclear localisation of Kin1. Yellow arrows indicate colocalisation of Kin1 or Kin2 with FAK at focal adhesions. Scale bar represents 50µm.

5.5. *In vitro* assessment of proliferation and clonogenicity in Kin1^{null}, Kin1^{wt} and Kin1^{AA} mouse SCC cell lines

We next set out to explore the *in vitro* role of Kin1 in proliferation of the three mouse SCC cell lines. A growing body of evidence suggests that cellular functions including proliferation [174][175], cell-ECM interactions [176], as well as gene and protein expression [177][178] vary between two-dimensional (2D) and three-dimensional (3D) cultures, which prompted us to examine cell proliferation in both systems.

We initially assessed the proliferation of Kin1^{null}, Kin1^{wt} and Kin1^{AA} SCC cell lines in 2D conditions. To achieve this, we seeded cells at low density on artificial substrate, which enabled the formation of 2D monolayers (**Fig.33.A.**). We then monitored cell density as a marker for proliferation in a 2D environment, in real time over the course of four days with the use of time-lapse microscopy. We observed no significant difference in cell density, and, thus, proliferation rate of Kin1^{null}, Kin1^{wt} and Kin1^{AA} cells in 2D culture conditions (**Fig.33.B.**).

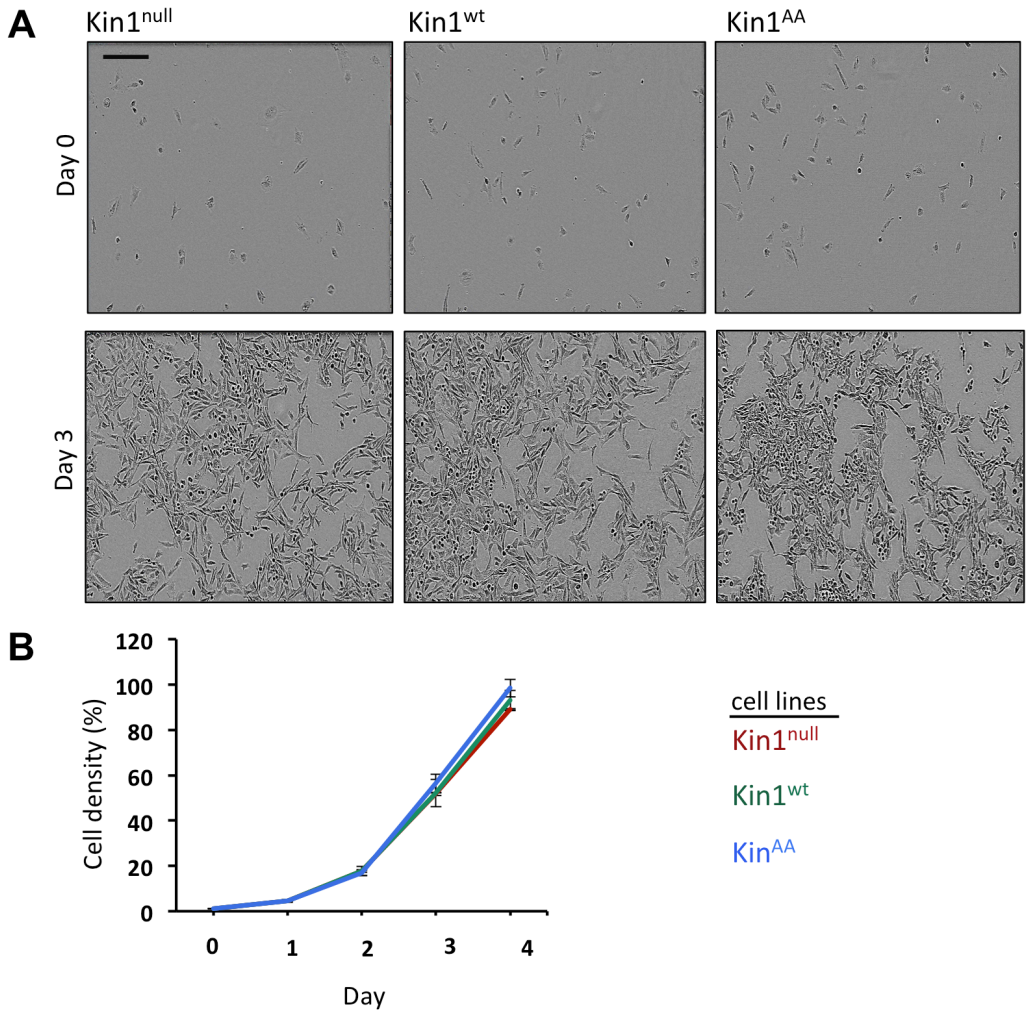

Figure 33: *In vitro* assessment of proliferation of Kin1^{null}, Kin1^{wt} and Kin1^{AA} SCC cell lines in 2D cell culture. Kin1^{null}, Kin1^{wt} and Kin1^{AA} SCC cells were seeded at low density on artificial substrate where they proceeded to proliferate and form 2D monolayers. Post-seeding, phase-contrast images of cells were captured every 3 hours by Incucyte live cell analysis system, and were, eventually, combined to form time-lapse microscopy movies. **A:** Representative phase-contrast images captured on Day0 and Day3 post-seeding. Scale bar represents 30µm. **B:** Quantification of cell density (% of well area covered by cells) of Kin1^{null}, Kin1^{wt} and Kin1^{AA} SCC cells was performed at Day0, Day1, Day2, Day3 and Day4 post-seeding, using data generated automatically by Incucyte control software. Results presented as mean ± SEM. one-way ANOVA with Tukey's multiple comparison test; p-value > 0.05.

We proceeded to evaluate proliferation of the three SCC cell lines in a 3D environment with the use of methylcellulose-over-agarose proliferation assay. Single-cell suspensions of Kin1^{null}, Kin1^{wt} and Kin1^{AA} SCC cells were seeded on low-adherent agarose plates with methylcellulose media, which facilitated the gradual growth of single cells into 3D spheroids **(Fig.34.A.)**. Cell proliferation was reflected by spheroid growth, monitored by measuring the average area of individual 3D spheroids from Day1, which is when spheroids started forming, until Day6 post-seeding.

We observed growth in all spheroids from Day1 until Day3, after which it proceeded to decline in Kin1^{wt} and Kin1^{AA} spheroids and arrest in Kin1^{null} spheroids **(Fig.34.B.)**. We found that by Day3, Kin1^{null} spheroids were significantly larger when compared to Kin1^{wt} and Kin1^{AA} cell lines **(Fig.34.B.)**. Despite not reaching significance following statistical analysis, we observed that Kin1^{wt} spheroids were slightly larger than Kin1^{AA} spheroids at Day3 and Day6 **(Fig.34.B.)**.

By Day3 there was still a number of Kin1^{null}, Kin1^{wt} and Kin1^{AA} single cells, which had not managed to grow into spheroids. We thus, proceeded to assess the clonogenicity of each cell line, by measuring the percentage of Kin1^{null}, Kin1^{wt} and Kin1^{AA} 3D spheroids that had formed by Day3. Following analysis, we detected that Kin1^{null} SCC cells had formed a significantly greater percentage of 3D spheroids and, thus, had the highest clonogenicity when compared to Kin1^{wt} and Kin1^{AA} SCC cells **(Fig.34.C.)**.

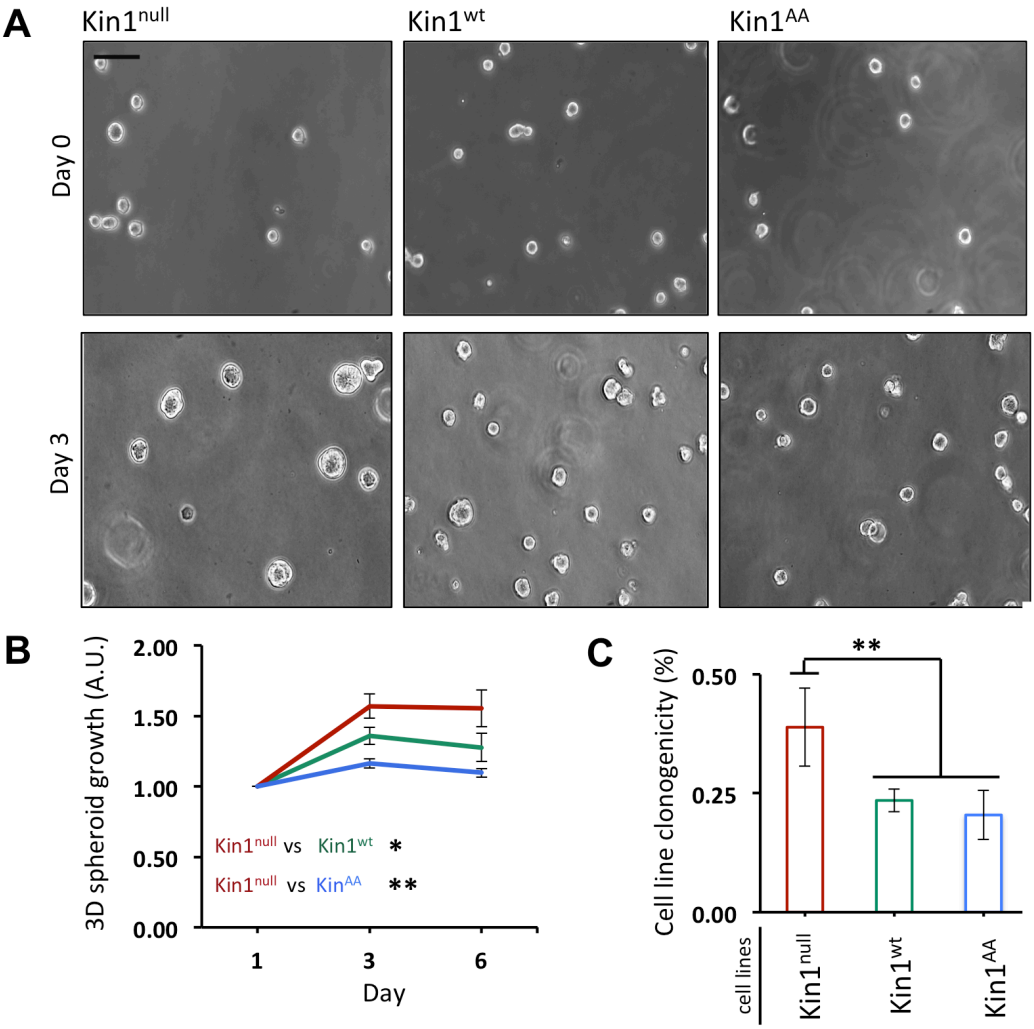

Figure 34: *In vitro* assessment of proliferation and clonogenicity of Kin1^{null}, Kin1^{wt} and Kin1^{AA} SCC cell lines in 3D cell culture. Single-cell suspension of Kin1^{null}, Kin1^{wt} and Kin1^{AA} SCC cells was seeded in methylcellulose-over-agarose assay to enable the gradual growth of single cells into 3D spheroids. **A:** Representative phase-contrast images captured on Day0 and Day3 post-seeding. Scale bar represents 125µm. **B:** 3D spheroid growth was determined by manual quantification of spheroid area from Day1 to Day6 post-seeding with ImageJ software. A collection of cells was considered as a spheroid if it occupied an area ≥ 3 times larger than the average area of a single cell. Manual quantification of the single-cell area was performed at Day0 post-seeding with ImageJ software. 5 low-power fields were analysed per cell line. one-way ANOVA with Tukey's multiple comparison test. **C:** Quantification of cell line clonogenicity was determined by measuring the percentage of 3D spheroids at Day3 in Kin1^{null}, Kin1^{wt} and Kin1^{AA} SCC cell lines. one-way ANOVA with Tukey's multiple comparison test. **B-C:** Results presented as mean ± SEM. p-value > 0.05, * p-value ≤ 0.05, ** p-value ≤ 0.01

5.6. *In vivo* assessment of Kin1^{null}, Kin1^{wt} and Kin1^{AA} mouse SCC tumour growth

We next sought to determine whether growth of Kin1^{null}, Kin1^{wt} and Kin1^{AA} mouse SCC cell lines *in vitro* reflected *in vivo* tumour growth, by carrying out bilateral subcutaneous implantations of SCC cells in 7-week old CD-1 nude mice.

We initially injected 0.50x10^6 Kin1^{null} or Kin1^{wt} SCC cells per mouse flank, in order to assess differences between growth of Kin1^{null} and Kin1^{wt} tumours (tumour growth study A) **(Fig.35.A.)**. Subsequently, to compare the growth of Kin1^{AA} tumours against Kin1^{null} and Kin1^{wt} tumour growth, we also carried out injections of 1.00x10^6 and 0.25x10^6 Kin1^{null}, Kin1^{wt} or Kin1^{AA} SCC cells per mouse flank, during tumour growth study B **(Fig.35.B.)** and C **(Fig.35.C.)**, respectively. Injections of different number of cells in every tumour growth study allowed us to scrutinise if the number of SCC cells injected affected tumour growth and, thus, reproducibility of results. Signs of tumour ulceration led to termination of studies at Day 24.

Overall, we observed that differences in growth between Kin1^{null}, Kin1^{wt} and Kin1^{AA} tumours started to appear between Day10 and Day17 post-implantation, as prior to that all tumours had similar volume **(Fig.35.A-C.)**. Kin1^{null} tumours were significantly larger than Kin1^{wt} tumours in every growth study **(Fig.35.A-C.)**. According to tumour volume data from growth study B, Kin1^{null} tumours were significantly larger than Kin1^{wt} and Kin1^{AA} tumours, and Kin1^{wt} tumours were also significantly larger than Kin1^{AA} tumours (**Fig.35.B.**). This growth trend was reflected between tumours of growth study C, but difference between Kin1^{wt} and Kin1^{AA} tumours was not statistically significant (**Fig.35.C.**). Interestingly, despite injection of different SCC cell number, Kin1^{null} tumours had reached comparable size by Day24 in growth studies B and C, which was

also observed for Kin1^{AA} tumours, whereas Kin^{wt} tumours were significantly smaller in study C compared to study B **(Fig.35.D.)**. This accounts for the non-statistically significant difference between Kin1^{wt} and Kin1^{AA} tumours in growth study C **(Fig.35.C.)**. Combination of growth rate data from growth studies B and C allowed us to examine statistical significance between Kin1^{null}, Kin1^{wt} and Kin1^{AA} tumour growth across both studies, whilst circumventing the variability in tumour volume values. We found that overall, Kin1^{null} tumours had significantly greater growth rate than Kin1^{wt} and Kin1^{AA} tumours, and Kin1^{wt} tumours had significantly higher growth rate than Kin1^{AA} tumours **(Fig.35.D.)**.

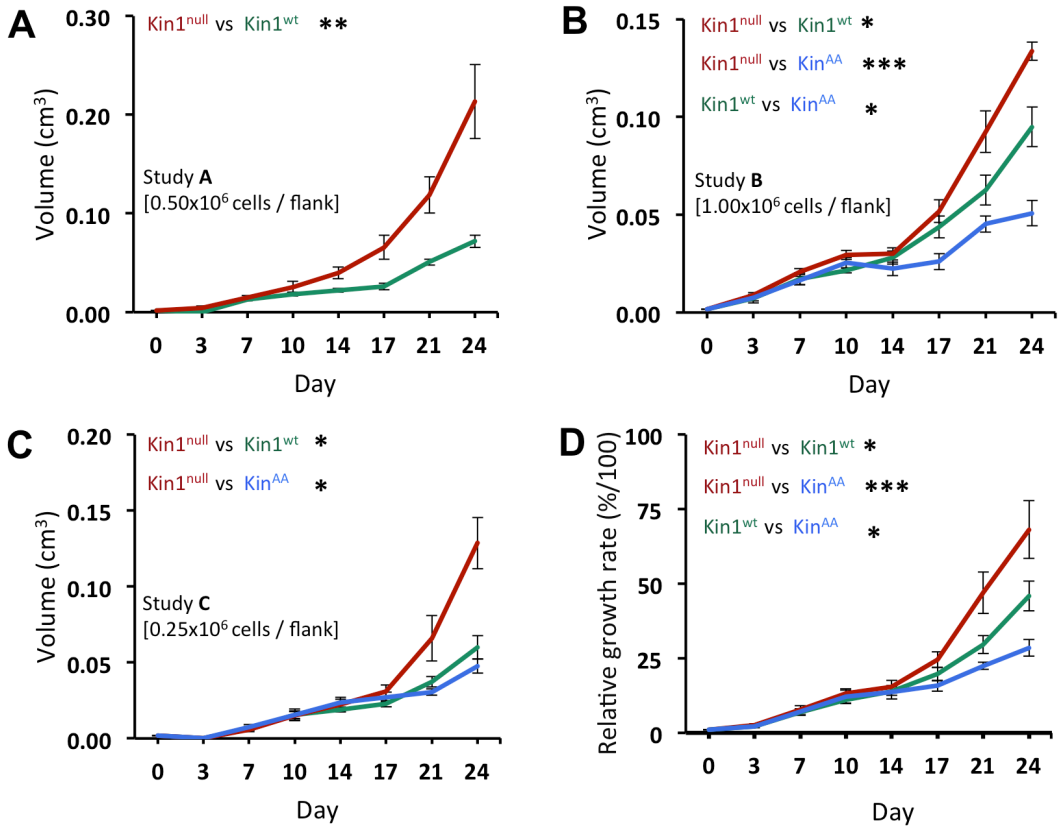

Figure 35: ***In vivo*** **assessment of Kin1^{null}, Kin1^{wt} and Kin1^{AA} SCC tumour growth.** Bilateral subcutaneous implantations of **A:** 0.50x10^6 Kin1^{null} and Kin1^{wt}, **B:** 1.00x10^6 Kin1^{null}, Kin1^{wt} and Kin1^{AA} and **C:** 0.25x10^6 Kin1^{null}, Kin1^{wt} and Kin1^{AA} SCC cells were administrated in CD-1 nude mice. **A-C:** Tumour volume was quantified over the course of 24 days. Only statistical analysis using values obtained at Day24 is shown. **A:** Unpaired t-test. **B:** one-way ANOVA with Tukey's multiple comparison test. **C:** Kruskal-Wallis ANOVA with Dunn's multiple comparison test. **D:** Combination of tumour growth rate values from studies B and C represents the percentage/100 of change of tumour measurements against initial tumour measurements that were considered as a baseline start of 1. one-way ANOVA with Tukey's multiple comparison test. **A-D:** Results presented as mean ± SEM. p-value > 0.05, * p-value ≤ 0.05, ** p-value ≤ 0.01, *** p-value < 0.001.

5.7. Morphological assessment of Kin1^{null}, Kin1^{wt} and Kin1^{AA} mouse SCC tumours

Initially, morphology and tumour structure were assessed by H&E staining, which showed that all tumours were highly invasive to skeletal muscle **(Fig.36.)**.

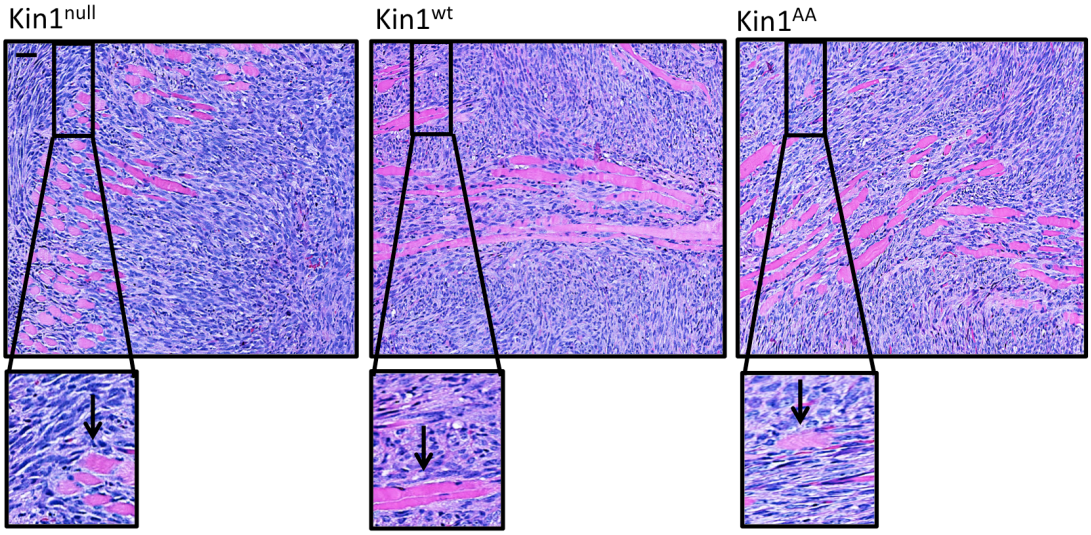

Figure 36: Morphological assessment of Kin1^{null}, Kin1^{wt} and Kin1^{AA} SCC tumours. Representative IHC images of H&E staining that was performed on Kin1^{null}, Kin1^{wt} and Kin1^{AA} SCC tumours from growth study C. Arrows indicate skeletal muscle being invaded by tumours cells. Mag x20. The scale bar represents 50µm.

We observed a spindle-like nuclear morphology across Kin1^{null}, Kin1^{wt} and Kin1^{AA} tumours **(Fig.37.A)**. Upon closer inspection we saw that Kin1^{null} tumour nuclei displayed a more elongated structure when compared to Kin1^{wt} and Kin1^{AA} nuclei **(Fig.37.A)**. Nuclear length analysis on tumours from growth study C confirmed our observation, as it showed that Kin1^{null} tumour nuclei were significantly longer than Kin1^{wt} nuclei **(Fig.37.B.)**. We also observed that quantification of Kin1^{null} and Kin1^{AA} nuclear length reflected our observation, as Kin1^{null} nuclei showed a tendency towards a longer structure compared to Kin1^{AA} nuclei, albeit not reaching statistical significance **(Fig.37.B.)**. We believe that the variability in average nuclear length measurements within Kin1^{null} and Kin1^{AA} tumours prevented the difference between Kin1^{null} and Kin1^{AA} tumours nuclear length reaching significance and analysis of further tumours will be required to confirm this. There was no significant difference in the average area occupied by each Kin1^{null}, Kin1^{wt} and Kin1^{AA} nucleus in tumours from growth study C **(Fig.37.C)**.

Furthermore, we observed that Kin1^{null} tumours displayed higher nuclear density and lower ECM deposition compared to Kin1^{wt} and Kin1^{AA} tumours **(Fig.37.A.)**. To assess our observation on nuclear density more closely, we measured the percentage of tumour area covered by all nuclei within various fields of tumours from growth study C. We found that Kin1^{null} tumours displayed a significantly higher nuclear density when compared to Kin1^{wt} and Kin1^{AA} counterparts **(Fig.37.D.)**.

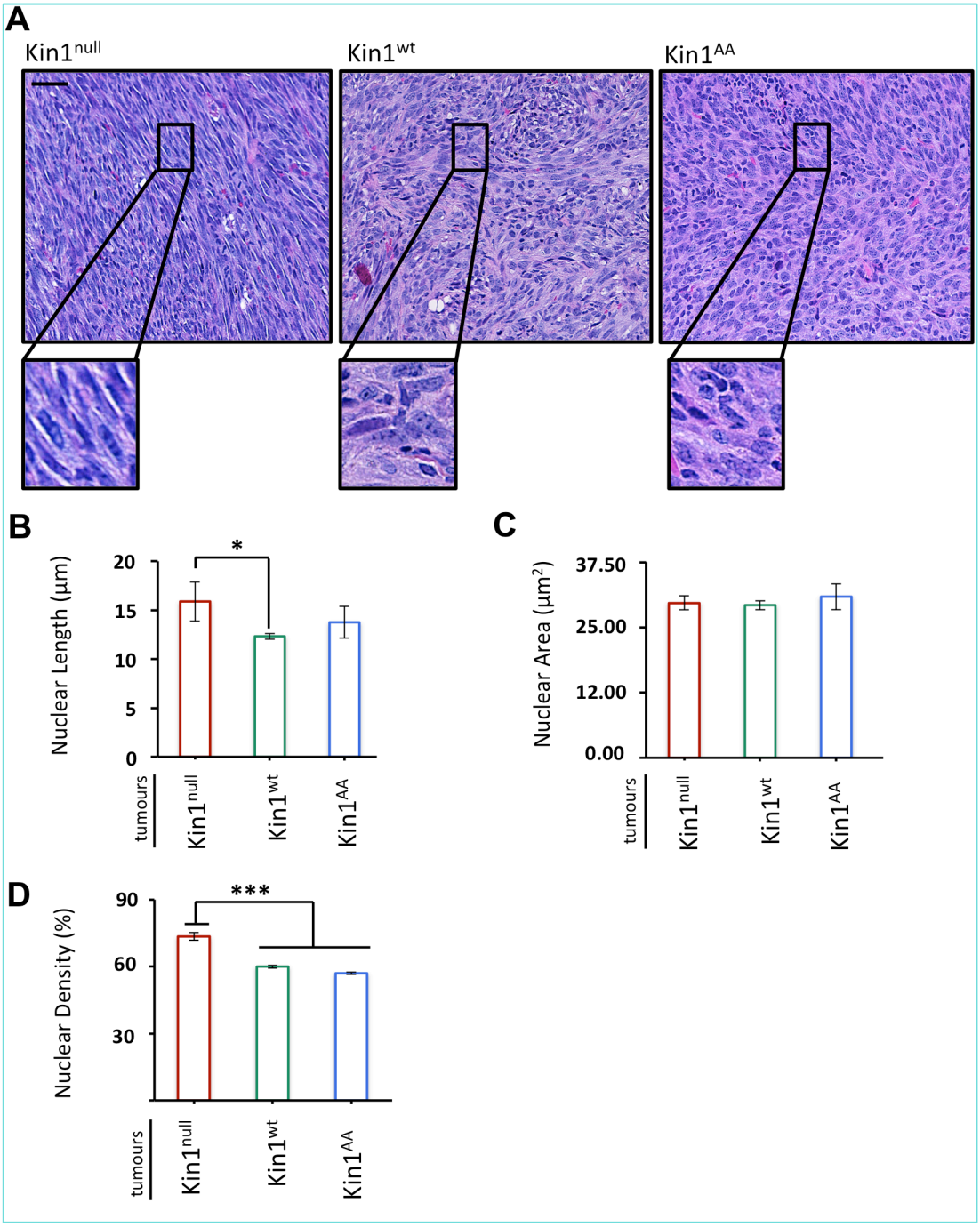

Figure 37: Analysis of nuclear length, nuclear area and nuclear density in Kin1^{null}, Kin1^{wt} and Kin1^{AA} SCC tumours. H&E staining was performed on Kin1^{null}, Kin1^{wt} and Kin1^{AA} SCC tumours from growth study C. **A:** Representative IHC images of H&E staining that display features such as tumour nuclear structure and density. Mag x40. The scale bar represents 50µm. **B:** Quantification of nuclear length was performed manually with ImageJ software. 5 nuclei from 5 representative high-power fields were analysed per Kin1^{null}, Kin1^{wt} and Kin1^{AA} tumour (n=4). Results presented as mean ± SEM. Kruskal-Wallis ANOVA with Dunn's multiple comparison test. **C:** Quantification of area occupied by each nucleus was performed manually with ImageJ software. Area of 5 individual nuclei from 5

representative high-power fields was analysed per $Kin1^{null}$, $Kin1^{wt}$ and $Kin1^{AA}$ tumour (n=4). Results presented as mean ± SEM. one-way ANOVA with Tukey's multiple comparison test. **D:** Quantification of nuclear density was performed automatically with ImageJ software by calculating the percentage of tumour field area covered by nuclei. Segmentation of higher intensity nuclear pixels from lower intensity background pixels was performed automatically with Threshold plugin of ImageJ. Nuclear density from 10 low-power fields was analysed per $Kin1^{null}$, $Kin1^{wt}$ and $Kin1^{AA}$ tumour (n=4). one-way ANOVA with Tukey's multiple comparison test. **B-D:** Results presented as mean ± SEM. p-value > 0.05, * p-value ≤ 0.05, *** p-value ≤ 0.001.

To evaluate ECM deposition in tumours, we measured collagen-I deposition within Kin1^{null} and Kin1^{wt} tumours with the use of second harmonic microscopy (**Fig.38.A.**). We found that Kin1^{null} tumours from growth studies A and C had a significantly lower collagen-I compared to Kin1^{wt} tumours (**Fig.38.B-C.**).

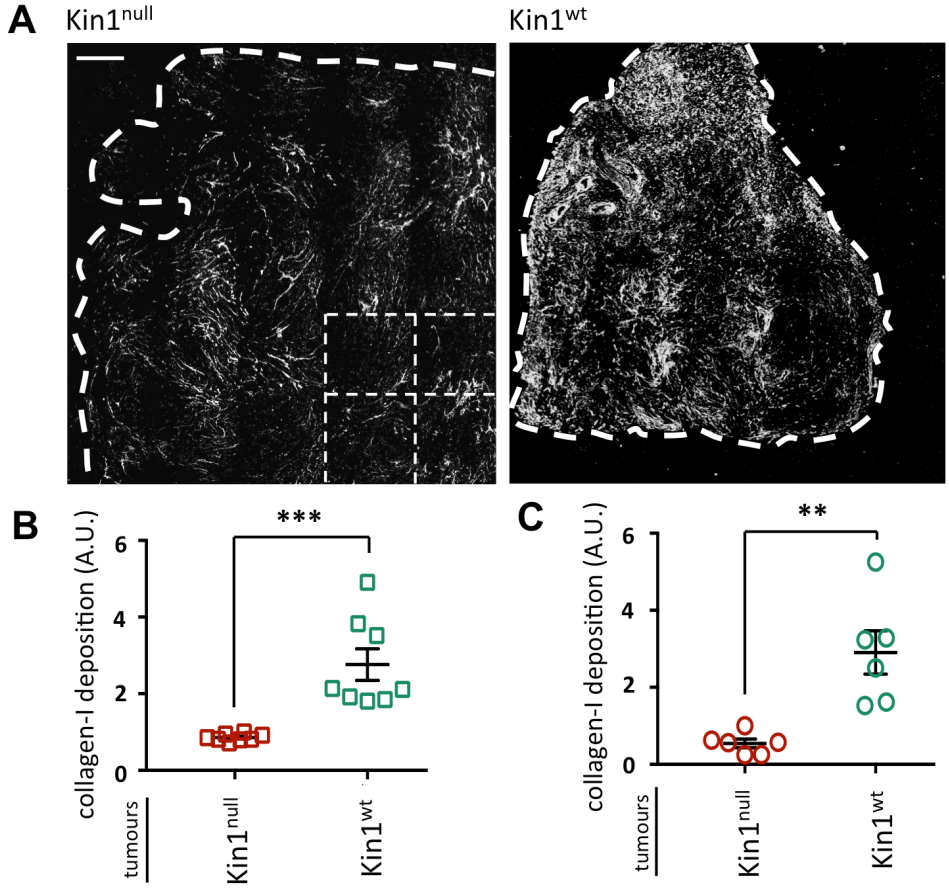

Figure 38: Analysis of collagen-I deposition in Kin1^{null} and Kin1^{wt} SCC tumours. Collagen-I deposition was measured in Kin1^{null} and Kin1^{wt} tumours from growth studies A and C with second harmonic microscopy. **A:** Representative images of collagen-I deposition in Kin1^{null} and Kin1^{wt} tumours from growth study C. Tumour perimeter is defined with the dashed white line. The scale bar represents 10µm. **B-C:** Quantification of collagen-I deposition was performed automatically with ImageJ by calculating the fraction of Integrated Density (sum of pixel value) of collagen-I over tissue autofluorescence, thus taking into account the size of each tumour. One image was analysed per tumour, which was composed by 25 individual images, examples of which are pointed out by the grid. Results presented as scatter plot ± SEM. Every value within each growth study's tumour cohort was normalised against the highest Kin1^{null} tumour value. Unpaired t-test; ** p-value ≤ 0.01, *** p-value ≤ 0.001. **B:** Squares represent values of individual tumours from growth study A. **C:** Circles represent values of individual tumours from growth study C.

5.8. Immunohistochemical assessment of proliferation, apoptosis and vascularization in Kin1^{null} and Kin1^{wt} mouse SCC tumours

Cellular proliferation and apoptosis, as well as tumour angiogenesis are potent regulatory forces of tumour growth and development. Our objective was to address whether Kin1 regulates the above processes, which would, ultimately, help us understand if this contributes to the significant differences in tumour growth observed between Kin1^{null} and Kin1^{wt} SCC tumours.

We initially scored cells within Kin1^{null} and Kin1^{wt} tumours from growth studies A and C that were positive for cellular proliferation marker Ki67 **(Fig.39.A.)**. Overall, we observed that cells from Kin1^{null} tumours proliferated significantly more compared to Kin1^{wt} cells **(Fig.39.B-C.)**.

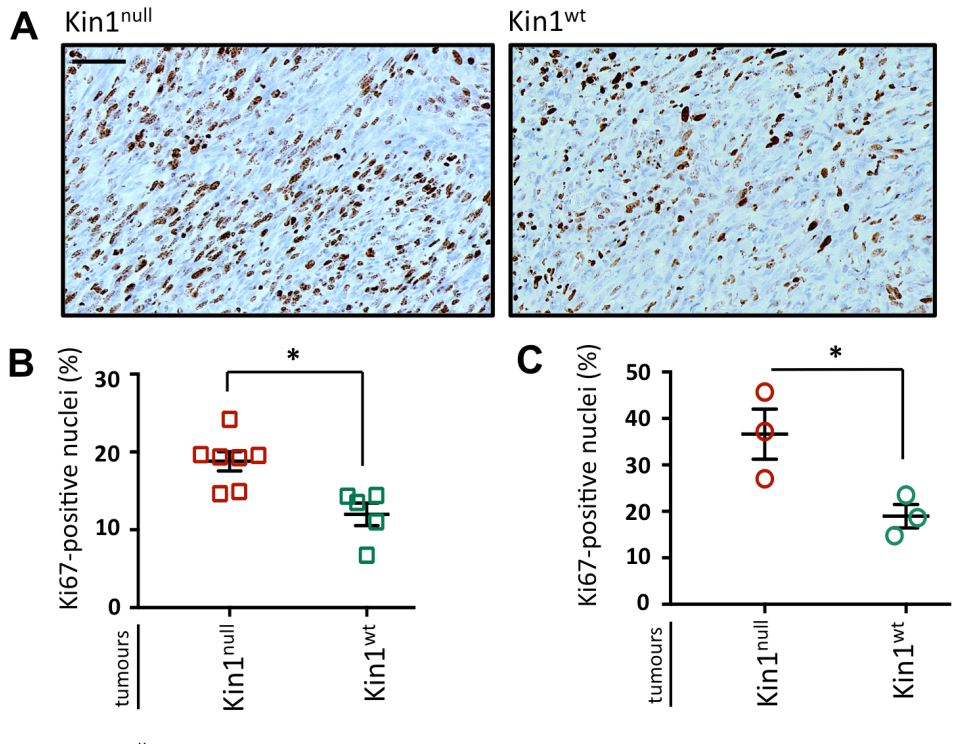

Figure 39: Analysis of proliferation in Kin1^{null} and Kin1^{wt} SCC tumours. IHC was performed with a Ki-67 antibody on Kin1^{null} and Kin1^{wt} tumours from growth studies A and C. **A:** Representative images of Ki-67 staining in Kin1^{null} and Kin1^{wt} tumours from growth study A. Mag x40. The scale bar represents

50µm. **B-C:** Quantification of the percentage of Ki-67-positive nuclei was performed automatically with Immunoratio plugin of ImageJ software [128]. 15 or more high-power fields were analysed per Kin1^{null} and Kin1^{wt} tumour. Results presented as scatter plot ± SEM. Unpaired t-test; * p-value ≤ 0.05. **B:** Squares represent values of individual tumours from growth study A. **C:** Circles represent values of individual tumours from growth study C.

To define any differences in apoptosis between Kin1^{null} and Kin1^{wt} tumours we scored nuclei that were positive for the apoptosis marker casp-3 **(Fig.40.A.)**. We overall observed a very low percentage of apoptotic cells and no statistical difference in apoptosis between Kin1^{null} and Kin1^{wt} tumours from growth study B **(Fig.40.B.)**.

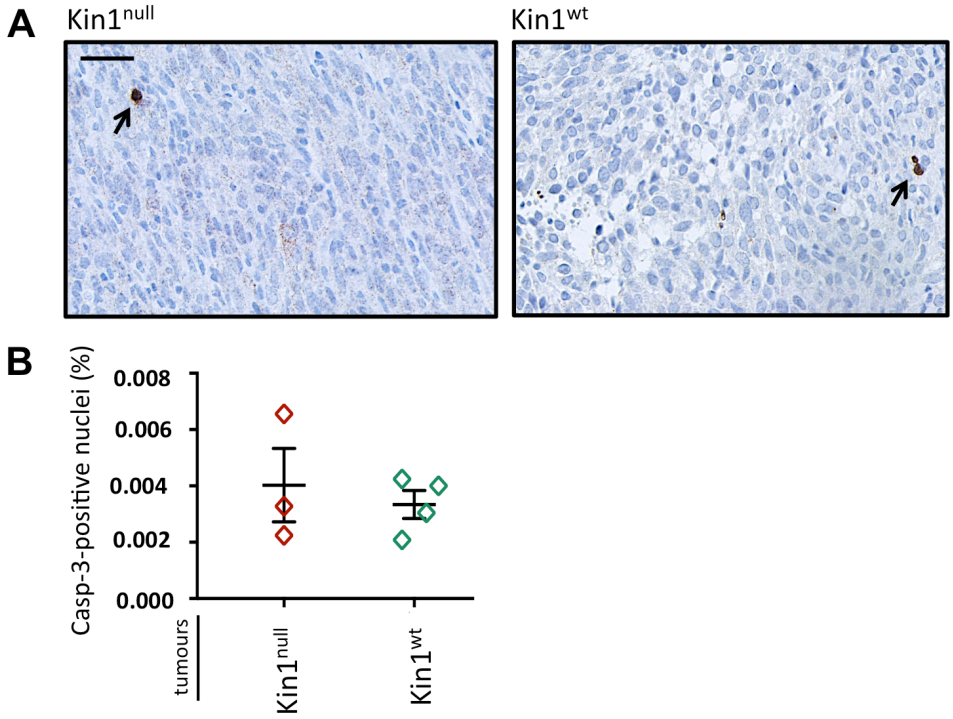

Figure 40: Analysis of apoptosis in Kin1^{null} and Kin1^{wt} SCC tumours. IHC was performed with a casp-3 antibody on Kin1^{null} and Kin1^{wt} tumours from growth study B. **A:** Representative images of casp-3 staining in Kin1^{null} and Kin1^{wt} tumours from growth study B. Mag x40. The scale bar represents 50µm. **B:** Quantification of the percentage of casp-3-positive nuclei was performed automatically with Immunoratio plugin of ImageJ software [128]. 15 high-power fields were analysed per Kin1^{null} and Kin1^{wt} tumour. Results presented as scatter plot ± SEM. Unpaired t-test; p-value > 0.05. Diamonds represent values of individual tumours from growth study B.

Finally, to determine whether angiogenesis is linked to the growth differences observed in our tumour models, we quantified vascularisation of tumours by measuring tumour Vascular Surface Area (VSA). This was achieved by calculating the percentage of tumour area covered by blood vessels positive for endothelial marker CD31. VSA was evaluated by performing IF on tumours from growth study A and IHC on tumours from growth study B **(Fig.41.A-B.)**. Results from both immunostaining studies showed that Kin1^{null} tumours had a significantly higher VSA compared to Kin1^{wt} tumours **(Fig.41.C-D.)**.

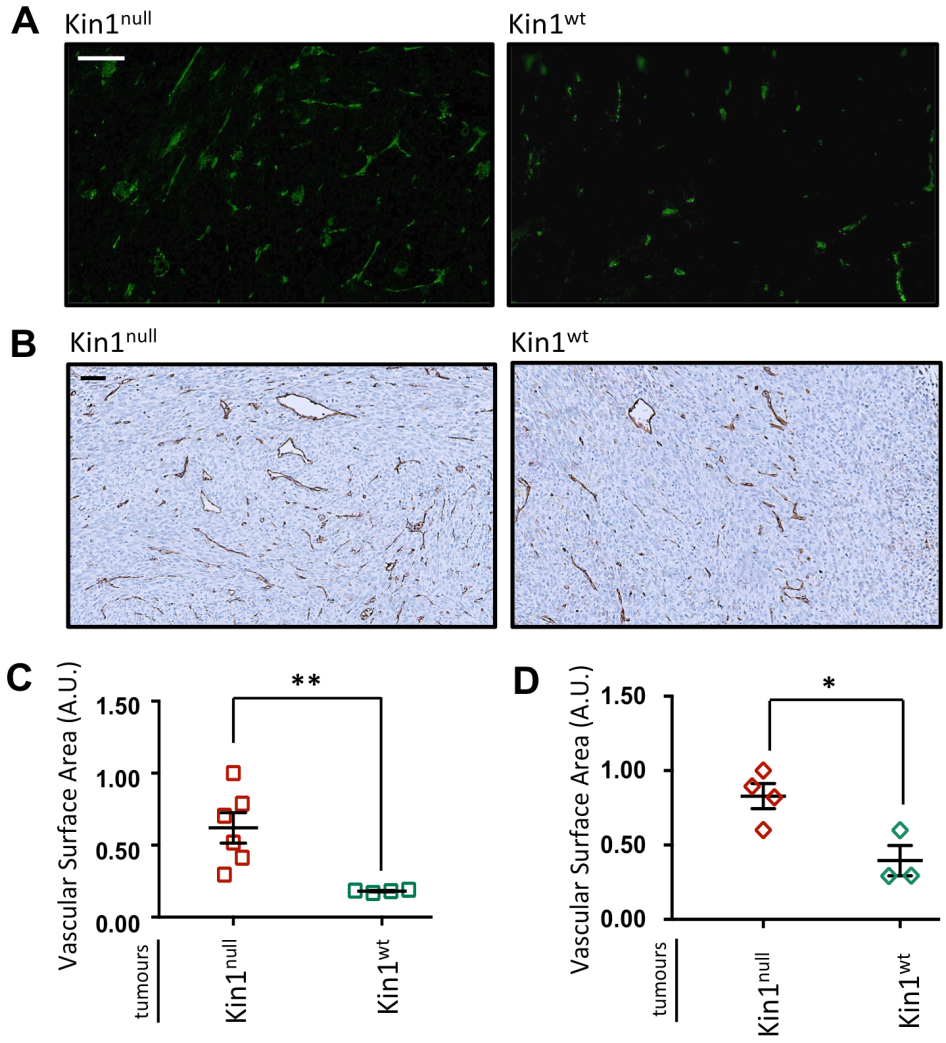

Figure 41: Analysis of VSA in Kin1^{null} and Kin1^{wt} SCC tumours. Immunostaining was performed with a CD31 antibody on Kin1^{null} and Kin1^{wt} tumours from growth studies B and C. **A:** Representative IF images of CD31 staining in Kin1^{null} and Kin1^{wt} tumours from growth study A. Mag x20. The scale bar represents 50µm. **B:** Representative IHC images of CD31 staining in Kin1^{null} and Kin1^{wt} tumours from growth study B. Mag x40. The scale bar represents 50µm. **C-D:** Quantification of VSA was performed

automatically with ImageJ software by calculating the percentage of tumour field area covered by CD31-positive vessels. Segmentation of higher intensity vessel pixels from lower intensity background pixels was performed automatically with Threshold plugin of ImageJ. 15 low-power fields were analysed per $Kin1^{null}$ and $Kin1^{wt}$ tumour. Results presented as scatter plot ± SEM. Every value within each growth's study tumour cohort was normalised against the highest $Kin1^{null}$ tumour value. **C:** Mann-Whitney U Test. **D:** Unpaired t-test. **C-D:** * p-value ≤ 0.05, ** p-value ≤ 0.01. C: Squares represent values of individual tumours from growth study A. **D:** Diamonds represent values of individual tumours from growth study B.

5.9. Comparative RNA-Seq analysis of gene expression changes in Kin1^{null} and Kin1^{wt} mouse SCC tumours

We next employed RNA-Seq to characterise the transcriptome of Kin1^{null} and Kin1^{wt} tumours and, thus, determine changes in signaling pathways, which could account for the variations in tumour growth, cellular proliferation and angiogenesis between the two tumour sets. RNA-Seq was performed on three Kin1^{null} tumours (volumes: 0.14cm^3, 0.21cm^3, 0.25cm^3) and three Kin1^{wt} tumours (volumes: 0.05cm^3, 0.07cm^3, 0.08cm^3), which were collected from growth study A 24 days following the injection of Kin1^{null} and Kin1^{wt} SCC cells in CD-1 nude mice. As half of every tumour was fixed for immunohistochemical analysis, RNA extraction was performed in the other tumour half, which was snap frozen in liquid N_2 immediately following its extraction.

Reads were mapped to the mouse mm9 reference genome, as described in **Chapter 2, Section 2.7.2**. Construction of Principal Component Analysis (PCA) plot was performed by Dr Stuart Aitken and revealed a 63% variance in gene expression between Kin1^{null} and Kin1^{wt} tumours (**Fig.42.**). Genes with a q value (p value adjusted for multiple testing) of less than 0.05 were considered differentially expressed. **Table 4** shows the 10 most highly enriched genes in the Kin1^{null} and Kin1^{wt} tumours.

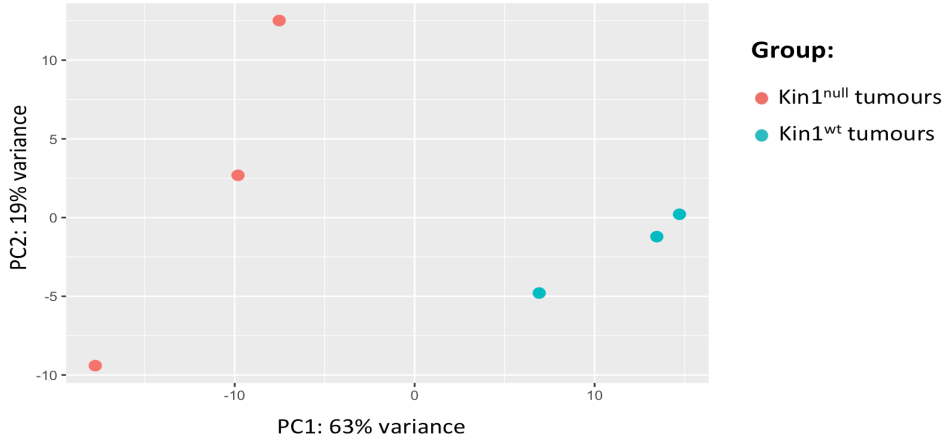

Figure 42: PCA of RNA-Seq results: PCA plot generated from the DESeq2 analysis of gene count data shows that Kin1^{null} and Kin1^{wt} samples are separated on the first principle component, as is desirable.

	Gene	Kin1^{null} (FPKM)	Kin1^{wt} (FPKM)	log2_fold change	q-value
A	*Cstf2,Mir3112*	143.57	2.19	6.03	0.002
	Gzmg	295.04	7.38	5.32	0.002
	Mir1894,Ppp1r10	357.52	10.89	5.04	0.002
	Nr4a1	76.19	2.83	4.75	0.002
	Mmp-13	47.86	2.16	4.47	0.002
	Ggt1	3.76	0.17	4.44	0.002
	1110038B12Rik,AC087117.1,AC087117.2,Snord52	1764.74	81.32	4.44	0.002
	Gpr110	25.96	1.32	4.30	0.002
	Mmp-3	620.64	34.83	4.16	0.002
	Ccl9	278.16	17.12	4.02	0.004
B	*Fxyd1*	1.80	42.34	-4.56	0.030
	Myh4	0.31	7.49	-4.59	0.003
	Tnnt3	6.44	162.83	-4.66	0.002
	Atp1a2	0.23	5.97	-4.71	0.040
	Mir5113,Tnrc6b	1.68	49.04	-4.87	0.002
	Adamts-17	0.13	3.77	-4.88	0.002
	Smoc1	0.15	4.65	-4.95	0.040
	Klra17	2.11	100.66	-5.58	0.002
	Ttn	0.05	2.94	-5.94	0.002
	Neu2	0.05	3.44	-6.21	0.020

Table 4: Analysis of RNA-Seq results from Kin1^{null} and Kin1^{wt} SCC tumours: Differential expression was analysed by Cuffdiff[275] and by DESeq2[276], which provided lists of differentially expressed genes by two alternative statistical techniques, by Dr Stuart Aitken Table showcases examples from differential expression of 20 genes with lo2 fold change >4 between Kin1^{null} and Kin1^{wt} tumours. FPKM=Fragments Per Kilobase of Exon Per Million Fragments Mapped. **(A)** Most highly enriched genes in Kin1^{null} tumours. **(B)** Most highly enriched genes in Kin1^{wt} tumours.

5.10. Exploring gene expression changes identified through RNA-Seq in Kin1^{null} and Kin1^{wt} mouse SCC tumours, and in Kin1^{null}, Kin1^{wt} and Kin1^{null} and Kin1^{AA} mouse SCC cell lines

Quantitative real-time PCR (q-PCR) assays were employed to validate expression changes in genes selected from RNA-Seq result analysis, principally due to their biological function. We evaluated gene expression changes between Kin1^{null} and Kin1^{wt} tumours from growth studies A, B and/or C, and between Kin1^{null}, Kin1^{wt} and Kin1^{AA} SCC cell lines grown as artificial monolayers (2D cell culture) and as 3D spheroids in low-adherent plates (3D cell culture).

Overall, we observed a strong correlation and a similar gene expression trend between RNA-Seq based transcript abundance estimation (FPKM: Fragments Per Kilobase of Exon Per Million Fragments Mapped) and q-PCR assays, highlighting the accuracy of the latter analysis.

We also explored correlation between expression levels of various genes and tumour volume. For each correlation assessment, we calculated both the Pearson product-moment correlation coefficient, which measured the strength and the direction of a linear relationship between two variables, as well as the statistical significance of the correlation coefficient. Due to the small tumour sample size of each growth study ($n \leq 8$), as well as variability within Kin1^{null} and/or Kin1^{wt} tumour values from each growth study, it was sometimes difficult to reach significance following statistical analysis. Nevertheless, even without statistical significance, we often observed a strong correlation trend between gene expression and tumour volume, which would be misleading if we did not take into account. Thus, for the purposes of this study we valued, and therefore commented on, strength of correlation coefficient rather than p-value. Interpretation of degree of correlation is based on "Correlation Coefficient Interpretation Guide" **(Table 5)** **[132]**[132].

	Very strong	Strong	Moderate	Weak	No correlation
Negative Correlation:	-0.9 to -1	-0.7 to -0.9	-0.5 to -0.7	-0.3 to -0.5	0 to -0.3
Positive Correlation:	0.9 to 1	0.7 to 0.9	0.5 to 0.7	0.3 to 0.5	0 to 0.3

Table 5: Correlation Coefficient Interpretation Guide. Correlation coefficient ranges from -1 (a perfect negative correlation) to 1 (a perfect positive correlation).

5.10.1. Validation of genetic loss of *Fermt1* gene in Kin1^{null} mouse SCC tumours

We initially validated the genetic loss of *Fermt1* in Kin1^{null} tumours and successful re-expression of wild-type *Fermt1* in Kin1^{wt} SCC tumours from growth study A **(Fig.43.i.)**. There was no correlation between *Fermt1* expression in Kin1^{wt} tumours and tumour volume **(Fig.43.ii.)**.

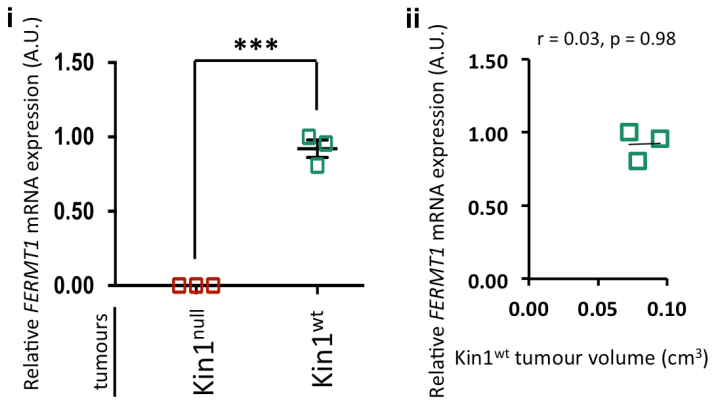

Figure 43: Analysis of *Fermt1* gene expression levels in Kin1^{null} and Kin1^{wt} tumours. q-PCR assay was performed using DNA from Kin1^{null} and Kin1^{wt} tumours from growth study A. **(i):** Quantification of relative *Fermt1* mRNA expression in relation to *Gapdh* expression in Kin1^{null} and Kin1^{wt} tumours. Results presented as scatter plot ± SEM. Every value was normalised against the highest Kin1^{wt} tumour value. Squares represent values of individual tumours from growth study A. **(ii):** Pearson's correlation between relative *Fermt1* expression and tumour volume in Kin1^{wt} tumours. r= correlation coefficient value. **(i-ii):** Unpaired t-test; p-value > 0.05, *** p-value ≤ 0.001.

5.10.2. Analysis of expression of Metalloproteinase genes in Kin1^{null} and Kin1^{wt} mouse SCC tumours, and in Kin1^{null}, Kin1^{wt} and Kin1^{AA} mouse SCC cells

Kin1^{null} and Kin1^{wt} tumours presented variations in expression of genes encoding enzymes that belong to the Metalloproteinase protein family, whose members play a role in the metabolic degradation of ECM components in physiological and pathological conditions. Metalloproteinases are categorized in four distinct groups; "classical" Matrix Metalloproteinases (MMPs), which are secreted as soluble enzymes, transmembrane proteins membrane-type MMPs (MT-MMPs), ADAMs (a disintegrin and metalloproteinase), which contain a unique integrin receptor-binding domain (disintegrin), and ADAMTS (a disintegrin and metalloproteinase with thrombospondin motif), which are secreted MMPs and contain disintegrin as well as a thrombospondin (TSP-1) domain in their C-terminal region [179].

In the following sections, we explored expression levels of genes that encode proteins from three of the four different Metalloproteinase sub-families: MMPs, MT-MMPs and ADAMTSs in Kin1^{null} and Kin1^{wt} tumours. We also explored expression levels of MMP genes in Kin1^{null}, Kin1^{wt} and Kin1^{AA} SCC cell lines grown in 2D and 3D cultures.

5.10.2.1. Analysis of expression of "classical" Matrix Metalloproteinase (MMP) genes *Mmp3* and *MMP13* in Kin1^{null} and Kin1^{wt} mouse SCC tumours, and in Kin1^{null}, Kin1^{wt} and Kin1^{AA} mouse SCC cells

According to RNA-Seq results, *Mmp3* mRNA expression in Kin1^{null} tumours was ~4-fold higher in comparison to Kin1^{wt} tumours (**Table 4**). Q-PCR assay in tumour samples isolated from growth studies A and C validated that Kin1^{null} tumours had a significantly higher *Mmp3* expression in comparison to Kin1^{wt} tumours (**Fig.44.A.i.,B.i.**). We found a very strong, positive correlation between *Mmp3* expression and volume of Kin1^{null} tumours from both growth studies (**Fig.44.A.ii.,B.ii.**). Moreover, we detected a strong and moderate, negative correlation between *Mmp3* expression and volume of Kin1^{wt} tumours from growth studies A and C, respectively (**Fig.44.A.iii.,B.iii**).

In vitro evaluation of gene expression showed that overall, *Mmp3* expression was significantly higher in Kin1^{wt} and Kin1^{AA} cells grown in 3D culture in comparison to Kin1^{wt} and Kin1^{AA} cells in 2D culture (**Fig.44.C.i.**). Although not significant, Kin1^{null} cells from 3D culture followed the above trend, as they also showed slightly higher *Mmp3* expression levels compared to 2D culture Kin1^{null} cells (**Fig.44.C.i.**). In 2D culture, Kin1^{null} cells showed a higher *Mmp3* expression compared to Kin1^{wt} cells (**Fig.44.C.ii.**), which reflects the *Mmp3* expression pattern between Kin1^{null} and Kin1^{wt} tumours (**Fig.44.A.i.,B.i.**). Moreover, in 2D culture Kin1^{AA} cells expressed comparable *Mmp3* levels to Kin1^{null} SCC cells, and significantly higher *Mmp3* levels than Kin1^{wt} cells (**Fig.44.C.ii.**). In contrast to 2D culture, Kin1^{null} cells from 3D culture expressed significantly lower *Mmp3* levels compared to Kin1^{wt} counterparts (**Fig.44.C.i.**), which also contrasts *Mmp3* expression pattern between Kin1^{null} and Kin1^{wt} tumours (**Fig.44.A.i.,B.i.**). Moreover, *Mmp3* levels in Kin1^{AA} 3D cell culture were similar to Kin1^{wt}, and significantly higher than Kin1^{null} SCC cells (**Fig.44.C.i.**).

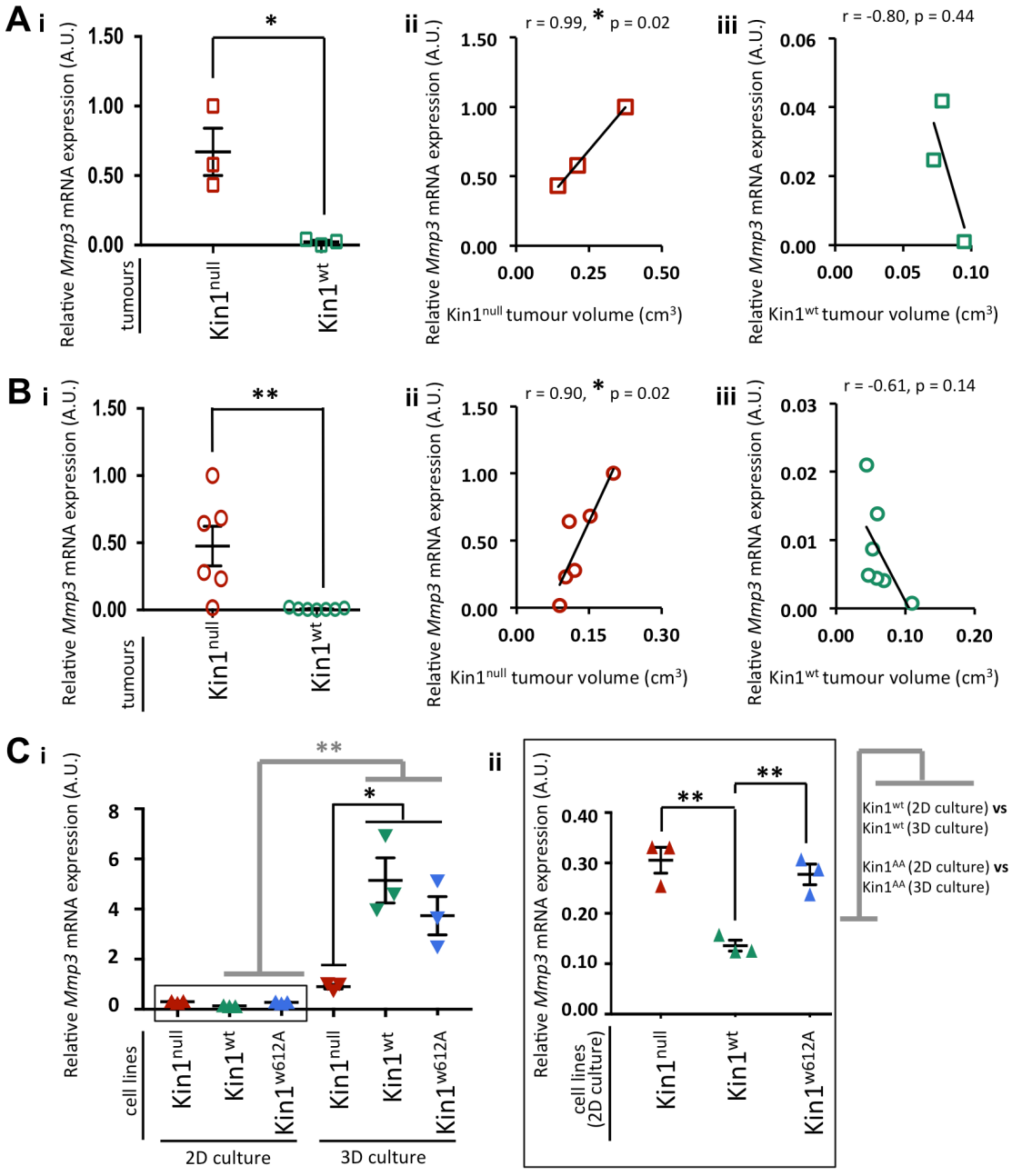

Figure 44: Analysis of *Mmp3* gene expression levels in Kin1^{null} and Kin1^{wt} SCC tumours and Kin1^{null}, Kin1^{wt} and Kin1^{AA} SCC cell lines. q-PCR assay was performed using cDNA from Kin1^{null} and Kin1^{wt} tumours from growth studies A and C. **A(i),B(i):** Quantification of relative *Mmp3* mRNA expression in relation to *Gapdh* expression in Kin1^{null} and Kin1^{wt} tumours. Results presented as scatter plot ± SEM. Every value within each growth's study tumour cohort was normalised against the highest Kin1^{null} tumour value. **A(ii-iii),B(ii-iii):** Pearson's correlation between relative *Mmp3* expression and tumour volume in Kin1^{null} and Kin1^{wt} tumours. r= correlation coefficient value. **A-B:** Unpaired t-test; * p-value ≤ 0.05, ** p-value ≤ 0.01. **A:** Squares represent values of individual tumours from growth study A. **B:**

Circles represent values of individual tumours from growth study C. **C(i) :** Quantification of relative *Mmp3* mRNA expression in relation to *Gapdh* expression in Kin1^{null}, Kin1^{wt} and Kin1^{AA} SCC cell lines grown in 2D and 3D cell culture. Results presented as scatter plot ± SEM. Every value within each cell line was normalised against the highest value from Kin1^{null} 3D culture cells. Three biological replicates were analysed per cell line. one-way ANOVA with Tukey's multiple comparison test; p-value > 0.05, * p-value ≤ 0.05, ** p-value ≤ 0.01. Thick grey line indicates that statistical testing compared *Mmp3* expression in Kin1^{wt} and Kin1^{AA} SCC cells grown in 2D culture against their 3D counterparts. **(ii):** Magnification of **C(i)** graph of cell lines grown in 2D cell culture.

IF results showed that Kin1^{null} tumours expressed significantly higher levels of MMP3 protein compared to Kin1^{wt} tumours (**Fig.45.B.**), thus reflecting our findings on *Mmp3* gene expression in our tumour samples (**Fig.45.A.i.,B.i.**). In both Kin1^{null} and Kin1^{wt} tumours MMP3 was localised in the cytoplasm and the extracellular space. (**Fig.45.A.**). Likewise, western blot analysis of MMP3 expression levels in Kin1^{null}, Kin1^{wt} and Kin1^{AA} cell lines grown in 2D and 3D cultures mirrored *in vitro Mmp3* gene expression trends (**Fig.45.C.**). In 2D culture, Kin1^{null} and Kin1^{AA} cells had similar levels between them, and higher MMP3 levels compared to Kin1^{wt} cells (**Fig.45.C.**). In 3D culture, Kin1^{null} cells showed lower MMP3 expression compared to Kin1^{wt} and Kin1^{AA} cells (**Fig.45.C.**).

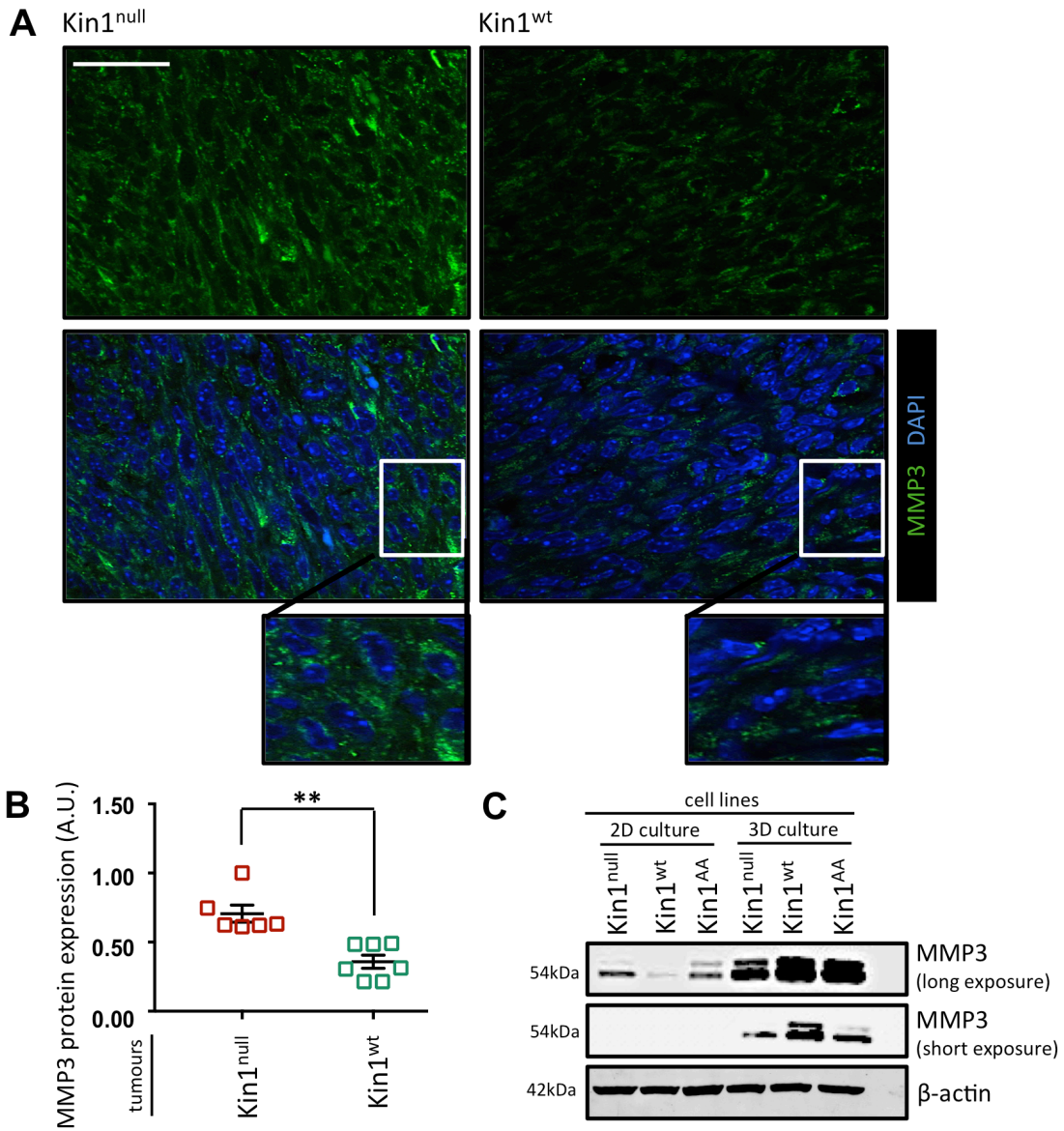

Figure 45: Analysis of MMP3 protein expression levels in Kin1^{null} and Kin1^{wt} SCC tumours and in Kin1^{null}, Kin1^{wt} and Kin1^{AA} SCC cell lines. IF was performed with an MMP3 antibody on Kin1^{null} and Kin1^{wt} tumours from growth study A. **A:** Representative IF images of MMP3 staining in Kin1^{null} and Kin1^{wt} tumours from growth study A. The scale bar represents 50µm. **B:** Quantification of MMP3 expression was performed automatically with ImageJ software by calculating the Raw Integrated Density (sum of pixel value) of every image. 10 representative high-power fields were analysed per Kin1^{null} and Kin1^{wt} tumour. Results presented as scatter plot ± SEM. Every value within each growth's study tumour cohort was normalised against the highest Kin1^{null} tumour value. Mann-Whitney; ** p-value ≤ 0.01. Squares represent values of individual tumours from growth study A. **C:** Western blot analysis of MMP-3 expression in Kin1^{null}, Kin1^{wt} and Kin1^{AA} SCC cell lines grown in 2D and 3D cell culture. Arrows indicate MMP-3 bands. Each lane contains 15 µg of lysate. β-actin was used as loading control.

RNA-Seq data revealed a ~4-fold higher *Mmp13* expression in Kin1^{null} compared to Kin1^{wt} SCC tumours **(Table 4)**, which resembled our results on *Mmp3* expression. q-PCR analysis validated that Kin1^{null} tumours from growth studies A and C had greater *Mmp13* levels than Kin1^{wt} SCC tumours **(Fig.46.A.i.,B.i.)**. Correlation analysis between *Mmp13* expression and tumour volume presented a similar trend with the correlation between *Mmp3* expression and tumour volume **(Fig.46.A.ii-iii.,B.ii-iii.)**. Samples from growth study A showed a strong, positive and a very strong, negative correlation between *Mmp13* expression and Kin1^{null} and Kin1^{wt} tumour volume, respectively **(Fig.46.A.ii-iii.)**. Similarly, in samples from growth study C, *Mmp13* expression had a weak, positive and a strong, negative correlation with Kin1^{null} and Kin1^{wt} tumour volume, respectively **(Fig.46.B.ii-iii.)**.

Similarly to the *in vitro Mmp3* expression pattern **(Fig.45.C.i.)**, Kin1^{null}, Kin1^{wt} and Kin1^{AA} cell lines grown in 3D culture had significantly higher *Mmp13* levels when compared to 2D culture counterparts **(Fig.46.C.i.)**. Overall, 2D and 3D culture cells displayed similar *Mmp13* expression pattern **(Fig.46.C.i-ii.)**. We noticed that Kin1^{null} 2D and 3D culture cells had lower *Mmp13* levels compared to Kin1^{wt} equivalents, although the difference was significant only in cells from 2D culture **(Fig.46.C.i-ii.)**. Although not significant, we observed that in both 2D and 3D culture cells, *Mmp13* expression in Kin1^{AA} cells was, similarly to Kin1^{null} cells, lower than *Mmp13* expression in Kin1^{wt} cells **(Fig.46.C.i-ii.)**.

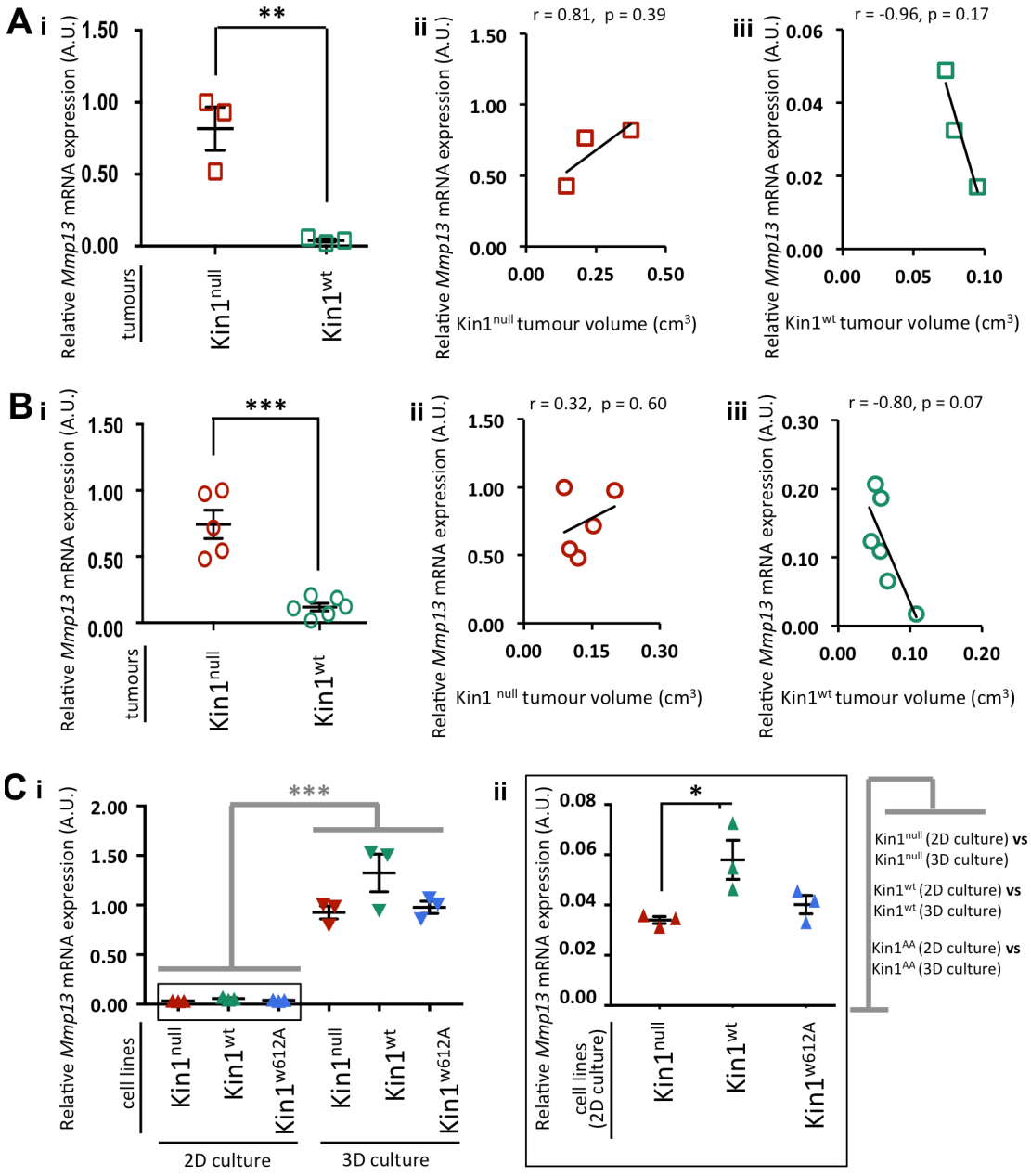

Figure 46: Analysis of *Mmp13* gene expression levels in Kin1^{null} and Kin1^{wt} SCC tumours and Kin1^{null}, Kin1^{wt} and Kin1^{AA} SCC cell lines. q-PCR assay was performed using cDNA from Kin1^{null} and Kin1^{wt} tumours from growth studies A and C. **A(i),B(i):** Quantification of relative *Mmp13* mRNA expression in relation to *Gapdh* expression in Kin1^{null} and Kin1^{wt} tumours. Results presented as scatter plot ± SEM. Every value within each growth's study tumour cohort was normalised against the highest Kin1^{null} tumour value. **A(ii-iii),B(ii-iii):** Pearson's correlation between relative *Mmp13* expression and tumour volume in Kin1^{null} and Kin1^{wt} tumours. r= correlation coefficient value. **A-B:** Unpaired t-test; p-value > 0.05, ** p-value ≤ 0.01, *** p-value ≤ 0.001. **A:** Squares represent values of individual tumours from growth study A. **B:** Circles represent values of individual tumours from growth study C.

C(i): Quantification of relative *Mmp13* mRNA expression in relation to *Gapdh* expression in Kin1^{null}, Kin1^{wt} and Kin1^{AA} SCC cell lines grown in 2D and 3D cell culture. Results presented as scatter plot ± SEM. Every value within each cell line was normalised against the highest value from Kin1^{null} 3D culture cells. Three biological replicates were analysed per cell line. one-way ANOVA with Tukey's multiple comparison test; p-value > 0.05, * p-value ≤ 0.05, *** p-value ≤ 0.001. Thick grey line indicates that statistical testing compared *Mmp3* expression in Kin1^{null}, Kin1^{wt} and Kin1^{AA} SCC cells grown in 2D culture against their 3D counterparts **(ii):** Magnification of C(i) graph of cell lines grown in 2D cell culture.

5.10.2.2. Analysis of expression of Membrane-Type Matrix Metalloproteinase (MT-MMP) genes *Mmp15* in Kin1^{null} and Kin1^{wt} mouse SCC tumours

According to RNA-Seq **(not included in Table 4),** expression levels of MT-MMP gene *Mmp15* did not vary significantly between Kin1^{null} and Kin1^{wt} tumours. This was confirmed by q-PCR assay, which revealed no changes in *Mmp15* expression between Kin1^{null} and Kn1^{wt} tumours from growth studies B and C (**Fig.47.A.i.,B.i.**). Correlation coefficient analysis between *Mmp15* expression and tumour volume provided inconsistent results among different growth study tumour cohorts. In particular, volume of Kin1^{null} tumours from growth study B had weak, positive correlation, whereas from study C had a strong, negative correlation with *Mmp15* expression (**Fig.47.A.ii.,B.ii.**),. Moreover, volume of Kin1^{wt} tumours from growth study B had no correlation, whereas from study C has moderate, positive correlation with *Mmp15* expression (**Fig.47.A.iii.,B.iii.**).

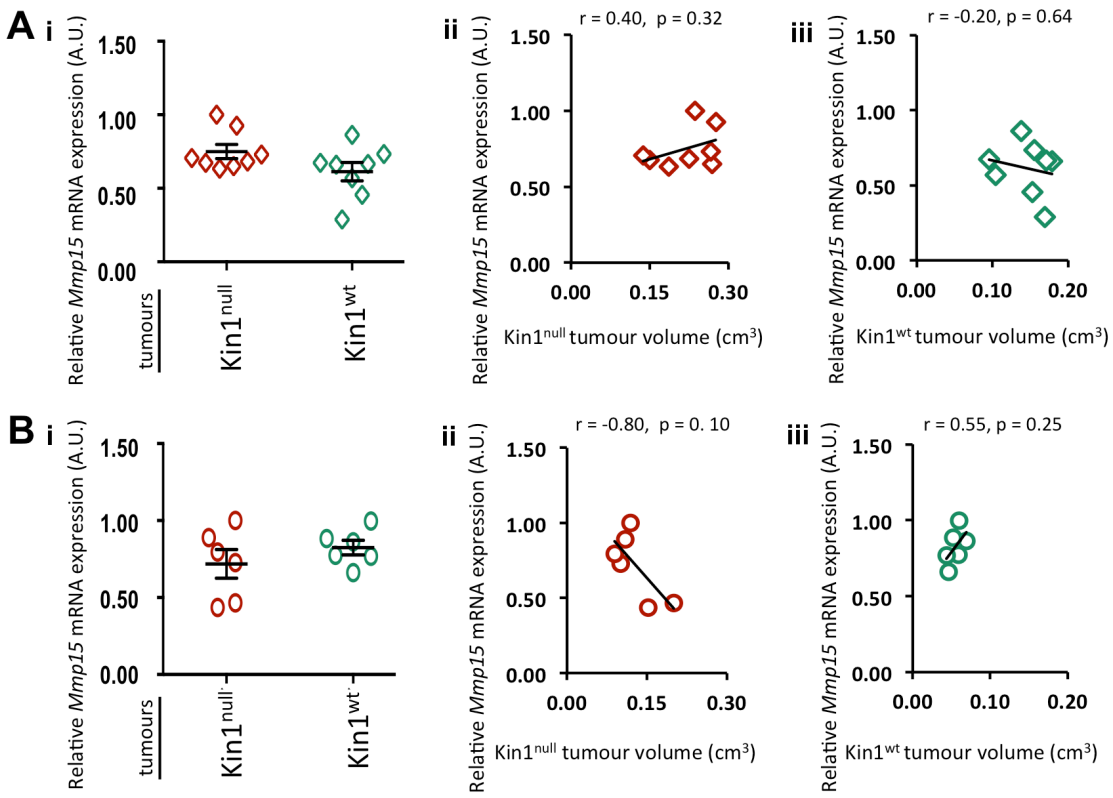

Figure 47: Analysis of *Mmp15* gene expression levels in Kin1^{null} and Kin1^{wt} SCC tumours. q-PCR assay was performed cDNA from Kin1^{null} and Kin1^{wt} tumours from growth studies B and C. **A(i),B(i):** Quantification of relative *Mmp15* mRNA expression in relation to *Gapdh* expression in Kin1^{null} and Kin1^{wt} tumours. Results presented as scatter plot ± SEM. Every value within each growth's study tumour cohort was normalised against the highest Kin1^{null} tumour value. **A(ii-iii),B(ii-iii):** Pearson's correlation between relative *Mmp15* expression and tumour volume in Kin1^{null} and Kin1^{wt} tumours. r= correlation coefficient value. **A-B:** Unpaired t-test; p-value > 0.05. **A:** Diamonds represent values of individual tumours from growth study B. **B:** Circles represent values of individual tumours from growth study C.

5.10.2.3. Analysis of expression of "A Disintegrin and Metalloproteinase with Thrombospondin motif" (ADAMTS) genes *Adamts6*, *Adamts12* and *Adamts17* in Kin1^{null} and Kin1^{wt} mouse SCC tumours

Adamts17 expressed ~5-fold lower transcript levels in Kin1^{null} SCC tumours when compared to Kin1^{wt} tumours, according to RNA-Seq (**Table 4**). On the other hand, gene expression profiling revealed that various other Adamts genes, such as *Adamts6* and *Adamts12* presented no significant changes between Kin1^{null} and Kin1^{wt} tumours.

Similarly to RNA-Seq results **(not included in Table 4)**, we detected no changes in the expression levels of *Adamts6* and *Adamts12* between Kin1^{null} and Kin1^{wt} tumours from growth study B (**Fig.48.A.i.,B.i.**). *Adamts6* levels had a strong and weak, negative correlation with volume of Kin1^{null} and Kin1^{wt} tumours, respectively (**Fig.48.A.ii-iii.**). Kin1^{null} tumour volume showed weak, negative correlation, whereas Kin1^{wt} tumour volume showed a moderate, positive correlation with *Adamts12* expression levels (**Fig.48.B.ii-iii.**).

Finally, we validated that *Adamts17* levels were significantly lower in Kin1^{null} compared to Kin1^{wt} tumours from growth study B (**Fig.48.C.i.**). Furthermore, we detected a moderate, negative, and a strong, positive correlation between *Adamts17* expression and volume of Kin1^{null} and Kin1^{wt} tumours, respectively (**Fig.48.C.ii-iii.**).

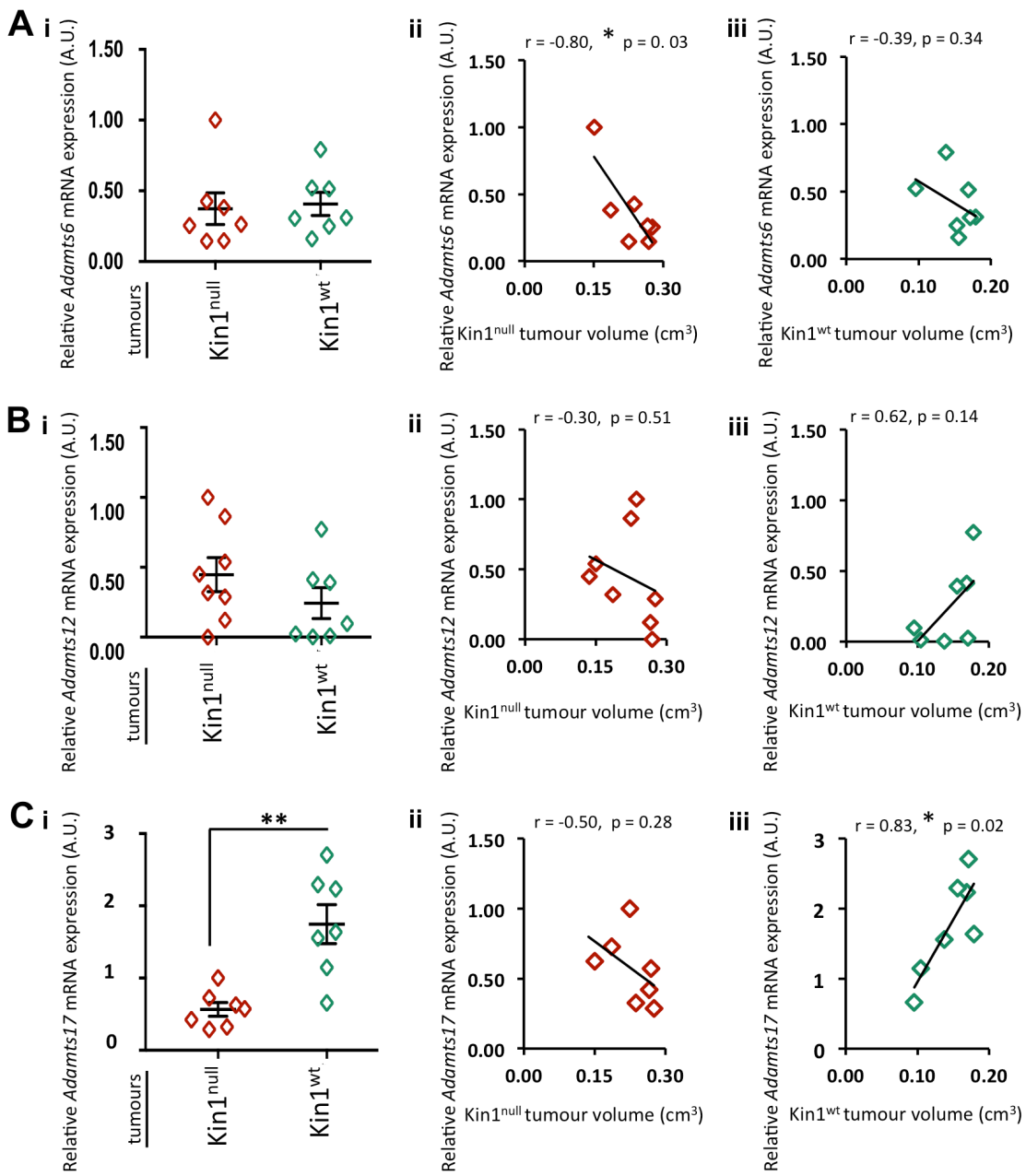

Figure 48: Analysis of *Adamts6, Adamts12* and *Adamts17* gene expression levels in Kin1^{null} and Kin1^{wt} SCC tumours. q-PCR assay was performed using cDNA from Kin1^{null} and Kin1^{wt} tumours from growth study B. **A(i),B(i),C(i):** Quantification of relative *Adamts6*, *Adamts12* and *Adamts17* mRNA expression in relation to *Gapdh* expression in Kin1^{null} and Kin1^{wt} tumours. Results presented as scatter plot ± SEM. Every value within each growth's study tumour cohort was normalised against the highest Kin1^{null} tumour value. **A:** Mann-Whitney. **B-C:** Unpaired t-test. **A(ii-iii),B(ii-iii),C(ii-iii):** Pearson's correlation between relative *Adamts6*, *Adamts12* and *Adamts17* expression and tumour volume in Kin1^{null} and Kin1^{wt} tumours. r= correlation coefficient value. Unpaired t-test. **A-C:** p-value >

0.05, * p-value ≤ 0.05, ** p-value ≤ 0.01. Diamonds represent values of individual tumours from growth study B.

5.10.3. Analysis of expression of angiogenesis factors in Kin1^{null} and Kin1^{wt} mouse SCC tumours

RNA-Seq revealed that various angiogenesis related genes were enriched in Kin1^{null} tumours compared to Kin1^{wt} tumours. In particular, we identified that *Angiopoietin1*, which encodes a promoter of angiogenesis [180][181], had a ~2-fold **(q-value=0.007, not shown in Table 4)** higher expression in Kin1^{null} compared to Kin1^{wt} SCC tumours. Similarly, *Vcam1* (Vascular Cell Adhesion Molecule-1), which also encodes a pro-angiogenic protein [182], had ~2-fold **(q-value=0.002, not shown in Table 4)** significantly higher expression levels in Kin1^{null} tumours when compared to Kin1^{wt} tumours. Finally, Kin1^{null} tumours had ~2-fold higher expression of *Hif1α* (Hypoxia-inducible factor 1α) **(q-value=0.046, not shown in Table 4)** in comparison to Kin1^{wt} tumours, which encodes a protein heavily implicated in promotion of angiogenesis under hypoxic conditions [183].

Primers for a number of the above genes, such as *Angpt1*, resulted in nonspecific annealing and primer elongation events, which prevented us from validating RNA-Seq variations in this gene. As a result, we used q-PCR to validate expression changes of *Hif1a*, for which we had a reliable set of primer, and to explore expression of other angiogenesis-related genes, in Kin1^{null} and Kin1^{wt} tumours.

5.10.3.1. Analysis of expression of *Hif1α* gene in Kin1^{null} and Kin1^{wt} mouse SCC tumours

Q-PCR analysis confirmed significantly higher *Hifıα* expression levels in Kinı^{null} tumours compared to Kinı^{wt} tumours from growth study C (**Fig.49.i.**). No correlation was observed between Kinı^{null} tumour volume and *Hifıα* expression levels (**Fig.49.ii.**), whereas we found a moderate, negative correlation between Kinı^{wt} tumour volume and *Hifıα* expression (**Fig.49.iii.**).

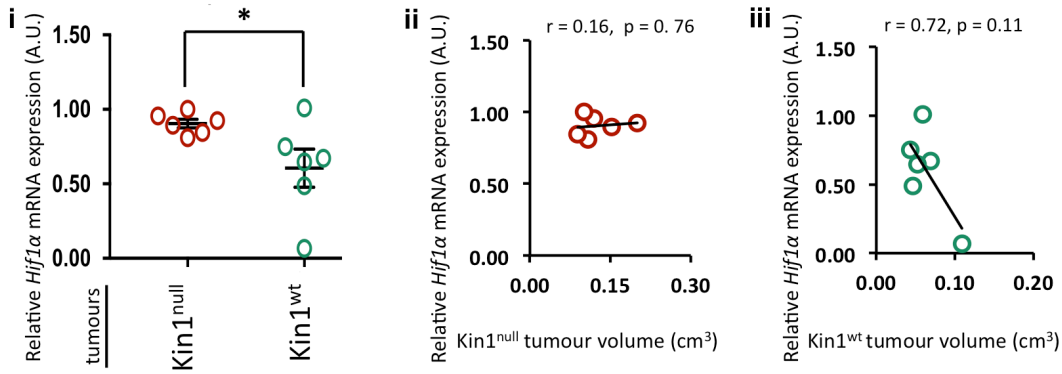

Figure 49: Analysis of *Hif1α* gene expression levels in Kin1^{null} and Kin1^{wt} SCC tumours. q-PCR assay was performed using cDNA from Kin1^{null} and Kin1^{wt} tumours from growth study C. **(i):** Quantification of relative *Hif1α* mRNA expression in relation to *Gapdh* expression in Kin1^{null} and Kin1^{wt} tumours. Results presented as scatter plot ± SEM. Every value within each growth's study tumour cohort was normalised against the highest Kin1^{null} tumour value. **(ii-iii):** Pearson's correlation between relative *Hif1α* expression and tumour volume in Kin1^{null} and Kin1^{wt} tumours. r= correlation coefficient value. **(i-iii):** Unpaired t-test; p-value > 0.05, * p-value ≤ 0.05. Circles represent values of individual tumours from growth study C.

5.10.3.2. Analysis of expression of *Vegfa (Vascular endothelial growth a), Flt1 (FMS-like tyrosine kinase 1)* and *Kdr (Kinase insert domain receptor)* gene in Kin1^{null} and Kin1^{wt} mouse SCC tumours

VEGFA is one of the primary factors driving expansion of the vascular bed in physiological and pathological processes [184]. Thus, despite not being included in the array of differentially expressed genes identified through RNA-Seq, we examined expression of *Vegfa* as well as *Flt1* and *Kdr*, which encode two of VEGFA's main receptors VEGFR1 (VEGF Receptor 1) and VEGFR2, respectively.

We did not observe any statistically significant difference between *Vegfa, Flt1* or *Kdr* between Kin1^{null} and Kin1^{wt} tumours **(Fig.5o.A.i.,B.i.,C.i.)**. However, the volume of Kin1^{null} tumours had a strong, weak and very strong, negative correlation with levels of *Vegfa*, *Flt1* and *Kdr,* respectively **(Fig.5o.A.ii.,B.ii.,C.ii.)**. Inversely, volume of Kin1^{wt} tumours had a very strong, moderate and very strong, positive correlation with *Vegfa*, *Kdr* and *Flt1* levels, respectively **(Fig.5o.A.iii., B.iii., C.iii.)**.

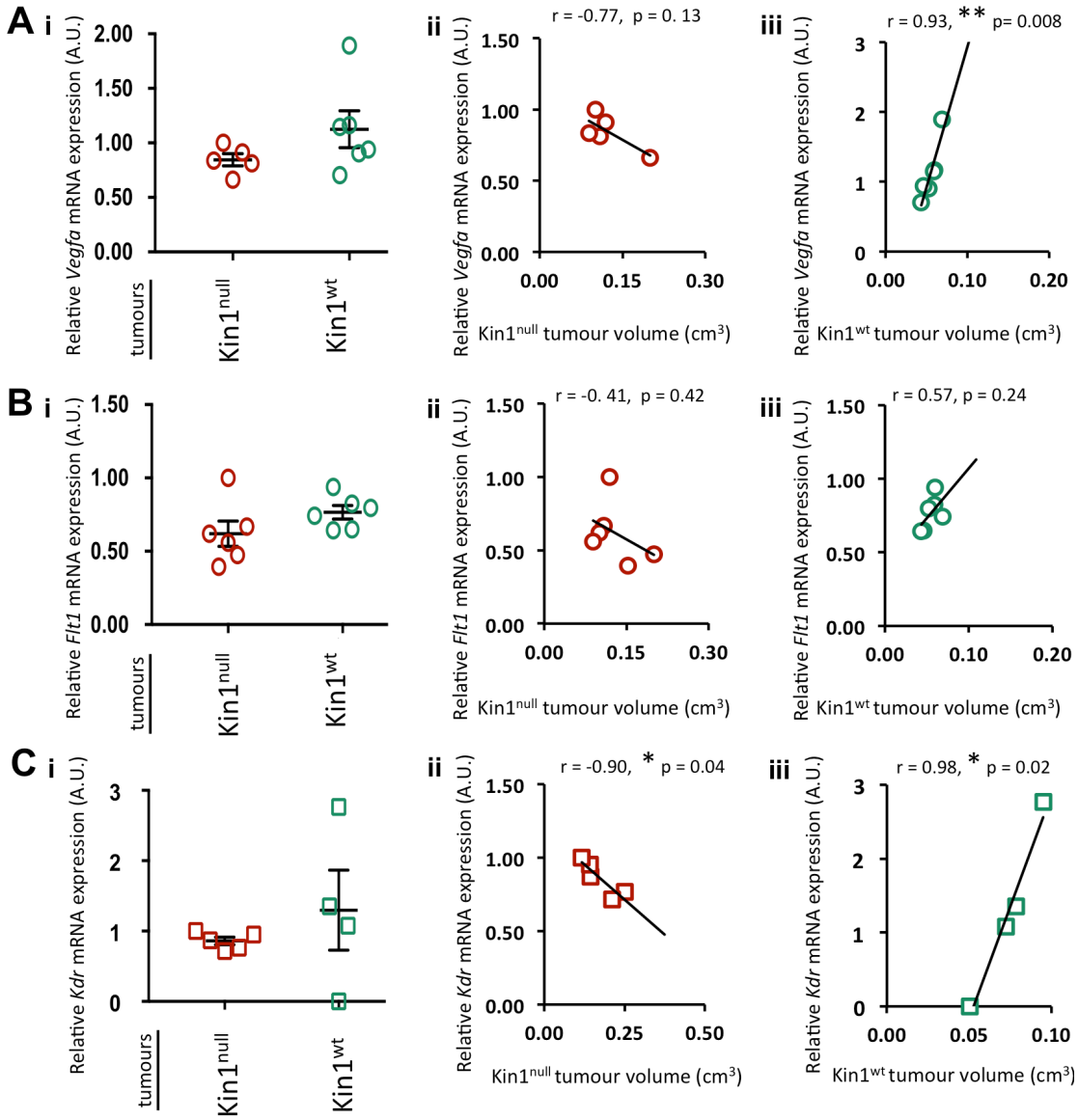

Figure 50: Analysis of *Vegfa, Flt1* and *Kdr* gene expression levels in Kin1^{null} and Kin1^{wt} SCC tumours. q-PCR assay was performed using cDNA from Kin1^{null} and Kin1^{wt} tumours from growth study C or A. **A(i),B(i),C(i):** Quantification of relative *Vegfa, Flt1* and *Kdr* mRNA expression in relation to *Gapdh* expression in Kin1^{null} and Kin1^{wt} tumours. Results presented as scatter plot ± SEM. Every value within each growth's study tumour cohort was normalised against the highest Kin1^{null} tumour value. **A(ii-iii),B(ii-iii),C(ii-iii):** Pearson's correlation between relative *Vegfa, Flt1* and *Kdr* expression and tumour volume in Kin1^{null} and Kin1^{wt} tumours. r= correlation coefficient value. **A-C:** Unpaired t-test; p-value > 0.05, * p-value ≤ 0.05, ** p-value ≤ 0.01. **A-B:** Circles represent values of individual tumours from growth study C. **C:** Squares represent values of individual tumours from growth study A.

5.10.3.3. Analysis of expression of Thbs1 gene in Kin1^{null} and Kin1^{wt} mouse SCC tumours

Despite not being identified through RNA-Seq, we also examined expression of *Thbs1* gene, which encodes Thrombospondin 1 (TSP1), an adhesive glycoprotein and a potent endogenous inhibitor of angiogenesis [185][186]. Following q-PCR analysis in samples from growth studies A and B, we detected significantly lower *Thbs1* expression in Kin1^{null} compared to Kin1^{wt} tumours (**Fig.51.A.i.,B.i.**). Volume of Kin1^{null} tumours from growth study A had no correlation with *Thbs1* levels, whereas from growth study B had a weak, positive correlation with *Thbs1* levels (**Fig.51.A.ii.,B.ii.**). Overall, Kin1^{wt} tumour volumes from studies A and B showed strong positive correlation with *Thbs1* levels (**Fig.51.A.iii.,B.iii.**).

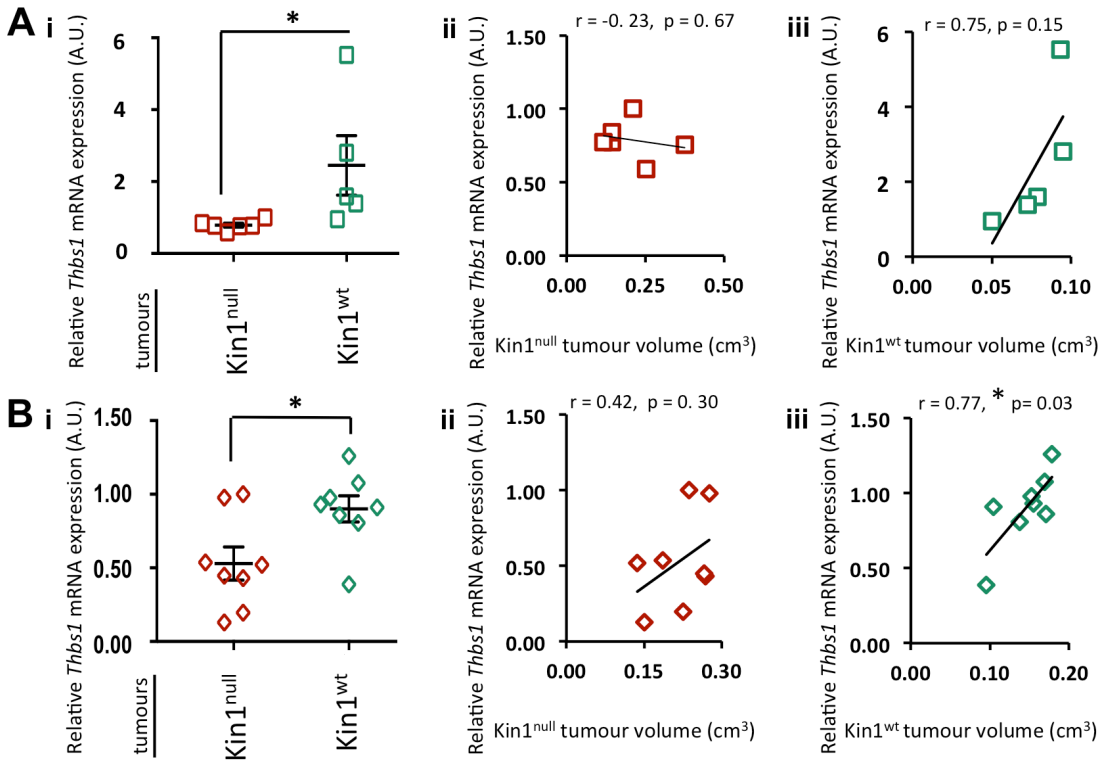

Figure 51: Analysis of *Thbs1* gene expression levels in Kin1^{null} and Kin1^{wt} SCC tumours. q-PCR assay was performed using cDNA from Kin1^{null} and Kin1^{wt} tumours from growth study A and B. **A(i),B(i):** Quantification of relative *Thbs1* mRNA expression in relation to *Gapdh* expression in Kin1^{null} and Kin1^{wt} tumours. Results presented as scatter plot ± SEM. Every value within each growth's study tumour cohort was normalised against the highest Kin1^{null} tumour value. **A(ii-iii),B(ii-iii):** Pearson's correlation between relative *Thbs1* expression and tumour volume in Kin1^{null} and Kin1^{wt} tumours. r= correlation coefficient value. **A-B:** Unpaired t-test; p-value > 0.05, * p-value ≤ 0.05. **A:** Squares represent values of individual tumours from growth study A. **B:** Diamonds represent values of individual tumours from growth study B.

5.10.4. Analysis of expression of chemokines in Kin1^{null} and Kin1^{wt} mouse SCC tumours

RNA-Seq revealed that Kin1^{null} SCC tumours had enrichment in genes that encode chemokines. Chemokines, which are chemoattractants that play a role in recruiting and, subsequently, directing migration of immune cells, and are subdivided into four subfamilies based on their N-terminus structure [187]. Compared to Kin1^{wt} tumours, we found that Kin1^{null} tumours had significantly higher expression in genes encoding chemokines from the C-X-C subfamily, whose N-terminus contains two cysteines separated by a variable amino acid, and the C-C subfamily, characterised by an N-terminus with two adjacent cysteine residues [186].

We saw that expression of *Cxcl1 (C-X-C motif ligand 1)* and *Cxcl5* chemokines was ~3- **(q-value=0.007, data not shown in Table 4)** and ~2-fold **(q-value=0.002, data not shown in Table 4)** higher in Kin1^{null} compared to Kin1^{wt} tumours. We proceeded to confirm that *Cxcl1* levels in Kin1^{null} tumours were significantly higher compared to Kin1^{wt} ones from growth study C **(Fig.521.A.i.)**. Moreover, we observed that *Cxcl1* levels had a strong, positive correlation with Kin1^{null} tumour volume, and, a very strong, negative correlation with Kin1^{wt} tumour volume **(Fig.52.A.ii-iii.)**.

Moreover, we detected that levels of *Ccl2 (C-C motif ligand 2)* and *Ccl7* chemokine genes were ~2-fold higher **(q-value=0.003, data not shown in Table 4)**, and levels of *Ccl9* were ~4-fold **(q-value=0.004, Table 4)** higher in Kin1^{null} tumours compared to Kin1^{wt} tumours. Q-PCR assay confirmed that Kin1^{null} tumours from growth study C had significantly higher levels of *Ccl2* and *Ccl7* compared to Kin1^{wt} counterparts **(Fig.52.B.i.,C.i.)**. Correlation analysis indicated that levels of *Ccl2* and *Ccl7* had a strong and a moderate, positive correlation with volume of Kin1^{null} tumours **(Fig.52.B.ii.,C.ii.)**. In

contrast, *Ccl2* and *Ccl7* expression had a strong, negative correlation with Kin1^{wt} tumour volume (**Fig.52.B.iii.,C.iii.**).

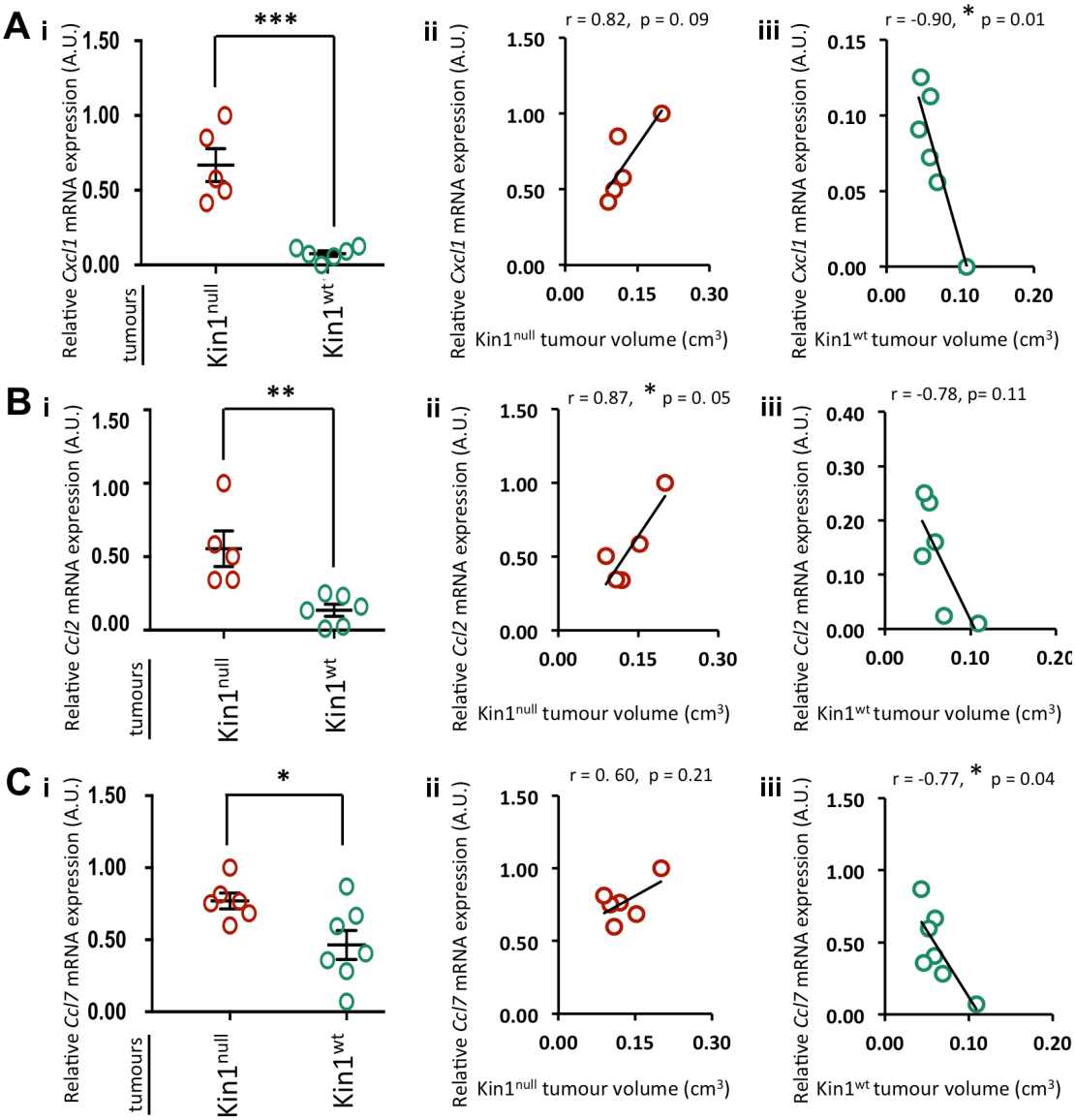

Figure 52: Analysis of *Cxcl1, Ccl2* and *Ccl7* gene expression levels in Kin1^{null} and Kin1^{wt} SCC tumours. q-PCR assay was performed using cDNA from Kin1^{null} and Kin1^{wt} tumours from growth study C. **A(i),B(i),C(i):** Quantification of relative *Cxcl1, Ccl2* and *Ccl7* mRNA expression in relation to *Gapdh* expression in Kin1^{null} and Kin1^{wt} tumours. Results presented as scatter plot ± SEM. Every value within each growth's study tumour cohort was normalised against the highest Kin1^{null} tumour value. **A(ii-iii),B(ii-iii),C(ii-iii):** Pearson's correlation between relative *Cxcl1, Ccl2* and *Ccl7* expression and tumour volume in Kin1^{null} and Kin1^{wt} tumours. r= correlation coefficient value. Unpaired t-test; p-value > 0.05, * p-value ≤ 0.05, ** p-value ≤ 0.01 *** p-value ≤ 0.001. Circles represent values of individual tumours from growth study C.

The most significant gene expression changes between Kin1^{null} and Kin1^{wt} SCC tumours are summarised below in **Table 6**.

	Mean relative mRNA expression (A.U.)								
Gene name	Tumour samples from growth experiment A		Statistical signifi-cance	Tumour samples from growth experiment B		Statistical signifi-cance	Tumour samples from growth experiment C		Statistical signifi-cance
	Kin1 null	**Kin1 wt**		**Kin1 null**	**Kin1 wt**		**Kin1 null**	**Kin1 wt**	
Mmp3	0.670	0.022	*	---	---	---	0.480	0.008	**
Mmp13	0.817	0.040	**	---	---	---	0.743	0.118	***
Adamts17	---	---	---	0.567	1.747	**	---	---	---
Hif1α	---	---	---	---	---	---	0.904	0.605	*
Thbs1	0.789	2.451	*	0.530	0.901	*	---	---	---
Cxcl1	---	---	---	---	---	---	0.668	0.076	***
Ccl2	---	---	---	---	---	---	0.554	0.135	**
Ccl7	---	---	---	---	---	---	0.769	0.464	*

Table 6: Summary of the most important gene expression alterations between Kin1^{null} and Kin1^{wt} SCC tumours. Results were obtained by performing a q-PCR assay and using cDNA from tumour samples from growth experiment A, or/and B, or/and C. Dark grey colour indicates the growth experiment from which tumour samples had been tested. p-value > 0.05, * p-value ≤ 0.05, ** p-value ≤ 0.01 *** p-value ≤ 0.001.

5.11. Discussion

Despite the array of data that showcase a role for Kin1 as a promoter of proliferation and clonogenicity *in vitro* [115], and tumour growth and progression *in vivo* [111][112][115], absence of Kin1, paradoxically, predisposes KS patients to the development of cutaneous SCC [2][10][11][12]. In the majority of non-KS related cases, SCC is usually localised and typically treatable [188]. However, in KS patients who develop SCC, particularly in their extremities, cancer is usually aggressive and metastatic, which can even result in amputation of the affected limb, lymph node excision as well as death. The reason behind the enigmatic, aggressive nature of KS-related SCC has not been addressed. The aim of this study was, therefore, to examine the role of Kin1 in cutaneous SCC, both *in vitro* and *in vivo*, and propose a mechanistic explanation for the behaviour of KS-related SCC.

To achieve this, we used mouse SCC cell lines that had derived from SCC tumours previously generated following the application of two-stage chemical carcinogenesis protocol [126][127] **(Fig.30.A.)**. Use of Kin1-knockout ($Kin1^{null}$) SCC cell line **(Fig.31.A.i.)**, and $Kin1^{wt}$ SCC cell line in which wild-type *Fermt1* had been re-expressed in $Kin1^{null}$ SCC cells **(Fig.31.A.ii.)** enabled us to scrutinise various biological processes, such as cellular proliferation and tumour growth, in the absence and presence of Kin1. We also inspected if the role of Kin1 in SCC cells and tumours relies upon one of its principal functions as an integrin co-activator, by using a mouse SCC cell line generated following re-expression of mutant *Fermt1* QW611/612AA in $Kin1^{null}$ SCC cells ($Kin1^{AA}$) **(Fig.31.A.iii.)**. Kin1-W611/612A is unable to β1- or β3-integrins, and its expression was shown to lead to impaired integrin activation [49][53].

5.11.1. Role of Kin1 in *in vitro* proliferation

We were first interested in addressing the *in vitro* role of Kin1 towards proliferation of mouse SCC cells, which, prior to this study, has never been

studied. The function of Kin1 in cellular proliferation surfaced a decade ago, when lack of Kin1 was associated with strongly diminished keratinocyte proliferation in KS epidermis and cultivated KS keratinocytes [8]. Likewise, in previous chapters we have shown that loss of Kin1 reduced keratinocyte proliferation in mouse epidermis **(Fig.9.)**, which we hypothesise to occur via defects in mitotic spindle.

It is possible that if the role of Kin1 in maintenance of mitotic homeostasis applies to SCC cells as well, then enhanced spindle abnormalities in Kin1^{null} mouse SCC cells could contribute to cell proliferation and tumour growth. Proper chromosome segregation ensures the maintenance of a diploid karyotype, with missegregation defects often identified as a causal factor of an aneuploid genome [189][190][191]. Aneuploidy can act as a promoter of tumourigenesis and tumour evolution, as the lost or gained chromosomes can harbour loci of tumour suppressor or tumour promoting genes, respectively. *In vivo* studies have correlated aneuploidy with enhanced tumour growth [192] and increased tumour vascularisation [193]. Future examination of mitotic spindle fidelity in mouse SCC tumours will be important in determining whether the potential role of Kin1 in mitosis in SCC contributes to differences between Kin1^{null} and Kin1^{wt} SCC tumour biology.

Fermt1 ablation in mice [54] and depletion of Kin1 in HaCaT immortalised keratinocytes [142] has also been shown to lower keratinocyte proliferation. Finally, stable expression of Kin1 in KS keratinocytes enhanced cell proliferation [94], which, in line with the aforementioned findings, highlights the requirement of Kin1 for keratinocyte proliferation. A regulatory role for Kin1 in proliferation was also demonstrated in MCF7 breast cancer cells, in which overexpression of Kin1 enhanced proliferation and clonogenicity [115].

Despite detecting no proliferation changes amongst Kin1^{null}, Kin1^{wt} and Kin1^{AA}

SCC cell lines cultivated in 2D conditions (**Fig.33.**), we detected significant changes in proliferation and clonogenic potential between cell lines grown in 3D conditions (**Fig.34.**). In particular, Kin1^{null} SCC cells had significantly higher proliferation and clonogenic potential compared to Kin1^{wt} and Kin1^{AA} SCC cells in a 3D environment (**Fig.34.B-C.**). This indicated that in our model, lack of Kin1 granted SCC cells with a proliferative advantage over cells expressing wild-type Kin1 or the non-integrin binding mutant Kin1-QW611/612AA. To our knowledge, this is the first time that expression of Kin1 is shown to reduce proliferation *in vitro*. This correlates with the effects that we see on *in vivo* growth of the SCC tumors and could be appointed to the fact that, in contrast to 2D monolayers, 3D cultures bare a greater physiological relevance to *in vivo* tissue architecture and environment [194].

5.11.2. Role of Kin1 in tumour growth and progression

Kin1^{null} tumours were significantly bigger and had a significantly higher growth rate compared to Kin1^{wt} and Kin1^{AA} tumours (**Fig.35.**). Taken together with our in vitro data this highlights that absence of Kin1 elevates SCC tumour growth, and denotes an *in vitro* and *in vivo* inhibitory role for Kin1 in SCC proliferation and growth. Differences between Kin1^{null} and Kin1^{wt} tumour growth reflect the enhanced proliferation in Kin1^{null} tumours, as evident by Ki-67 staining (**Fig.39.A-C.**), which is in line with our proposition for an anti-proliferative role for Kin1 in SCC. To our knowledge, analogous function for Kin1 in tumour growth has only been remarked in one other study, where expression of Kin1 reduced non-small-cell lung cancer xenograft tumour growth and *in vitro* cell migration [120].

In sharp contrast, numerous studies demonstrated a pro-tumourigenic part for Kin1 in various other types of cancer. Silencing of Kin1 prevented tumour growth in a mouse model of breast cancer [115], and expression of Kin1 was higher in hepatocellular carcinoma than in normal tissue, where it positively

correlated with tumour volume [112]. Kin1 overexpression was also noted in colon, lung and bladder cancer, and in pancreatic cancer cell lines, in comparison to healthy tissue and cells [110][111][115]. In a variety of cancers Kin1 expression also promoted key factors of tumour progression. Overexpression of Kin1 in hepatocellular carcinoma presented a positive correlation with tumour metastatic status and unfavourable overall survival [112], and depletion of Kin1 inhibited breast tumour metastasis in an orthotopic mouse model [115]. Likewise, depletion of Kin1 *in vitro* decreased migratory and invasive properties of pancreatic cancer cells [111]. Thus, our findings indicate for the first time an *in vitro* and *in vivo* anti-proliferative/anti-growth role for Kin1 in mouse SCC model.

5.11.3. Role of Kin1-integrin interaction in tumour growth and proliferation

Separate studies have reported impaired β1 integrin activation in cells that lack Kin1 or express Kin1-W611/612A mutant. Reduced β1 integrin activation has been reported in Kin1-deficient immortal keratinocytes [88] and in intestinal epithelial cells with complete loss of Kin1 [54]. Similarly, cells expressing Kin1-W611/612A mutant protein displayed significant decrease in β3- and β1 integrin binding and activation [49][53][54].

Our lab has simultaneously examined β1 integrin activation in mouse SCC cells that lack Kin1 ($Kin1^{null}$), express wild-type Kin1 ($Kin1^{wt}$) or express Kin1-QW611/612AA mutant protein ($Kin1^{AA}$). Both $Kin1^{null}$ and $Kin1^{AA}$ SCC cell lines, which behaved in a diametrically contrasting manner in proliferation **(Fig.34.)** and tumour growth **(Fig.35.)**, displayed significant reduction in β1 integrin activation when compared to $Kin1^{wt}$ counterpart **(Fig.53. by Dr Hila Emmert)**. However, β1 integrin activation was significantly higher in $Kin1^{AA}$ SCC cells than $Kin1^{null}$ SCC cells **(Fig.53. by Dr Hila Emmert)**. These observations imply that role of Kin1 in proliferation and tumour growth in our mouse SCC model

is independent from its role in β1 integrin activation. However, to examine this theory additional studies have to be performed, such as proliferation and tumour growth assays in the same mouse SCC model following depletion of β1 integrin.

Activation of integrins at focal adhesions is not a function restricted to Kin1, which also could explain the β1 integrin activation observed even in complete absence of Kin1 **(Fig.53. by Dr Hila Emmert)**. Kin2, which is expressed at focal adhesions in all three mouse SCC cell lines **(Fig.33.B.)** is also capable of integrin activation and was shown to partially compensate for Kin1 loss in integrin activation in keratinocytes [88][195]. Moreover, as previously mentioned **(Chapter 1, Section 1.5.)**, while synergy between kindlins and talins is essential for maximal integrin activation, mutations that inhibit - kindlin-integrin binding still permit talin-mediated integrin activation, but block the kindlin enhancement effect *in vitro* [54][68]. This offers a potential explanation for integrin activation at Kin1^{null} and Kin1^{AA} SCC cells, where Kin1 cannot bind β1- and β3- integrins, and yet β1 integrin activation still occurs.

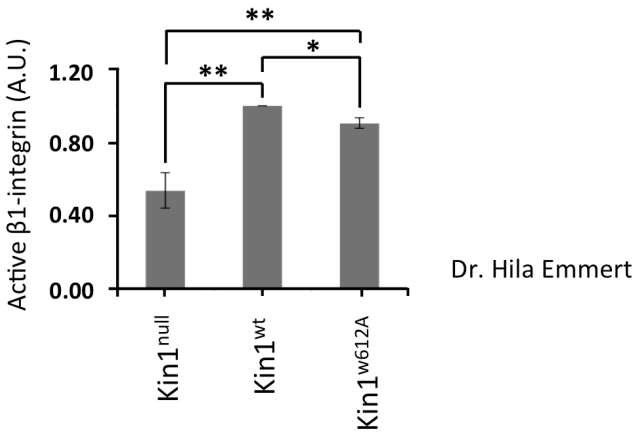

Figure 53: Analysis of β1 integrin activation in Kin1^{null}, Kin1^{wt} and Kin1^{AA} SCC cells. Flow cytometry was performed with a 9EG7 antibody, which reacts with active β1 integrin[307], on Kin1^{null}, Kin1^{wt} and Kin1^{AA} SCC cells. Quantification of active β1 integrin was performed in relation to total β1 integrin levels. Results presented as mean ± SEM. Kin1^{null} and Kin1^{AA} values were normalised against the highest Kin1^{wr} value. one-way ANOVA with Tukey's multiple comparison test; p-value > 0.05, * p-value ≤ 0.05, ** p-value ≤ 0.01.

Although we have not examined this, we hypothesise that higher β1 integrin activation in Kin1^{AA} SCC cells could suggest that, additionally to QW611/612 Kin1-integrin binding site, other β1 integrin binding sites are mapped to Kin1 and are important for integrin activation and binding. Examples include K610 and I651, both of which were identified on human Kin1, and their mutagenesis strongly inhibited binding to β1 integrin tails [49]. In support of this we saw Kin1-QW611/612AA localisation at focal adhesions **(Fig.32.A.)**. However, in other studies this integrin binding mutant failed to accumulate at focal adhesions [49][170] and compromised activation of β1- and β3-integrins [37][49] in NIH-3T3 and CHO cells, respectively. Kin1 has various binding partners that are part of focal adhesion macromolecular assemblies, including Kin2, FAK and migfilin [142][196], which could potentially retain Kin1 at focal adhesions in SCC cells in the absence of integrin binding.

5.11.4. Role of Kin1 in regulating the tumour microenvironment

It has emerged that interactions of abnormal cells that encompass malignant potential with their microenvironment can aid tumour development and progression. Key constituents of the microenvironment include the tumours surrounding supportive ECM and components of the immune system and vasculature. Therefore, examining the interplay between mouse SCC tumours and their microenvironment would provide us with a better understanding regarding the differences in growth, proliferation and angiogenesis between Kin1^{null} and Kin1^{wt} tumours.

5.11.4.1. Role of Kin1 in regulating angiogenesis

Tumour growth depends on adequate supply of nutrients and oxygen and removal of catabolites via the tumour's vascular network, which is formed through angiogenesis, a well-established hallmark of cancer [197]. Compared to Kin1^{wt} tumours, Kin1^{null} SCC tumours had higher vascularisation **(Fig.41.)**, which could stem from enhanced expression of angiogenic activators and

supressed expression of angiogenic inhibitors in Kin1^{null} tumours. A key promoter of angiogenesis in hypoxic areas such as localised ischemia and tumours [183] is HIF1A, and expression of *Hif1a* mRNA was significantly higher in Kin1^{null} tumours compared to Kin1^{wt} tumours **(Fig.49.i.)**. Higher expression of *Hif-1a* suggests a more hypoxic environment in Kin1^{null} tumours, which has been linked to a more clinically aggressive metastatic behaviour [198]. Kin1^{null} SCC tumours also presented a lower expression of *Thbs1* **(Fig.51.i.,B.i.)**, which encodes TSP1, an anti-angiogenic protein that exerts an inhibitory outcome on tumour vascularity and positively correlates with lower tumour invasion and better overall prognosis [199][200].

Thus, we show for the first time an *in vivo* anti-angiogenic role for Kin1 in mouse SCC model. This may offer an insight to the properties of SCC developed in KS patients and a potential link between the aggressive nature of KS SCC tumours and enhanced growth as well as angiogenesis.

Induction of tumour vasculature, termed the "angiogenic switch", can occur at different points within tumour development/progression. For example, neovascularisation can happen in premalignant or dormant lesions where it aids progression to malignancy [201], as well as in malignant tumours to sustain and enhance propagation following, for example, the induction of hypoxia. We are not aware, yet, whether angiogenesis is the cause of tumour growth in our model, or was consequentially induced by mouse SCC tumours to support tumour gradual growth, or a combination of the two. Dissecting the cause-and-effect relationship between angiogenesis and growth in our tumour model will help us understand tumour evolution and maintenance in our mouse SCC model and, ultimately, SCC patients in KS.

5.11.4.2. Role of Kin1 in regulating the ECM

5.11.4.2.1. Role of Kin1 in regulating MMPs

MMP3 and MMP13 are members of the MMP subfamily of metalloproteinases, which are potent enzymes that, once activated, degrade and, ultimately, remodel ECM [202]. *Mmp3* and *Mmp13* were significantly upregulated in Kin1^{null} SCC tumours **(Table 4)** **(Fig.44.A.i.,B.i.)**, **(Fig.46.A.i.,B.i.)**. Changes observed in *Mmp3* expression between tumours translated in the protein level **(Fig.45.B.)**. We detected cytoplasmic and extracellular localisation of MMP3, as MMPs are synthesised and stored in the cytoplasm prior to secretion and engage in proteolytic degradation of macromolecules in the ECM [203].

Notably, Kin1^{null} tumours had lower expression of collagen-I, one of the most abundant proteins in the ECM, compared to Kin1^{wt} tumours **(Fig.38)**, which we believe may explain why morphological evaluation of tumour histology indicated lower ECM deposition in Kin1^{null} tumours **(Fig.37.A.)**, and link to the higher *Mmp3* and *Mmp13* expression in Kin1^{null} tumours **(Fig.44.A.i.,B.i.)**, **(Fig.45.A(i),B(i))**. Gel zymography is an important experiment to be performed in the future, as it will determine the proteolytic activity of MMP3 and MMP13 in tumours, and provide a direct link between these MMPs and degradation of ECM components.

MMPs are able to degrade and structurally reform the ECM as well as the vascular basement membrane, which allows migration of vascular endothelial cells and potentiates formation of new blood vessels. Specific MMPs, including MMP3, contribute to angiogenesis in more ways than ECM remodelling. Examples include release of ECM-tethered angiogenic growth factors, such as basic fibroblast growth factor [204], and exposure of cryptic pro-angiogenic sites, such as α5β3 integrin-binding sites that are normally hidden within matrix-immobilised collagen type IV [205]. Thus, increased *Mmp3* and *Mmp13* expression in Kin1^{null} tumours could connect to the enhanced vasculature, and

enhanced *Hif1a* and suppressed *Thbs1* expression, observed in Kin1^{null} tumours.

As with various other MMPs, MMP3- and MMP13-mediated augmentation of angiogenesis, which can occur at various stages of tumour development and/or progression, contributes to tumour growth enhancement, as noted by studies in glioblastoma, gastric cancer and melanoma [206]–[208]. Moreover, proteolytic processing by MMPs can regulate tumour growth by increasing bioavailability of growth factors that are otherwise bound to ECM or to cell membranes. Prominent examples include degradation of insulin-like growth-factor-binding proteins by MMP3 and MMP7, which facilitates bioavailability of insulin-like growth factor (IGF), an anti-apoptotic and mitogenic factor, favouring cancer cell proliferation [209][210]. MMP3 and MMP7 are also capable of shedding of transmembrane HB-EGF (heparin-binding epidermal growth factor-like growth factor), another potent mitogenic factor that promote proliferation [211][212].

In line with these findings, our results showed that *Mmp3* and *Mmp13* levels correlated positively with volume of Kin1^{null} tumours and negatively with volume of Kin1^{wt} tumours **(Fig.44.A.ii-iii.,B.ii-iii.), (Fig.46.A.ii-iii.,B.ii-iii.)**. Overall, our data imply a potential link between *Mmp3* and *Mmp13* levels and tumour growth in our model. Our data may also suggest a multifunctional role for *Mmp3* and *Mmp13*, which could be context- and expression level-dependent, in our mouse SCC tumour model. *In vivo* tumour growth studies with MMP3 or MMP13-deficient mouse SCC cells, will offer an insight on whether these MMPs play a role in tumour growth in our model, and whether this role is regulated by Kin1. Future correlation analysis between *Mmp3* and *Mmp13* levels and vascularisation in our samples, which we were unable to perform as there was no overlap between the tumours in which we examined CD31 expression and *Mmp3* and *Mmp13* levels, will reveal if there is a connection between *Mmp3, Mmp13* and angiogenesis in our mouse model.

Collectively, our data on *Mmp3* and *Mmp13* expression *in vitro* **(Fig.44.C.)**, **(Fig.46.C.)** did not reflect *Mmp3* and *Mmp13* expression *in vivo*, nor did they reflect a pattern that could underline proliferation and clonogenicity data in 2D and 3D conditions. Dissimilarity between *in vivo* and *in vitro* data in *Mmp3* and *Mmp13* expression suggests differences between the potential mechanism that controls cell proliferation *in vitro* and *in vivo*.

Interestingly, our report is not the first study to show a connection between Kin1 and MMPs. As aforementioned, only one other study shows Kin1 as an inhibitor of tumour growth, which also reported downregulation of *Mmp7*, *Mmp9* and *Mmp13* following ectopic expression of Kin1 in non-small cell lung cancer *in vitro* [120]. Moreover, Kin1 deficient immortalised HaCat keratinocytes expressed higher levels of MMP2 and MMP9 [213]. Thus, our findings are in concert with literature, demonstrating that Kin1 is a negative regulator of various MMPs in more than one cell types.

Finally, another important function of MMPs in cancer is promotion of metastasis, which they achieve by removing physical barriers posed by basement membranes within the ECM thus allowing cell invasion, intravasation and extravasation. This is shown by the fact that depletion of loss of MMP3 reduced invasion in gastric cancer cells in vitro [214] and spontaneous lung metastasis in mammary carcinoma in vivo [215], respectively. Moreover, thyroid cancer cohort study found that expression of MMP13 was increased in metastatic versus primary tumours [216], and silencing of MMP13 in melanoma and thyroid cancer cells decreased metastasis in vivo [215][217].

Two critical steps of the metastatic process are intravasation and extravasation. Intravasation involves movement of cancer cells in tumour embedded or neighbouring blood vessels that allow them to travel via

circulation, and they are termed as circulating tumour cells (CTCs). Following arrest of CTCs in the capillary bed, cells then traverse the endothelial cell lining of vascular wall in a process termed extravasation, and invade the extravascular tissue where they establish metastasis. Inhibition of MMP3 was linked to inhibited intravasation in an orthotopic ovarian cancer model, whereas MMP13 was shown to promote extravasation of colorectal cancer cells in the liver microenvironment [218]. Thus, elevated *Mmp3* and *Mmp13* expression may predict enhanced metastatic ability for $Kin1^{null}$ SCC tumours compared to $Kin1^{wt}$ counterparts via augmented intravasation and extravasation.

Histological examination indicated that all SCC tumours were invasive to skeletal muscle **(Fig.36.)**, but we have yet to examine any potential variation in invasive and metastatic capacity between $Kin1^{null}$ and $Kin1^{wt}$ SCC tumours. To scrutinise this, we will search for levels of CTC in the bloodstream, which is a biomarker readily used in estimation of intravasation and metastatic progression [219]. Moreover, tail-vein injections will result in intravessel growth of $Kin1^{null}$ and $Kin1^{wt}$ SCC cells in the lung microenvironment, which will help interrogate subsequent extravasation and lung colonisation. Finally, examination of metastatic burden in lymph nodes, liver, lung and other organs following termination of future tumour growth experiment, and tumour extraction, will help us further define any differences in metastatic ability amongst $Kin1^{null}$ and $Kin1^{wt}$ SCC tumours.

5.11.4.2.2. Role of Kin1 in regulating ADAMTSs

Various genes from the ADAMTS subfamily of metalloproteinases, such as *Adamts17* were identified through RNA-Seq and validated through q-PCR as having significantly lower expression in $Kin1^{null}$ compared to $Kin1^{wt}$ tumours **(Table 4), (Fig.48.C.i.)**, contrary to the expression pattern observed in MMP genes. Our data parallel numerous literature findings that show that

expression of ADAMTS genes is reduced in a variety of cancers, including breast, lung and oesophageal SCC [220]–[223].

Due to limited research in *Adamts17*, its specific roles in cancer are unknown. However, research in various other ADAMTSs, such as ADAMTS1 and ADAMTS9, reveals an angiostatic role for these proteins [224][225]. As suggested by their nomenclature, ADAMTSs share a motif with TSP1, a protein shown to prohibit angiogenesis [199]. However, whereas not all peptides of TSP1 have shown to have anti-angiogenic effects, fragments shared by ADAMTSs and TSP1 were shown to be anti-angiogenic [226]–[228]. Our data, therefore, underline the link between ADAMTSs and TSP1, as, both *Adamts17* and *Thbs1* levels were lower in $Kin1^{null}$ compared to $Kin1^{wt}$ tumours **(Fig.48.C.i.)**, **(Fig.51.A.i.,B.i.)**.

Finally, we observed that *Adamts17* levels correlated with $Kin1^{null}$ and $Kin1^{wt}$ tumour volume in an opposing manner **(Fig.48.C.ii-iii.)**. This implies that via its role in angiogenesis, *Adamts17* expression might also influence tumour growth in a context-specific way, which, in this case, is the presence or absence of Kin1.

5.11.4.3. Role of Kin1 in regulating the immune system

Chemokines are chemoattractants that facilitate leukocyte directed motility, and are induced by inflammatory cytokines, pathogenic stimuli and growth factors [187]. Various studies have implicated expression of chemokines to malignancy, which occurs in a variety of ways.

We identified that a variety of genes that encode chemokines, such as *Cxcl1* **(Fig.52.A.i.)**, *Ccl2* **(Fig.52.B.i.)** and *Ccl7* **(Fig.52.C.i.)** had significantly higher expression in $Kin1^{null}$ compared to $Kin1^{wt}$ tumours. Interestingly, according to the RNA-Seq results $Kin1^{null}$ tumours also expressed significantly higher levels

of *Ccr1*, which encodes a chemokine receptor for both CCL7 and CCL9.

Various chemokines are overexpressed in cancer and stimulate cancer progression. In colorectal cancer expression of CXCL1, induced by prostanglandin E2, promoted angiogenesis [229], and overexpression of CXCL1 in gastric cancer cells *in vitro* promoted invasion, potentially via elevated activity of MMP2 and MMP9 [230].

CCL2 also plays an important role in tumourigenesis. It is upregulated in prostate cancer cells in vitro and in human cancers [231], and its expression correlated with advanced stage in prostate cancer patients [232]. Moreover, CCL2 was produced by prostate cancer cells in vitro, which promoted proliferation and invasion[231]. The proliferative and migratory effect of CCL2 to prostate cancer cells were shown to occur directly on tumour cell growth *in vitro*, via the PI3 Kinase/AKT signalling pathway and activation of p70-S6 kinase [233], and via indirect effect on tumour microenvironment by regulation of tumour-associated macrophage (TAM) infiltration into the tumour bed *in vivo* [231].

Immune cells such as TAMs and cancer-associated fibroblasts (CAFs) are known to contribute to malignant progression and have been previously linked to expression level changes in key components of the tumour microenvironment. TAMs can stimulate expression of mitogenic stimuli and induce angiogenesis during tumour growth via the production of various angiogenic factors, such as VEGF, PDGF and MMPs. Moreover, levels of *CCL2* have previously correlated with accumulation of TAMs and microvessel density in primary breast cancer [234]. Finally, CCL2- and CCL5- mediated TAM infiltration was documented to promote growth and cancer cell dissemination in breast cancer *in vivo* [235].

Similarly to TAMs, CAFs have also been associated with the presence of chemokines, such as CCL2. In particular, fibroblast activation protein (FAP) was shown to trigger induction of a subset of CAFs in a murine tumour model, which were a key source of CCL2 [236]. In fact, FAP-mediated CCL2 upregulation and STAT3 activation in CAFs promoted tumour growth, which was abrogated in mice deficient for CCR2, which is the receptor for CCL2 [236]. Interestingly, similar results were noted clinically, where a positive correlation between stromal expression of FAP, p-STAT3 and CCL2 was observed in human intrahepatic cholangiocarcinoma, a highly aggressive liver cancer [236]. It is, thus, possible, that observed differences in expression levels of chemokines, such as *Ccl2*, as well as of various MMPs and angiogenic factors between $Kin1^{null}$ and $Kin1^{wt}$ SCC tumours are associated with enhanced infiltration of immune system components.

Notably, a central function of TAMs is the production of pro-inflammatory cytokines such as IL-6 (Interleukin-6) [237][238], which is normally expressed by T cells and macrophages and whose expression is associated with stimulation of tumour angiogenesis, enhanced cell invasiveness, advanced tumour stage [239][240]. Interestingly, KS keratinocytes from numerous KS patients have exhibited characteristics of inflammatory response, such as increased secretion of pro-inflammatory cytokines, including IL-6, and infiltration of macrophages [54][213][241]. It is possible that long-term blistering and continuous skin fragility in KS skin could provoke chronic inflammation, which, can be a pathological trigger for tumour initiation and progression. In the future we will explore this avenue via examining presence of cytokines such as IL-6 in $Kin1^{null}$ and $Kin1^{wt}$ SCC tumours.

CCL2 was also shown to induce angiogenesis directly via upregulation of *HIF1a* levels and, in turn, induced VEGFA expression [242]. Interestingly, we observed no significant changes in expression of *Vegfa* (**Fig.50.A.i.**), or *Flt1*

(**Fig.50.B.i.**) and *Kdr* (**Fig.50.C.i.**) between Kin1^{null} and Kin1^{wt} tumours, which suggests that VEGA, VEGFR1 and VEGFR2 do not participate in enhancement of angiogenesis in our model.

Furthermore, expression of CCL7 and its receptor CCR2, and infiltration of CCR2-positive TAMs was higher in tumour cells of renal cell cancer brain metastasis compared to primary tumours, indicating a connection between CCL7 and metastasis [243]. CCL7 overexpression enhanced tumour growth and induced liver and lung metastasis in colorectal cancer via activation of ERK-JNK signalling pathway [244].

Interestingly, we observed that *Cxcl1* (**Fig.52.A.ii-iii.**), *Ccl2* (**Fig.52.B.ii-iii.**) and *Ccl7* (**Fig.52.C.ii-iii.**) expression correlated positively with Kin1^{null} tumour volume and negatively with Kin1^{wt} tumour volume, which mirrors the correlation pattern between *Mmp3* and *Mmp13* between and Kin1^{null} and Kin1^{wt} tumour volume. This suggests that in our mouse SCC model various chemokines may influence tumour growth in a different manner in the presence or absence of Kin1.

5.11.5. Role of Kin1 in tumour growth in Kin1^{null}, Kin1^{wt} and Kin1^{AA}

Met-1 mammary tumours

Interestingly, data from our lab showed that in mouse Met-1 mammary tumours Kin1 depletion affected tumour growth, but in an overall different manner than the mouse SCC tumour model. Met-1 tumour growth study demonstrated that Kin1^{wt} and Kin1^{AA} tumours had a higher growth rate than Kin1^{null} tumours, but showed no variation in growth between them (**Fig.54. by Georgia Dodd**). This resembles *in vitro* and *in vivo* data that show a role for Kin1 as a proliferation and growth promoter in breast cancer [115], but contradicts growth of mouse SCC tumours in our study (**Fig.35.D.**). High variability in growth rate of Kin1^{AA} tumours could have prevented the

difference between Kin1^{null} and Kin1^{AA} tumours reaching significance, but further studies will be required to confirm this.

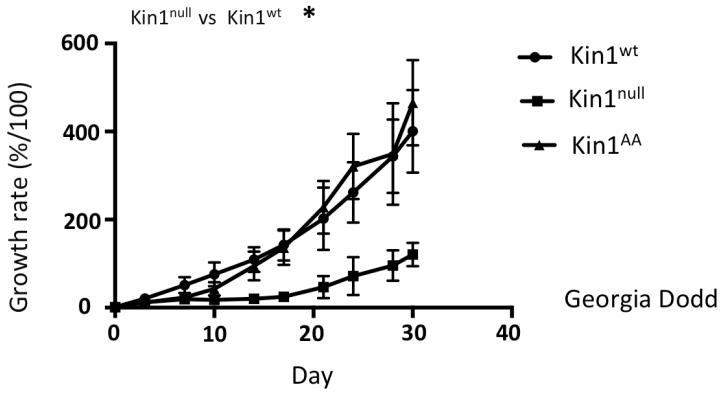

Figure 54: Assessment of Kin1^{null}, Kin1^{wt} and Kin1^{AA} Met-1 tumour growth. Bilateral subcutaneous implantations of 4x10^6 Kin1^{null}, Kin1^{wt} and Kin1^{AA} Met-1 cells were administrated in CD-1 nude mice. Tumour volume was quantified over the course of 30 days. Only statistical analysis using values obtained at Day30 is shown. Results presented as mean ± SEM. one-way ANOVA with Tukey's multiple comparison test; p-value > 0.05, * p-value ≤ 0.05. (Experiment performed by Georgia Dodd).

5.11.6. Summary and future work

Overall, we found that in our mouse SCC model, Kin1 inhibits cell proliferation, tumour growth and angiogenesis, both *in vitro* and *in vivo*. Although we do not yet know the mechanisms that regulate cell proliferation in 3D conditions *in vitro*, we have identified a variety of changes in tumour microenvironment that may contribute to differences in tumour growth between Kin1^{null} and Kin1^{wt} SCC tumours. Kin1 expression supresses expression of *Mmp3,* MMP3 and *Mmp13* which are known to induce tumour growth, angiogenesis and metastasis, and induces expression of *Adamts17*, which belongs to a family of angiostatic factors. Moreover, presence of Kin1 reduces expression of various chemokines, including *Ccl2* and *Cxcl1*, which have been shown to induce pro-angiogenic and pro-metastatic response, sometimes via involvement of MMPs. Interestingly, expression of various MMPs and chemokines correlates in a positive manner with Kin1^{null} tumour volume and in a negative manner with Kin1^{wt} tumour volume in our mouse SCC model.

It is, therefore, likely that a signalling axis exists between chemokines and metalloproteinases in our model that exerts anti- or pro-tumourigenic and angiogenic effects in the presence or absence of Kin1, respectively, in a context-specific manner. Silencing of chemokines and MMPs regulated by Kin1 will help us establish whether differences in tumour growth between $Kin1^{null}$ and $Kin1^{wt}$ SCC tumours occur in a chemokine-metalloproteinase-dependent manner, and further define the interrelationship between Kin1 and tumour microenvironment.

SCC tumours developed by KS patients are highly aggressive and metastatic, but the mechanism accountable for this feature remains elusive. Here we identify important roles for Kin1 in SCC, which offer a mechanistic insight to the development of aggressive SCC in KS, and may ultimately provide therapeutic targets for SCC's management.

Chapter 6: discussion

Kindler syndrome is an extremely rare genetic disorder, characterised by skin blistering, epidermal atrophy and predisposition to aggressive SCC. As with other variants of EB, treatment of the disease is mainly symptomatic and of preventative nature, such as avoidance of physical trauma and management of skin wounds.

6.1. Therapeutic avenues for KS and other types of EB

Despite the potential benefits of therapies aimed at symptom relief, there is still a need for a systemic therapeutic approach for KS and other subtypes of EB, and research has shown promise towards the development of effective treatments and therapies.

6.1.1. Allogeneic bone marrow transplantation

Plasticity in bone marrow (BM) stem cells enables them to not only regenerate the haematopoietic system, but differentiate into other organs such as skin and aid cutaneous tissue repair [245]–[247]. BM transplantation has also shown promise in ameliorating RDEB, which is caused by loss-of-function mutations in *COLVIIA1* gene. BM cells from healthy donors were capable of migrating to affected skin lesions, restore production of Collagen VII protein and skin structure, and mediate wound healing in animals and in clinical trial [248]–[250].

However, BM transplantation relies on a suitable human leukocyte antigen-matched donor, which not every patient has, and, despite the potential benefits, remains a high-risk therapeutic approach. This is due to complications such as profound immunodeficiency, which is common after allogeneic transplantation, and graft versus host disease. Thus, this presents a

key limitation to clinical application of allogeneic transplant therapy to RDEB and other genodermatoses, such as KS.

6.1.2. Autologous gene therapy

Autologous cell transplantation should evade these complications, but requires correction of defective genes. Gene therapy can be delivered via viral or non-viral gene systems, and this approach has shown promise for RDEB. Codon-optimised Collagen VII was delivered in cultured RDEB patient fibroblasts via a lentiviral-engineered platform, which restored protein expression levels [251]. Collagen VII-expressing RDEB fibroblasts were subsequently incorporated on a bioengineered human skin graft that was, in turn, grafted on mouse skin, which resulted in functional recovery of RDEB fibroblasts and morphological correction of the epidermis in RDEB human:murine skin graft model [249].

Ex vivo *FERMT1* gene delivery in KS patient keratinocytes and autologous transplantation of corrected patient keratinocytes on affected areas of KS patient skin holds potential for repair of affected KS epidermis. Nevertheless, both viral- and nonviral-mediated gene therapy have been reported to sometimes lead to undesirable off-target side effects such as toxicity, presenting a limitation to this approach [252][253].

6.1.3. Revertant mosaicism

Interestingly various patients that suffer from genetic diseases that affect self-generating organs, such as blood and skin, have exhibited Revertant mosaicism (RM), a naturally occurring phenomenon that involves spontaneous reversion of inherited pathogenic mutations in somatic cells [254][255]. RM has also been reported in a variety of skin disorders, including EB subtypes RDEB [256] and KS [257][258], where patients exhibit multiple

revertant, normal-appearing skin patches that contrast their otherwise atrophic skin.

In KS patients with revertant patches are positive for restoration of the *FERMT1* reading frame, and *FERMT1* mRNA and Kin1 expression over the entire length of the biopsy, similar to normal skin [255][256]. Signs of KS epidermal atrophy, such as low epidermal thickness, decreased keratinocyte proliferation and cleaved dermoepidermal junction are restored in revertant skin patches [255][256]. Notably, higher β1 integrin activation is found at focal adhesion of revertant keratinocytes, compared to non-revertant KS counterparts [258].

Corrected revertant keratinocytes offer a unique opportunity for autologous cell therapy in genodermatoses such as KS, as *in vivo* restoration obviates the need for further genetic repair of the diseased skin, and the development of an immune response. Punch graft transplantation of autologous revertant skin in affected areas of the epidermis of a JEB patient resulted in revertant skin expansion and phenotypical and genotypical cutaneous correction [259]. However, although beneficial, such approach cannot treat the entire body surface, and, thus, does not accommodate the need for desired universal therapy in KS and EB patients.

In vitro cultivation and expansion of autologous keratinocyte stem cells, an approach routinely used to form transplantable epidermal sheets to treat burn victims [260], also presents limitations in EB diseases, as chronic wounding and non-healing tissue repair can lead to exhaustion and paucity of keratinocyte stem cell population [261]. To circumvent that, researchers have shown that induced pluripotent stem cells can be derived from both mutant and revertant skin of an affected individual, which can differentiate into stratified skin epithelium [256]. Such approach not only supports the

likelihood of generating life-long supply of patient-specific keratinocytes, but abolishes the need for RM, which is unknown if it occurs on every KS/EB individual.

6.2. A role for Kin1 in skin homeostasis

Epidermal atrophy, which results in thin and fragile skin, is often characterised by progressive deterioration, making it one of the major clinical features of KS and other subtypes of EB. Our research has shown a novel role for Kin1 in skin homeostasis and may, ultimately, open up new therapeutic approaches, which could help to relieve the epidermal atrophy and fragility symptoms of KS.

We demonstrated for the first time that short-term loss of Kin1 in adult mouse epidermis reduces keratinocyte proliferation, a feature that has been linked to epidermal atrophy in KS patients and mice with congenital loss of Kin1 [8][54]. We have also shown that adult mice with short-term loss of Kin1 had decreased mitotic index, and abnormalities in important features of mitotic spindles, such as spindle orientation and tubulin acetylation that is a well-established readout of microtubule stability [137]-[140]. This implies that skin atrophy and reduced keratinocyte proliferation in KS patients may be linked to faulty mitosis.

Our *in vitro* data complemented our *in vivo* findings, showing that Kin1 depletion in human epithelial cell lines increased spindle abnormalities, which were rescued via chemical inhibition of tubulin deacetylase HDAC6. Together these data led us to conclude that *in vitro,* depletion of Kin1 reduces tubulin acetylation, weakens spindle stability and, ultimately, impairs proper mitosis, potentially via enhancement of HDAC6 expression.

If our *in vitro* findings translate *in vivo*, a potential therapeutic avenue for skin atrophy in KS patients would be pharmacological inhibition of HDAC6, which

could restore correct mitotic function and, ultimately, keratinocyte proliferation and skin homeostasis. For this to be implemented, additional studies must be performed to examine in greater detail the role of Kin1 in mitosis *in vivo*, and the protein's relationship with HDAC6.

Translation of scientific discoveries into novel therapies for human diseases, such as KS, necessitates development of suitable animal models that can ultimately replicate the pathophysiology of human disease. Short-term or long-term loss of Kin1 in epidermis of adult K14Cre-Kin1$^{fl/fl}$ FVB mice did not replicate skin atrophy phenotype observed in KS patients, as revealed by histological examination. In contrast, long-term loss of Kin1 in C57BL/6 mouse epidermis, which occurred during embryonic development, provoked exhaustion of keratinocyte stem cell compartments and resulted in KS-like phenotypes, including skin atrophy and poikiloderma [119]. Lack of epidermal abnormalities in our model could stem from various factors, including inability of Kin1 to regulate an already established adult stem cell population and/or from the fact that epidermal stem cell population of C57BL/6 mice is more susceptible to Kin1 loss compared to that in FVB mice. As elaborated in **Chapter 3, Section 3.6.2**, taking into consideration such factors is key for developing a mouse model that would appropriately allow us to study if loss of Kin1 causes skin atrophy via regulation of mitosis.

An attractive alternative to genetically modified animals would be the development of a humanised mouse model via xenotransplantation of human KS skin onto mice. This technique was first achieved in 1973, and human grafts were capable of preserving skin phenotype and accompanying genetic and molecular characteristics of diseases such as RDEB in mice [262]. By examining if defective mitosis underlines skin atrophy in KS skin, and the molecular mechanisms behind it, we will be able to identify molecular targets whose clinical inhibition could relieve KS-related skin atrophy, such as HDAC6.

Over the past few years, clinical HDAC6 inhibition has gained substantial interest, as besides its role α-tubulin deacetylation, HDAC6 also promotes deacetylation of cortactin and heat shock protein 90, a process that promotes endothelial cell migration, angiogenesis and stabilises survival/anti-apoptotic factors [263][264]. A variety of HDAC6 inhibitors have been identified, some of which have been approved for cutaneous treatment of cutaneous T-cell lymphoma [265]. If we confirm that *in vivo* Kin1 regulates mitosis in an HDAC6 dependent manner, then application of HDAC6 inhibitors on mouse and humanised mouse model of KS will help us assess whether this could restore mitosis and, ultimately, skin homeostasis in KS patients.

6.3. A role for Kin1 in the development of SCC

Patients of KS and of other EB subtypes are predisposed to the development of aggressive SCC, which increases morbidity and mortality amongst KS patients. To our knowledge, the mechanism that underlines EB patients to SCC predisposition remains unknown.

A single *in vivo* study recapitulated tumour susceptibility in Kin1-null C57BL/6 mice, and defined a tumour suppressor role for Kin1, which controls homeostasis of cutaneous epithelial stem cells by maintaining a balance between Wnt-β-catenin-mediated growth-promoting signals and TGF-β-mediated growth-inhibiting signals [119]. As a staggering 70% of KS patients over 45 years old develop SCC [9], targeting Wnt signalling could represent a chemo preventative option. However, this will require a fine balancing act, wherein the tumour-promoting functions of Wnt signalling in SCC are abolished without interfering with other key roles of Wnt signalling in functions such as insulin sensitivity and bone development.

Nevertheless, many tumours developed by C57BL/6 animals were benign, including trichofolluculoma-like lesions and papillomas, and were only slightly larger in mice with Kin1 loss, which does not recapitulate the malignancy and aggressiveness of SCC tumours observed in KS patients [119]. This could be due to the fact that C57CL/6 mouse is less susceptible to development of SCC tumours compared to other mouse strains, such as FVB, or that the cell of origin in the mouse does not reflect that seen in the human disease.

In this thesis we explored molecular mechanisms that underline aggressiveness of SCC tumours developed in KS, and overall showed that Kin1 plays a role in SCC development and that this may be via regulation of tumour microenvironment. We demonstrated that, compared to $Kin1^{wt}$ SCC cells, injection of $Kin1^{null}$ SCC cells in CD-1 nude mice resulted in greater tumour growth, enhanced vascularisation and increased expression of tumour microenvironment factors known to promote tumour growth, angiogenesis and metastasis, such as MMPs and chemokines.

It is important to validate our findings in an *in vivo* model with genetic resemblance to KS. Loss of Kin1 during embryonic development via establishment of K5-Cre/$Kin1^{fl/fl}$ mice will allow us to recapitulate the genetic background of KS. Subsequently assessment of growth, vascularisation, histopathology and gene expression profile in SCC tumours that develop spontaneously or following DMBA treatment will reveal if Kin1 has a function in SCC tumour development in this model. Finally, choice of FVB mice will aid SCC tumour development due to their susceptibility to carcinogenesis in several organ sites, including skin [155]. Moreover, FVB mice will allow us to scrutinise the role of Kin1 in regulation of immune system factors, such as chemokines, in a more representative manner, as, contrary to CD-1 nude mice, FVB strains have an intact immune system.

If we eventually define a causal relationship between enhanced MMP and chemokine expression, and tumour growth and progression in our model, use of MMP and chemokine inhibitors could be an important step towards defining therapeutic points of clinical intervention for SCC in KS.

Thus, by exploring the mechanism via which Kin1 regulates skin homeostasis and the development and nature of SCC in KS, we have defined potential molecular targets for clinical management of prominent and life-threatening KS pathologies, such as skin atrophy and aggressive SCC.

6.4. Concluding Remarks

In this study we explored molecular mechanisms that underline KS features such as reduced keratinocyte proliferation and aggressive nature of SCC. We show that Kin1 is important for keratinocyte proliferation and mitosis and, ultimately, epidermal homeostasis *in vivo*, and, for the first time, that Kin1 plays a key role in orientation and tubulin acetylation of mitotic spindles in mouse epidermis **(Figure 55.A.)**. We also demonstrate a novel role for Kin1 in chromosome segregation *in vitro*, which, along with spindle orientation, is regulated by Kin1 in an HDAC6 dependent manner **(Figure 55.A.)**. We further characterise the *in vitro* roles of Kin1 and Kin2 in mitosis with the use of live cell imaging. We define an overlapping function of the two protein isoforms in spindle orientation, and a distinct function of Kin1 in chromosome segregation and of Kin2 in mitotic spindle formation. Finally, we examine the tumour suppressor role of Kin1 in SCC and reveal a role for Kin1 in inhibition of cell proliferation and tumour growth **(Figure 55.B.)**. We provide evidence that Kin1 also plays a central role in regulation of tumour microenvironment and represses vascularisation and expression of angiogenesis markers, as well as expression of factors known to promote tumour progression, such as MMPs and chemokines. In conclusion, this study reveals important roles and an

insight to molecular mechanisms via which Kin1 controls skin homeostasis and development of SCC.

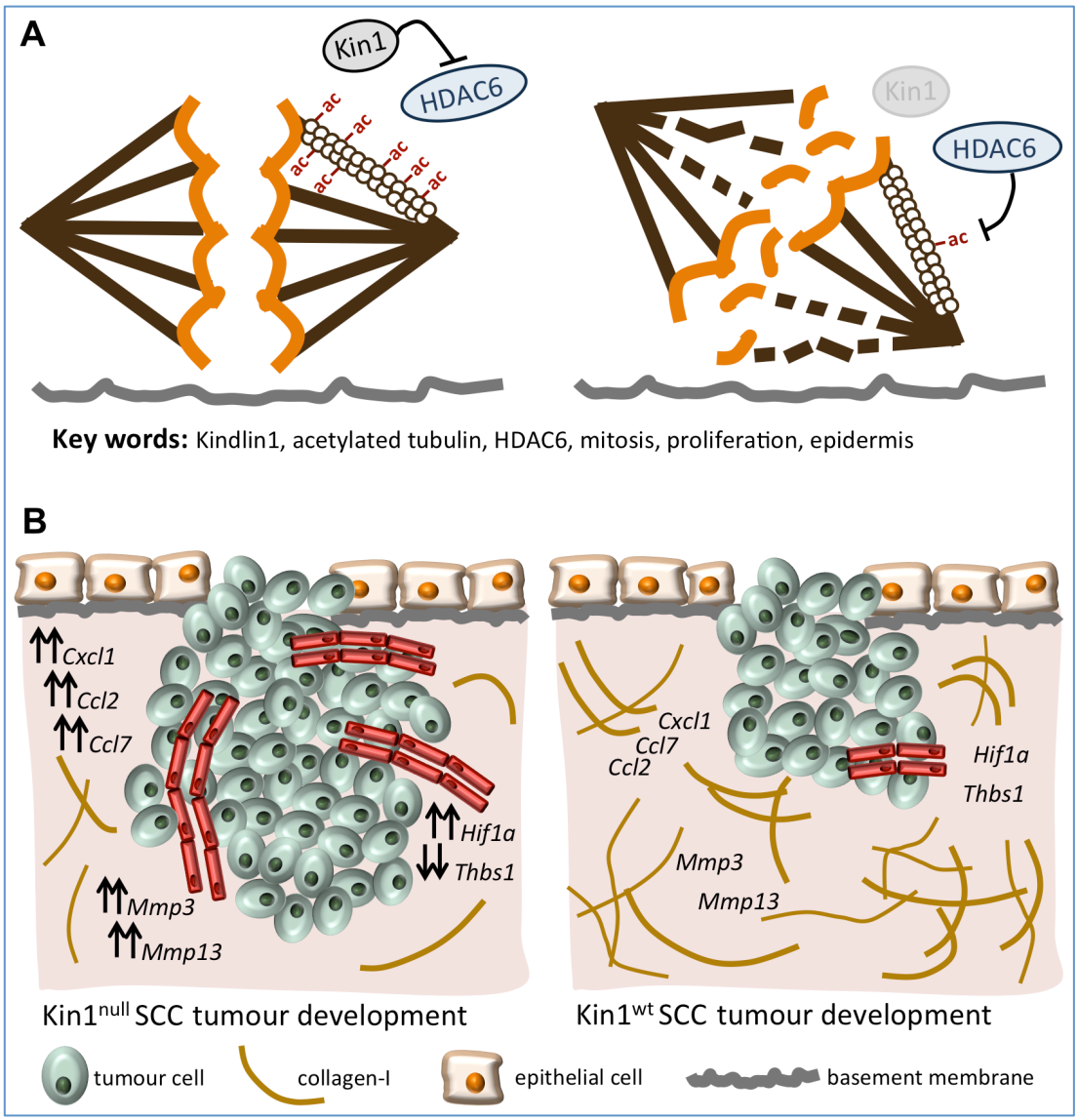

Figure 55: The role of Kin1 in skin homeostasis and the development of SCC. A. We believe that Kin1 contributes to skin homeostasis by safeguarding the fidelity of mitosis in mouse keratinocytes. According to our in vivo and in vitro findings, loss of Kin1 in mouse epidermis or depletion of Kin1 from epithelial cell lines elevates the incidence of unstable mitotic spindles, resulting in increased presence of spindle misorientation and lagging sister chromatids. Notably, we also show that enhanced spindle misorientation in Kin1-null mouse epidermis elevates the incident of asymmetrical cell division, which reduces keratinocyte proliferation, thus, highlighting the role of Kin1 in skin homeostasis. Finally, data from this study, as well as data from our lab conclude that Kin1 ensures normal mitosis via inhibition of HDAC6, a key a-tub deacetylase, which preserves the levels of acetylated tubulin across mitotic spindles and, thus, the stability of the mitotic spindle apparatus. **B.**

In this study we show that presence of Kin1 has a regulatory role within the microenvironment of SCC tumours, which hinders the development of SCC. As a result, loss of Kin1 results in deregulation of key components of the tumour microenvironment, including MMPs, chemokines and angiogenesis factors, which likely underlines the development of favorable conditions for upregulated SCC tumour growth, such as the enhancement of vasculature and the reduction of collagen-I, a key component of the ECM, that we observe in $Kin1^{null}$ SCC tumours.

Bibliography

[1] Y. Suga, R. Tsuboi, Y. Hashimoto, H. Yaguchi, and H. Ogawa, 'A Japanese case of Kindler syndrome', *Int. J. Dermatol.*, vol. 39, no. 4, pp. 284–286, 2000.

[2] K. Arita, V. Wessagowit, A. C. Inamadar, A. Palit, H. Fassihi, J. E. Lai-Cheong, C. Pourreyron, A. P. South, and J. A. McGrath, 'Unusual molecular findings in Kindler syndrome', *Br. J. Dermatol.*, vol. 157, no. 6, pp. 1252–1256, 2007.

[3] L. Mendes, L. Nogueira, V. Vilasboas, C. Talhari, S. Talhari, and M. Santos, 'Kindler syndrome: report of two cases.', *An. Bras. Dermatol.*, vol. 87, no. 5, pp. 779–81, 2012.

[4] S. Hacham-Zadeh and A. A. Garfunkel, 'Kindler syndrome in two related Kurdish families.', *Am. J. Med. Genet.*, vol. 20, no. 1, pp. 43–48, 1985.

[5] R. C. Sharma, V. Mahajan, N. L. Sharma, and A. K. Sharma, 'Kindler syndrome', in *International Journal of Dermatology*, 2003, vol. 42, no. 9, pp. 727–732.

[6] N. Suman, S. Kaur, S. Kaur, and V. Sarangal, 'Kindler's syndrome: A rare case report.', *Contemp. Clin. Dent.*, vol. 5, no. 2, pp. 217–220, 2014.

[7] S. K. Ghosh, D. Bandyopadhyay, J. Das, G. Chatterjee, and S. Sarkar, 'Kindler'S syndrome: a case series of three Indian children', *Indian J Dermatol*, vol. 55, pp. 393–396, 2010.

[8] C. Herz, M. Aumailley, C. Schulte, U. Schlötzer-Schrehardt, L. Bruckner-Tuderman, and C. Has, 'Kindlin-1 is a phosphoprotein involved in regulation of polarity, proliferation, and motility of epidermal keratinocytes', *J. Biol. Chem.*, vol. 281, no. 47, pp. 36082–36090, 2006.

[9] C. Has, D. Castiglia, M. del Rio, M. Garcia Diez, E. Piccinni, D. Kiritsi, J. Kohlhase, P. Itin, L. Martin, J. Fischer, G. Zambruno, and L. Bruckner-Tuderman, 'Kindler syndrome: Extension of FERMT1 mutational spectrum and natural history', *Hum. Mutat.*, vol. 32, no. 11, pp. 1204–1212, 2011.

[10] H. Mizutani, K. Masuda, N. Nakamura, H. Takenaka, D. Tsuruta, and N. Katoh, 'Cutaneous and laryngeal squamous cell carcinoma in mixed epidermolysis Bullosa, Kindler Syndrome', *Case Rep. Dermatol.*, vol. 4, no. 2, pp. 133–138, 2012.

[11] G. H. S. Ashton, W. H. I. McLean, A. P. South, N. Oyama, F. J. D. Smith, R. Al-Suwaid, A. Al Ismaily, D. J. Atherton, C. A. Harwood, I. M. Leigh, C. Moss, B. Didona, G. Zambruno, A. Patrizi, R. A. J. Eady, and J. A. McGrath, 'Recurrent Mutations in Kindlin-1, a Novel Keratinocyte Focal Contact Protein, in the Autosomal Recessive Skin Fragility and Photosensitivity Disorder, Kindler Syndrome', *J. Invest. Dermatol.*, vol. 122, no. 1, pp. 78–83, 2004.

[12] C. Has, V. Wessagowit, M. Pascucci, C. Baer, B. Didona, C. Wilhelm, C. Pedicelli, A. Locatelli, J. Kohlhase, G. H. S. Ashton, G. Tadini, G.

Zambruno, L. Bruckner-Tuderman, J. a McGrath, and D. Castiglia, 'Molecular basis of Kindler syndrome in Italy: novel and recurrent Alu/Alu recombination, splice site, nonsense, and frameshift mutations in the KIND1 gene.', *J. Invest. Dermatol.*, vol. 126, no. 8, pp. 1776–83, 2006.

[13] E. Cardin-Langlois, D. Hanna, M. St-Amant, and F. Croteau, 'Invasive squamous cell carcinoma of the hand in a patient with Kindler syndrome: Case report and literature review', *Can. J. Plast. Surg.*, vol. 18, no. 3, pp. e41-43, 2010.

[14] P. O. Emanuel, D. Rudikoff, and R. G. Phelps, 'Aggressive squamous cell carcinoma in Kindler syndrome.', *Skinmed*, vol. 5, no. 6, pp. 305–307, 2006.

[15] T. Techanukul, G. Sethuraman, A. Zlotogorski, L. Horev, M. Macarov, A. Trainer, K. Fong, M. Lens, L. Medenica, V. Ramesh, J. A. Mcgrath, and J. E. Lai-Cheong, 'Novel and recurrent FERMT1 gene mutations in kindler syndrome', *Acta Derm. Venereol.*, vol. 91, no. 3, pp. 267–270, 2011.

[16] C. B. Wiebe, G. Petricca, L. Häkkinen, G. Jiang, C. Wu, and H. S. Larjava, 'Kindler syndrome and periodontal disease: review of the literature and a 12-year follow-up case.', *J. Periodontol.*, vol. 79, no. 5, pp. 961–6, 2008.

[17] D. N. Ricketts, C. L. Morgan, J. M. McGregor, and P. R. Morgan, 'Kindler syndrome: a rare cause of desquamative lesions of the gingiva.', *Oral Surg. Oral Med. Oral Pathol. Oral Radiol. Endod.*, vol. 84, no. 5, pp. 488–491, 1997.

[18] C. B. Wiebe, H. Penagos, N. Luong, J. Slots, E. J. Epstein, D. Siegel, L. Hakkinen, E. E. Putnins, and H. S. Larjava, 'Clinical and microbiologic study of periodontitis associated with Kindler syndrome.', *J. Periodontol.*, vol. 74, no. 1, pp. 25–31, 2003.

[19] C. B. Wiebe, J. G. Silver, and H. S. Larjava, 'Early-onset periodontitis associated with Weary-Kindler syndrome: a case report.', *J. Periodontol.*, vol. 67, no. 10, pp. 1004–1010, 1996.

[20] J. S. Kern, C. Herz, E. Haan, D. Moore, S. Nottelmann, T. Von Lilien, P. Greiner, A. Schmitt-Graeff, O. G. Opitz, L. Bruckner-Tuderman, and C. Has, 'Chronic colitis due to an epithelial barrier defect: The role of kindlin-I isoforms', *J. Pathol.*, vol. 213, no. 4, pp. 462–470, 2007.

[21] E. Sadler, A. Klausegger, W. Muss, U. Deinsberger, G. Pohla-Gubo, M. Laimer, C. Lanschuetzer, J. W. Bauer, and H. Hintner, 'Novel KIND1 gene mutation in Kindler syndrome with severe gastrointestinal tract involvement.', *Arch. Dermatol.*, vol. 142, no. 12, pp. 1619–24, 2006.

[22] A. L. Krunic, L. Medenica, A. Novak, G. Carlos, and R. E. Clark, 'Hereditary bullous acrokeratotic poikiloderma of Weary-Kindler associated with pseudoainhum and sclerotic bands', *Int J Dermatol*, vol. 36, no. 7, pp. 529–533, 1997.

[23] H. Penagos, M. Jaen, M. T. Sancho, M. R. Saborio, V. G. Fallas, D. H. Siegel, and I. J. Frieden, 'Kindler syndrome in native Americans from Panama: report of 26 cases.', *Arch. Dermatol.*, vol. 140, no. 8, pp. 939–

944, 2004.
[24] F. Jobard, B. Bouadjar, F. Caux, S. Hadj-Rabia, C. Has, F. Matsuda, J. Weissenbach, M. Lathrop, J. F. Prud'homme, and J. Fischer, 'Identification of mutations in a new gene encoding a FERM family protein with a pleckstrin homology domain in Kindler syndrome', *Hum. Mol. Genet.*, vol. 12, no. 8, pp. 925–935, 2003.
[25] M. Sipahier, 'Epidermolysis bullosa: a case report', *Quintessence Int*, vol. 25, pp. 839–843, 1994.
[26] E. B. Freeman, J. K??glmeier, A. E. Martinez, J. E. Mellerio, L. Haynes, N. J. Sebire, K. J. Lindley, and N. Shah, 'Gastrointestinal complications of epidermolysis bullosa in children', *Br. J. Dermatol.*, vol. 158, no. 6, pp. 1308–1314, 2008.
[27] A. B. Novaes Júnior, J. C. Teles, G. C. Sousa, N. G. Angulo, and A. B. Novaes, 'Periodontal aspects of hereditary epidermolysis bullosa.', *Braz. Dent. J.*, vol. 2, no. 1, pp. 59–68, 1991.
[28] J. A. McGrath, O. M. Schofield, B. J. Mayou, P. H. McKee, and R. A. Eady, 'Epidermolysis bullosa complicated by squamous cell carcinoma: report of 10 cases.', *J. Cutan. Pathol.*, vol. 19, no. 2, pp. 116–23, 1992.
[29] J. D. Fine, R. A. J. Eady, E. A. Bauer, J. W. Bauer, L. Bruckner-Tuderman, A. Heagerty, H. Hintner, A. Hovnanian, M. F. Jonkman, I. Leigh, J. A. McGrath, J. E. Mellerio, D. F. Murrell, H. Shimizu, J. Uitto, A. Vahlquist, D. Woodley, and G. Zambruno, 'The classification of inherited epidermolysis bullosa (EB): Report of the Third International Consensus Meeting on Diagnosis and Classification of EB', *J. Am. Acad. Dermatol.*, vol. 58, no. 6, pp. 931–950, 2008.
[30] M. Floeth and L. Bruckner-Tuderman, 'Digenic junctional epidermolysis bullosa: mutations in COL17A1 and LAMB3 genes.', *Am. J. Hum. Genet.*, vol. 65, pp. 1530–1537, 1999.
[31] I. Yordanova, 'Epidermolysis Bullosa Simplex Dowling-Meara - A case report', *J. IMAB - Annu. Proceeding (Scientific Pap.*, vol. 14, 1, no. 2008, pp. 59–62, 2009.
[32] R. Varki, S. Sadowski, J. Uitto, and E. Pfendner, 'Epidermolysis bullosa. II. Type VII collagen mutations and phenotype-genotype correlations in the dystrophic subtypes.', *J. Med. Genet.*, vol. 44, no. 3, pp. 181–92, 2007.
[33] L. Bruckner-Tuderman and C. Has, 'Disorders of the cutaneous basement membrane zone-The paradigm of epidermolysis bullosa', *Matrix Biol.*, vol. 33, pp. 29–34, 2014.
[34] R. Windoffer, M. Beil, T. M. Magin, and R. E. Leube, 'Cytoskeleton in motion: The dynamics of keratin intermediate filaments in epithelia', *J. Cell Biol.*, vol. 194, no. 5, pp. 669–678, 2011.
[35] A. P. Kowalczyk, T. S. Stappenbeck, D. A. D. Parry, H. L. Palka, M. L. A. Virata, E. A. Bornslaeger, L. A. Nilles, and K. J. Green, 'Structure and function of desmosomal transmembrane core and plaque molecules', *Biophys. Chem.*, vol. 50, no. 1–2, pp. 97–112, 1994.
[36] Y. Gache, S. Chavanas, J. P. Lacour, G. Wiche, K. Owaribe, and G.

Meneguzzi, 'Defective Expression of Plectin / HD1 in Epidermolysis Bullosa Simplex', vol. 97, no. 10, pp. 2289–2298, 1996.
[37] J. E. Lai-Cheong, M. Parsons, A. Tanaka, S. Ussar, A. P. South, S. Gomathy, J. B. Mee, J.-B. Barbaroux, T. Techanukul, N. Almaani, S. E. Clements, I. R. Hart, and J. A. McGrath, 'Loss-of-function FERMT1 mutations in kindler syndrome implicate a role for fermitin family homolog-1 in integrin activation.', *Am. J. Pathol.*, vol. 175, no. 4, pp. 1431–41, 2009.
[38] D. Kiritsi, C. Has, and L. Bruckner-Tuderman, 'Laminin 332 in junctional epidermolysis bullosa', *Cell Adhesion and Migration*, vol. 7, no. 1. pp. 135–141, 2013.
[39] J. W. Bauer and C. Lanschuetzer, 'Type XVII collagen gene mutations in junctional epidermolysis bullosa and prospects for gene therapy', *Clin. Exp. Dermatol.*, vol. 28, no. 1, pp. 53–60, 2003.
[40] H. Schumann, D. Kiritsi, M. Pigors, I. Hausser, J. Kohlhase, J. Peters, H. Ott, L. Hyla-Klekot, E. Gacka, A. L. Sieron, M. Valari, L. Bruckner-Tuderman, and C. Has, 'Phenotypic spectrum of epidermolysis bullosa associated with ??6??4 integrin mutations', *Br. J. Dermatol.*, vol. 169, no. 1, pp. 115–124, 2013.
[41] A. H. Chishti, A. C. Kim, S. M. Marfatia, M. Lutchman, M. Hanspal, H. Jindal, S. C. Liu, P. S. Low, G. A. Rouleau, N. Mohandas, J. A. Chasis, J. G. Conboy, P. Gascard, Y. Takakuwa, S. C. Huang, E. J. Benz, A. Bretscher, R. G. Fehon, J. F. Gusella, V. Ramesh, F. Solomon, V. T. Marchesi, S. Tsukita, S. Tsukita, M. Arpin, D. Louvard, N. K. Tonks, J. M. Anderson, A. S. Fanning, P. J. Bryant, D. F. Woods, and K. B. Hoover, 'The FERM domain: A unique module involved in the linkage of cytoplasmic proteins to the membrane', *Trends Biochem. Sci.*, vol. 23, no. 8, pp. 281–282, 1998.
[42] M. C. Frame, H. Patel, B. Serrels, D. Lietha, and M. J. Eck, 'The FERM domain: organizing the structure and function of FAK.', *Nat. Rev. Mol. Cell Biol.*, vol. 11, no. 11, pp. 802–814, 2010.
[43] B. T. Goult, M. Bouaouina, D. S. Harburger, N. Bate, B. Patel, N. J. Anthis, I. D. Campbell, D. A. Calderwood, I. L. Barsukov, G. C. Roberts, and D. R. Critchley, 'The Structure of the N-Terminus of Kindlin-1: A Domain Important for ??IIb??3 Integrin Activation', *J. Mol. Biol.*, vol. 394, no. 5, pp. 944–956, 2009.
[44] D. A. Calderwood, R. Zent, R. Grant, D. J. G. Rees, R. O. Hynes, and M. H. Ginsberg, 'The talin head domain binds to integrin ?? subunit cytoplasmic tails and regulates integrin activation', *J. Biol. Chem.*, vol. 274, no. 40, pp. 28071–28074, 1999.
[45] M. Moes, S. Rodius, S. J. Coleman, S. J. Monkley, E. Goormaghtigh, L. Tremuth, C. Kox, P. P. G. Van Der Holst, D. R. Critchley, and N. Kieffer, 'The integrin binding site 2 (IBS2) in the talin rod domain is essential for linking integrin ?? subunits to the cytoskeleton', *J. Biol. Chem.*, vol. 282, no. 23, pp. 17280–17288, 2007.

[46] J. D. Humphries, A. Byron, and M. J. Humphries, 'Integrin ligands at a glance', *J. Cell Sci.*, vol. 119, no. 19, pp. 3901–3903, 2006.
[47] N. Beglova, S. C. Blacklow, J. Takagi, and T. a Springer, 'Cysteine-rich module structure reveals a fulcrum for integrin rearrangement upon activation.', *Nat. Struct. Biol.*, vol. 9, no. 4, pp. 282–7, 2002.
[48] D. A. Calderwood, B. Yan, J. M. De Pereda, B. G. Alvarez, Y. Fujioka, R. C. Liddington, and M. H. Ginsberg, 'The phosphotyrosine binding-like domain of talin activates integrins', *J. Biol. Chem.*, vol. 277, no. 24, pp. 21749–21758, 2002.
[49] D. S. Harburger, M. Bouaouina, and D. A. Calderwood, 'Kindlin-1 and -2 directly bind the C-terminal region of ?? integrin cytoplasmic tails and exert integrin-specific activation effects', *J. Biol. Chem.*, vol. 284, no. 17, pp. 11485–11497, 2009.
[50] Y. Q. Ma, J. Qin, C. Wu, and E. F. Plow, 'Kindlin-2 (Mig-2): A co-activator of ??3 integrins', *J. Cell Biol.*, vol. 181, no. 3, pp. 439–446, 2008.
[51] L. A. Yates, A. K. Füzéry, R. Bonet, I. D. Campbell, and R. J. C. Gilbert, 'Biophysical analysis of kindlin-3 reveals an elongated conformation and maps integrin binding to the membrane-distal β-subunit NPXY motif', *J. Biol. Chem.*, vol. 287, no. 45, pp. 37715–37731, 2012.
[52] M. Moser, B. Nieswandt, S. Ussar, M. Pozgajova, and R. Fässler, 'Kindlin-3 is essential for integrin activation and platelet aggregation.', *Nat. Med.*, vol. 14, no. 3, pp. 325–30, 2008.
[53] H. Patel, J. Zich, B. Serrels, C. Rickman, K. G. Hardwick, M. C. Frame, and V. G. Brunton, 'Kindlin-1 regulates mitotic spindle formation by interacting with integrins and Plk-1.', *Nat. Commun.*, vol. 4, no. May, p. 2056, 2013.
[54] S. Ussar, M. Moser, M. Widmaier, E. Rognoni, C. Harrer, O. Genzel-Boroviczeny, and R. Fässler, 'Loss of kindlin-1 causes skin atrophy and lethal neonatal intestinal epithelial dysfunction', *PLoS Genet.*, vol. 4, no. 12, 2008.
[55] G. Zhang, Y. Gu, R. Begum, H. Chen, X. Gao, J. A. McGrath, M. Parsons, and B. Song, 'Kindlin-1 Regulates Keratinocyte Electrotaxis', *J. Invest. Dermatol.*, pp. 1–11, 2016.
[56] M. Mehrbod, S. Trisno, and M. R. K. Mofrad, 'On the activation of integrin ??iIb??3: Outside-in and inside-out pathways', *Biophys. J.*, vol. 105, no. 6, pp. 1304–1315, 2013.
[57] M. A. M??ller, L. Brunie, A. S. B??cher, H. Kessler, K. E. Gottschalk, and U. Reuning, 'Cytoplasmic salt bridge formation in integrin ??v??3 stabilizes its inactive state affecting integrin-mediated cell biological effects', *Cell. Signal.*, vol. 26, no. 11, pp. 2493–2503, 2014.
[58] N. J. Anthis, N. J. Anthis, K. L. Wegener, K. L. Wegener, F. Ye, F. Ye, C. Kim, C. Kim, B. T. Goult, B. T. Goult, E. D. Lowe, E. D. Lowe, I. Vakonakis, I. Vakonakis, N. Bate, N. Bate, D. R. Critchley, D. R. Critchley, M. H. Ginsberg, M. H. Ginsberg, I. D. Campbell, and I. D. Campbell, 'The structure of an integrin/talin complex reveals the basis of

inside-out signal transduction', *EMBO J.*, vol. 28, no. 22, pp. 3623–3632, 2009.
[59] V. Martel, C. Racaud-Sultan, S. Dupe, C. Marie, F. Paulhe, A. Galmiche, M. R. Block, and C. Albiges-Rizo, 'Conformation, Localization, and Integrin Binding of Talin Depend on Its Interaction with Phosphoinositides', *J. Biol. Chem.*, vol. 276, no. 24, pp. 21217–21227, 2001.
[60] A. C. Kalli, I. D. Campbell, and M. S. P. Sansom, 'Multiscale simulations suggest a mechanism for integrin inside-out activation.', *Proc. Natl. Acad. Sci. U. S. A.*, vol. 108, no. 29, pp. 11890–5, 2011.
[61] E. Goksoy, Y. Q. Ma, X. Wang, X. Kong, D. Perera, E. F. Plow, and J. Qin, 'Structural Basis for the Autoinhibition of Talin in Regulating Integrin Activation', *Mol. Cell*, vol. 31, no. 1, pp. 124–133, 2008.
[62] B. T. Goult, M. Bouaouina, P. R. Elliott, N. Bate, B. Patel, A. R. Gingras, J. G. Grossmann, G. C. K. Roberts, D. A. Calderwood, D. R. Critchley, and I. L. Barsukov, 'Structure of a double ubiquitin-like domain in the talin head: a role in integrin activation', *EMBO J.*, vol. 29, no. 6, pp. 1069–1080, 2010.
[63] M. Bouaouina, B. T. Goult, C. Huet-Calderwood, N. Bate, N. N. Brahme, I. L. Barsukov, D. R. Critchley, and D. A. Calderwood, 'A conserved lipid-binding loop in the kindlin FERM F1 domain is required for kindlin-mediated ??IIb??3 integrin coactivation', *J. Biol. Chem.*, vol. 287, no. 10, pp. 6979–6990, 2012.
[64] H. D. Perera, Y. Q. Ma, J. Yang, J. Hirbawi, E. F. Plow, and J. Qin, 'Membrane binding of the N-terminal ubiquitin-like domain of kindlin-2 is crucial for its regulation of integrin activation', *Structure*, vol. 19, no. 11, pp. 1664–1671, 2011.
[65] J. Liu, K. Fukuda, Z. Xu, Y. Q. Ma, J. Hirbawi, X. Mao, C. Wu, E. F. Plow, and J. Qin, 'Structural basis of phosphoinositide binding to kindlin-2 protein pleckstrin homology domain in regulating integrin activation', *J. Biol. Chem.*, vol. 286, no. 50, pp. 43334–43342, 2011.
[66] L. A. Yates, C. N. Lumb, N. N. Brahme, R. Zalyte, L. E. Bird, L. De Colibus, R. J. Owens, D. A. Calderwood, M. S. P. Sansom, and R. J. C. Gilbert, 'Structural and functional characterization of the kindlin-1 pleckstrin homology domain', *J. Biol. Chem.*, vol. 287, no. 52, pp. 43246–43261, 2012.
[67] S. Tadokoro, S. J. Shattil, K. Eto, V. Tai, R. C. Liddington, J. M. de Pereda, M. H. Ginsberg, and D. a Calderwood, 'Talin binding to integrin beta tails: a final common step in integrin activation.', *Science (80-.).*, vol. 302, no. 5642, pp. 103–106, 2003.
[68] F. Ye, G. Hu, D. Taylor, B. Ratnikov, A. A. Bobkov, M. A. McLean, S. G. Sligar, K. A. Taylor, and M. H. Ginsberg, 'Recreation of the terminal events in physiological integrin activation', *J. Cell Biol.*, vol. 188, no. 1, pp. 157–173, 2010.
[69] T. M. Rogalski, G. P. Mullen, M. M. Gilbert, B. D. Williams, and D. G. Moerman, 'The UNC-112 gene in Caenorhabditis elegans encodes a novel

component of cell-matrix adhesion structures required for integrin localization in the muscle cell membrane', *J. Cell Biol.*, vol. 150, no. 1, pp. 253–264, 2000.

[70] D. H. Siegel, G. H. S. Ashton, H. G. Penagos, J. V Lee, H. S. Feiler, K. C. Wilhelmsen, A. P. South, F. J. D. Smith, A. R. Prescott, V. Wessagowit, N. Oyama, M. Akiyama, D. Al Aboud, K. Al Aboud, A. Al Githami, K. Al Hawsawi, A. Al Ismaily, R. Al-Suwaid, D. J. Atherton, R. Caputo, J.-D. Fine, I. J. Frieden, E. Fuchs, R. M. Haber, T. Harada, Y. Kitajima, S. B. Mallory, H. Ogawa, S. Sahin, H. Shimizu, Y. Suga, G. Tadini, K. Tsuchiya, C. B. Wiebe, F. Wojnarowska, A. B. Zaghloul, T. Hamada, R. Mallipeddi, R. a J. Eady, W. H. I. McLean, J. a McGrath, and E. H. Epstein, 'Loss of kindlin-1, a human homolog of the Caenorhabditis elegans actin-extracellular-matrix linker protein UNC-112, causes Kindler syndrome.', *Am. J. Hum. Genet.*, vol. 73, no. 1, pp. 174–187, 2003.

[71] H. Qu, Y. Tu, X. Shi, H. Larjava, M. a Saleem, S. J. Shattil, K. Fukuda, J. Qin, M. Kretzler, and C. Wu, 'Kindlin-2 regulates podocyte adhesion and fibronectin matrix deposition through interactions with phosphoinositides and integrins.', *J. Cell Sci.*, vol. 124, no. Pt 6, pp. 879–891, 2011.

[72] T. Kiema, Y. Lad, P. Jiang, C. L. Oxley, M. Baldassarre, K. L. Wegener, I. D. Campbell, J. Yl??nne, and D. A. Calderwood, 'The molecular basis of filamin binding to integrins and competition with talin', *Mol. Cell*, vol. 21, no. 3, pp. 337–347, 2006.

[73] Y. Tu, S. Wu, X. Shi, K. Chen, and C. Wu, 'Migfilin and Mig-2 link focal adhesions to filamin and the actin cytoskeleton and function in cell shape modulation', *Cell*, vol. 113, no. 1, pp. 37–47, 2003.

[74] M. Das, S. S. Ithychanda, J. Qin, and E. F. Plow, 'Migfilin and filamin as regulators of integrin activation in endothelial cells and neutrophils', *PLoS One*, vol. 6, no. 10, 2011.

[75] S. S. Ithychanda, M. Das, Y. Q. Ma, K. Ding, X. Wang, S. Gupta, C. Wu, E. F. Plow, and J. Qin, 'Migfilin, a molecular switch in regulation of integrin activation', *J. Biol. Chem.*, vol. 284, no. 7, pp. 4713–4722, 2009.

[76] Y. Lad, P. Jiang, S. Ruskamo, D. S. Harburger, J. Ylänne, I. D. Campbell, and D. A. Calderwood, 'Structural basis of the migfilin-filamin interaction and competition with integrin β tails', *J. Biol. Chem.*, vol. 283, no. 50, pp. 35154–35163, 2008.

[77] S. C. Fagerholm, H. S. Lek, and V. L. Morrison, 'Kindlin-3 in the immune system.', *Am. J. Clin. Exp. Immunol.*, vol. 3, no. 1, pp. 37–42, 2014.

[78] D. Bouvard, L. Vignoud, S. Dupé-Manet, N. Abed, H. N. Fournier, C. Vincent-Monegat, S. Francesco Retta, R. Fässler, and M. R. Block, 'Disruption of focal adhesions by integrin cytoplasmic domain-associated protein-1α', *J. Biol. Chem.*, vol. 278, no. 8, pp. 6567–6574, 2003.

[79] W. Liu, K. M. Draheim, R. Zhang, D. A. Calderwood, and T. J. Boggon, 'Mechanism for KRIT1 Release of ICAP1-Mediated Suppression of Integrin Activation', *Mol. Cell*, vol. 49, no. 4, pp. 719–729, 2013.

[80] S. S. Ithychanda, D. Hsu, H. Li, L. Yan, D. Liu, M. Das, E. F. Plow, and J. Qin, 'Identification and characterization of multiple similar ligand-binding repeats in filamin: Implication on filamin-mediated receptor clustering and cross-talk', *J. Biol. Chem.*, vol. 284, no. 50, pp. 35113–35121, 2009.
[81] B. N. Kahner, H. Kato, A. Banno, M. H. Ginsberg, S. J. Shattil, and F. Ye, 'Kindlins, integrin activation and the regulation of talin recruitment to ??IIb??3', *PLoS One*, vol. 7, no. 3, 2012.
[82] K. Bledzka, J. Liu, Z. Xu, H. Dhanuja Perera, S. P. Yadav, K. Bialkowska, J. Qin, Y. Q. Ma, and E. F. Plow, 'Spatial coordination of kindlin-2 with talin head domain in interaction with integrin ?? cytoplasmic tails', *J. Biol. Chem.*, vol. 287, no. 29, pp. 24585–24594, 2012.
[83] D. a Calderwood, I. D. Campbell, and D. R. Critchley, 'Talins and kindlins: partners in integrin-mediated adhesion.', *Nat. Rev. Mol. Cell Biol.*, vol. 14, no. 8, pp. 503–17, 2013.
[84] K. R. Legate, S. A. Wickström, and R. Fässler, 'Genetic and cell biological analysis of integrin outside-in signaling', *Genes and Development*, vol. 23, no. 4. pp. 397–418, 2009.
[85] M. A. Arnaout, B. Mahalingam, and J.-P. Xiong, 'Integrin Structure, Allostery, and Bidirectional Signaling', *Annu. Rev. Cell Dev. Biol.*, vol. 21, pp. 381–410, 2005.
[86] J. Zhu, C. V. Carman, M. Kim, M. Shimaoka, T. A. Springer, and B. H. Luo, 'Requirement of ?? and ?? subunit transmembrane helix separation for integrin outside-in signaling', *Blood*, vol. 110, no. 7, pp. 2475–2483, 2007.
[87] H. Priddle, L. Hemmings, S. Monkley, A. Woods, B. Patel, D. Sutton, G. A. Dunn, D. Zicha, and D. R. Critchley, 'Disruption of the talin gene compromises focal adhesion assembly in undifferentiated but not differentiated embryonic stem cells', *J. Cell Biol.*, vol. 142, no. 4, pp. 1121–1133, 1998.
[88] Y. He, P. Esser, A. Heinemann, L. Bruckner-Tuderman, and C. Has, 'Kindlin-1 and -2 have overlapping functions in epithelial cells: Implications for phenotype modification', *Am. J. Pathol.*, vol. 178, no. 3, pp. 975–982, 2011.
[89] K. E. Gottschalk and H. Kessler, 'A computational model of transmembrane integrin clustering', *Structure*, vol. 12, no. 6, pp. 1109–1116, 2004.
[90] B. Geiger and A. Bershadsky, 'Assembly and mechanosensory function of focal contacts', *Current Opinion in Cell Biology*, vol. 13, no. 5. pp. 584–592, 2001.
[91] S. Ussar, H.-V. Wang, S. Linder, R. Fässler, and M. Moser, 'The Kindlins: subcellular localization and expression during murine development.', *Exp. Cell Res.*, vol. 312, no. 16, pp. 3142–3151, 2006.
[92] I. Djaafri, F. Khayati, S. Menashi, J. Tost, M.-P. Podgorniak, A. Sadoux, A. Daunay, L. Teixeira, J. Soulier, A. Idbaih, N. Setterblad, F. Fauvel, F.

Calvo, A. Janin, C. Lebbé, and S. Mourah, 'A novel tumor suppressor function of Kindlin-3 in solid cancer.', *Oncotarget*, vol. 5, no. 19, pp. 8970–8985, 2014.

[93] K. Bialkowska, Y. Q. Ma, K. Bledzka, K. Sossey-Alaoui, L. Izem, X. Zhang, N. Malinin, J. Qin, T. Byzova, and E. F. Plow, 'The integrin co-activator kindlin-3 is expressed and functional in a non-hematopoietic cell, the endothelial cell', *J. Biol. Chem.*, vol. 285, no. 24, pp. 18640–18649, 2010.

[94] C. Margadant, M. Kreft, G. Zambruno, and A. Sonnenberg, 'Kindlin-1 Regulates Integrin Dynamics and Adhesion Turnover', *PLoS One*, vol. 8, no. 6, 2013.

[95] S. Raghavan, C. Bauer, G. Mundschau, Q. Li, and E. Fuchs, 'Conditional ablation of ??1 integrin in skin: Severe defects in epidermal proliferation, basement membrane formation, and hair follicle invagination', *J. Cell Biol.*, vol. 150, no. 5, pp. 1149–1160, 2000.

[96] C. Brakebusch, R. Grose, F. Quondamatteo, a Ramirez, J. L. Jorcano, a Pirro, M. Svensson, R. Herken, T. Sasaki, R. Timpl, S. Werner, and R. Fässler, 'Skin and hair follicle integrity is crucially dependent on beta 1 integrin expression on keratinocytes.', *EMBO J.*, vol. 19, no. 15, pp. 3990–4003, 2000.

[97] S. Kloeker, M. B. Major, D. A. Calderwood, M. H. Ginsberg, D. A. Jones, and M. C. Beckerle, 'The Kindler Syndrome Protein Is Regulated by Transforming Growth Factor-?? and Involved in Integrin-mediated Adhesion', *J. Biol. Chem.*, vol. 279, no. 8, pp. 6824–6833, 2004.

[98] E. Piccinni, G. Di Zenzo, R. Maurelli, E. Dellambra, M. Teson, C. Has, G. Zambruno, and D. Castiglia, 'Induction of senescence pathways in Kindler syndrome primary keratinocytes', *Br. J. Dermatol.*, vol. 168, no. 5, pp. 1019–1026, 2013.

[99] E. Montanez, S. Ussar, M. Schifferer, M. B??sl, R. Zent, M. Moser, and R. F??ssler, 'Kindlin-2 controls bidirectional signaling of integrins', *Genes Dev.*, vol. 22, no. 10, pp. 1325–1330, 2008.

[100] N. L. Malinin, L. Zhang, J. Choi, A. Ciocea, O. Razorenova, Y.-Q. Ma, E. A. Podrez, M. Tosi, D. P. Lennon, A. I. Caplan, S. B. Shurin, E. F. Plow, and T. V Byzova, 'A point mutation in KINDLIN3 ablates activation of three integrin subfamilies in humans', *Nat. Med.*, vol. 15, no. 3, pp. 313–318, 2009.

[101] L. Svensson, K. Howarth, A. McDowall, I. Patzak, R. Evans, S. Ussar, M. Moser, A. Metin, M. Fried, I. Tomlinson, and N. Hogg, 'Leukocyte adhesion deficiency-III is caused by mutations in KINDLIN3 affecting integrin activation', *Nat. Med.*, vol. 15, no. 3, pp. 306–312, 2009.

[102] C. Margadant, M. Kreft, D. J. De Groot, J. C. Norman, and A. Sonnenberg, 'Distinct roles of talin and kindlin in regulating integrin ??5??1 function and trafficking', *Curr. Biol.*, vol. 22, no. 17, pp. 1554–1563, 2012.

[103] M. Kr??ger, M. Moser, S. Ussar, I. Thievessen, C. A. Luber, F. Forner, S. Schmidt, S. Zanivan, R. F??ssler, and M. Mann, 'SILAC Mouse for

Quantitative Proteomics Uncovers Kindlin-3 as an Essential Factor for Red Blood Cell Function', *Cell*, vol. 134, no. 2, pp. 353–364, 2008.
[104] G. Y. Jung, Y. J. Park, and J. S. Han, 'Mediation of Rac1 activation by kindlin-2: An essential function in osteoblast adhesion, spreading, and proliferation', *J. Cell. Biochem.*, vol. 112, no. 9, pp. 2541–2548, 2011.
[105] X. Wu, H. Jiang, J. Chen, Q. Hu, J. Zhang, and J. Wang, '[Kindlin-2 regulates migration and adhesion of vascular smooth muscle cells via beta1-integrin].', *Zhonghua Xin Xue Guan Bing Za Zhi*, vol. 42, no. 11, pp. 938–943, 2014.
[106] C. Wu, H. Jiao, Y. Lai, W. Zheng, K. Chen, H. Qu, W. Deng, P. Song, K. Zhu, H. Cao, D. L. Galson, J. Fan, H.-J. Im, Y. Liu, J. Chen, D. Chen, and G. Xiao, 'Kindlin-2 controls TGF-β signalling and Sox9 expression to regulate chondrogenesis.', *Nat. Commun.*, vol. 6, no. May, p. 7531, 2015.
[107] R. Ruppert, M. Moser, M. Sperandio, E. Rognoni, M. Orban, W.-H. Liu, A. S. Schulz, R. A. J. Oostendorp, S. Massberg, and R. Fässler, 'Kindlin-3-mediated integrin adhesion is dispensable for quiescent but essential for activated hematopoietic stem cells.', *J. Exp. Med.*, vol. 212, no. 9, pp. 1415–32, 2015.
[108] Z. Xu, J. Cai, J. Gao, G. C. White, F. Chen, and Y. Q. Ma, 'Interaction of kindlin-3 and ??<inf>2</inf>-integrins differentially regulates neutrophil recruitment and NET release in mice', *Blood*, vol. 126, no. 3, pp. 373–377, 2015.
[109] a. Bandyopadhyay, G. Rothschild, S. Kim, D. a. Calderwood, and S. Raghavan, 'Functional differences between kindlin-1 and kindlin-2 in keratinocytes', *J. Cell Sci.*, vol. 125, no. 9, pp. 2172–2184, 2012.
[110] E. J. Weinstein, M. Bourner, R. Head, H. Zakeri, C. Bauer, and R. Mazzarella, 'URP1: A member of a novel family of PH and FERM domain-containing membrane-associated proteins is significantly over-expressed in lung and colon carcinomas', *Biochim. Biophys. Acta - Mol. Basis Dis.*, vol. 1637, no. 3, pp. 207–216, 2003.
[111] P. Mahawithitwong, K. Ohuchida, N. Ikenaga, H. Fujita, M. Zhao, S. Kozono, K. Shindo, T. Ohtsuka, S. Aishima, K. Mizumoto, and M. Tanaka, 'Kindlin-1 expression is involved in migration and invasion of pancreatic cancer', *Int. J. Oncol.*, vol. 42, no. 4, pp. 1360–1366, 2013.
[112] H. X. Ma, Q. H. Shu, J. J. Pan, D. Liu, G. L. Xu, J. S. Li, J. L. Ma, W. D. Jia, J. H. Yv, and Y. S. Ge, 'Expression of Kindlin-1 in human hepatocellular carcinoma and its prognostic significance', *Tumor Biol.*, vol. 36, no. 6, pp. 4235–4241, 2015.
[113] Z. An, K. Dobra, J. G. Lock, S. Strömblad, A. Hjerpe, and H. Zhang, 'Kindlin-2 is expressed in malignant mesothelioma and is required for tumor cell adhesion and migration', *Int. J. Cancer*, vol. 127, no. 9, pp. 1999–2008, 2010.
[114] K. Sossey-Alaoui, E. Pluskota, G. Davuluri, K. Bialkowska, M. Das, D. Szpak, D. J. Lindner, E. Downs-Kelly, C. L. Thompson, and E. F. Plow, 'Kindlin-3 enhances breast cancer progression and metastasis by

activating Twist-mediated angiogenesis', *FASEB J.*, vol. 28, no. 5, pp. 2260–2271, 2014.
[115] S. Sin, F. Bonin, V. Petit, D. Meseure, F. Lallemand, I. Biche, A. Bellahcne, V. Castronovo, O. De Wever, C. Gespach, R. Lidereau, and K. Driouch, 'Role of the focal adhesion protein kindlin-1 in breast cancer growth and lung metastasis', *J. Natl. Cancer Inst.*, vol. 103, no. 17, pp. 1323–1337, 2011.
[116] Y. Yu, J. Wu, L. Guan, L. Qi, Y. Tang, B. Ma, J. Zhan, Y. Wang, W. Fang, and H. Zhang, 'Kindlin 2 promotes breast cancer invasion via epigenetic silencing of the microRNA200 gene family', *Int. J. Cancer*, vol. 133, no. 6, pp. 1368–1379, 2013.
[117] B. Guo, J. Gao, J. Zhan, and H. Zhang, 'Kindlin-2 interacts with and stabilizes EGFR and is required for EGF-induced breast cancer cell migration', *Cancer Lett.*, vol. 361, no. 2, pp. 271–281, 2015.
[118] E. Pluskota, J. J. Dowling, N. Gordon, J. A. Golden, D. Szpak, X. X. Z. West, C. Nestor, Y. Q. Ma, K. Bialkowska, T. Byzova, and E. F. Plow, 'The integrin coactivator Kindlin-2 plays a critical role in angiogenesis in mice and zebrafish', *Blood*, vol. 117, no. 18, pp. 4978–4987, 2011.
[119] E. Rognoni, M. Widmaier, M. Jakobson, R. Ruppert, S. Ussar, D. Katsougkri, R. T. Böttcher, J. E. Lai-Cheong, D. B. Rifkin, J. a McGrath, and R. Fässler, 'Kindlin-1 controls Wnt and TGF-β availability to regulate cutaneous stem cell proliferation.', *Nat. Med.*, vol. 20, no. 4, pp. 350–359, 2014.
[120] J. Zhan, X. Zhu, Y. Guo, Y. Wang, Y. Wang, G. Qiang, M. Niu, J. Hu, J. Du, Z. Li, J. Cui, B. Ma, W. Fang, and H. Zhang, 'Opposite Role of Kindlin-1 and Kindlin-2 in Lung Cancers', *PLoS One*, vol. 7, no. 11, 2012.
[121] Y. Ren, H. Jin, Z. Xue, Q. Xu, S. Wang, G. Zhao, J. Huang, and H. Huang, 'Kindlin-2 inhibited the growth and migration of colorectal cancer cells', *Tumor Biol.*, vol. 36, no. 6, pp. 4107–4114, 2015.
[122] A. D. Edelstein, M. A. Tsuchida, N. Amodaj, H. Pinkard, R. D. Vale, and N. Stuurman, 'Advanced methods of microscope control using μManager software', *Journal of Biological Methods*, vol. 1, no. 2. p. e10, 2014.
[123] A. K. Indra, X. Warot, J. Brocard, J. M. Bornert, J. H. Xiao, P. Chambon, and D. Metzger, 'Temporally-controlled site-specific mutagenesis in the basal layer of the epidermis: Comparison of the recombinase activity of the tamoxifen-inducible Cre-ER(T) and Cre-ER(T2) recombinases', *Nucleic Acids Res.*, vol. 27, no. 22, pp. 4324–4327, 1999.
[124] M. Li, a K. Indra, X. Warot, J. Brocard, N. Messaddeq, S. Kato, D. Metzger, and P. Chambon, 'Skin abnormalities generated by temporally controlled RXRalpha mutations in mouse epidermis.', *Nature*, vol. 407, no. 6804, pp. 633–636, 2000.
[125] R. Feil, J. Brocard, B. Mascrez, M. LeMeur, D. Metzger, and P. Chambon, 'Ligand-activated site-specific recombination in mice.', *Proc. Natl. Acad. Sci. U. S. A.*, vol. 93, no. 20, pp. 10887–90, 1996.

[126] G. W. Mclean, K. Brown, M. I. Arbuckle, A. W. Wyke, T. Pikkarainen, E. Ruoslahti, and M. C. Frame, 'Advances in Brief Decreased Focal Adhesion Kinase Suppresses Papilloma Formation during Experimental Mouse Skin Carcinogenesis 1', *Proteins*, pp. 8385–8389, 2001.
[127] M. Quintanilla, K. Brown, M. Ramsden, and A. Balmain, '(10)Carcinogen-specific mutation and amplification of Ha-ras during mouse skin carcinogenesis.', *Nature*, vol. 322, no. 6074, pp. 78–80, 1986.
[128] V. J. Tuominen, S. Ruotoistenmäki, A. Viitanen, M. Jumppanen, and J. Isola, 'ImmunoRatio: a publicly available web application for quantitative image analysis of estrogen receptor (ER), progesterone receptor (PR), and Ki-67.', *Breast Cancer Res.*, vol. 12, no. 4, p. R56, 2010.
[129] C. Trapnell, D. G. Hendrickson, M. Sauvageau, L. Goff, J. L. Rinn, and L. Pachter, 'Differential analysis of gene regulation at transcript resolution with RNA-seq.', *Nat. Biotechnol.*, vol. 31, no. 1, pp. 46–53, 2013.
[130] S. Anders and W. Huber, 'Differential expression analysis for sequence count data.', *Genome Biol.*, vol. 11, no. 10, p. R106, 2010.
[131] K. J. Livak and T. D. Schmittgen, 'Analysis of relative gene expression data using real-time quantitative PCR and the 2(-Delta Delta C(T)) Method', *Methods*, vol. 25, no. 4, pp. 402–408, 2001.
[132] D. A. Agunbiade and P. I. Ogunyinka, 'Effect of Correlation Level on the Use of Auxiliary Variable in Double Sampling for Regression Estimation', vol. 2013, no. October, pp. 312–318, 2013.
[133] C. V. Krishna, N. V. Parmar, and C. Has, 'Kindler syndrome with severe mucosal involvement in childhood', *Clin. Exp. Dermatol.*, vol. 39, no. 3, pp. 340–343, 2014.
[134] C. Tapia, H. Kutzner, T. Mentzel, S. Savic, D. Baumhoer, and K. Glatz, 'Two mitosis-specific antibodies, MPM-2 and phospho-histone H3 (Ser28), allow rapid and precise determination of mitotic activity.', *Am. J. Surg. Pathol.*, vol. 30, no. 1, pp. 83–89, 2006.
[135] T. Lechler and E. Fuchs, 'Asymmetric cell divisions promote stratification and differentiation of mammalian skin.', *Nature*, vol. 437, no. 7056, pp. 275–80, 2005.
[136] N. D. Poulson and T. Lechler, 'Robust control of mitotic spindle orientation in the developing epidermis', *J. Cell Biol.*, vol. 191, no. 5, pp. 915–922, 2010.
[137] F. Toyoshima and E. Nishida, 'Integrin-mediated adhesion orients the spindle parallel to the substratum in an EB1- and myosin X-dependent manner.', *EMBO J.*, vol. 26, no. 6, pp. 1487–1498, 2007.
[138] Y. Yang, M. Liu, D. Li, J. Ran, J. Gao, S. Suo, S.-C. Sun, and J. Zhou, 'CYLD regulates spindle orientation by stabilizing astral microtubules and promoting dishevelled-NuMA-dynein/dynactin complex formation.', *Proc. Natl. Acad. Sci. U. S. A.*, pp. 1–6, 2014.
[139] G. Piperno, M. LeDizet, and X. J. Chang, 'Microtubules containing acetylated alpha-tubulin in mammalian cells in culture.', *J. Cell Biol.*, vol. 104, no. 2, pp. 289–302, 1987.

[140] K. Acevedo, R. Li, P. Soo, R. Suryadinata, B. Sarcevic, V. A. Valova, M. E. Graham, P. J. Robinson, and O. Bernard, 'The phosphorylation of p25/TPPP by LIM kinase 1 inhibits its ability to assemble microtubules', *Exp. Cell Res.*, vol. 313, no. 20, pp. 4091–4106, 2007.
[141] V. M. Fernandes, K. McCormack, L. Lewellyn, and E. M. Verheyen, 'Integrins Regulate Apical Constriction via Microtubule Stabilization in the Drosophila Eye Disc Epithelium', *Cell Rep.*, vol. 9, no. 6, pp. 2043–2055, 2014.
[142] X. Shi, Y. Yao, Y. Wang, Y. Zhang, Q. Huang, J. Zhou, M. Liu, and D. Li, 'Cep70 regulates microtubule stability by interacting with HDAC6', *FEBS Lett.*, vol. 589, no. 15, pp. 1771–1777, 2015.
[143] C. M. Lanschuetzer, W. H. Muss, M. Emberger, G. Pohla-Gubo, A. Klausegger, J. W. Bauer, and H. Hintner, 'Characteristic immunohistochemical and ultrastructural findings indicate that Kindler's syndrome is an apoptotic skin disorder.', *J. Cutan. Pathol.*, vol. 30, no. 9, pp. 553–560, 2003.
[144] C. Has, C. Herz, E. Zimina, H.-Y. Qu, Y. He, Z.-G. Zhang, T.-T. Wen, Y. Gache, M. Aumailley, and L. Bruckner-Tuderman, 'Kindlin-1 Is required for RhoGTPase-mediated lamellipodia formation in keratinocytes.', *Am. J. Pathol.*, vol. 175, no. 4, pp. 1442–52, 2009.
[145] a J. Zhu, I. Haase, and F. M. Watt, 'Signaling via beta1 integrins and mitogen-activated protein kinase determines human epidermal stem cell fate in vitro.', *Proc. Natl. Acad. Sci. U. S. A.*, vol. 96, no. 12, pp. 6728–6733, 1999.
[146] R. Grose, C. Hutter, W. Bloch, I. Thorey, F. M. Watt, R. Fassler, C. Brakebusch, and S. Werner, 'A crucial role of beta 1 integrins for keratinocyte migration in vitro and during cutaneous wound repair', *Development*, vol. 129, no. 9, pp. 2303–2315, 2002.
[147] C. G. Reverte, A. Benware, C. W. Jones, and S. E. LaFlamme, 'Perturbing integrin function inhibits microtubule growth from centrosomes, spindle assembly, and cytokinesis', *J. Cell Biol.*, vol. 174, no. 4, pp. 491–497, 2006.
[148] F. Toyoshima, S. Matsumura, H. Morimoto, M. Mitsushima, and E. Nishida, 'PtdIns(3,4,5)P3 Regulates Spindle Orientation in Adherent Cells', *Dev. Cell*, vol. 13, no. 6, pp. 796–811, 2007.
[149] E. J. Morris, K. Assi, B. Salh, and S. Dedhar, 'Integrin-linked kinase links dynactin-1/dynactin-2 with cortical integrin receptors to orient the mitotic spindle relative to the substratum.', *Sci. Rep.*, vol. 5, p. 8389, 2015.
[150] L. M. Machesky and A. Hall, 'Role of actin polymerization and adhesion to extracellular matrix in Rac- and Rho-induced cytoskeletal reorganization', *J. Cell Biol.*, vol. 138, no. 4, pp. 913–926, 1997.
[151] M. Ginsberg, M. D. Pierschbacher, E. Ruoslahti, G. Marguerie, and E. Plow, 'Inhibition of fibronectin binding to platelets by proteolytic fragments and synthetic peptides which support fibroblast adhesion', *J.*

Biol. Chem., vol. 260, no. 7, pp. 3931–3936, 1985.
[152] K. Loulier, J. D. Lathia, V. Marthiens, J. Relucio, M. R. Mughal, S. C. Tang, T. Coksaygan, P. E. Hall, S. Chigurupati, B. Patton, H. Colognato, M. S. Rao, M. P. Mattson, T. F. Haydar, and C. Ffrench-Constant, '??1 integrin maintains integrity of the embryonic neocortical stem cell niche', *PLoS Biol.*, vol. 7, no. 8, 2009.
[153] N. Akhtar and C. H. Streuli, 'An integrin–ILK–microtubule network orients cell polarity and lumen formation in glandular epithelium', *Nat. Cell Biol.*, vol. 15, no. 1, pp. 17–27, 2013.
[154] K. Dan and Y. Tanaka, 'Attachment of one spindle pole to the cortex in unequal cleavage', *Ann. N. Y. Acad. Sci.*, vol. 582, pp. 108–119, 1990.
[155] J. T. Thaiparambil, C. M. Eggers, and A. I. Marcus, 'AMPK regulates mitotic spindle orientation through phosphorylation of myosin regulatory light chain.', *Mol. Cell. Biol.*, vol. 32, no. 16, pp. 3203–17, 2012.
[156] H. Patel, I. Stavrou, R. L. Shrestha, V. Draviam, M. C. Frame, and V. G. Brunton, 'Kindlin1 regulates microtubule function to ensure normal mitosis.', *J. Mol. Cell Biol.*, p. mjw009-, 2016.
[157] C. D. Woodworth, E. Michael, L. Smith, K. Vijayachandra, A. Glick, H. Hennings, and S. H. Yuspa, 'Strain-dependent differences in malignant conversion of mouse skin tumors is an inherent property of the epidermal keratinocyte', *Carcinogenesis*, vol. 25, no. 9, pp. 1771–1778, 2004.
[158] V. Vasioukhin, L. Degenstein, B. Wise, and E. Fuchs, 'The magical touch: genome targeting in epidermal stem cells induced by tamoxifen application to mouse skin', *Proc Natl Acad Sci U S A*, vol. 96, no. 15, pp. 8551–8556, 1999.
[159] C. Byrne, M. Tainsky, and E. Fuchs, 'Programming gene expression in developing epidermis.', *Development*, vol. 120, no. 9, pp. 2369–2383, 1994.
[160] M. Tarutani, S. Itami, M. Okabe, M. Ikawa, T. Tezuka, K. Yoshikawa, T. Kinoshita, and J. Takeda, 'Tissue-specific knockout of the mouse Pig-a gene reveals important roles for GPI-anchored proteins in skin development.', *Proc. Natl. Acad. Sci. U. S. A.*, vol. 94, no. 14, pp. 7400–7405, 1997.
[161] G. W. McLean, N. H. Komiyama, B. Serrels, H. Asano, L. Reynolds, F. Conti, K. Hodivala-Dilke, D. Metzger, P. Chambon, S. G. N. Grant, and M. C. Frame, 'Specific deletion of focal adhesion kinase suppresses tumor formation and blocks malignant progression', *Genes Dev.*, vol. 18, no. 24, pp. 2998–3003, 2004.
[162] J. Bai, R. Binari, J.-Q. Ni, M. Vijayakanthan, H.-S. Li, and N. Perrimon, 'RNA interference screening in Drosophila primary cells for genes involved in muscle assembly and maintenance.', *Development*, vol. 135, no. 8, pp. 1439–49, 2008.
[163] A. Matsuyama, T. Shimazu, Y. Sumida, A. Saito, Y. Yoshimatsu, D. Seigneurin-Berny, H. Osada, Y. Komatsu, N. Nishino, S. Khochbin, S. Horinouchi, and M. Yoshida, 'In vivo destabilization of dynamic

microtubules by HDAC6-mediated deacetylation', *EMBO J.*, vol. 21, no. 24, pp. 6820–6831, 2002.
[164] C. Hubbert, A. Guardiola, R. Shao, Y. Kawaguchi, A. Ito, A. Nixon, M. Yoshida, X.-F. Wang, and T.-P. Yao, 'HDAC6 is a microtubule-associated deacetylase.', *Nature*, vol. 417, no. 6887, pp. 455–458, 2002.
[165] S. J. Haggarty, K. M. Koeller, J. C. Wong, C. M. Grozinger, and S. L. Schreiber, 'Domain-selective small-molecule inhibitor of histone deacetylase 6 (HDAC6)-mediated tubulin deacetylation.', *Proc. Natl. Acad. Sci. U. S. A.*, vol. 100, no. 8, pp. 4389–94, 2003.
[166] R. A. Green, R. Wollman, and K. B. Kaplan, 'APC and EB1 Function Together in Mitosis to Regulate Spindle Dynamics and Chromosome Alignment', *Mol. Biol. Cell*, vol. 16, pp. 4609–4622, 2005.
[167] J. Costa, C. Fu, V. M. Khare, and P. T. Tran, 'Csi2P Modulates Microtubule Dynamics and Organizes the Bipolar Spindle for Chromosome Segregation', *Mol. Biol. Cell*, vol. 25, no. 24, pp. 3900–3908, 2014.
[168] J. Joseph M. Varberg, a Leah R. Padgett, a Gustavo Arrizabalaga, a, b William J. Sullivan, 'TgATAT-Mediated-Tubulin Acetylation Is Required for Division of the Protozoan Parasite Toxoplasma gondii', *mSpere*, vol. 1, no. 1, pp. 1–16, 2016.
[169] S. E. LaFlamme, B. Nieves, D. Colello, and C. G. Reverte, 'Integrins as regulators of the mitotic machinery', *Current Opinion in Cell Biology*, vol. 20, no. 5. pp. 576–582, 2008.
[170] C. Huet-Calderwood, N. N. Brahme, N. Kumar, A. L. Stiegler, S. Raghavan, T. J. Boggon, and D. a Calderwood, 'Differential binding to the ILK complex determines kindlin isoform adhesion localization and integrin activation.', *J. Cell Sci.*, pp. 4308–4321, 2014.
[171] X. Zhang, G. Jiang, Y. Cai, S. J. Monkley, D. R. Critchley, and M. P. Sheetz, 'Talin depletion reveals independence of initial cell spreading from integrin activation and traction.', *Nat. Cell Biol.*, vol. 10, no. 9, pp. 1062–1068, 2008.
[172] E. L. Abel, J. M. Angel, K. Kiguchi, and J. DiGiovanni, 'Multi-stage chemical carcinogenesis in mouse skin: fundamentals and applications.', *Nat. Protoc.*, vol. 4, no. 9, pp. 1350–62, 2009.
[173] X. Shi, Y. Q. Ma, Y. Tu, K. Chen, S. Wu, K. Fukuda, J. Qin, E. F. Plow, and C. Wu, 'The MIG-2/integrin interaction strengthens cell-matrix adhesion and modulates cell motility', *J. Biol. Chem.*, vol. 282, no. 28, pp. 20455–20466, 2007.
[174] A. C. Luca, S. Mersch, R. Deenen, S. Schmidt, I. Messner, K. L. Schäfer, S. E. Baldus, W. Huckenbeck, R. P. Piekorz, W. T. Knoefel, A. Krieg, and N. H. Stoecklein, 'Impact of the 3D Microenvironment on Phenotype, Gene Expression, and EGFR Inhibition of Colorectal Cancer Cell Lines', *PLoS One*, vol. 8, no. 3, 2013.
[175] V. M. Weaver, O. W. Petersen, F. Wang, C. A. Larabell, P. Briand, C. Damsky, and M. J. Bissell, 'Reversion of the malignant phenotype of

human breast cells in three- dimensional culture and in vivo by integrin blocking antibodies', *J. Cell Biol.*, vol. 137, no. 1, pp. 231–245, 1997.
[176] L. Zhou, G. Huang, S. Wang, J. Wu, W. G. Lee, Y. Chen, F. Xu, and T. Lu, 'Advances in cell-based biosensors using three-dimensional cell-encapsulating hydrogels', *Biotechnology Journal*, vol. 6, no. 12. pp. 1466–1476, 2011.
[177] O. M. Maria, O. Maria, Y. Liu, S. V Komarova, and S. D. Tran, 'Matrigel improves functional properties of human submandibular salivary gland cell line.', *Int. J. Biochem. Cell Biol.*, vol. 43, no. 4, pp. 622–31, 2011.
[178] K. J. Price, A. Tsykin, K. M. Giles, R. T. Sladic, M. R. Epis, R. Ganss, G. J. Goodall, and P. J. Leedman, 'Matrigel Basement Membrane Matrix influences expression of microRNAs in cancer cell lines', *Biochem. Biophys. Res. Commun.*, vol. 427, no. 2, pp. 343–348, 2012.
[179] C. J. Malemud, 'Matrix metalloproteinases (MMPs) in health and disease: an overview', *Front. Biosci.*, vol. 11, no. 1, p. 1696, 2006.
[180] C. Suri, P. F. Jones, S. Patan, S. Bartunkova, P. C. Maisonpierre, S. Davis, T. N. Sato, and G. D. Yancopoulos, 'Requisite role of angiopoietin-1, a ligand for the TIE2 receptor, during embryonic angiogenesis', *Cell*, vol. 87, no. 7, pp. 1171–1180, 1996.
[181] W. Shim, 'Angiopoietin 1 Promotes Tumor Angiogenesis and Tumor Vessel Plasticity of Human Cervical Cancer in Mice', *Exp. Cell Res.*, vol. 279, no. 2, pp. 299–309, 2002.
[182] Y. Bin Ding, G. Y. Chen, J. G. Xia, X. W. Zang, H. Y. Yang, and L. Yang, 'Association of VCAM-1 overexpression with oncogenesis, tumor angiogenesis and metastasis of gastric carcinoma', *World J. Gastroenterol.*, vol. 9, no. 7, pp. 1409–1414, 2003.
[183] M. I. Koukourakis, A. Giatromanolaki, E. Sivridis, C. Simopoulos, H. Turley, K. Talks, K. C. Gatter, and A. L. Harris, 'Hypoxia-inducible factor (HIF1A and HIF2A), angiogenesis, and chemoradiotherapy outcome of squamous cell head-and-neck cancer', *Int. J. Radiat. Oncol. Biol. Phys.*, vol. 53, no. 5, pp. 1192–1202, 2002.
[184] A. Hoeben, B. Landuyt, M. S. Highley, H. Wildiers, A. T. Van Oosterom, and E. a De Bruijn, 'Vascular endothelial growth factor and angiogenesis.', *Pharmacol. Rev.*, vol. 56, no. 4, pp. 549–580, 2004.
[185] S. Kaur, G. Martin-Manso, M. L. Pendrak, S. H. Garfield, J. S. Isenberg, and D. D. Roberts, 'Thrombospondin-1 inhibits VEGF receptor-2 signaling by disrupting its association with CD47', *J. Biol. Chem.*, vol. 285, no. 50, pp. 38923–38932, 2010.
[186] M. L. Iruela-Arispe, M. Lombardo, H. C. Krutzsch, J. Lawler, and D. D. Roberts, 'Inhibition of angiogenesis by thrombospondin-1 is mediated by 2 independent regions within the type 1 repeats.', *Circulation*, vol. 100, no. 13, pp. 1423–1431, 1999.
[187] F. Balkwill, 'Cancer and the chemokine network', *Nat. Rev. Cancer*, vol. 4, no. 7, pp. 540–550, 2004.
[188] L. Jennings and C. D. Schmults, 'Management of high-risk cutaneous

squamous cell carcinoma.', *J. Clin. Aesthet. Dermatol.*, vol. 3, no. 4, pp. 39–48, 2010.
[189] H. Zhou, J. Kuang, L. Zhong, W. L. Kuo, J. W. Gray, a Sahin, B. R. Brinkley, and S. Sen, 'Tumour amplified kinase STK15/BTAK induces centrosome amplification, aneuploidy and transformation.', *Nat. Genet.*, vol. 20, no. october, pp. 189–193, 1998.
[190] A. H. Yang, D. Kaushal, S. K. Rehen, K. Kriedt, M. A. Kingsbury, M. J. McConnell, and J. Chun, 'Chromosome segregation defects contribute to aneuploidy in normal neural progenitor cells.', *J. Neurosci.*, vol. 23, no. 32, pp. 10454–62, 2003.
[191] P. Duesberg and R. Li, 'Multistep carcinogenesis: a chain reaction of aneuploidizations.', *Cell cycle (Georgetown, Tex.)*, vol. 2, no. 3. pp. 202–210, 2003.
[192] B. A. A. Weaver, A. D. Silk, C. Montagna, P. Verdier-Pinard, and D. W. Cleveland, 'Aneuploidy Acts Both Oncogenically and as a Tumor Suppressor', *Cancer Cell*, vol. 11, no. 1, pp. 25–36, 2007.
[193] E. Cristi, G. Perrone, G. Toscano, a Verzì, S. Nori, D. Santini, G. Tonini, a Vetrani, a Fabiano, and C. Rabitti, 'Tumour proliferation, angiogenesis, and ploidy status in human colon cancer.', *J. Clin. Pathol.*, vol. 58, no. 11, pp. 1170–4, 2005.
[194] A. Pastuła, M. Middelhoff, A. Brandtner, M. Tobiasch, B. Höhl, A. H. Nuber, I. E. Demir, S. Neupert, P. Kollmann, G. Mazzuoli-Weber, and M. Quante, 'Three-Dimensional Gastrointestinal Organoid Culture in Combination with Nerves or Fibroblasts: A Method to Characterize the Gastrointestinal Stem Cell Niche', *Stem Cells Int.*, vol. 2016, 2016.
[195] M. Theodosiou, M. Widmaier, R. T. Böttcher, E. Rognoni, M. Veelders, M. Bharadwaj, A. Lambacher, K. Austen, D. J. Müller, R. Zent, and R. Fässler, 'Kindlin-2 cooperates with talin to activate integrins and induces cell spreading by directly binding paxillin', *Elife*, vol. 5, no. JANUARY2016, 2016.
[196] J. E. Lai-Cheong, S. Ussar, K. Arita, I. R. Hart, and J. a McGrath, 'Colocalization of kindlin-1, kindlin-2, and migfilin at keratinocyte focal adhesion and relevance to the pathophysiology of Kindler syndrome.', *J. Invest. Dermatol.*, vol. 128, no. 9, pp. 2156–65, 2008.
[197] D. Hanahan, 'The Hallmarks of Cancer', *Cell*, vol. 100, no. 1, pp. 57–70, 2000.
[198] K. Sundfør, H. Lyng, and E. K. Rofstad, 'Tumour hypoxia and vascular density as predictors of metastasis in squamous cell carcinoma of the uterine cervix.', *Br. J. Cancer*, vol. 78, no. 6, pp. 822–7, 1998.
[199] L. Yao, Y. L. Zhao, S. Itoh, S. Wada, L. Yue, and I. Furuta, 'Thrombospondin-1 expression in oral squamous cell carcinomas: Correlations with tumor vascularity, clinicopathological features and survival', *Oral Oncol.*, vol. 36, no. 6, pp. 539–544, 2000.
[200] T. Fleitas, V. Martinez-Sales, V. Vila, E. Reganon, D. Mesado, M. Martin, J. Gomez-Codina, J. Montalar, and G. Reynes, 'VEGF and TSP1 levels

correlate with prognosis in advanced non-small cell lung cancer', *Clinical and Translational Oncology*, vol. 15, no. 11. pp. 897–902, 2013.
[201] M. S. O'Reilly, L. Holmgren, C. Chen, and J. Folkman, 'Angiostatin induces and sustains dormancy of human primary tumors in mice', *Nat. Med.*, vol. 2, no. 6, pp. 689–692, 1996.
[202] T. E. Cawston and D. A. Young, 'Proteinases involved in matrix turnover during cartilage and bone breakdown', *Cell and Tissue Research*, vol. 339, no. 1. pp. 221–235, 2010.
[203] S. K. Sinha, K. Asotra, H. Uzui, S. Nagwani, V. Mishra, and T. B. Rajavashisth, 'Nuclear localization of catalytically active MMP-2 in endothelial cells and neurons', *Am. J. Transl. Res.*, vol. 6, no. 2, pp. 155–162, 2014.
[204] J. M. Whitelock, A. D. Murdoch, R. V Iozzo, and P. A. Underwood, 'The Degradation of Human Endothelial Cell-derived Perlecan and Release of Bound Basic Fibroblast Growth Factor by Stromelysin , Collagenase , Plasmin , and Heparanases *', vol. 271, no. 17, pp. 10079–10086, 1996.
[205] J. Xu, D. Rodriguez, E. Petitclerc, J. J. Kim, M. Hangai, S. Moon Yuen, G. E. Davis, and P. C. Brooks, 'Proteolytic exposure of a cryptic site within collagen type IV is required for angiogenesis and tumor growth in vivo', *J. Cell Biol.*, vol. 154, no. 5, pp. 1069–1079, 2001.
[206] S. Briggs, K. Stephenson, J. Holliday, R. Peckham, D. Arthur, M. Papanikolaou, A. Butt, A. Pickford, G. Pilkington, and H. L. Fillmore, 'O4.03 * GLIOBLASTOMA STIMULATED ANGIOGENESIS IS MEDIATED BY MMP-3 ACTIVATED MMP-1 VIA BRAIN ENDOTHELIAL CELL ASSOCIATED PROTEASE ACTIVATED RECEPTOR 1 (PAR1) AND IS ENHANCED UNDER HYPOXIC CONDITIONS', *Neuro. Oncol.*, vol. 16, no. suppl 2, p. ii7-ii7, 2014.
[207] X. Jin, M. Yagi, N. Akiyama, T. Hirosaki, S. Higashi, C. Y. Lin, R. B. Dickson, H. Kitamura, and K. Miyazaki, 'Matriptase activates stromelysin (MMP-3) and promotes tumor growth and angiogenesis', *Cancer Sci.*, vol. 97, no. 12, pp. 1327–1334, 2006.
[208] W. Lederle, B. Hartenstein, A. Meides, H. Kunzelmann, Z. Werb, P. Angel, and M. M. Mueller, 'MMP13 as a stromal mediator in controlling persistent angiogenesis in skin carcinoma', *Carcinogenesis*, vol. 31, no. 7, pp. 1175–1184, 2009.
[209] S. Mañes, E. Mira, M. Mar, A. Ciprés, J. Mari, M. Aracil, G. Márquez, C. Marti, S. Man, M. Barbacid, A. Cipre, P. Ferna, G. Ma, and C. Martı, 'CELL BIOLOGY AND METABOLISM : Identification of Insulin-like Growth Factor-binding Protein-1 as a Potential Physiological Substrate for Human Identification of Insulin-like Growth Factor-binding Protein-1 as a Potential Physiological Substrate for Human S', vol. 272, no. 41, pp. 25706–25712, 1997.
[210] M. Nakamura, S. Miyamoto, H. Maeda, G. Ishii, T. Hasebe, T. Chiba, M. Asaka, and A. Ochiai, 'Matrix metalloproteinase-7 degrades all insulin-like growth factor binding proteins and facilitates insulin-like growth

factor bioavailability', *Biochem. Biophys. Res. Commun.*, vol. 333, no. 3, pp. 1011–1016, 2005.
[211] M. Suzuki, G. Raab, M. A. Moses, C. A. Fernandez, and M. Klagsbrun, 'Matrix metalloproteinase-3 releases active heparin-binding EGF-like growth factor by cleavage at a specific juxtamembrane site', *J. Biol. Chem.*, vol. 272, no. 50, pp. 31730–31737, 1997.
[212] A. K. Kivisaari, M. Kallajoki, R. Ala-Aho, J. A. McGrath, J. W. Bauer, R. K??nigov??, M. Medvecz, W. Beckert, R. Gr??nman, and V. M. K??h??ri, 'Matrix metalloproteinase-7 activates heparin-binding epidermal growth factor-like growth factor in cutaneous squamous cell carcinoma', *Br. J. Dermatol.*, vol. 163, no. 4, pp. 726–735, 2010.
[213] H. Qu, T. Wen, M. Pesch, and M. Aumailley, 'Partial loss of epithelial phenotype in kindlin-1-deficient keratinocytes', *Am. J. Pathol.*, vol. 180, no. 4, pp. 1581–1592, 2012.
[214] S. Gencer, A. Cebeci, and M. B. Irmak-Yazicioglu, 'Silencing of the MMP-3 gene by siRNA transfection in gastric cancer AGS cells', *J. Gastrointest. Liver Dis.*, vol. 20, no. 1, pp. 19–26, 2011.
[215] D. Banik, C. S. Netherby, P. N. Bogner, and S. I. Abrams, 'MMP3-Mediated tumor progression is controlled transcriptionally by a novel IRF8-MMP3 interaction', *Oncotarget*, vol. 6, no. 17, pp. 15164–79, 2015.
[216] P. Zigrino, I. Kuhn, T. Bäuerle, J. Zamek, J. W. Fox, S. Neumann, A. Licht, M. Schorpp-Kistner, P. Angel, and C. Mauch, 'Stromal expression of MMP-13 is required for melanoma invasion and metastasis.', *J. Invest. Dermatol.*, vol. 129, pp. 2686–2693, 2009.
[217] J. R. Wang, X. H. Li, X. J. Gao, S. C. An, H. Liu, J. Liang, K. Zhang, Z. Liu, J. Wang, Z. Chen, and W. Sun, 'Expression of MMP-13 is associated with invasion and metastasis of papillary thyroid carcinoma', *Eur. Rev. Med. Pharmacol. Sci.*, vol. 17, no. 4, pp. 427–435, 2013.
[218] A. M. Mendonsa, M. N. VanSaun, A. Ustione, D. W. Piston, B. M. Fingleton, and D. L. Gorden, 'Host and tumor derived MMP13 regulate extravasation and establishment of colorectal metastases in the liver.', *Mol. Cancer*, vol. 14, no. 1, p. 49, 2015.
[219] C. Alix-Panabieŕes and K. Pantel, 'Circulating tumor cells: Liquid biopsy of cancer', *Clinical Chemistry*, vol. 59, no. 1. pp. 110–118, 2013.
[220] G. E. Lind, K. Kleivi, G. I. Meling, M. R. Teixeira, E. Thiis-Evensen, T. O. Rognum, and R. A. Lothe, 'ADAMTS1, CRABP1, and NR3C1 identified as epigenetically deregulated genes in colorectal tumorigenesis.', *Cell. Oncol.*, vol. 28, no. 5–6, pp. 259–72, 2006.
[221] P. H. Y. Lo, a C. C. Leung, C. Y. C. Kwok, W. S. Y. Cheung, J. M. Y. Ko, L. C. Yang, S. Law, L. D. Wang, J. Li, E. J. Stanbridge, G. Srivastava, J. C. O. Tang, S. W. Tsao, and M. L. Lung, 'Identification of a tumor suppressive critical region mapping to 3p14.2 in esophageal squamous cell carcinoma and studies of a candidate tumor suppressor gene, ADAMTS9.', *Oncogene*, vol. 26, no. 1, pp. 148–57, 2007.
[222] H. Jin, X. Wang, J. Ying, a H. Y. Wong, H. Li, K. Y. Lee, G. Srivastava, a

T. C. Chan, W. Yeo, B. B. Y. Ma, T. C. Putti, M. L. Lung, Z.-Y. Shen, L.-Y. Xu, C. Langford, and Q. Tao, 'Epigenetic identification of ADAMTS18 as a novel 16q23.1 tumor suppressor frequently silenced in esophageal, nasopharyngeal and multiple other carcinomas.', *Oncogene*, vol. 26, no. 53, pp. 7490–7498, 2007.

[223] S. Porter, S. D. Scott, E. M. Sassoon, M. R. Williams, J. L. Jones, A. C. Girling, R. Y. Ball, and D. R. Edwards, 'Dysregulated Expression of Adamalysin-Thrombospondin Genes in Human Breast Carcinoma', *Clin. Cancer Res.*, vol. 10, no. 7, pp. 2429–2440, 2004.

[224] M. L. Iruela-Arispe, D. Carpizo, A. Luque, D. Lq, W. Uhvxowv, L. Q. Uhjuhvvlrq, R. I. Wxpru, L. Q. Wkh, I. Lv, W. Xqghuvwdqglqj, W. K. H. Phfkdqlvpv, W. Frqwuro, W. K. H. Qhrydvfxodu, R. U. Kdow, S. Ydvfxodu, J. Dqg, U. Fdqfhu, D. Iru, W. Wkh, Y. Lv, W. Xqolnh, W. Fhoov, W. K. H. Fhooxodu, and G. Uhvlvwdqfh, 'ADAMTS1: a matrix metalloprotease with angioinhibitory properties', *Ann N Y Acad Sci*, vol. 995, pp. 183–190, 2003.

[225] B.-H. Koo, D. M. Coe, L. J. Dixon, R. P. T. Somerville, C. M. Nelson, L. W. Wang, M. E. Young, D. J. Lindner, and S. S. Apte, 'ADAMTS9 is a cell-autonomously acting, anti-angiogenic metalloprotease expressed by microvascular endothelial cells.', *Am. J. Pathol.*, vol. 176, no. 3, pp. 1494–1504, 2010.

[226] S. Sharghi-Namini, H. Fan, K. N. Sulochana, P. Potturi, W. Xiang, Y. S. Chong, Z. Wang, H. Yang, and R. Ge, 'The first but not the second thrombospondin type 1 repeat of ADAMTS5 functions as an angiogenesis inhibitor', *Biochem. Biophys. Res. Commun.*, vol. 371, no. 2, pp. 215–219, 2008.

[227] S. S. Tolsma, O. V. Volpert, D. J. Good, W. A. Frazier, P. J. Polverini, and N. Bouck, 'Peptides derived from two separate domains of the matrix protein thrombospondin-1 have anti-angiogenic activity', *J. Cell Biol.*, vol. 122, no. 2, pp. 497–511, 1993.

[228] M. L. Iruela-Arispe, F. Vazquez, and M. A. Ortega, 'Antiangiogenic domains shared by thrombospondins and metallospondins, a new family of angiogenic inhibitors', *Ann N Y Acad Sci*, vol. 886, pp. 58–66, 1999.

[229] D. Wang, H. Wang, J. Brown, T. Daikoku, W. Ning, Q. Shi, A. Richmond, R. Strieter, S. K. Dey, and R. N. DuBois, 'CXCL1 induced by prostaglandin E2 promotes angiogenesis in colorectal cancer.', *J. Exp. Med.*, vol. 203, no. 4, pp. 941–51, 2006.

[230] W. L. Cheng, C. S. Wang, Y. H. Huang, M. M. Tsai, Y. Liang, and K. H. Lin, 'Overexpression of CXCL1 and its receptor CXCR2 promote tumor invasion in gastric cancer', *Ann. Oncol.*, vol. 22, no. 10, pp. 2267–2276, 2011.

[231] R. D. Loberg, C. Ying, M. Craig, L. Yan, L. A. Snyder, and K. J. Pienta, 'CCL2 as an important mediator of prostate cancer growth in vivo through the regulation of macrophage infiltration', *Neoplasia*, vol. 9, no. 7, pp. 556–562, 2007.

[232] H. Gustavsson, K. Jennbacken, K. Welén, and J.-E. Damber, 'Altered expression of genes regulating angiogenesis in experimental androgen-independent prostate cancer.', *Prostate*, vol. 68, no. 2, pp. 161–170, 2008.
[233] R. D. Loberg, L. L. Day, J. Harwood, C. Ying, L. N. St John, R. Giles, C. K. Neeley, and K. J. Pienta, 'CCL2 is a potent regulator of prostate cancer cell migration and proliferation', *Neoplasia*, vol. 8, no. 7, pp. 578–586, 2006.
[234] H. Saji, M. Koike, T. Yamori, S. Saji, M. Seiki, K. Matsushima, and M. Toi, 'Significant correlation of monocyte chemoattractant protein-1 expression with neovascularization and progression of breast carcinoma', *Cancer*, vol. 92, no. 5, pp. 1085–1091, 2001.
[235] S. Svensson, A. Abrahamsson, G. V. Rodriguez, A. K. Olsson, L. Jensen, Y. Cao, and C. Dabrosin, 'CCL2 and CCL5 are novel therapeutic targets for estrogen-dependent breast cancer', *Clin. Cancer Res.*, vol. 21, no. 16, pp. 3794–3805, 2015.
[236] X. Yang, Y. Lin, Y. Shi, B. Li, W. Liu, W. Yin, Y. Dang, Y. Chu, J. Fan, and R. He, 'FAP Promotes immunosuppression by cancer-associated fibroblasts in the tumor microenvironment via STAT3-CCL2 Signaling', *Cancer Res.*, vol. 76, no. 14, pp. 4124–4135, 2016.
[237] S. Wan, E. Zhao, I. Kryczek, L. Vatan, A. Sadovskaya, G. Ludema, D. M. Simeone, W. Zou, and T. H. Welling, 'Tumor-associated macrophages produce interleukin 6 and signal via STAT3 to promote expansion of human hepatocellular carcinoma stem cells', *Gastroenterology*, vol. 147, no. 6, pp. 1393–1404, 2014.
[238] A. Isobe, K. Sawada, Y. Kinose, C. Ohyagi-Hara, E. Nakatsuka, H. Makino, T. Ogura, T. Mizuno, N. Suzuki, E. Morii, K. Nakamura, I. Sawada, A. Toda, K. Hashimoto, S. Mabuchi, T. Ohta, K. I. Morishige, H. Kurachi, and T. Kimura, 'Interleukin 6 receptor is an independent prognostic factor and a potential therapeutic target of ovarian cancer', *PLoS One*, vol. 10, no. 2, 2015.
[239] H. Xu, W. Lai, Y. Zhang, L. Liu, X. Luo, Y. Zeng, H. Wu, Q. Lan, and Z. Chu, 'Tumor-associated macrophage-derived IL-6 and IL-8 enhance invasive activity of LoVo cells induced by PRL-3 in a KCNN4 channel-dependent manner', *BMC Cancer*, vol. 14, p. 330, 2014.
[240] Y. Guo, F. Xu, T. Lu, Z. Duan, and Z. Zhang, 'Interleukin-6 signaling pathway in targeted therapy for cancer', *Cancer Treatment Reviews*, vol. 38, no. 7. pp. 904–910, 2012.
[241] A. Heinemann, Y. He, E. Zimina, M. Boerries, H. Busch, N. Chmel, T. Kurz, L. Bruckner-Tuderman, and C. Has, 'Induction of phenotype modifying cytokines by FERMT1 mutations', *Hum. Mutat.*, vol. 32, no. 4, pp. 397–406, 2011.
[242] K. H. Hong, J. Ryu, and K. H. Han, 'Monocyte chemoattractant protein-1-induced angiogenesis is mediated by vascular endothelial growth factor-A', *Blood*, vol. 105, no. 4, pp. 1405–1407, 2005.
[243] L. Wyler, C. U. Napoli, B. Ingold, T. Sulser, M. Heikenwälder, P.

Schraml, and H. Moch, 'Brain metastasis in renal cancer patients: metastatic pattern, tumour-associated macrophages and chemokine/chemoreceptor expression.', *Br. J. Cancer*, vol. 7, no. November, pp. 1–9, 2013.
[244] Y. S. Lee, S. Kim, S. Song, H. K. Hong, Y. Lee, B. Y. Oh, W. Y. Lee, and Y. B. Cho, 'Crosstalk between CCL7 and CCR3 promotes metastasis of colon cancer cells via ERK-JNK signaling pathways', vol. 7, no. 24, 2016.
[245] D. S. Krause, N. D. Theise, M. I. Collector, O. Henegariu, S. Hwang, R. Gardner, S. Neutzel, and S. J. Sharkis, 'Multi-organ, multi-lineage engraftment by a single bone marrow-derived stem cell', *Cell*, vol. 105, no. 3, pp. 369–377, 2001.
[246] Y. Jiang, B. N. Jahagirdar, R. L. Reinhardt, R. E. Schwartz, C. D. Keene, X. R. Ortiz-Gonzalez, M. Reyes, T. Lenvik, T. Lund, M. Blackstad, J. Du, S. Aldrich, A. Lisberg, W. C. Low, D. a Largaespada, and C. M. Verfaillie, 'Pluripotency of mesenchymal stem cells derived from adult marrow.', *Nature*, vol. 418, no. 6893, pp. 41–49, 2002.
[247] E. V. Badiavas, M. Abedi, J. Butmarc, V. Falanga, and P. Quesenberry, 'Participation of bone marrow derived cells in cutaneous wound healing', *J. Cell. Physiol.*, vol. 196, no. 2, pp. 245–250, 2003.
[248] J. Tolar, I. Y. Akemi, M. Riddle, R. T. McElmurry, M. Osborn, L. Xia, T. Lund, C. Slattery, J. Uitto, A. M. Christiano, J. E. Wagner, and B. R. Blazar, 'Amelioration of epidermolysis bullosa by transfer of wild-type bone marrow cells', *Blood*, vol. 113, no. 5, pp. 1167–1174, 2009.
[249] T. Chino, K. Tamai, T. Yamazaki, S. Otsuru, Y. Kikuchi, K. Nimura, M. Endo, M. Nagai, J. Uitto, Y. Kitajima, and Y. Kaneda, 'Bone marrow cell transfer into fetal circulation can ameliorate genetic skin diseases by providing fibroblasts to the skin and inducing immune tolerance.', *Am. J. Pathol.*, vol. 173, no. 3, pp. 803–814, 2008.
[250] J. E. Wagner, A. Ishida-Yamamoto, J. a McGrath, M. Hordinsky, D. R. Keene, D. T. Woodley, M. Chen, M. J. Riddle, M. J. Osborn, T. Lund, M. Dolan, B. R. Blazar, and J. Tolar, 'Bone marrow transplantation for recessive dystrophic epidermolysis bullosa.', *N. Engl. J. Med.*, vol. 363, no. 7, pp. 629–639, 2010.
[251] C. Georgiadis, F. Syed, A. Petrova, A. Abdul-Wahab, S. M. Lwin, F. Farzaneh, L. Chan, S. Ghani, R. A. Fleck, L. Glover, J. R. McMillan, M. Chen, A. J. Thrasher, J. A. McGrath, W.-L. Di, and W. Qasim, 'Lentiviral Engineered Fibroblasts Expressing Codon Optimized COL7A1 Restore Anchoring Fibrils in RDEB.', *J. Invest. Dermatol.*, no. August, pp. 1–29, 2015.
[252] S. J. Howe, M. R. Mansour, K. Schwarzwaelder, C. Bartholomae, M. Hubank, H. Kempski, M. H. Brugman, K. Pike-Overzet, S. J. Chatters, D. De Ridder, K. C. Gilmour, S. Adams, S. I. Thornhill, K. L. Parsley, F. J. T. Staal, R. E. Gale, D. C. Linch, J. Bayford, L. Brown, M. Quaye, C. Kinnon, P. Ancliff, D. K. Webb, M. Schmidt, C. Von Kalle, H. B. Gaspar, and A. J. Thrasher, 'Insertional mutagenesis combined with acquired somatic

mutations causes leukemogenesis following gene therapy of SCID-X1 patients', *J. Clin. Invest.*, vol. 118, no. 9, pp. 3143–3150, 2008.
[253] S. Dinçer, M. Türk, and E. Pişkin, 'Intelligent polymers as nonviral vectors', *Gene Ther.*, vol. 12, pp. S139–S145, 2005.
[254] Y. Tone, T. Wada, F. Shibata, T. Toma, Y. Hashida, Y. Kasahara, S. Koizumi, and A. Yachie, 'Somatic revertant mosaicism in a patient with leukocyte adhesion deficiency type 1', *Blood*, vol. 109, no. 3, pp. 1182–1184, 2007.
[255] T. Wada, S. H. Schurman, G. J. Jagadeesh, E. K. Garabedian, D. L. Nelson, and F. Candotti, 'Multiple patients with revertant mosaicism in a single Wiskott-Aldrich syndrome family', *Blood*, vol. 104, no. 5, pp. 1270–1272, 2004.
[256] J. Tolar, J. A. McGrath, L. Xia, M. J. Riddle, C. J. Lees, C. Eide, D. R. Keene, L. Liu, M. J. Osborn, T. C. Lund, B. R. Blazar, and J. E. Wagner, 'Patient-specific naturally gene-reverted induced pluripotent stem cells in recessive dystrophic epidermolysis bullosa.', *J. Invest. Dermatol.*, vol. 134, no. 5, pp. 1246–54, 2014.
[257] D. Kiritsi, Y. He, A. M. G. Pasmooij, M. Onder, R. Happle, M. F. Jonkman, L. Bruckner-Tuderman, and C. Has, 'Revertant mosaicism in a human skin fragility disorder results from slipped mispairing and mitotic recombination', *J. Clin. Invest.*, vol. 122, no. 5, pp. 1742–1746, 2012.
[258] J. E. Lai-Cheong, C. Moss, M. Parsons, N. Almaani, and J. a McGrath, 'Revertant mosaicism in Kindler syndrome.', *J. Invest. Dermatol.*, vol. 132, no. 3 Pt 1, pp. 730–2, 2012.
[259] A. Gosty??ski, A. M. G. Pasmooij, and M. F. Jonkman, 'Successful therapeutic transplantation of revertant skin in epidermolysis bullosa', *J. Am. Acad. Dermatol.*, vol. 70, no. 1, pp. 98–101, 2014.
[260] M. De Luca, G. Pellegrini, and H. Green, 'Regeneration of squamous epithelia from stem cells of cultured grafts.', *Regen. Med.*, vol. 1, no. 1, pp. 45–57, 2006.
[261] V. Sebastiano, H. H. Zhen, B. Haddad, B. H. Derafshi, E. Bashkirova, S. P. Melo, P. Wang, T. L. Leung, Z. Siprashvili, A. Tichy, J. Li, M. Ameen, J. Hawkins, S. Lee, L. Li, A. Schwertschkow, G. Bauer, L. Lisowski, M. A. Kay, S. K. Kim, A. T. Lane, M. Wernig, and A. E. Oro, 'Human COL7A1-corrected induced pluripotent stem cells for the treatment of recessive dystrophic epidermolysis bullosa.', *Sci. Transl. Med.*, vol. 6, no. 264, p. 264ra163, 2014.
[262] Y. H. Kim, D. T. Woodley, K. C. Wynn, W. Giomi, and E. a Bauer, 'Recessive dystrophic epidermolysis bullosa phenotype is preserved in xenografts using SCID mice: development of an experimental in vivo model.', *The Journal of investigative dermatology*, vol. 98, no. 2. pp. 191–197, 1992.
[263] D. Kaluza, J. Kroll, S. Gesierich, T.-P. Yao, R. A. Boon, E. Hergenreider, M. Tjwa, L. Rössig, E. Seto, H. G. Augustin, A. M. Zeiher, S. Dimmeler, and C. Urbich, 'Class IIb HDAC6 regulates endothelial cell migration

and angiogenesis by deacetylation of cortactin', *EMBO J.*, vol. 30, no. 20, pp. 4142–4156, 2011.
[264] R. Rao, W. Fiskus, Y. Yang, P. Lee, R. Joshi, P. Fernandez, A. Mandawat, P. Atadja, J. E. Bradner, and K. Bhalla, 'HDAC6 inhibition enhances 17-AAG--mediated abrogation of hsp90 chaperone function in human leukemia cells.', *Blood*, vol. 112, no. 5, pp. 1886–1893, 2008.
[265] S. Dallavalle, C. Pisano, and F. Zunino, 'Development and therapeutic impact of HDAC6-selective inhibitors', *Biochemical Pharmacology*, vol. 84, no. 6. pp. 756–765, 2012.